Using Mercury Stable Isotopes to Identify Sources and Track Biogeochemical Cycling of Mercury in Freshwater Ecosystems

by

Elizabeth R. Crowther

A dissertation submitted in partial fulfillment
of the requirements for the degree of
Doctor of Philosophy
(Earth and Environmental Sciences)
in the University of Michigan
2023

Doctoral Committee:

Professor Joel D. Blum, Co-Chair
Associate Research Scientist Jason D. Demers, Co-Chair
Professor G. Allen Burton, Jr.
Professor Rose M. Cory
Professor Nathan D. Sheldon

Elizabeth R. Crowther

ecrowth@umich.edu

ORCID iD: 0000-0002-3976-3844

Acknowledgements

I would first like to thank both of my co-advisors, Dr. Jason Demers and Dr. Joel Blum, for being such great mentors and for helping to ensure that I had a positive graduate school experience. Thank you, Jason, for teaching me how to do good work in the field and in the lab, and for helping me to evolve my scientific writing skills. Thank you, Joel, for helping to ensure that I stayed on track with my research projects, and for offering fresh perspectives and advice both within and outside of my research. Thank you both for your guidance, support, and encouragement over the past five-and-a-half years.

I would also like to thank the other members of the BEIGL lab group, including our lab manager, Marcus Johnson, for both his technical support with lab instruments as well as his moral support during my phases of spending countless hours in the lab. Thank you especially for teaching me how to run the mass spectrometer independently. Thank you also to my other lab mates, including Dr. Jamie Gleason and graduate students Laura Motta Medina, Aaron Kurz, and Spencer Washburn, for helping to make my time in the lab enjoyable.

Thank you to the rest of my dissertation committee, including Dr. Rose Cory, Dr. Nathan Sheldon, and Dr. Allen Burton, for helping me to better articulate the main points of my research projects and for offering advice from their tangentially related fields about how I can connect my research to a broader audience. Thank you also to Dr. Scott Brooks for introducing me to mercury research while I was an undergraduate student, and for continuing to be involved with my graduate research. If I had not done an undergraduate internship with you, my life would be very different today.

Thank you to my graduate cohort – María, Prithvi, Marlon, Guolei, Sooyeon, Brie, Molly, and Tariq – for being so supportive and for making time to hang out together despite our busy schedules. I'm so glad that we remained close throughout graduate school and I'm very happy to have you as my friends. Thank you also to Natalie, my closest friend that I met in graduate school, for all of the encouragement you've given me over the years and for taking me on fun kayaking adventures. Also thank you to my therapist of three years, Mylah, for helping me when I had lost much of my motivation and needed to be kinder to myself.

Lastly, thank you to my family, especially my parents for always loving, supporting, and encouraging me. Thank you for instilling in me a strong work ethic and for raising me to value my education and the natural environment. Thank you to my grandparents and great grandparents for their endless love and support, and for listening to me talk about science even when they don't fully understand it. I only wish that all of my grandparents who saw me start graduate school could have been here to see me finish. To Cameron, my husband and best friend, I can't thank you enough for your support and encouragement. Thank you for keeping me sane during really challenging phases of graduate school and for celebrating the accomplishments I've made along the way.

Table of Contents

List of Tables

List of Figures

Abstract

Mercury is a trace metal toxin that is harmful to the health of humans and wildlife. Anthropogenic mercury released directly into waterbodies during mining activities or industrial processes may remain in the sediment and soil for decades or longer as legacy mercury. Mercury in the environment may also be converted into methylmercury, a more toxic and bioaccumulative form of mercury that biomagnifies in food webs. Throughout this dissertation, I applied measurements of mercury stable isotope ratios in sediment, fish, and aquatic invertebrate samples to study mercury biogeochemical cycling within East Fork Poplar Creek, a point-source contaminated stream ecosystem. In Chapter 2, I investigated the potential mechanisms by which legacy mercury within streambed sediment may be remobilized to the surface water as dissolved mercury. This was done by combining sequential extractions and mercury isotope analysis, through which I observed isotopic differences between various pools of mercury within the sediment. These isotopic signatures, along with previous measurements of the isotopic composition of surface water, pore water, and suspended particulates, suggested that small amounts of the largely-recalcitrant legacy mercury in the sediment is contributing to the flux of dissolved mercury along the flow path of the stream. In Chapter 3, I developed a method of extracting and isolating methylmercury from fish and aquatic invertebrates for isotope analysis. This method involved a novel combination of nitric acid digestion and anion-exchange resin separation, and successfully achieved high methylmercury recovery and purity. This method allows for direct determination of the isotopic composition of methylmercury within a variety of organisms, which enables the sources of methylmercury to the food web to be identified. In

Chapter 4, I applied this new methylmercury separation method to directly measure both the total mercury and methylmercury isotopic compositions of a range of aquatic organisms from East Fork Poplar Creek and a regional reference stream, Hinds Creek. This allowed for the identification of sources of methylmercury to the food webs of these streams, as well as a comparison of biogeochemical processing of methylmercury within freshwater stream ecosystems containing either natural background or highly elevated levels of mercury. I found that the two streams each contain multiple sources of methylmercury, with organisms from Hinds Creek ultimately deriving methylmercury from a combination of precipitation and dry deposition, and organisms from East Fork Poplar Creek ultimately deriving methylmercury from a combination of legacy and newly released mercury originating from an industrial point source. I also found that for both streams, multiple basal resources deliver methylmercury to the food web, including streambed sediment as well as biofilm and/or suspended particulates. Finally, I found that microbial demethylation tends to be an important reaction within streams containing either natural background or moderately elevated levels of mercury contamination, including Hinds Creek, but that isotope fractionation induced by microbial methylation tends to be more dominant relative to that induced by microbial demethylation within the most highly contaminated stream ecosystems, including East Fork Poplar Creek.

Chapter 1 Introduction

1.1 Mercury Biogeochemical Cycling in Freshwater Ecosystems

Mercury (Hg) is a toxic metal present in the atmosphere and in terrestrial and aquatic environments globally. Long-term exposure to high levels of mercury can cause negative health effects for wildlife and humans (Scheuhammer et al. 2007, Hong et al. 2012). Mercury is released to the environment through natural processes as well as anthropogenic activities such as coal combustion, artisanal small-scale gold mining, metals production, and other industrial processes (UNEP 2013). Atmospheric mercury can travel long distances before entering terrestrial and aquatic environments through precipitation or dry deposition. Even pristine environments contain mercury derived from anthropogenic emissions of mercury to the atmosphere, though concentrations of mercury in sediment and soil in point source contaminated environments are often orders of magnitude higher than those in natural background sites. Mercury within terrestrial and aquatic ecosystems may also be re-emitted to the atmosphere (Gaffney and Marley 2014), perpetuating the global mercury cycle.

Within a freshwater ecosystem, mercury can undergo numerous biogeochemical reactions. The two most common oxidation states of mercury in freshwater ecosystems are Hg(II) and Hg(0). Oxidized inorganic Hg(II) may be dissolved in water, precipitated as minerals, or adsorbed to various solid materials, and has a strong affinity for reduced sulfur functional groups. Reduced Hg(0) may be dissolved in water, volatilized to the atmosphere, or be present as liquid elemental mercury within some environments contaminated by mining or certain types of industrial activities. Mercury can be converted from one oxidation state to the other through

microbial, photochemical, and dark abiotic reduction and oxidation reactions (Morel et al. 1998). Additionally, inorganic mercury (iHg) may be converted into methylmercury (MeHg), a bioaccumulative neurotoxin, through microbial methylation. Pools of MeHg may be partially degraded by microbial or photochemical demethylation prior to bioaccumulating in organisms. Concentrations of MeHg in organisms increase with trophic level as MeHg biomagnifies in the food web, typically resulting in ~90-100% MeHg (MeHg / total Hg) in fish tissue and lower %MeHg values in lower trophic level invertebrates (Gentès et al. 2021).

In order to remediate mercury contaminated freshwater ecosystems, or to predict their natural rate of recovery, it is important to identify specific sources of mercury to the water and to the food web. For highly contaminated ecosystems, legacy mercury contamination can persist over long periods of time (Turner and Southworth 1999), and although a large proportion of anthropogenic legacy mercury contamination within sediment and soil is typically recalcitrant, smaller weakly-bound fractions may have the potential to be remobilized. For some contaminated waterbodies, it is unclear whether dissolved mercury concentrations in the surface water are sustained by diffuse legacy sources, new inputs from industrial activities, or ongoing deposition from atmospheric sources, or some combination of these. Additionally, because some pools of iHg within an ecosystem may be more bioavailable for methylation than others, it may be challenging to determine which basal resources are contributing neurotoxic MeHg to the food web. Measurements of mercury stable isotope ratios in sediment, water, aquatic organisms, and other environmental samples can aid in identifying sources of mercury to surface water and the food web, as well as determining which biogeochemical reactions are predominantly occurring within an ecosystem.

1.2 Mercury Stable Isotope Ratios

Mercury stable isotope ratios in environmental samples can be used to identify sources and track biogeochemical cycling of mercury within ecosystems. All natural samples containing mercury contain seven stable isotopes of mercury (^{196}Hg, ^{198}Hg, ^{199}Hg, ^{200}Hg, ^{201}Hg, ^{202}Hg, and ^{204}Hg), the ratios of which can be determined using cold vapor multiple collector inductively coupled plasma mass spectrometry (CV-MC-ICP-MS) (Lauretta et al. 2001, Blum and Bergquist 2007). Each of the biogeochemical reactions mentioned in the previous section, among others, result in mass-dependent fractionation (MDF) of mercury isotopes, and some additionally result in odd- or even-mass number mass-independent fractionation (odd-MIF or even-MIF) (Blum et al. 2014). This leads to different isotopic compositions within different pools of iHg and MeHg, which is useful for distinguishing between mercury sources and for tracking biogeochemical transformations of mercury.

Mass-dependent isotope fractionation (MDF) is reported as the permil (‰) deviation from the average of NIST SRM 3133 bracketing standards (Blum and Bergquist 2007) using delta notation:

$$\delta^{xxx}\text{Hg (‰)} = ([(^{xxx}\text{Hg}/^{198}\text{Hg})_{\text{sample}} / (^{xxx}\text{Hg}/^{198}\text{Hg})_{\text{NIST SRM 3133}}] - 1) * 1000$$

where xxx is the mass of each mercury isotope between ^{199}Hg and ^{204}Hg. Mass-dependent fractionation is reported with δ^{202}Hg values. Mass-independent isotope fractionation (MIF) is reported as the difference between the measured δ^{xxx}Hg value and that which is theoretically predicted by the kinetic mass-dependent fractionation law (Blum and Bergquist 2007) using capital delta notation:

$$\Delta^{xxx}\text{Hg (‰)} \approx \delta^{xxx}\text{Hg} - (\delta^{202}\text{Hg} * \beta)$$

where xxx is the mass of each mercury isotope ^{199}Hg, ^{200}Hg, ^{201}Hg, and ^{204}Hg, and β is a constant for each isotope (0.252, 0.502, 0.752, 1.493, respectively) (Blum and Bergquist 2007).

1.3 Dissertation Narrative

Historical releases of mercury from industrial sources has led to high levels of legacy mercury contamination in numerous waterbodies around the world, though the effects of anthropogenic legacy mercury on surface water dissolved mercury concentrations and levels of MeHg in aquatic food webs are not fully understood. This dissertation focuses on using measurements of mercury stable isotope ratios in sediment, fish, and aquatic invertebrate samples, in conjunction with previous mercury isotopic measurements of surface water, pore water, suspended particulates, and biofilm, to better understand the effects of legacy mercury in East Fork Poplar Creek (EFPC), a point source contaminated freshwater stream in Oak Ridge, TN, USA.

In Chapter 2, published in *Environmental Science: Processes & Impacts* (Crowther et al. 2021), I investigated the potential for remobilization of anthropogenic legacy mercury in EFPC from streambed sediment to the surface water dissolved phase. This stream was contaminated by the release of mercury from the Y-12 National Security Complex in the 1950s and early 1960s (Brooks and Southworth 2011), and levels of mercury in the sediment, soil, surface water, groundwater, and aquatic food web remain high today. I performed sequential extractions (Bloom et al. 2003) on EFPC streambed sediment and assessed the isotopic composition of water soluble, organically-bound, and recalcitrant pools of mercury within the sediment. The results of these measurements suggest that small amounts of the large recalcitrant mercury fraction may be released and then rapidly and weakly re-adsorb to the sediment, after which it may contribute dissolved mercury to the hyporheic pore water and surface water. The weakly-bound sediment

mercury fraction also appears to contribute mercury to other basal resources in the stream, such as biofilm and suspended particulates. Through this study, I also found that the baseline mercury isotopic composition of EFPC streambed sediment appears to have been set by equilibrium isotope effects during isotope exchange between coexisting Hg(0) and Hg(II) species (Zheng et al. 2019), which may have overprinted isotope fractionation signatures imparted by kinetic oxidation and reduction reactions.

In Chapter 3, published in *Analytical and Bioanalytical Chemistry* (Crowther et al. 2022), I developed a method of extracting and isolating MeHg from fish and aquatic invertebrates for compound-specific mercury isotopic analysis. This method uses a widely used hot nitric acid digestion procedure (Hammerschmidt and Fitzgerald 2005) followed by a batch anion-exchange resin separation procedure. Performance of this method was assessed using aqueous MeHg standards, four biological reference materials, and five types of natural biological samples collected from EFPC. Recovery of MeHg and the amount of iHg impurities were quantified after each step in the procedure to verify that MeHg was sufficiently recovered and isolated prior to isotope analysis. Measured MeHg isotopic compositions of reference materials closely aligned with those measured in other studies using different MeHg separation methods. Variable offsets between THg and MeHg isotopic composition were observed for reference materials and natural biological samples containing lower %MeHg, demonstrating distinct isotopic compositions of iHg and MeHg within some of the samples. This novel combination of nitric acid digestion and anion-exchange resin separation uses a single sample aliquot for MeHg concentration and isotopic analysis, which promotes a tight coupling between MeHg concentration, %MeHg, and MeHg isotopic composition for each sample. Additionally, this method is relatively simple and avoids some of the challenges associated with other MeHg separation techniques. The ability to

measure the THg and MeHg isotopic compositions of biological samples independently, and to calculate iHg isotopic compositions by mass balance, is useful for identifying the sources of mercury to aquatic food webs, especially those that may obtain iHg and/or MeHg from multiple isotopically distinct sources.

In Chapter 4, I measured THg and MeHg concentrations and THg isotope ratios in a variety of different types of fish and invertebrates collected from EFPC, as well as from a regional background stream, Hinds Creek (HC). I additionally measured the MeHg isotopic compositions of a subset of biological samples from each of the two streams using the MeHg separation method developed in Chapter 3. For some biological samples, iHg isotopic compositions could be calculated via mass balance using their THg and MeHg isotopic compositions and concentrations. In plotting THg isotope ratios against %MeHg values, I found nonlinear relationships for both streams, suggesting that aquatic organisms had obtained iHg and MeHg each from multiple combinations of sources. Calculated iHg isotope ratios as well as THg isotope ratios of low trophic level organisms were used to determine the most likely source(s) of iHg to each of the food webs. Directly measured MeHg isotope ratios as well as THg isotope ratios of high trophic level organisms were used to determine the most likely source(s) of MeHg to each of the food webs. Additionally, THg and MeHg isotopic compositions of aquatic organisms, as well as previously measured THg isotopic compositions of various basal resources, were used to determine the types of reactions and relative amounts of biogeochemical processing experienced by MeHg prior to its bioaccumulation in the food webs of each of the streams. These results were compared to previous studies of other waterbodies with variable levels of sediment THg concentrations to assess whether there may be any consistent differences in

biogeochemical cycling of mercury between natural background and point source contaminated waterbodies.

In Chapter 5, I summarize the key findings of this study on mercury biogeochemical cycling in EFPC and HC, and discuss how these findings may relate more broadly to other waterbodies with both high and low levels of mercury contamination. I also provide additional research questions and ideas for future research to further investigate and understand the impacts of anthropogenic legacy mercury on freshwater stream ecosystems.

References

Bloom, Nicolas S., Eve Preus, Jodie Katon, and Misti Hiltner. 2003. "Selective extractions to assess the biogeochemically relevant fractionation of inorganic mercury in sediments and soils." *Analytica Chimica Acta* 479 (2):233-248. doi: 10.1016/s0003-2670(02)01550-7.

Blum, Joel D., and Bridget A. Bergquist. 2007. "Reporting of variations in the natural isotopic composition of mercury." *Analytical and Bioanalytical Chemistry* 388:353-359. doi: 10.1007/s00216-007-1236-9.

Blum, Joel D., Laura S. Sherman, and Marcus W. Johnson. 2014. "Mercury isotopes in earth and environmental sciences." *Annual Review of Earth and Planetary Sciences* 42:249-269. doi: 10.1146/annurev-earth-050212-124107.

Brooks, Scott C., and George R. Southworth. 2011. "History of mercury use and environmental contamination at the Oak Ridge Y-12 Plant." *Environmental Pollution* 159 (1):219-228. doi: 10.1016/j.envpol.2010.09.009.

Crowther, Elizabeth R., Jason D. Demers, Joel D. Blum, Scott C. Brooks, and Marcus W. Johnson. 2021. "Use of sequential extraction and mercury stable isotope analysis to assess remobilization of sediment-bound legacy mercury." *Environmental Science: Processes & Impacts* 23:756-775. doi: 10.1039/d1em00019e.

Crowther, Elizabeth R., Jason D. Demers, Joel D. Blum, Scott C. Brooks, and Marcus W. Johnson. 2022. "Coupling of nitric acid digestion and anion-exchange resin separation for the determination of methylmercury isotopic composition within organisms." *Analytical and Bioanalytical Chemistry*. doi: 10.1007/s00216-022-04468-8.

Gaffney, Jeffrey S., and Nancy A. Marley. 2014. "In-depth review of atmospheric mercury: Sources, transformations, and potential sinks." *Energy and Emission Control Technologies* 2:1-21. doi: 10.2147/eect.s37038.

Gentès, Sophie, Brice Löhrer, Alexia Legeay, Agnès Feurtet Mazel, Pierre Anschutz, Céline Charbonnier, Emmanuel Tessier, and Régine Maury-Brachet. 2021. "Drivers of variability in mercury and methylmercury bioaccumulation and biomagnification in temperate freshwater lakes." *Chemosphere* 267:128890. doi: 10.1016/j.chemosphere.2020.128890.

Hammerschmidt, Chad R., and William F. Fitzgerald. 2005. "Methylmercury in mosquitoes related to atmospheric mercury deposition and contamination." *Environmental Science & Technology* 39:3034-3039. doi: 10.1021/es0485107.

Hong, Young-Seoub, Yu-Mi Kim, and Kyung-Eun Lee. 2012. "Methylmercury exposure and health effects." *Journal of Preventive Medicine and Public Health* 45 (6):353-363. doi: 10.3961/jpmph.2012.45.6.353.

Lauretta, Dante S., Bjoern Klaue, Joel D. Blum, and Peter R. Buseck. 2001. "Mercury abundances and isotopic compositions in the Murchison (CM) and Allende (CV) carbonaceous chondrites." *Geochimica et Cosmochimica Acta* 65:2807-2818. doi: 10.1016/s0016-7037(01)00630-5.

Morel, François M. M., Anne M. L. Kraepiel, and Marc Amyot. 1998. "The chemical cycle and bioaccumulation of mercury." *Annual Review of Ecology, Evolution, and Systematics* 29:543-566. doi: 10.1146/annurev.ecolsys.29.1.543.

Scheuhammer, Anton M., Michael W. Meyer, Mark B. Sandheinrich, and Michael W. Murray. 2007. "Effects of environmental methylmercury on the health of wild birds, mammals, and fish." *Ambio* 36 (1):12-18. doi: 10.1579/0044-7447(2007)36[12:eoemot]2.0.co;2.

Turner, R. R., and G. R. Southworth. 1999. *Mercury Contaminated Sites–Characterization, Risk Assessment and Remediation*, edited by R. Ebinghaus, R. R. Turner, L. D. de Lacerda, O. Vasiliev and W. Salomons, 89-112. Springer-Verlag Berlin Heidelberg.

UNEP. 2013. Global Mercury Assessment 2013: Sources, Emissions, Releases and Environmental Transport. Geneva, Switzerland: UNEP Chemicals Branch.

Zheng, Wang, Jason D. Demers, Xia Lu, Bridget A. Bergquist, Ariel D. Anbar, Joel D. Blum, and Baohua Gu. 2019. "Mercury stable isotope fractionation during abiotic dark oxidation in the presence of thiols and natural organic matter." *Environmental Science & Technology* 53:1853-1862. doi: 10.1021/acs.est.8b05047.

Chapter 2 Use of Sequential Extraction and Mercury Stable Isotope Analysis to Assess Remobilization of Sediment-Bound Legacy Mercury

Co-authored with Jason D. Demers, Joel D. Blum, Scott C. Brooks, and Marcus W. Johnson. Use of sequential extraction and mercury stable isotope analysis to assess remobilization of sediment-bound legacy mercury. *Environmental Science: Processes & Impacts*, 2021, **23**, 756–775, DOI: 10.1039/d1em00019e

Abstract: The goal of this project was to assess how anthropogenic legacy mercury (Hg) retained in streambed sediment may be remobilized to stream water. To do this, we performed sequential extractions and Hg isotope analyses on streambed sediment collected along the length of East Fork Poplar Creek, a point-source contaminated stream in Oak Ridge, Tennessee, USA. Legacy Hg within streambed sediment appears to have been isotopically fractionated by equilibrium isotope effects driven by isotope exchange between co-existing Hg(0) and Hg(II) species, probably over-printing fractionation patterns that would have been imparted by kinetic redox reactions. Weakly-bound and recalcitrant sediment Hg pools were isotopically similar to one another, suggesting that small amounts of recalcitrant Hg may be released and then rapidly and weakly re-adsorbed onto the sediment. This weakly-bound Hg pool appears to contribute dissolved Hg to the hyporheic pore water, which may subsequently enter the surface flow. The isotopic composition of the organically-bound sediment Hg pools, as well as biofilm and suspended particulates, converged with that of the weakly-bound and recalcitrant sediment Hg pools along the flow path. This appears to be indicative of both physical mixing with streambed sediment and the transfer of weakly-bound sediment Hg into biofilm and suspended particulates

followed by re-incorporation into the organically-bound sediment Hg pool. Overall, these results provide evidence that legacy Hg in the streambed is remobilized, enters the stream water as dissolved Hg, and may be incorporated into streambed biofilm, which constitutes a basal resource within the stream ecosystem.

2.1 Introduction

Mercury (Hg) is a toxic metal that is harmful to the health of humans and wildlife (Scheuhammer et al. 2007, Hong et al. 2012). Anthropogenic Hg has been emitted to the atmosphere through fossil fuel combustion, cement and metals production, waste incineration, and artisanal small-scale gold mining, or released directly to waterbodies during mercury and gold mining activities, chlor-alkali production, and other industrial processes (UNEP 2013). In point-source contaminated aquatic ecosystems, direct industrial releases of Hg can persist in sediment and soil for decades or longer (Turner and Southworth 1999). Although this legacy Hg primarily exists in recalcitrant forms (resistant to dissolution and mobilization), recent evidence suggests that some legacy Hg pools may be remobilized to surface water or become bioavailable for methylation and subsequent accumulation in the food web (Choe et al. 2004, Demers et al. 2018, Rudd et al. 2018, Janssen et al. 2020). In order to understand the long-term effects of legacy Hg on water quality and bioaccumulation, it is necessary to assess whether dissolved Hg in contaminated aquatic ecosystems can be derived from seemingly recalcitrant legacy sources in the sediment and soil. Quantifying the legacy Hg pools that may be available for remobilization, as well as the processes governing their release, is essential for predicting the timing and potential for recovery of aquatic ecosystems heavily contaminated with point-source Hg pollution.

In the 1950s and early 1960s, the Y-12 National Security Complex (Y-12) in Oak Ridge, Tennessee used approximately 11 million kg of liquid elemental mercury (Hg(0)) for lithium-6 isotope separation for use in nuclear weapons. During that time, ~193,000 kg of metallic Hg(0) was lost to the soil from spills and leaks within the Y-12 boundary (Rothschild et al. 1984, Brooks and Southworth 2011), and ~128,000 kg of Hg was discharged from Y-12 directly into East Fork Poplar Creek (EFPC), primarily in the form of dissolved and particulate-bound oxidized mercury (Hg(II)) (Brooks and Southworth 2011). The headwaters of EFPC originate from Y-12 and are comprised of industrial wastewater, storm water runoff, and contaminated groundwater. Although the release of Hg into EFPC has declined dramatically since the 1960s, total Hg flux measured at the Y-12 boundary has continued to fluctuate between 2.7 and 24 kg per year over the last two decades (WRRP and UCOR 2019). This has maintained unfiltered stream water total Hg concentrations of 198 to 1860 ng L^{-1} and dissolved Hg concentrations of 45 to 100 ng L^{-1} at the Y-12 boundary (WRRP and UCOR 2016, 2019).

In addition to continued Hg discharge from Y-12, Hg flux measurements in the lower reaches of EFPC indicate that the stream also receives significant amounts of Hg from diffuse legacy sources, such as hyporheic discharge and riparian floodplain inputs. Field studies have shown that 25 to 83% of the particulate-bound Hg flux and 6 to 36% of the dissolved Hg flux originates from diffuse legacy sources, as measured at a site ~18 km downstream of the Y-12 boundary (Demers et al. 2018, Peterson et al. 2018a). Although this recent research suggests that a substantial amount of Hg enters the stream from legacy sources, the specific sources (e.g., streambed sediment, stream bank soil, floodplain soil, and hyporheic pore water) and mechanisms of remobilization remain unclear.

Estimates of the current watershed inventories of Hg include 334 kg in the EFPC streambed (Brooks et al. 2017) and 57,000 kg in the floodplains (Watson et al. 2016b) downstream of Y-12. Each year, an estimated 26 to 38 kg of Hg are contributed to the streambed by bank erosion (Watson et al. 2016b, Watson et al. 2016a, Dickson et al. 2019). Results of previous sequential extractions show that EFPC soil and sediment contain high proportions of recalcitrant Hg (Brooks et al. 2017, Peterson et al. 2018b), likely in the form of mercuric sulfide (HgS). The presence of metacinnabar, a polymorph of HgS, has been confirmed in EFPC stream bank and floodplain soil using scanning electron microscopy with energy-dispersive x-ray spectrometry, along with transmission electron microscopy with select area electron diffraction (Barnett et al. 1997, Peterson et al. 2018b). While HgS is a poorly soluble form of Hg (Brezonik and Arnold 2011), chemical dissolution of solid HgS can occur by sulfide replacement with another ligand, by Hg replacement with another metal, or by sulfide ligand oxidation (Chen et al. 2017). For example, dissolved organic matter (DOM) with high aromaticity has been shown to enhance dissolution of HgS by replacing the sulfide ligand, forming dissolved Hg-DOM complexes (Ravichandran et al. 1998, Waples et al. 2005). Additionally, Vázquez-Rodríguez *et al.* (2015) found evidence of microbially mediated dissolution of HgS occurring within the hyporheic zone of EFPC. Turbulent hydrodynamic conditions or lowering of the water table may also lead to oxidative dissolution of HgS by high levels of dissolved oxygen, resulting in the release of dissolved Hg, as has been studied experimentally under dissolved oxygen concentrations that roughly meet or exceed 100% dissolved oxygen saturation (Hsieh et al. 1991, Barnett et al. 2001, Holley et al. 2007). Through these mechanisms, slow dissolution of legacy HgS and other Hg minerals in highly contaminated ecosystems can release a substantial amount

of dissolved Hg over time, which is more mobile and reactive and potentially more bioavailable for methylation.

Contaminated sediment and soil often contain numerous forms of Hg with diverse chemical and physical properties, making it difficult to isolate individual Hg compounds. However, several sequential extraction schemes have been developed to isolate operationally-defined pools of Hg (summarized by Issaro *et al.* (2009)). Although sequential extractions are limited in their ability to completely separate different forms of Hg, these operationally-defined pools can be used to generalize the potential mobility and bioavailability of Hg in sediment or soil. Sequential extraction analyses previously performed on EFPC stream bank soil and streambed sediment showed that 0.11 ± 0.06% (1SD, n=22) of the total Hg in bank soil (Dickson et al. 2019), and 0.18 to 0.30% (interquartile range, n=66) of the total Hg in streambed sediment (Brooks et al. 2017), was water soluble. Based on estimates of the total amount of Hg in the streambed, this suggests that 0.6 to 1 kg of the Hg in the entire streambed is weakly bound (Brooks et al. 2017, Demers et al. 2018). Similarly, annual dissolved Hg flux measurements in the lower reaches of the stream have ranged from 0.53 to 1.00 kg y^{-1} (Riscassi et al. 2016, Peterson et al. 2018a). While the results of water leaching experiments may not be directly comparable to dissolved Hg flux estimates in the stream, these values suggest that, despite the recalcitrant nature of the soil- and sediment-bound Hg, these legacy Hg sources could account for a large proportion of the dissolved Hg flux in the surface water (Demers et al. 2018, Peterson et al. 2018a). However, it is difficult to demonstrate the *in situ* dissolution of legacy Hg source(s) that contribute to the dissolved Hg flux in stream water, as well as to identify the biogeochemical processes influencing this remobilization.

Mercury stable isotope ratio measurements can be used to track Hg cycling through complex ecosystems. As demonstrated by laboratory experiments, Hg isotopes undergo mass-dependent fractionation (MDF) during all known biotic and abiotic chemical reactions, as well as mass-independent fractionation (MIF) during photochemical reactions and some dark abiotic reactions (Blum et al. 2014). The magnitude and sign (positive or negative) of MDF and MIF signatures in environmental samples are useful for determining which biogeochemical reactions are likely to have taken place within an ecosystem, and are also useful for distinguishing between different sources of Hg contamination. Previous and ongoing studies have characterized the Hg stable isotopic composition of surface water, hyporheic pore water, shallow riparian groundwater, suspended particulates, biofilm, streambed sediment, and fish collected from EFPC to identify sources of Hg to the sediment and the stream water (Bartov 2014, Donovan et al. 2014, Demers et al. 2018). These studies suggest that hyporheic pore water was predominantly responsible for the diffuse legacy input of dissolved Hg to the surface water (Demers et al. 2018). However, previous studies were unable to link the isotopic composition of the hyporheic pore water to its specific legacy source(s).

Different pools of Hg within a single legacy source may have unique isotopic signatures, as demonstrated by other studies that have paired leaching experiments with Hg isotope analysis (Stetson et al. 2009, Wiederhold et al. 2013, Yin et al. 2013, Wiederhold et al. 2015, Brocza et al. 2019, Grigg et al. 2018, Huang et al. 2021). Thus, isolating and analyzing individual Hg pools can aid in the investigation of *in situ* transformation and remobilization of legacy Hg. In this study, we used sequential extraction methods coupled with Hg stable isotope ratio measurements (1) to assess whether certain pools of legacy Hg within streambed sediment contribute dissolved Hg to the hyporheic pore water and/or surface water of EFPC and (2) to further investigate the

biogeochemical processes underlying the net flux of dissolved Hg into the surface water of EFPC from diffuse legacy sources. Our results are interpreted within the context of our previous investigations of Hg stable isotope fractionation patterns in the sediments, surface water, pore water, and biofilm in EFPC.

2.2 Methods

2.2.1 Streambed sediment sample collection

East Fork Poplar Creek is a 26-kilometer-long low order stream in the Valley and Ridge physiographic province of east Tennessee, USA. Streambed sediment was collected from four sites along EFPC under baseflow conditions during late summer 2017. Downstream sampling followed a gradient of decreasing dissolved and suspended particulate-bound total Hg concentrations (Peterson et al. 2016, Demers et al. 2018). Sampling sites were identified by their distance in river kilometers upstream of the confluence of Poplar Creek and EFPC. Streambed sediment was collected from EFK 22.3, EFK 18.0, EFK 15.8, and EFK 8.7, where EFK = East Fork and the number indicates creek kilometer. These locations correspond to hyporheic piezometer and groundwater well sites used for past and ongoing Hg studies (Watson et al. 2016b, Peterson et al. 2018b, Demers et al. 2018) (Figure 2.1).

Polycarbonate core tubes (4.5 cm diameter), cleaned with 10% HCl, were used to collect streambed sediment from depositional zones. Fifteen core samples of the top ~10 cm of sediment were collected at each site and were combined in a new 5-gallon plastic bucket that had been rinsed with stream water prior to use. Using stream water, sediment was wet sieved in the field into four size fractions: 1-2mm, 250µm-1mm, 125-250µm, and <125µm. Sediment samples were placed on ice in the field, frozen the same day upon arrival at the laboratory (within six hours), and were later freeze-dried, transferred to clean borosilicate glass jars, sealed in doubled Ziploc

bags, and then stored in the dark at room temperature. The <125µm size fraction was obtained by collecting the stream water that had flowed through the column of sieves into new trace metal clean 1 L HDPE bottles, which were put on ice in the field and frozen upon return to the laboratory the same day. Later, these sample bottles in which sediment had settled were thawed overnight at room temperature and the liquid overlaying the sediment was removed from the bottles using a vacuum pump before re-freezing and freeze drying the settled <125µm sediment fraction. The mass fraction of each grain size is provided in Table S2.1.

2.2.2 Bulk sediment mercury extraction by combustion

Aliquots of streambed sediment collected from EFK 22.3, EFK 18.0, EFK 15.8, and EFK 8.7 were prepared for analysis of total mercury (THg) concentration and Hg stable isotope ratios following a previously-described combustion procedure (Demers et al. 2013a). Freeze-dried sediment was ground in 2 g aliquots using a SPEX 8000 Mixer/Mill with an alumina grinding cylinder and ball, and stored in trace metal clean borosilicate glass vials prior to combustion. Four additional aliquots, one per size fraction, were ground separately as sample replicates. To avoid cross contamination, Ottawa Sand (quartz, Fisher Scientific) was ground between each sample, and the grinding cylinder and ball were rinsed thoroughly with deionized water and isopropanol. Aliquots of ground sediment (50 to 100 mg) were combusted in a two-stage furnace, and volatilized Hg(0) was trapped in a 24 g oxidizing solution of 1% $KMnO_4$ (w/w) in 10% H_2SO_4 (v/v) (hereafter, 1% $KMnO_4$). For each size fraction, a replicate aliquot of ground sediment from a single vial was combusted separately as an analytical process replicate. Trap solutions of 1% $KMnO_4$ were later reduced with hydroxylamine hydrochloride ($HONH_3Cl$), and a small aliquot was analyzed for THg concentration using cold vapor atomic fluorescence spectrometry (CVAFS; RA-3F, Nippon Instruments) following EPA Method 1631 (U.S. EPA

2002). Samples were analyzed in batches with quality control including calibration verification standards, secondary standards, and blanks (see Section 2.5.1 in the Supporting Information for details).

To reduce matrix interferences from combustion residues, aliquots of the 1% $KMnO_4$ combustion trap solutions were reduced with stannous chloride ($SnCl_2$), and Hg(0) was transferred to secondary 1% $KMnO_4$ trap solutions (Demers et al. 2013a). These secondary solutions were later reduced with $HONH_3Cl$, and a small aliquot was analyzed for THg concentration by CVAFS. This was done to assess the percent recovery of the transfer process and to allow matching of standard and sample concentrations for isotope analysis. Recovery of Hg after the transfer process was 95.6 ± 2.0% (1SD, n=27 including sediment samples and reference materials).

Procedural blanks and standard reference materials were combusted to monitor combustion performance. Average procedural blank 1% $KMnO_4$ solutions yielded 0.10 ng Hg (± 0.01 ng Hg, 1SD, n=4) prior to transfer, and 0.13 ng Hg (± 0.02 ng Hg, 1SD, n=4) after transfer, representing <0.2% of sample solution Hg mass. Standard reference materials included NIST SRM 2711 (Montana Soil; 6.25 ± 0.19 μg g^{-1} THg) with an average recovery of 105.1 ± 0.1% (1SD, n=2) and NIST SRM 1944 (NY/NJ Waterway Sediment; 3.4 ± 0.5 μg g^{-1} THg) with a recovery of 105.7% (n=1) relative to certified values.

2.2.3 Sequential extractions

Five-step sequential extractions were performed on sieved streambed sediment collected from EFK 22.3, EFK 18.0, and EFK 8.7 to separate and quantify individual pools of sediment-bound Hg. We followed the sequential extraction procedure developed by Bloom *et al.*, (2003) as this extraction method has been previously used to assess the forms of Hg in streambed

sediment, stream bank soil, historical release deposits, biofilm, and floodplain soil of EFPC (Liu et al. 2006, Southworth et al. 2010, Miller et al. 2013, Brooks et al. 2017, Peterson et al. 2018b). This sequential extraction procedure involved a series of five reagents of increasing chemical strength to extract operationally-defined pools of Hg, and included deionized water (F1), 0.1 M acetic acid (CH_3COOH) + 0.01 M trace metal grade HCl (F2), 1 M reagent grade KOH (F3), 12 M trace metal grade HNO_3 (F4), and aqua regia (F5) (see Section 2.5.2 in the Supporting Information for reagent preparation) (Bloom et al. 2003). We are aware that suggestions have been made to further optimize the sequential extraction procedure, such as decreasing the concentration of the HNO_3 step (Hall et al. 2005) and decreasing the leach time (Hall and Pelchat 2005). However, to allow for the most direct comparison with previous sequential extraction studies in EFPC, we chose to maintain the original Bloom *et al.* (2003) procedure.

Well-mixed sediment (but not ground) was weighed into 50-mL polypropylene centrifuge tubes (~0.4 g per tube), and the F1 reagent was added (~40 mL per tube), maintaining a 1:100 solid-to-liquid mass ratio. Because the F1 and F2 extractions were expected to release relatively small amounts of Hg, the contents of multiple centrifuge tubes (up to 2.4 g sediment with 240 mL reagent) were combined to yield enough Hg for isotope analysis. Centrifuge tubes were capped and rotated end-over-end for 21 ± 2 hours, then centrifuged for 20 minutes at 1560 rpm (450 x g). The supernatant was filtered using 0.45 µm cellulose nitrate filter cups (Nalgene) and poured into trace metal clean borosilicate glass bottles (Pyrex), combining the supernatant of multiple tubes representing the same sediment sample. An additional aliquot of the F1 reagent (~40 mL deionized water) was added to each centrifuge tube as a rinse step, which was then re-centrifuged, filtered, and added to the bottles. Extraction samples were brought to 1% BrCl and refrigerated, except for the F3 samples, which were brought to 5% BrCl, and some of the F5

samples, to which additional small aliquots of concentrated BrCl were later added until the solution remained yellow after shaking. This process was repeated for the F2, F3, and F4 reagents, using the respective reagent for the rinse steps. After the addition of the F5 reagent (aqua regia, 10 mL HCl + 3 mL HNO_3), centrifuge tubes were briefly hand shaken, and then the loosely-capped tubes were stored in a fume hood for ~24 hours. The centrifuge tubes were then diluted to 40 mL with deionized water and filtered, and then additional deionized water was used for the rinse step. To prevent degradation of the cellulose nitrate filters while filtering the F3, F4, and F5 reagents, 40-80 mL of deionized water was added to the filter cup along with the reagents, diluting the extraction solutions. Brominated solutions were kept in the dark and refrigerated at 4ºC until analysis.

To quantify the amount of Hg leached from the sediment by each reagent, the THg concentration of each extraction solution was measured using CVAFS following EPA Method 1631 (U.S. EPA 2002). To avoid matrix interferences from dissolved organic matter, an aliquot of each extraction solution was transferred to a 15-mL Teflon vial, diluted with 5% BrCl, and exposed to ultraviolet light for five to ten days prior to concentration analysis (Olson et al. 1997, Demers et al. 2013b). Samples were analyzed in batches with quality control including calibration verification standards, secondary standards, blanks, sample duplicates, and matrix spike recovery tests (see Section 2.5.1 in the Supporting Information for details). Procedural blanks, standard reference materials, and sample replicates were used to assess sequential extraction performance. Each of the five extractants were used for the procedural blanks, and average procedural blank solutions yielded 0.10 ng Hg (± 0.10 ng Hg, 1SD, n=20), typically representing <0.5% of sample solution Hg mass.

Sequential extraction experiments using pure Hg compounds have shown that individual forms of Hg are not always extracted by a single reagent and may be split into consecutively extracted fractions (Revis et al. 1989, Bloom et al. 2003, Hall et al. 2005). In addition, differing results within and between sequential extraction experiments (Bloom et al. 2003, Hall et al. 2005) may be attributed to variations in Hg concentration, matrix material, particle size, or impurities in mineral composition (Kim et al. 2003). For this study, rather than assigning specific Hg species to each extracted fraction, the five sequential extractions are thought of as a gradient of Hg compounds based on solubility and sorption properties, with some possible overlap between them (Figure S2.1). Throughout this paper, we use the phrases poorly soluble, strongly-bound, and recalcitrant to refer to the F4 and F5 sequential extractions, which likely contain mercuric sulfide and other poorly soluble Hg compounds (Bloom et al. 2003, Hall et al. 2005). For the middle of the gradient, we use the phrases organically-bound and intermediate solubility to refer to the F2 and F3 sequential extractions, though we acknowledge that not all of the organically-bound Hg in the sediment is captured by these extractions, nor are these extractions capturing organically-bound Hg exclusively (Eganhouse et al. 1978, Bloom et al. 2003). We use the phrases highly soluble, water-soluble, and weakly-bound to refer to the F1 sequential extractions, which likely contain a mixture of highly soluble Hg compounds, such as mercuric chloride and Hg bound to soluble organic matter, as well as readily exchanged sorbed forms of Hg (Bloom et al. 2003, Brocza et al. 2019).

2.2.4 Sample preparation for isotope analysis

Prior to isotope analysis, each sequential extraction sample was chemically reduced, and the resulting Hg(0) was purged from solution and re-oxidized in a 1% $KMnO_4$ trapping solution following previously described methods (Demers et al. 2013a). Briefly, aliquots of the already-

brominated extraction samples were diluted to 1 L with deionized water and then further acidified (0.5% HCl) and oxidized (1% BrCl). Samples were then pre-reduced with 1.0 mL of 30% $HONH_3Cl$ and allowed to react for 1-2 hours. Samples were reduced with ~100 mL of 10% $SnCl_2$ (in 10% HCl), and Hg(0) was purged from solution with gold-filtered clean-laboratory air and subsequently trapped in a 5-10 g oxidizing solution of 1% $KMnO_4$. The 1% $KMnO_4$ trap solutions were later reduced with $HONH_3Cl$, and a small aliquot was analyzed for THg concentration using CVAFS following EPA Method 1631 (U.S. EPA 2002) as previously described for combustion solutions. Purge and trap recovery of Hg from extraction samples was 99.7 ± 3.6% (1SD, n=89 including sediment samples and reference materials). Purge and trap procedural blanks and standards (12, 15, or 35 ng Hg; NIST SRM 3133) were used to monitor analytical performance. Procedural blank 1% $KMnO_4$ solutions, yielding 0.22 ng Hg (± 0.44 ng Hg, 1SD, n=10, with one anomalously high value at 1.38 ng Hg), typically represented <1% of sample solution Hg mass. Procedural standard recovery was 98.3 ± 4.2% (1SD, n=21), and procedural standards were not significantly fractionated isotopically relative to NIST SRM 3133 bracketing standards (Table S2.2).

2.2.5 Mercury isotope analysis

Following Hg extraction and pre-concentration procedures, the Hg isotopic composition of each 1% $KMnO_4$ trap solution was measured using cold vapor multiple collector inductively coupled plasma mass spectrometry (CV-MC-ICP-MS; Nu Instruments) following previously described methods (Lauretta et al. 2001, Blum and Bergquist 2007). Thallium (NIST SRM 997) was used as an internal standard to correct for instrumental mass bias, along with sample-standard bracketing with Hg standard NIST SRM 3133. On-peak zero corrections were applied to all masses.

Mass-dependent isotope fractionation (MDF) is reported as the permil (‰) deviation from the average of NIST SRM 3133 bracketing standards (Blum and Bergquist 2007) using delta notation:

$$\delta^{xxx}Hg\ (‰) = ([(^{xxx}Hg/^{198}Hg)_{sample} / (^{xxx}Hg/^{198}Hg)_{NIST\ SRM\ 3133}] - 1) * 1000$$

where xxx is the mass of each Hg isotope between ^{199}Hg and ^{204}Hg. Mass-dependent fractionation is reported with $\delta^{202}Hg$ values. Mass-independent isotope fractionation (MIF) is reported as the difference between the measured $\delta^{xxx}Hg$ value and that which is theoretically predicted by the kinetic mass-dependent fractionation law (Blum and Bergquist 2007), using capital delta notation:

$$\Delta^{xxx}Hg\ (‰) \approx \delta^{xxx}Hg - (\delta^{202}Hg * \beta)$$

where xxx is the mass of each Hg isotope (^{199}Hg, ^{200}Hg, ^{201}Hg, and ^{204}Hg), and β is a constant for each isotope (0.252, 0.502, 0.752, 1.493, respectively) (Blum and Bergquist 2007).

To characterize reproducibility of the mass spectrometry, each analytical session included 5 to 9 analyses of a secondary standard (UM-Almadén) at representative Hg concentrations (1 to 5 ng g^{-1}). We also measured the isotopic composition of each NIST SRM 3133 purge and trap standard once, and of each combustion reference material three times. To evaluate the external reproducibility and the accuracy of our results, we calculated the mean (± 2SE) for the collection of independent preparations of UM-Almadén and each reference material type (Table S2.2), and compared those means to the long-term average isotopic composition measured at the University of Michigan (Blum and Johnson 2017). We represent the uncertainty in the isotopic composition of Hg in combustion samples with the average uncertainty (2SD) across combustion reference material analyses (Table S2.3, Table S2.4). We represent the uncertainty in the isotopic

composition of Hg in sequential extraction samples with the average uncertainty (2SD) across all UM-Almadén analyses (Table S2.5, Table S2.6a-c, Table S7a-c).

2.2.6 Organic carbon analysis by loss-on-ignition

Organic carbon (OC) concentrations were determined following a loss-on-ignition (LOI) procedure (Wang et al. 2011) (Table S2.8). Sediment aliquots (~1.5 g) were taken from the same 2 g aliquots that had been ground for THg analysis (see Section 2.2.2) to ensure accurate calculation of THg per mass of organic carbon (μg THg g^{-1} OC) (Table S2.8). Sediment was weighed into disposable quartz fiber crucibles, which had been pre-baked in a muffle furnace at 800ºC for 12 hours. The sediment was then heated to 105ºC for 12 hours to remove moisture, then 500ºC for 12 hours to release organic matter, and then 800ºC for 12 hours to release carbonates. The sediment was cooled to room temperature in a desiccator, and mass loss was measured after each 12-hour cycle. The percentage of mass loss after 500ºC was converted to a percentage of organic carbon by dividing the value by 2, based on the assumption that carbon makes up ~50% of organic matter (Pribyl 2010). Process blanks (pre-baked empty crucibles) and standard reference materials were used to monitor LOI performance. Mass loss from blanks was 0.08 to 0.46 mg (n=2) after 500ºC, representing <1% of average sample mass loss. Based on calculated percentages of organic carbon, NIST SRM 1944 (NY/NJ Waterway Sediment) had an average recovery of 99.6 ± 0.6% (n=2) relative to its certified %OC value of 4.4 ± 0.3%.

2.2.7 Statistical analysis

All statistical analyses were conducted using publicly available Python packages. To assess whether there were significant differences in isotopic composition among sequential extraction fractions, we used a series of significance tests. First, we used two-tailed paired-

samples t-tests (paired by size fraction) to assess whether there were significant offsets in isotopic composition between the F2 and F3 Hg fractions, and between the F4 and F5 Hg fractions, at each sampling site (Table S2.9). Given that the F2 and F3 fractions were isotopically similar, and that the F4 and F5 fractions were isotopically similar (see Section 2.3.4), we calculated the un-weighted average isotopic composition of the F2 and F3 Hg fractions (denoted as F2F3), and of the F4 and F5 Hg fractions (denoted as F4F5) for each sediment sample. We used paired samples t-tests with a Bonferroni adjustment for multiple comparisons to assess whether there were significant differences in isotopic composition among the F1, F2F3, and F4F5 Hg fractions (Table S2.10). Samples were paired by sediment size fraction within each site, such that F1, F2F3, and F4F5 were being compared within a single sediment sample. We also repeated this three-group comparison, but used the F3 Hg fraction in place of the F2F3 fraction (Table S2.11) in order to assess the influence of the F2 extraction samples which were analyzed at lower concentrations and tended to have higher within-site variability in isotopic composition than the other Hg fractions. Finally, we repeated these statistical assessments using independent sample averages (i.e., across all sediment size fractions within each site) and Tukey multiple comparisons tests (Table S2.12, Table S2.13). This was done to assess whether the results from our paired within-size-fraction comparisons could be more generally applied to assess differences among sequential extraction fractions at a broader scale that would be more relevant to interpreting the influence of legacy Hg sources on the isotopic composition of pore water and surface water. We found similar outcomes regardless of whether we used significance tests on paired samples or independent samples (see Section 2.3.4).

To determine slopes for Δ^{199}Hg versus δ^{202}Hg and Δ^{199}Hg versus Δ^{201}Hg plots, the York regression was used, which incorporates uncertainty in the X and Y variables (York 1966). These

slopes were generated using IsoplotR (Vermeesch 2018), which requires 1SE as the error input term. For combustion samples this is represented by the average 1SE value across combustion reference material analyses, and for sequential extraction samples this is represented by the average 1SE value across all UM-Almadén analyses.

2.3 Results and Discussion

2.3.1 Assessment of sequential extraction methods

Standard reference materials were used to assess the mass balance associated with the sequential extraction procedure. Based on the sum of the amount of Hg released in the five sequential extractions, NIST SRM 2711 had an average recovery of 95.4 ± 1.7% (1SD, n=3) and NIST SRM 1944 had a recovery of 102.3% (n=1) relative to certified values. The relative distribution of Hg fractions extracted from NIST SRM 2711 was reasonably similar to that reported by Bloom *et al*. (2003) (Table S2.5). The calculated isotopic composition (THg_{calc}) of reference materials was based on the weighted average of sequential extraction Hg concentrations (Table S2.5). These values were within error of the isotopic composition obtained by combustion of bulk material (Table S2.2), and also agreed with the long-term average isotopic composition of the reference materials measured at the University of Michigan (Blum and Johnson 2017). A comparison of the isotopic signatures associated with sequential extractions of NIST SRM 2711 across multiple studies is provided in the Supporting Information (see Section 2.5.3).

Total Hg concentrations and isotopic compositions of EFPC sediment samples obtained by the weighted average of sequential extractions also generally agreed with those obtained by whole sample combustion (Figure S2.2, Figure S2.3). However, the relative percent difference between average THg concentrations obtained from combustions and sequential extractions was

larger for the 1-2mm size fraction (23.9 ± 12.7%, 1SD, n=3) than for the other three size fractions (3.9 ± 2.5%, 1SD, n=9) (Figure S2.2). Additionally, only for the 1-2mm size fraction at EFK 22.3 did the THg concentration and isotopic composition significantly differ between the sample aliquots used for sequential extractions and each of the two combustion replicates (Figure S2.2, Figure S2.3a, Table S2.4, Table S2.6a). These differences may have been due to greater heterogeneity within subsamples of this larger sediment size fraction, whereby individual grains of sediment with anomalous THg concentrations or isotope ratios may have had a stronger influence on the THg concentration and/or isotopic composition of the bulk sediment sample compared to smaller grain sizes.

The sequential extraction procedure was repeated two times for EFK 18.0: 250µm-1mm sediment (Table S2.7a) and three times for NIST SRM 2711 (Table S2.7b) to evaluate the variability in concentration and isotopic composition of the extracted Hg fractions. Partial sequential extraction replicates (only the first two extraction steps) were also performed on all size fractions of EFK 8.7 sediment as an additional evaluation of the variability within the F1 and F2 extraction steps (Table S2.7a). Differences in δ^{202}Hg and Δ^{199}Hg values between sequential extraction replicates were within analytical uncertainty (14 of 16 replicates), except for δ^{202}Hg values of the F2 extraction replicates of NIST SRM 2711 (Table S2.7b) and of the F1 extraction replicates for the EFK 8.7 250µm-1mm sediment (Table S2.7a). Aside from these two anomalies, our sequential extraction replicates suggest that each sequential extraction was consistently targeting a specific pool of Hg that was isotopically similar across replicates and in some cases was isotopically distinguishable from other Hg pools.

When using a sequential extraction procedure to isolate Hg pools for isotopic analysis, it is important that the extraction procedure does not induce artificial isotope fractionation. This

may be the result of incomplete dissolution/desorption of a target or non-target Hg pool. Based on kinetic fractionation mechanisms in which lighter isotopes react more quickly, it is expected that artificially induced isotope fractionation would result in lower δ^{202}Hg values in earlier extractions. In our sequential extractions, the only consistent offset in δ^{202}Hg was between the F4 and F5 pools, and the F4 pool had more positive δ^{202}Hg values (Table S2.6a-c) which is the opposite of what would be expected if this offset was caused by the extraction procedure itself. Additionally, Wiederhold *et al.* (2015) demonstrated that partial dissolution of HgS and organically-bound Hg using 6 M HCl and 6 M HNO_3 did not result in isotope fractionation between the dissolved and residual fractions. A similar lack of fractionation has also been shown for iron isotopes during dissolution of goethite, an iron oxide mineral, using 0.5 M HCl (Wiederhold et al. 2006). Overall, complete recoveries, consistent isotopic composition across sequential extraction replicates, and the apparent lack of artificial isotope fractionation suggests that the sequential extraction procedure used in our study was reliable for investigating the isotopic composition of individual operationally-defined pools of Hg within our sediment samples.

2.3.2 Mechanistic controls on the mercury isotopic composition of streambed sediment

Across all sampling sites, a majority (82-93%) of the sediment in the <2mm bulk samples had a diameter between 250µm and 2mm, while the 125-250µm and <125µm size fractions made up 2-4% and 5-14% of the bulk sediment, respectively (Table S2.1). Total Hg concentrations for EFPC streambed sediment ranged from 7.14 to 41.8 µg g^{-1} (based on combustion), with THg concentrations generally decreasing along the flow path for smaller size fractions and increasing along the flow path for larger size fractions (Figure S2.2, Table S2.3). These concentrations were similar to the range of sediment Hg concentrations reported in other

recent studies of EFPC sediment (Southworth et al. 2010, Donovan et al. 2014, Brooks et al. 2017), and were much higher than those of regional background sites (Donovan et al. 2014).

Across all sites and sediment size fractions, EFPC streambed sediment δ^{202}Hg values ranged from -0.24‰ to 0.24‰ (± 0.09‰, 2SD) and Δ^{199}Hg values ranged from -0.12‰ to -0.05‰ (± 0.02‰, 2SD) based on combustion (Figure S2.4, Table S2.3). Associated Δ^{200}Hg and Δ^{204}Hg values were essentially zero, averaging 0.00‰ ± 0.01‰ (1SD, n=16) for both Δ^{200}Hg and Δ^{204}Hg (Table S2.3), suggesting minimal contribution of Hg to the sediment from precipitation or dry deposition (Gratz et al. 2010, Chen et al. 2012, Demers et al. 2013a). This overall range in Hg isotope values is similar to that of streambed sediment samples reported previously for EFPC (Donovan et al. 2014, Bartov 2014). Across all sites and sediment size fractions, there were no overall trends in δ^{202}Hg or Δ^{199}Hg versus 1/THg (Figure S2.5), and when separated by size fraction, even the strongest trend was not statistically significant (smallest p-value for δ^{202}Hg vs. 1/THg was 0.082 for the <125µm size fraction). The lack of a relationship between isotope ratios and 1/THg concentration indicates that variations in THg concentration and isotopic signatures among sediment samples do not appear to be driven predominantly by the mixing of two isotopically distinct sources.

EFPC streambed sediment had a Δ^{199}Hg/δ^{202}Hg slope of -0.11 (± 0.01, 1SE, n=16) and a Δ^{199}Hg/Δ^{201}Hg slope of 1.37 (± 0.21, 1SE, n=16) (Figure S2.4). These slope values, as well as the relatively small magnitude of the measured Δ^{199}Hg values, suggest that mass-dependent and nuclear volume-dependent fractionation effects may be partially responsible for the observed range in isotopic composition of the streambed sediment. Equilibrium mass-dependent fractionation causes shifts in δ^{202}Hg values due to the tendency of heavier Hg isotopes to be enriched in compounds with shorter, stiffer bonds (higher vibrational frequency) (Schauble 2007,

Wiederhold et al. 2010). Nuclear volume fractionation also causes shifts in δ^{202}Hg values due to the tendency of Hg isotopes with a larger nuclear radius (which are less strongly bound to electrons) to be enriched in compounds that give Hg a more positive partial charge (Schauble 2007, Wiederhold et al. 2010). For redox reactions, both of these isotope effects would result in higher δ^{202}Hg values in the oxidized Hg(II) phase, though these isotope effects also apply to non-redox reactions. Nuclear volume fractionation additionally causes shifts in Δ^{199}Hg and Δ^{201}Hg values, with a characteristic Δ^{199}Hg/Δ^{201}Hg ratio of ~1.5 to 1.6, due to the nuclear radius of Hg isotopes not scaling linearly with mass, with the two odd-numbered isotopes having smaller nuclear radii than what is expected based on the linear relationship between nuclear radius and mass for the five even-numbered isotopes (Wiederhold et al. 2010). Equilibrium mass-dependent fractionation and nuclear volume fractionation have been shown experimentally to cause equilibrium isotope effects during isotope exchange between liquid and gaseous Hg(0) (Estrade et al. 2009, Ghosh et al. 2013), between coexisting Hg(II) species (Wiederhold et al. 2010, Jiskra et al. 2012), and between coexisting Hg(0) and Hg(II) species (Bartov 2014, Zheng et al. 2019). The results of these experimental studies have generally aligned with theoretical calculations of equilibrium fractionation factors (Schauble 2007, Wiederhold et al. 2010, Jiskra et al. 2012, Yang and Liu 2015) and have demonstrated Δ^{199}Hg/δ^{202}Hg slopes of -0.1 to -0.2 and Δ^{199}Hg/Δ^{201}Hg slopes of ~1.5 to 1.6. These values are within the range of uncertainty in the slopes for EFPC streambed sediment, suggesting that equilibrium isotope effects may at least partially account for the range in isotopic composition of the sediment.

Nuclear volume fractionation has also been shown to occur alongside kinetic mass-dependent fractionation, which causes shifts in δ^{202}Hg values due to the tendency of lighter Hg isotopes to react faster (due to their higher zero-point energy) and therefore be enriched in the

products of a reaction (Buchachenko 2009). Kinetic mass-dependent fractionation and nuclear volume fractionation have been shown to occur together during some kinetic reactions, such as evaporation of liquid Hg(0) (Estrade et al. 2009), dark abiotic reduction of Hg(II) (Zheng and Hintelmann 2009, 2010b), and dark abiotic oxidation of Hg(0) (Zheng et al. 2019). Similar to equilibrium reactions involving nuclear volume fractionation, these studies have also demonstrated $\Delta^{199}Hg/\Delta^{201}Hg$ slopes of ~1.5 to 1.6, though the measured $\Delta^{199}Hg/\delta^{202}Hg$ slopes have been shown to be more variable (both steeper and shallower) than those of equilibrium reactions. Importantly, experimental studies have shown that equilibrium isotope effects can overwrite initial kinetic isotope effects as a reaction progresses, which can alter the $\Delta^{199}Hg/\delta^{202}Hg$ slope (Zheng et al. 2019).

Of the reactions mentioned above, some are more likely to have influenced the isotopic composition of EFPC streambed sediment than others. For example, of the 11 million kg of liquid Hg(0) historically used at Y-12, only ~0.3% was lost to the atmosphere (Brooks and Southworth 2011), and so evaporation of Hg(0) would not have caused significant isotope fractionation within the remaining liquid Hg(0). On the other hand, an estimated 1.2 ± 0.3% of the liquid Hg(0) historically used at Y-12 was oxidized and released directly to EFPC, mainly through a nitric acid washing procedure (Brooks and Southworth 2011). This process could have resulted in isotopic fractionation of the Hg(II) released to EFPC relative to the initial Hg(0) source. Dark abiotic oxidation of Hg(0), followed by isotope exchange between coexisting Hg(0) and Hg(II) species, has been experimentally shown to shift the oxidized Hg(II) phase toward more positive $\delta^{202}Hg$ and more negative $\Delta^{199}Hg$ values relative to the reduced Hg(0) phase (Zheng et al. 2019). In that study, the equilibrium isotope effect had overwritten the initial kinetic isotope effect (which initially had a steeper $\Delta^{199}Hg/\delta^{202}Hg$ slope), resulting in a

$\Delta^{199}Hg/\delta^{202}Hg$ slope of -0.12 (± 0.01, 1SE, n=40) and a $\Delta^{199}Hg/\Delta^{201}Hg$ slope of 1.28 (± 0.19, 1SE, n=49) (or 1.62 ± 0.14, 1SE, n=49, if the regression analysis was forced through the origin) (Zheng et al. 2019). This is consistent with the isotopic composition of EFPC streambed sediment, which primarily contains Hg(II) species, being offset toward higher $\delta^{202}Hg$ and lower $\Delta^{199}Hg$ values relative to the assumed isotopic composition of the historically used liquid Hg(0) (Figure 2.2). Although the exact isotopic composition of this historical liquid Hg(0) source is not known, commercial sources of liquid Hg(0) obtained from the major Hg mines around the world have an average $\delta^{202}Hg$ value of -0.38 ± 0.34‰ (1SD, n=13) and near-zero $\Delta^{199}Hg$ (Sun et al. 2016). Isotope fractionation by dark abiotic oxidation and equilibrium isotope effects could have largely occurred in the Y-12 facility during the nitric acid washing procedure. Once released from Y-12, much of the Hg(II) would have become associated with the streambed sediment through processes such as HgS precipitation, mineral sorption, and thiol ligand binding. Based on experimental studies, these processes may have shifted the isotopic composition of the sediment-bound Hg toward slightly lower $\delta^{202}Hg$ values, depending on what proportion of the Hg bound to the sediment (Wiederhold et al. 2010, Jiskra et al. 2012, Foucher et al. 2013, Smith et al. 2015) (Figure 2.2). Isotope fractionation by dark abiotic oxidation and equilibrium isotope effects could have also occurred (and could still be occurring) in the environment surrounding Y-12 where liquid Hg(0) was released to the soil through spills and leaks (Rothschild et al. 1984), and where Hg(0)-contaminated groundwater is known to enter the surface flow (Brooks and Southworth 2011). For *in situ* processes, however, there would need to be subsequent separation of the Hg(0) and Hg(II) phases, which could be achieved through preferential sorption of Hg(II) to sediment and/or volatilization of Hg(0). In addition to dark abiotic oxidation, equilibrium isotope effects between Hg(0) and Hg(II) species could also accompany Hg reduction processes,

so long as the reduced Hg(0) does not volatilize immediately after being formed. For example, the isotopic composition of EFPC surface water suggests that photochemical reduction of Hg(II) is likely occurring along the flow path (see Section 2.3.6.2) (Demers et al. 2018). The coexisting Hg(0) and Hg(II) involved in Hg reduction processes could undergo equilibrium isotope exchange, which would shift the Hg(II) phase toward higher δ^{202}Hg and lower Δ^{199}Hg values. The Hg(II) could then be associated with the streambed sediment more so than the Hg(0) phase due to differences in sorption characteristics and/or volatilization of Hg(0).

Overall, it appears that equilibrium isotope effects that occur alongside Hg oxidation and reduction processes could have played an important role in determining the isotopic composition of the high-concentration streambed sediment within EFPC. Zheng *et al.* (2019) stated that isotope exchange "could be ubiquitous" across a variety of biogeochemical reactions, including both oxidation and reduction reactions, which could alter isotopic signatures within ecosystems. Both Bartov (2014) and Zheng *et al.* (2019) pointed out that fractionation by isotope exchange reactions could overwrite initial fractionation by kinetic reactions. This could potentially make it difficult to deduce which kinetic reactions may have been dominant historically, especially for ecosystems in which both Hg oxidation and Hg reduction are possible. We suspect that equilibrium isotope effects may have the potential to set the "baseline" Hg isotopic composition for sediment and soil within ecosystems that contain both Hg(0) and Hg(II) species, including both non-contaminated and contaminated environments. In particular, it may be worth considering the potential impact of equilibrium isotope effects between Hg(0) and Hg(II) species for ecosystems with a known Hg(0) contamination source, such as within industrial sites and near Hg or gold mining sites. As an example, waterbodies downstream of several historical Hg mines in the California Coast Range have been impacted by Hg(II) and may also have been

impacted by Hg(0) as a result of losses during on-site HgS ore roasting processes (Schnabel et al. 1998, Rytuba 2000). One such waterbody is Cache Creek, for which an investigation of the isotopic composition of the sediment revealed a $\Delta^{199}Hg/\delta^{202}Hg$ slope of -0.12 (± 0.02, 1SE, n=11) and a $\Delta^{199}Hg/\Delta^{201}Hg$ slope of 1.69 (± 0.34, 1SE, n=11) (Donovan et al. 2016). These slope values, along with the lack of a relationship between Hg isotope ratios and 1/THg concentration, suggest that the isotopic composition of the sediment has been influenced by biogeochemical reactions involving mass-dependent fractionation and nuclear volume fractionation, which could include equilibrium isotope effects between Hg(0) and Hg(II) species.

2.3.3 Sequential extractions: Mercury concentrations

Across all sites and size fractions, a majority of the Hg was strongly bound to the sediment, found mostly in the F4 and F5 fractions, which together made up 94.6 ± 5.2% (1SD, n=12) of the THg (Figure 2.3, Table S2.6a-c). The F3 fractions were the next largest, which made up a larger percentage of THg at the downstream site than at the two upstream sites (5.3 to 20.5% at EFK 8.7, compared to 1.7 to 2.5% at EFK 18.0 and 1.5 to 3.8% at EFK 22.3) (Figure 2.3, Table S2.6a-c). These higher proportions at EFK 8.7 were driven by higher concentrations of Hg in the F3 fractions across all sediment grain sizes, as well as an especially low THg concentration for the 125-250µm size fraction (Table S2.6c). Note that methylmercury typically makes up <0.05% of THg within EFPC streambed sediment (Southworth et al. 2010, Olsen et al. 2016, Watson et al. 2016b, Brooks et al. 2017) and thus would typically represent <3% of the F3 Hg fraction. The F1 fractions made up 0.7 ± 0.4% (1SD, n=12) of the THg, and the proportion of the F2 fractions was even smaller. The relative proportions among these Hg fractions, as well as the increasing proportion of the F3 fraction along the flow path, aligns with observations by Brooks *et al.* (2017) using the same sequential extraction method on EFPC streambed sediment.

Despite the higher proportions and higher concentrations of Hg in the F3 fractions at EFK 8.7 (Table S2.6c), which are thought to primarily represent organically-bound Hg, the organic carbon concentrations of the sediment generally decreased along the flow path (Table S2.8), accentuating increases in the ratio of F3-extracted Hg to organic carbon along the flow path. At the two upper sites (EFK 22.3 and EFK 18.0), the amount of Hg in the F3 fractions (Hg_{F3}) relative to the organic carbon (OC) content of the sediment was consistent across all sediment size fractions, averaging 26.0 ± 7.1 μg Hg_{F3} g^{-1} OC (1SD, n=8). This concentration increased substantially for all but the smallest size fraction at EFK 8.7, averaging 197 ± 35 μg Hg_{F3} g^{-1} OC (1SD, n=3) (Figure S2.6, Table S2.8). This 7.6-fold increase in the Hg_{F3}:OC ratio was driven by both an increase in the Hg_{F3} concentration of the sediment (Table S2.6a-c) as well as a decrease in the organic carbon concentration (Table S2.8), and suggests that the Hg content of the organic matter within the streambed sediment generally increases downstream, though the explanation for this trend is unclear.

2.3.4 Sequential extractions: Mercury isotopic composition

Across all sequential extractions of EFPC streambed sediment, δ^{202}Hg values ranged from -0.64‰ to 0.49‰ (± 0.08‰, 2SD) and Δ^{199}Hg values ranged from -0.16‰ to 0.04‰ (± 0.05‰, 2SD) (Figure 2.4, Figure S2.3, Table S2.6a-c). Sequential extractions had a $\Delta^{199}Hg/\delta^{202}Hg$ slope of -0.15 (± 0.01, 1SE, n=60) and a $\Delta^{199}Hg/\Delta^{201}Hg$ slope of 1.57 (± 0.16, 1SE, n=60) (Figure S2.7). As with the bulk sediment, Δ^{200}Hg and Δ^{204}Hg values of the sequential extractions were essentially zero, averaging 0.00‰ ± 0.02‰ (1SD, n=60) for both Δ^{200}Hg and Δ^{204}Hg (Table S2.6a-c), suggesting minimal contribution of Hg to any of the individual sediment Hg fractions from precipitation or dry deposition (Gratz et al. 2010, Chen et al. 2012, Demers et al. 2013a).

In general, the F2 and F3 Hg fractions had a positive offset in Δ^{199}Hg values relative to the other sediment Hg fractions (Figure 2.4, Figure S2.8). For each of the three sampling sites, the isotopic composition of the F2 and F3 Hg fractions within individual sediment size fractions were similar to one another (Figure S2.8), as the mean offsets in δ^{202}Hg and Δ^{199}Hg values between the F2 and F3 fractions for each site were not significantly different from zero (Table S2.9). Results of pairwise comparisons between the F4 and F5 Hg fractions within individual size fractions were more variable. The mean offset in Δ^{199}Hg values between the F4 and F5 Hg fractions for each site ranged from 0.00 ± 0.02‰ to -0.01 ± 0.02‰ (Figure S2.8), indicating no significant difference within individual size fractions at either EFK 22.3 or EFK 18.0 (Table S2.9). Although our statistical analyses did suggest that there was a difference in Δ^{199}Hg values between F4 and F5 fractions at EFK 8.7, this appeared to be driven by an exceptionally small mean offset and standard deviation (-0.01 ± 0.00‰) (Table S2.9), and thus we deemed differences in Δ^{199}Hg values between the F4 and F5 Hg fractions to be negligible overall. The mean offset in δ^{202}Hg values between F4 and F5 Hg fractions was more variable (Figure S2.8), increasing from 0.16 ± 0.12‰ ($p=0.075$, $n=4$) at EFK 22.3 to 0.34 ± 0.07‰ at EFK 8.7 ($p=0.002$, $n=4$) (Table S2.9). Nonetheless, based on their similarity in Δ^{199}Hg values, we chose to combine the F4 and F5 Hg fractions for our subsequent assessments. This approach was further supported by our unpaired tests of F2 vs. F3 Hg fractions, and F4 vs. F5 Hg fractions, within each sampling site which indicated that neither F2 and F3, nor F4 and F5, could be consistently resolved from one another at the streambed level (i.e., across all size fractions within each site) (Table S2.12). This becomes important when tracking sources through the stream ecosystem.

Based on the isotopic similarity of the F2 and F3 Hg fractions, and the F4 and F5 Hg fractions, we calculated the un-weighted average isotopic composition of the F2 and F3 fractions (hereafter, F2F3) and of the F4 and F5 fractions (hereafter, F4F5) for each sediment sample (Figure 2.5). We then made a three-group comparison of means among the F1, F2F3, and F4F5 Hg fractions using data paired within individual sediment size fractions (Table S2.10), as well as with unpaired data within each site (Table S2.13). One key result was that the F1 and F4F5 Hg fractions were statistically indistinguishable at all three sites, in terms of both δ^{202}Hg and Δ^{199}Hg values, using paired and unpaired data (Table S2.10, Table S2.13). The F1 Hg fraction was also similar to the F2F3 Hg fraction with respect to δ^{202}Hg values, for both paired and unpaired data, driven in part by the high variability in the F2F3 δ^{202}Hg values (Table S2.10, Table S2.13). However, the F1 Hg fraction differed from the F2F3 Hg fraction with respect to Δ^{199}Hg values at our site furthest upstream, EFK 22.3, but the Δ^{199}Hg values of these Hg fractions were not significantly different at EFK 18.0 or EFK 8.7, in terms of both paired and unpaired data, as F2F3 Δ^{199}Hg values decreased along the flow path (Figure 2.5, Table S2.10, Table S2.13). The F2F3 Hg fraction δ^{202}Hg and Δ^{199}Hg values also were significantly offset from F4F5 δ^{202}Hg and Δ^{199}Hg values paired within individual size fractions at EFK 22.3 (Table S2.10), although using unpaired data δ^{202}Hg values of the F2F3 and F4F5 fractions were not significantly different at EFK 22.3 (Table S2.13). Along the flow path, F2F3 δ^{202}Hg values increased and Δ^{199}Hg values decreased (Figure 2.5, Table S2.13), becoming indistinguishable from F4F5 values paired within individual sediment size fractions (Table S2.10). Although these patterns of convergence in F2F3 and F4F5 Hg fractions were not observed for δ^{202}Hg values at the streambed level (i.e., because δ^{202}Hg values of F2F3 fractions did not statistically differ from F4F5 at EFK 22.3 using unpaired data), this convergence between F2F3 and F4F5 Hg fractions remained strong with respect to

Δ^{199}Hg values compared at the streambed level, that is, across all sediment size fractions at each site (Table S2.13). Thus, a second key result was that overall the isotopic composition of the F2F3 Hg pool in the sediment appeared to converge with that of the F1 and F4F5 Hg pools along the flow path.

We note that this convergence in isotopic composition of F2F3 Hg pools with F1 and F4F5 Hg pools was partially driven by high variability in the isotopic composition of the F2 Hg fraction, which is consistent with the concept of small Hg pools being more easily isotopically fractionated relative to large pools. When we excluded the F2 Hg fractions from this analysis, the support for converging isotopic compositions along the flow path was somewhat weakened. Without F2 included in our paired samples statistical model, the F3 Hg fractions consistently had a significantly positive mean offset in Δ^{199}Hg values relative to both the F1 and F4F5 Hg pools at all three sites, although these differences did decline in magnitude along the flow path, as supported by concomitantly increasing p-values (Table S2.11). Nonetheless, the remainder of our discussion is based on the complete dataset, including the F2 Hg fractions, and suggests that (*i*) the F1 and F4F5 Hg pools have similar isotopic compositions throughout all sediment size fractions at all sites, and (*ii*) the isotopic composition of the F2F3 Hg pool appears to converge with that of the F1 and F4F5 Hg pools along the flow path, especially with respect to Δ^{199}Hg values.

2.3.5 Sediment as a potential source of dissolved mercury to stream water

2.3.5.1 Weakly-bound mercury in sediment may be derived from more recalcitrant pools

In our sequential extractions, the weakly-bound F1 sediment Hg fractions were isotopically more similar to the strongly-bound F4F5 Hg fractions than to the moderately-bound F2F3 Hg fractions (Figure 2.4, Table S2.10). One possible explanation is that within the

streambed sediment, poorly soluble high-concentration Hg pools (F4F5) may slowly release dissolved Hg into the pore water, some of which may subsequently re-adsorb onto the sediment as a weakly-bound pool (F1). This weakly adsorbed Hg could accumulate on the sediment, retaining its isotopic composition and later be released to the stream water.

Poorly soluble Hg pools in the streambed sediment, likely made up largely of HgS, can be partially released if sulfide is replaced with dissolved organic matter with high aromaticity (Ravichandran et al. 1998, Waples et al. 2005), or by oxidative dissolution by high levels of dissolved oxygen (Hsieh et al. 1991, Barnett et al. 2001, Holley et al. 2007) or with the help of sulfur-oxidizing bacteria (Vázquez-Rodríguez et al. 2015). Several laboratory experiments have also demonstrated re-adsorption of Hg onto HgS minerals (Hsieh et al. 1991, Barnett et al. 2001, Holley et al. 2007, Jiang et al. 2016), as well as adsorption of Hg onto sediment and soil which have a variety of different sorption sites with varying affinities for Hg (Yin et al. 1997, Pelcová et al. 2010). Although Hg re-adsorbed onto HgS would be relatively strongly bound (Hasany et al. 1999), Hg that has re-adsorbed onto weaker sorption sites within the sediment could potentially be represented in the F1 sediment extractions. Additionally, after performing leaching experiments on EFPC stream bank soil, Peterson *et al.* (2018b) suggested that differences in the amount of Hg released during their experiments might have been due to re-adsorption of Hg onto soil particles. Zhang *et al.* (2021) also saw evidence of re-adsorption of Hg after it had been released from EFPC streambed sediment. These studies lend support to our suggestion that dissolution of small amounts of HgS and other Hg compounds, followed by re-adsorption of Hg(II) onto the sediment and eventual re-release of the weakly-bound Hg into the stream water, could be part of a mechanism by which sediment-bound legacy Hg contributes dissolved Hg to the stream. This could explain why weakly-bound Hg in the sediment (represented by the F1

extraction) is not completely depleted over time, but rather may be replenished by the release of strongly-bound Hg from more recalcitrant compounds that are subsequently re-adsorbed to the sediment.

One key assumption within our hypothesis that weakly-bound Hg within the sediment (F1 pool) is derived from the more abundant recalcitrant Hg (F4F5 pool), is that the processes involved do not induce significant isotope fractionation. To our knowledge, no study has assessed the isotopic fractionation that may be associated with processes that remobilize Hg within recalcitrant Hg compounds (e.g., DOM dissolution of HgS) (Wiederhold 2015). Although kinetic and equilibrium reactions typically result in isotope fractionation (Blum et al. 2014), dissolution of minerals occurs only at the surface of the mineral, and this limits the possibility of large isotope fractionation effects (Wiederhold et al. 2006). Extraction experiments also suggest that recalcitrant Hg pools could be partially dissolved without fractionation. For example, Wiederhold *et al.* (2015) showed that partial dissolution of HgS and organically-bound Hg using 6 M HCl and 6 M HNO_3 resulted in no measurable Hg isotope fractionation. Additionally, in sequential extractions performed on unroasted HgS ore, small water-soluble Hg pools were isotopically similar to the bulk material (Wiederhold et al. 2013). Brocza *et al.* (2019) suggested that the extent to which various sequential extraction experiments have found isotopically distinct fractions of Hg within solid samples appears to be highly dependent on site-specific Hg speciation and spatial heterogeneity. In sequential extractions performed on contaminated soils and calcine waste from Hg mining sites, water-soluble Hg fractions tended to be isotopically heavier than recalcitrant Hg (Stetson et al. 2009, Wiederhold et al. 2013, Yin et al. 2013), but in another study involving sequential extractions of soil and sediment downstream of an industrial facility, water-soluble Hg fractions were found to be isotopically similar to recalcitrant Hg

(Grigg et al. 2018). Additionally, for sequential extractions performed on soil core samples from a $HgCl_2$-contaminated industrial site, water-soluble Hg fractions tended to be isotopically heavier than recalcitrant Hg for soil samples with the highest THg concentrations and the largest relative proportions of more mobile forms of Hg. However, for samples with lower THg concentrations that were dominated by recalcitrant forms of Hg, water-soluble Hg fractions tended to be isotopically similar to recalcitrant Hg (Brocza et al. 2019). Although some of the evidence provided here may be site-specific, these results suggest that within EFPC, where the streambed sediment is dominated by HgS (Barnett et al. 1997, Peterson et al. 2018b) and other recalcitrant forms of Hg (F4+F5 make up 94.6 ± 5.2% of THg, 1SD, n=12), dissolution of recalcitrant Hg could plausibly occur without inducing significant isotope fractionation.

Adsorption of dissolved Hg onto solid minerals has been experimentally shown to induce isotope fractionation by enriching the adsorbed Hg in lighter isotopes relative to the dissolved phase (Jiskra et al. 2012). This fractionation is hypothesized to be the result of equilibration between neutral and positively charged Hg(II) complexes, in which positively charged complexes are generally isotopically lighter and have a higher affinity for binding onto surfaces than neutral complexes. However, as the fraction of adsorbed Hg approaches 100%, the degree of fractionation decreases until the isotopic composition of the adsorbed phase matches that of the original dissolved Hg (Jiskra et al. 2012). Several experimental studies have demonstrated that adsorption of Hg onto solid HgS (Hsieh et al. 1991, Barnett et al. 2001, Holley et al. 2007, Jiang et al. 2016) and onto contaminated and non-contaminated sediment and soil (Yin et al. 1997, Pelcová et al. 2010, Zhang et al. 2021) can occur rapidly and, in some cases, nearly completely. This suggests that subsequent to dissolution of small portions of HgS and other Hg minerals, rapid re-adsorption could feasibly occur without significant isotope fractionation. This

re-adsorbed Hg would likely be released during different steps within the sequential extraction procedure, with Hg re-adsorbed to weak sorption sites potentially being released in the F1 extraction. This could explain the similarity in isotopic composition of our F1 and F4F5 sediment Hg fractions. Additional studies that investigate the isotope fractionation involved with partial dissolution of HgS, and re-adsorption of Hg onto HgS and other sorption sites within sediment, will be required to further assess this hypothesis.

2.3.5.2 Comparison of sequential extractions, surface water, and pore water

While the proportions of Hg released by the F1 extractions were small (Table S2.6a-c), this amount is not insignificant. Based on dissolved Hg flux measurements (Riscassi et al. 2016) and previous sequential extractions of EFPC streambed sediment (Brooks et al. 2017), Demers *et al.* (2018) calculated that the release of the water-soluble fraction of Hg in the streambed (i.e., the F1 pool) would be enough to sustain the annual dissolved Hg flux to the surface water, so long as the water-soluble fraction in the sediment is replenished. Demers *et al.* (2018) further suggested that soluble pools of Hg in the sediment could be replenished by stream bank erosion, however sequential extractions of EFPC stream bank soil later revealed that the proportion of water-soluble Hg in bank soil was even lower than the proportion of water-soluble Hg in streambed sediment (Dickson et al. 2019). Weakly-bound Hg in the streambed sediment could also potentially be replenished by the contaminated stream water flowing over the sediment, although this would not represent a net flux of dissolved Hg to the surface water, as has been observed (Demers et al. 2018, Peterson et al. 2018a). Moreover, dissolved Hg in the surface water near our sampling sites consistently had positive Δ^{199}Hg values (Figure 2.6) (Demers et al. 2018), while the F1 sediment Hg fractions had negative Δ^{199}Hg values, suggesting that surface water is not the primary contributor of weakly-bound Hg in the sediment. Instead, the results of

this study suggest that the weakly-bound Hg in the sediment could be derived from and replenished by the more abundant recalcitrant fractions in the sediment, which would be a sustainable source for many years. This finding, along with the similarities in isotopic composition between the F1 and F4F5 Hg pools, suggests that small amounts of strongly-bound Hg may continuously be remobilized, contributing to both the weakly-bound Hg pools in the sediment and to the dissolved Hg in the stream water.

Previous Hg flux measurements have revealed that between EFK 23.4 and EFK 5.0, diffusive legacy sources contribute 6 to 36% of the total dissolved Hg flux, depending on hydrologic connectivity (Demers et al. 2018, Peterson et al. 2018a). In a previous Hg isotope study at EFPC, Demers *et al.* (2018) suggested that hyporheic pore water contributes to this dissolved Hg flux and influences the isotopic composition of the surface water, increasing its δ^{202}Hg values along the flow path. In that study, hyporheic pore water samples with the highest dissolved Hg concentrations tended to have negative Δ^{199}Hg values and relatively higher, positive δ^{202}Hg values, while surface water and low-concentration pore water samples tended to have positive Δ^{199}Hg values and relatively lower, negative δ^{202}Hg values (Figure 2.6). It is possible that these high-concentration pore water samples contained remobilized legacy Hg released from the sediment, leading to their high dissolved Hg concentrations and isotopic signatures that were shifted toward those of the F1, F4, and F5 Hg pools in the sediment. Additionally, at the two upstream sites (EFK 22.3 and EFK 18.0), δ^{202}Hg values of the F1 sediment Hg fractions were near-zero or slightly negative, while at the downstream site (EFK 8.7), δ^{202}Hg values of the F1 Hg fractions were near-zero or slightly positive (Figure 2.4, Figure S2.3). Thus, weakly-bound Hg in the streambed sediment and hotspots of dissolved Hg in the hyporheic pore water may contribute to the flux of dissolved Hg entering the surface water in a

matter that is consistent with the observed increase in δ^{202}Hg values of the surface water dissolved phase along the flow path, which aligns with the interpretations made by Demers *et al*. (2018)

2.3.6 Interactions between sediment and biofilm

2.3.6.1 Biofilm and suspended particulates as sources of organically-bound mercury to the streambed sediment

The F2 and F3 Hg fractions within each sediment size fraction, which had similar Hg isotopic compositions to one another (Table S2.9), were likely dominated by organically-bound Hg (Bloom et al. 2003). Suspended particulates within EFPC have been found to be largely composed of diatoms and mineral particles coated with organic matter (Gu et al. 2014), so suspended particulates are one likely source of organic matter and organically-bound Hg to the streambed sediment. Another likely source is the nearly-ubiquitous streambed biofilm layer within EFPC, which may be incorporated into the sediment as it goes through cycles of growth and decay and is washed downstream, making it a continuous source of organic matter and organically-bound Hg to the sediment.

The Hg concentration of the F2F3 Hg fractions (Hg_{F2F3}) across all sediment samples ranged from 0.30 to 1.72 µg Hg_{F2F3} g^{-1} sediment, which accounted for 1.6 to 21% (median = 2.6%) of the THg measured (n=12) (Table S2.6a-c). When normalized to the organic carbon content of each sediment sample, the concentration of the F2F3 Hg fractions ranged from 15.5 to 237 µg Hg_{F2F3} g^{-1} OC, with a median value of 32.1 µg Hg_{F2F3} g^{-1} OC (values for Hg_{F2F3} are similar to Hg_{F3} in Figure S2.6, Table S2.8). In comparison, a previous study found that the concentration of the F2F3 Hg pools in EFPC streambed biofilm ranged from 2.23 to 4.95 µg Hg_{F2F3} g^{-1} biofilm, which accounted for 15 to 25% (median = 16%) of the THg measured (n=4)

(Southworth et al. 2010). Organic carbon concentrations were not measured for this small set of biofilm samples, but a larger and more recently collected EFPC biofilm sample set was found to consist of an average of 11.7 ± 6.1% organic carbon (1SD, n=64, measured via loss-on-ignition). For reference, the larger set of biofilm samples that were analyzed for organic carbon had an average THg concentration of 9.2 ± 6.6 µg THg g^{-1} biofilm (1SD, n=64), and the smaller set of biofilm samples that had been used for sequential extractions had an average THg concentration of 22.9 ± 9.5 µg THg g^{-1} biofilm (1SD, n=4) (Southworth et al. 2010). While not a perfect comparison, we used these two sample sets to calculate the concentration of the F2F3 Hg pools in biofilm normalized to the average organic carbon content, which ranged from 19.1 to 42.2 µg Hg_{F2F3} g^{-1} OC, with a median value of 24.7 µg Hg_{F2F3} g^{-1} OC. These concentrations within the biofilm appear to be high enough that a significant portion of the F2F3 Hg pool in the sediment could have been derived from the streambed biofilm layer.

The F2 and F3 sediment-bound Hg pools in this study had isotopic compositions similar to the EFPC biofilm and suspended particulates analyzed by Demers *et al.* (2018) at each site along the stream (Figure 2.7). As previously reported, the isotopic composition of biofilm and suspended particulates shifted along the flow path, with increasing δ^{202}Hg and decreasing Δ^{199}Hg values that converged with the isotopic composition of <125µm streambed sediment (Donovan et al. 2014, Demers et al. 2018). These trends are similar to the shifts in isotopic composition of our F2F3 Hg pool toward that of the F1 and F4F5 Hg pools along the flow path, as determined through statistical analyses (Figure 2.5, Figure 2.7, Table S2.10) (see Section 2.3.4). This similar shift in isotopic composition further suggests that the F2 and F3 Hg pools in the sediment may have been derived from biofilm and/or suspended particulates. Note that methylmercury typically makes up <0.2% and <0.05% of THg within EFPC biofilm and streambed sediment,

respectively (Southworth et al. 2010, Olsen et al. 2016, Watson et al. 2016b, Brooks et al. 2017), which translates to methylmercury making up <1.3% and <3% of the F2F3 Hg fractions within biofilm and streambed sediment, respectively. Thus, while methylation and demethylation reactions may induce isotope fractionation in the pool of methylmercury within the biofilm and sediment, these reactions are not likely to be responsible for the shift in isotopic composition of the biofilm or the F2 and F3 sediment Hg pools along the flow path.

Altogether, the concentration of the F2F3 Hg fraction (normalized to organic carbon content) in biofilm relative to streambed sediment, as well as the similarity in the isotopic composition of biofilm, suspended particulates, and the F2 and F3 sediment Hg fractions, suggests that biofilm and/or suspended particulates are likely sources of organically-bound Hg to the sediment and are responsible for the shift in isotopic composition of the F2 and F3 sediment Hg pools along the flow path (Figure 2.7). This hypothesis relies on the assumption that the organically-bound Hg pool (F2F3) within biofilm and suspended particulates is isotopically similar to bulk biofilm and suspended particulates, which has not been assessed and will require further study.

2.3.6.2 Mechanisms influencing the mercury isotopic composition of biofilm and suspended particulates

Demers *et al.* (2018) proposed that the shift in Hg isotopic composition of EFPC biofilm and suspended particulates along the flow path (i.e., toward higher δ^{202}Hg values and slightly lower Δ^{199}Hg values) could result from suspended particulates being modified as they move downstream by a process similar to nutrient spiraling (Newbold et al. 1981), being repeatedly deposited into the streambed biofilm layer where photochemical and microbial Hg reduction processes could alter their isotopic composition before being re-suspended. This combination of

reactions was proposed to explain the shift in isotopic composition of suspended particulates and biofilm along the flow path while simultaneously accounting for the observed transient increases in Δ^{199}Hg values of the surface water dissolved phase (Demers et al. 2018), which may have resulted from the pulsed release of Hg(0) (with relatively higher Δ^{199}Hg values) to the dissolved phase from the suspended particulates and/or biofilm by photochemical reduction of thiol-bound Hg(II) along the stream (Zheng and Hintelmann 2010a). This combination of reactions was also proposed based on the observed Δ^{199}Hg/Δ^{201}Hg slope of 0.98 (± 0.18, 1SE, n=24) for suspended particulates (Demers et al. 2018), which aligns with the experimentally determined Δ^{199}Hg/Δ^{201}Hg slope of 1.0 to 1.3 for photochemical reduction of Hg(II) (Bergquist and Blum 2007, Zheng and Hintelmann 2009, 2010a). The slope of 0.98 for suspended particulates was obtained using the ordinary least squares regression (Demers et al. 2018), although by using the York regression, which accounts for uncertainty in both the X and Y variables (York 1966), the Δ^{199}Hg/Δ^{201}Hg slope value for suspended particulates is calculated to be 1.33 (± 0.27, 1SE, n=24). Although this higher value is still within the range of experimentally determined slopes for photochemical reduction, especially given that all Δ^{199}Hg and Δ^{201}Hg values were ≤ 0.3‰ (Blum et al. 2014), it opens up the possibility that processes involving nuclear volume fractionation, which typically have a Δ^{199}Hg/Δ^{201}Hg slope of 1.5 to 1.6 (Wiederhold et al. 2010, Zheng and Hintelmann 2009, 2010b, Ghosh et al. 2013, Yang and Liu 2015, Zheng et al. 2019), could also have influenced the isotopic composition of the suspended particulates. Additionally, the Δ^{199}Hg/δ^{202}Hg slope for suspended particulates was -0.11 (± 0.03, 1SE, n=24) (Demers et al. 2018). These slopes are very similar to the slope values for bulk streambed sediment in this study (Figure S2.4, Figure S2.9), which we propose were likely driven by equilibrium isotope effects between coexisting Hg(0) and Hg(II) species (Zheng et al. 2019) (see Section 2.3.2). Based on

these similar slopes, as well as the convergence in δ^{202}Hg and Δ^{199}Hg values of the suspended particulates and biofilm with those of the streambed sediment (Demers et al. 2018). we offer an overall simpler explanation for the evolution of the isotopic composition of suspended particulates and biofilm along the flow path. We suggest that this shift is simply due to mixing with fine-grained streambed sediment, which could account for the relatively large increase in δ^{202}Hg values of the suspended particulates and biofilm along the flow path, negating the need for microbial Hg reduction in the previous explanation (which shifts the oxidized phase toward higher δ^{202}Hg values). Mixing with streambed sediment could also account for the small decrease in Δ^{199}Hg values along the flow path, although photochemical reduction of thiol-bound Hg(II) in the particulate phase would still be required to explain the transient increases in Δ^{199}Hg values of the surface water dissolved phase.

2.3.6.3 Evidence for the transfer of weakly-bound mercury from streambed sediment to biofilm and suspended particulates

Within the streambed sediment, the F2F3 pools of Hg also increased in δ^{202}Hg and decreased in Δ^{199}Hg values along the flow path, converging with the isotopic composition of the F1 and F4F5 sediment Hg pools (Figure 2.4, Figure 2.5). Physical incorporation of fine sediment grains into the biofilm and suspended particulates would primarily contribute recalcitrant forms of Hg, potentially altering the isotopic composition of these materials. Physical mixing with sediment, however, would likely not have significantly altered the isotopic composition of the organically-bound Hg pools within the biofilm and suspended particulates. Thus, we would not expect subsequent incorporation of biofilm and suspended particulates into the streambed sediment to alter the isotopic composition of the F2F3 sediment Hg pools along the flow path. However, relatively weakly-bound Hg (i.e., from the F1 pool), which itself may be derived from

the more recalcitrant F4F5 pools (see Section 2.3.5.1), could have been dissolved and transferred into biofilm and suspended particulates where it may have become bound to organic ligands. Then, as biofilm and suspended particulates became physically incorporated into the streambed sediment along the flow path, this organically-bound Hg could have been contributed to the F2F3 sediment Hg pools. This would have caused the F2F3 Hg pools in the sediment to become isotopically more similar to recalcitrant forms of Hg, and thus could explain the convergence in isotopic composition of the F2F3 Hg pool with the F1 and F4F5 Hg pools within the streambed sediment along the flow path (Figure 2.4, Figure 2.5).

This explanation of F2F3 isotopic convergence with F1 and F4F5 Hg pools in the streambed sediment would also require no (or net zero) isotope fractionation during the transfer of weakly-bound (F1) Hg from sediment to biofilm and suspended particulates, and the re-incorporation of Hg from biofilm and suspended particulates into the organically-bound (F2F3) sediment Hg pool. While this seems somewhat unlikely, the fractionation that results from this process is difficult to predict without knowing the chemical form of weakly-bound Hg in the sediment. Regardless of potential fractionation, the near-quantitative transfer of small pools of Hg from the F1 to the F2F3 fraction could be achieved with no *net* fractionation. Additionally, the physical incorporation of biofilm and suspended particulates into the streambed along the flow path, which would contribute organically-bound Hg to the F2F3 pool in the sediment, would not be expected to induce isotope fractionation.

Overall, we suggest that physical mixing with fine-grained streambed sediment (along with photochemical reduction of thiol-bound Hg(II)) could explain the shifts in isotopic composition of the bulk biofilm and suspended particulates along the flow path. At the same time, our sequential extraction data suggest that the F2F3 Hg pools in the streambed sediment

likely originate from organically-bound Hg in biofilm and suspended particulates, and that dissolution and transfer of weakly-bound (F1) Hg from the sediment to the biofilm and suspended particulates, followed by re-incorporation into the organically-bound (F2F3) sediment Hg pool, could explain the shifts in isotopic composition of the F2F3 sediment Hg pools along the flow path. However, to evaluate the likelihood of this scenario, more process-specific experimental isotope fractionation studies will need to be undertaken to identify the biogeochemical processes involved and the potential fractionation that each process may or may not induce.

2.4 Conclusions and Implications

In this study, we measured THg concentrations and Hg isotope ratios in four size fractions of streambed sediment collected from four sites along East Fork Poplar Creek, and also performed five-step sequential extractions and Hg isotope analyses on sediment from three of these sites. We found that there were no significant correlations between isotope ratios and THg concentration for any of the sediment size fractions, suggesting that variations in THg concentration and isotopic signatures were not driven by mixing between two sources with distinct Hg concentrations and isotopic compositions. Instead, based on the $\Delta^{199}Hg/\Delta^{201}Hg$ and $\Delta^{199}Hg/\delta^{202}Hg$ slope values for streambed sediment, we suggest that the isotopic composition of the sediment appears to have been influenced by equilibrium reactions involving nuclear volume fractionation, including equilibrium isotope exchange between coexisting Hg(0) and Hg(II) species. The isotope fractionation imparted on the sediment by equilibrium isotope effects may have over-printed that of kinetic Hg oxidation and reduction reactions, such as oxidation of metallic Hg(0) prior to and after being released from Y-12, as well as *in situ* reduction of Hg(II) within the stream. The equilibrium isotope effect appears to control the overall isotopic

composition of the recalcitrant Hg pool throughout the stream ecosystem (Figure 2.2). The results of our study provide an *in situ* ecosystem-based example of how equilibrium isotope effects may have over-printed isotope fractionation signatures imparted by kinetic oxidation and reduction reactions, as hypothesized by Bartov (2014) and later observed experimentally by Zheng *et al*. (2019) Equilibrium isotope effects between redox species may be especially relevant for ecosystems that have been contaminated with both Hg(0) and Hg(II), such as industrial and mining sites.

Similar to previous studies (Southworth et al. 2010, Brooks et al. 2017), our sequential extractions showed that recalcitrant forms of Hg make up a majority of the Hg in EFPC streambed sediment, followed by Hg compounds of intermediate solubility such as organically-bound Hg, and small but significant amounts of weakly-bound Hg (Figure 2.3, Table S2.6a-c). The similarity in isotopic composition between the F1 and F4F5 sediment Hg fractions suggests that the weakly-bound pool may be derived from the strongly-bound legacy Hg through dissolution and rapid re-adsorption to the sediment. This implies that weakly-bound Hg pools in the sediment may continually be replenished by the large reservoir of recalcitrant Hg in the streambed, which itself is also replenished by stream bank erosion (Watson et al. 2016b, Watson et al. 2016a), suggesting that the streambed sediment will likely be a source of dissolved Hg for many years. Dissolution of legacy Hg from streambed sediment can help explain the isotopic composition of hyporheic pore water samples with high dissolved Hg concentrations, which had higher δ^{202}Hg values and lower Δ^{199}Hg values than surface water and low-concentration pore water (Demers et al. 2018), and appeared to be influenced by the F1, F4, and F5 Hg pools in the streambed sediment (Figure 2.6). The elevated δ^{202}Hg values of the high-concentration pore water, as well as the increase in δ^{202}Hg values of the F1 sediment Hg fractions along the flow

path (Figure 2.4), align with the increasing δ^{202}Hg values of the surface water dissolved phase along the flow path (Demers et al. 2018). This suggests that hyporheic pore water and weakly-bound sediment Hg pools are likely sources of dissolved Hg to the surface water, contributing to the diffuse Hg flux which makes up 6 to 36% of the total dissolved Hg flux along the stream (Demers et al. 2018, Peterson et al. 2018a). Together, these isotope data and flux measurements suggest that even if the upstream point-source were to cease delivering dissolved Hg to the stream, dissolved Hg concentrations in the surface water would likely remain elevated due to the release of dissolved Hg from the streambed. The slow release of dissolved Hg from seemingly recalcitrant legacy sources may be common among other legacy Hg-contaminated stream ecosystems, and should be considered when evaluating the potential for ecosystem recovery from historical Hg inputs.

Along the flow path, the isotopic composition of the F2 and F3 sediment Hg pools, as well as EFPC biofilm and suspended particulates (Demers et al. 2018), shifted toward higher δ^{202}Hg and lower Δ^{199}Hg values (Figure 2.5, Figure 2.7). These similarities suggest that the F2 and F3 sediment Hg pools were predominantly derived from biofilm and/or suspended particulates. As suggested by Demers *et al.* (2018), shifts in isotopic composition of the biofilm and suspended particulates may have resulted from photochemical and microbial Hg reduction processes, which could also explain the transient increases in Δ^{199}Hg values of the surface water dissolved phase along the flow path. We also provide an alternative explanation, in which the shift in isotopic composition of biofilm and suspended particulates along the flow path is simply driven by mixing with fine-grained streambed sediment, though photochemical reduction in the particulate phase would still be required to explain the isotopic patterns in the dissolved phase. Additionally, it appears that weakly-bound sediment Hg is transferred into the biofilm and

suspended particulates, which may subsequently contribute to and shift the isotopic composition of the organically-bound sediment Hg pools as the biofilm and suspended particulates become incorporated into the streambed sediment along the flow path. Biofilm is known to be a site for enhanced Hg methylation within EFPC (Olsen et al. 2016) and other streams, thus legacy Hg that is transferred into biofilm may be more available for methylation and subsequent bioaccumulation in the food web. Additionally, Zhang *et al.* (2019) recently showed that in a laboratory setting, up to 7% of EFPC sediment-bound Hg was available for microbial methylation without first being dissolved. For most of our sediment samples, this percentage is greater than the F1, F2, and F3 Hg fractions combined (Table S2.6a-c). Further studies will be required to determine which of the sediment Hg pools would be preferentially methylated, and to assess the potential transfer of legacy Hg from sediment into biofilm, its transformation into methylmercury, and its incorporation into the food web.

Our coupling of sequential extractions and Hg isotope analysis has highlighted knowledge gaps in our understanding of the mechanisms underlying the biogeochemical cycling of Hg within contaminated stream ecosystems and their associated isotope fractionation patterns. In particular, sequential extraction results point toward a mechanism of dissolution of recalcitrant legacy Hg that does not induce significant isotope fractionation. While the observed isotopic fractionation, or lack-thereof, in our study (and others) suggests that dissolution of recalcitrant Hg may indeed be occurring within the environment, isotope fractionation during dissolution of HgS by most reactions (e.g., dissolution by dissolved organic matter, high levels of dissolved oxygen, or sulfur-oxidizing bacteria) has not been experimentally evaluated. Moreover, the processes that control the transfer of Hg from weakly-bound fractions to organically-bound fractions need to be identified and their isotopic systematics described. Also, for contaminated

ecosystems that are known to contain both Hg(0) and Hg(II), it is worth considering the degree to which equilibrium isotope effects may be ubiquitously over-printing fractionation signatures from kinetic reaction mechanisms, as may be indicated by previous experimental results involving isotope exchange following dark abiotic oxidation (Zheng et al. 2019). To better constrain and interpret field observations of Hg isotopic composition, it will be necessary to continue to experimentally assess the isotope fractionation associated with environmentally-relevant processes and to expand upon our catalogue of process-specific diagnostic Hg fractionation patterns (i.e., characteristic isotope ratios and slopes).

Overall, Hg isotopic analysis of EFPC surface water, hyporheic pore water, biofilm, suspended particulates, and streambed sediment sequential extractions has provided evidence that sediment-bound legacy Hg may be remobilized within contaminated streams. Together with dissolved Hg flux measurements, this information further suggests that recalcitrant legacy Hg has the potential to be a long-term source of dissolved Hg to stream water, as the large reservoirs of recalcitrant Hg may continue to release small, but meaningful, amounts of Hg. Moreover, our sequential extraction data suggest that remobilized recalcitrant legacy Hg may be incorporated into streambed biofilm, a basal resource of aquatic food webs. Thus, along with reducing dissolved Hg inputs from upstream point sources, remediation efforts focused on the streambed sediment-bound Hg would also likely decrease surface water dissolved Hg concentrations and may also decrease THg and methylmercury concentrations in aquatic organisms.

Acknowledgements

We thank Todd Olsen for assistance in collecting the biofilm samples that were used for the organic carbon analysis. This manuscript was improved substantially thanks to the thoughtful comments of Jan Wiederhold and two anonymous reviewers. This research was supported by the

U.S. Department of Energy (DOE), Office of Science, Biological and Environmental Research (BER), Subsurface Biogeochemical Research (SBR) program under Award No. DE-SC0016489 and is also a product of the Mercury Science Focus Area (SFA) at Oak Ridge National Laboratory (ORNL). ORNL is managed by UT-Battelle, LLC for the DOE under Contract No. DE-AC05-00OR22725.

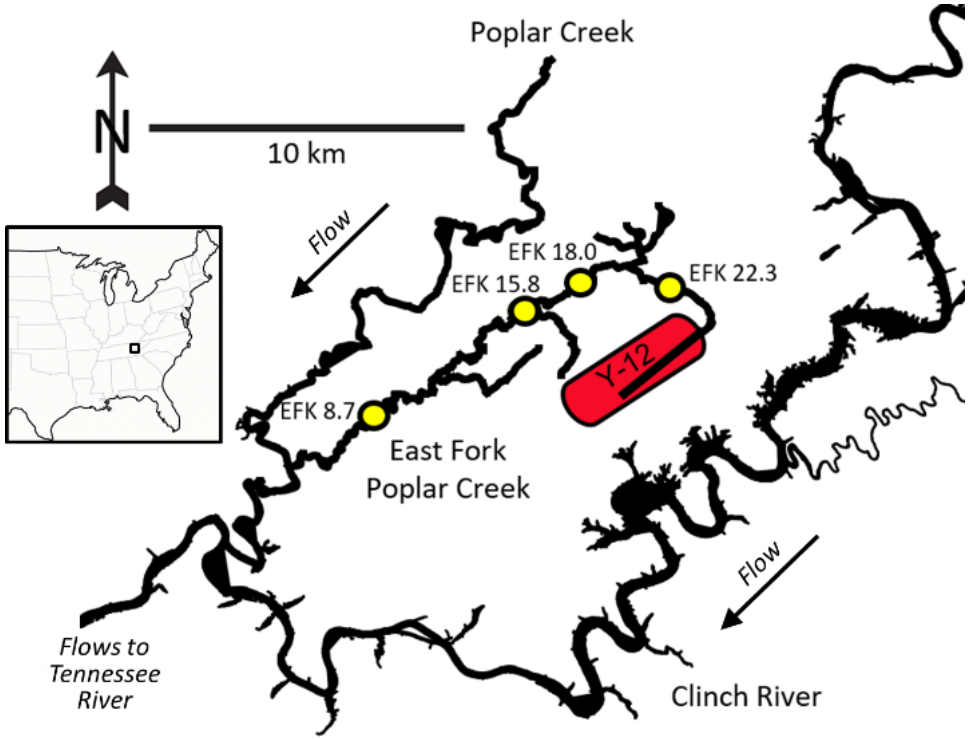

Figure 2.1. Map of East Fork Poplar Creek in Oak Ridge, Tennessee, USA.

Map highlights the Y-12 National Security Complex (red oval) and the four streambed sediment collection sites: EFK 22.3, EFK 18.0, EFK 15.8, and EFK 8.7 (yellow circles).

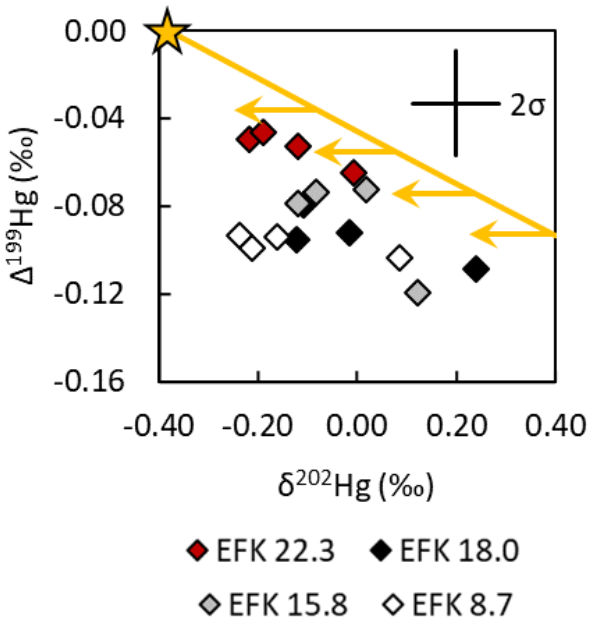

Figure 2.2. Total Hg isotopic composition of EFPC streambed sediment, measured via combustion.

Analytical uncertainty in delta values is shown as the average uncertainty (2SD) across combustion reference material analyses (see Section 2.2.5). The gold star represents the assumed isotopic composition of metallic Hg(0) historically used at Y-12 (average isotopic composition of -0.38 ± 0.34‰ δ^{202}Hg and near-zero Δ^{199}Hg) (Sun et al. 2016). The diagonal line represents the equilibrium isotope effect driven by isotope exchange between coexisting Hg(0) and Hg(II) species (Δ^{199}Hg/δ^{202}Hg slope of -0.12 ± 0.01, 1SE) (Zheng et al. 2019). This is followed by precipitation of HgS and other minerals (Foucher et al. 2013, Smith et al. 2015), sorption of Hg(II) to mineral surfaces (Jiskra et al. 2012), and/or binding of Hg(II) to thiol ligands within organic matter (Wiederhold et al. 2010) (horizontal arrows pointing toward lower δ^{202}Hg values for the solid phase).

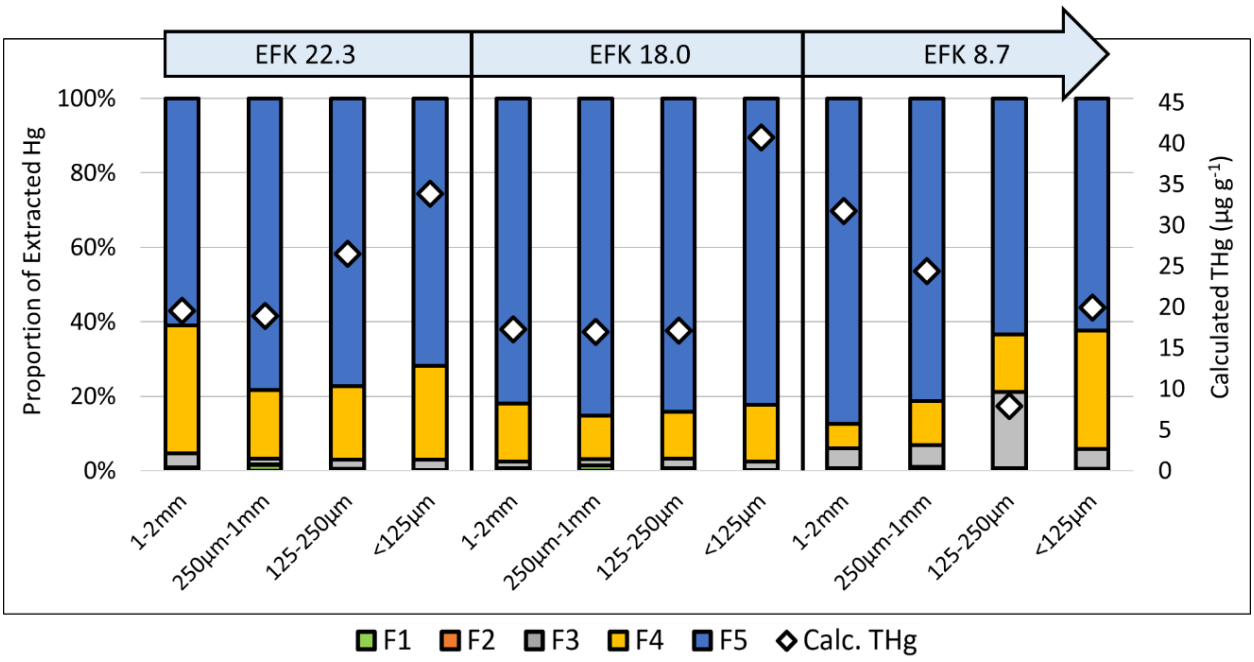

Figure 2.3. Proportions of Hg fractions extracted from EFPC streambed sediment (bar graph, left axis) and total Hg concentration calculated from the sum of sequential extractions (white diamonds, right axis).

Note that the proportions of F1 and F2 are too small to be visible on the figure.

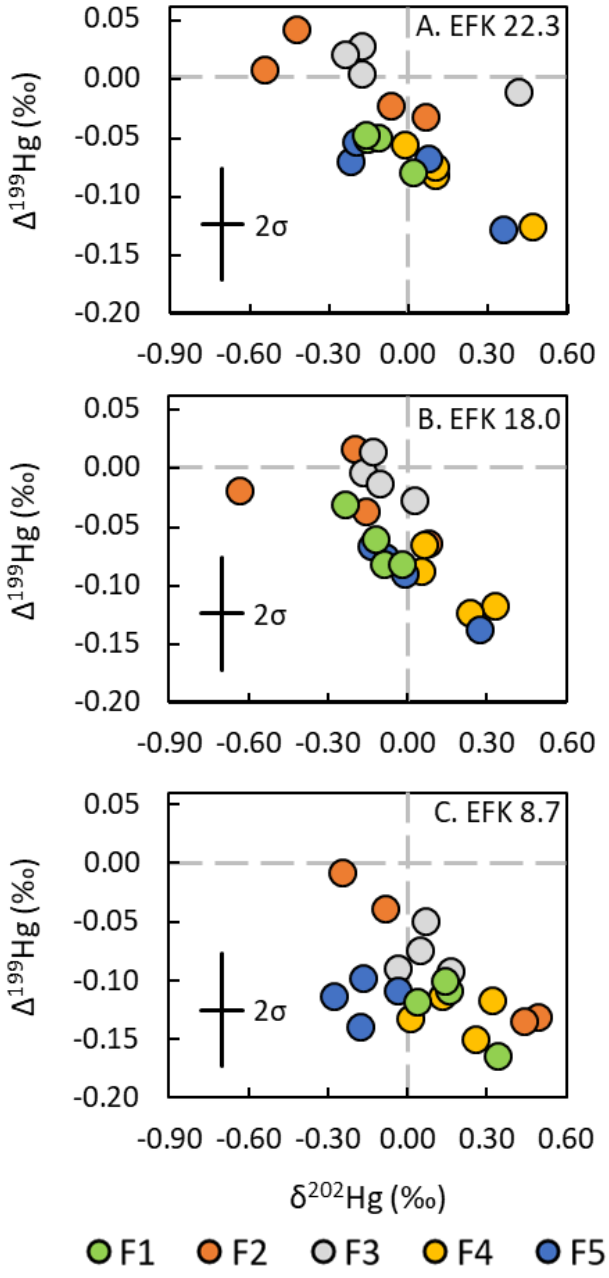

Figure 2.4. Mercury isotopic composition of sequential extractions of EFPC streambed sediment collected from (A) EFK 22.3, (B) EFK 18.0, and (C) EFK 8.7.

Analytical uncertainty in delta values is shown as the average uncertainty (2SD) across all UM-Almadén analyses (see Section 2.2.5). Symbols of the same color represent different sediment size fractions.

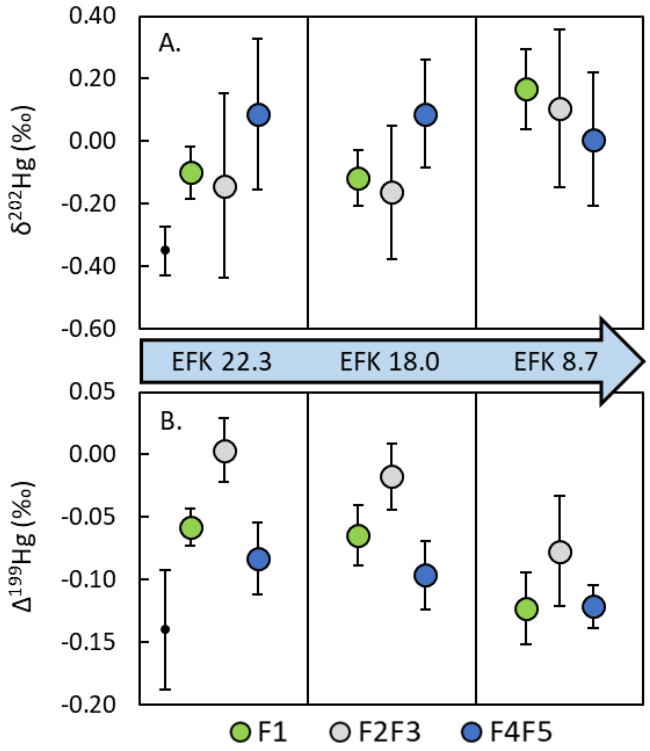

Figure 2.5. Average Hg isotopic composition of sequential extractions of EFPC streambed sediment. Shown are (A) δ^{202}Hg and (B) Δ^{199}Hg values for F1, F2F3, and F4F5 Hg fractions averaged across all size fractions within each sampling site.

Isotopic compositions of the F2F3 and F4F5 Hg fractions were calculated based on the unweighted average of F2 and F3, and of F4 and F5 fractions, respectively. Error bars represent 1SD associated with each average δ^{202}Hg or Δ^{199}Hg value (n=4 for F1 fractions, n=8 for F2F3 and F4F5 fractions). Average and 1SD values match those reported in Table S2.13. Analytical uncertainty in delta values is shown as the average uncertainty (2SD) across all UM-Almadén analyses (see Section 2.2.5).

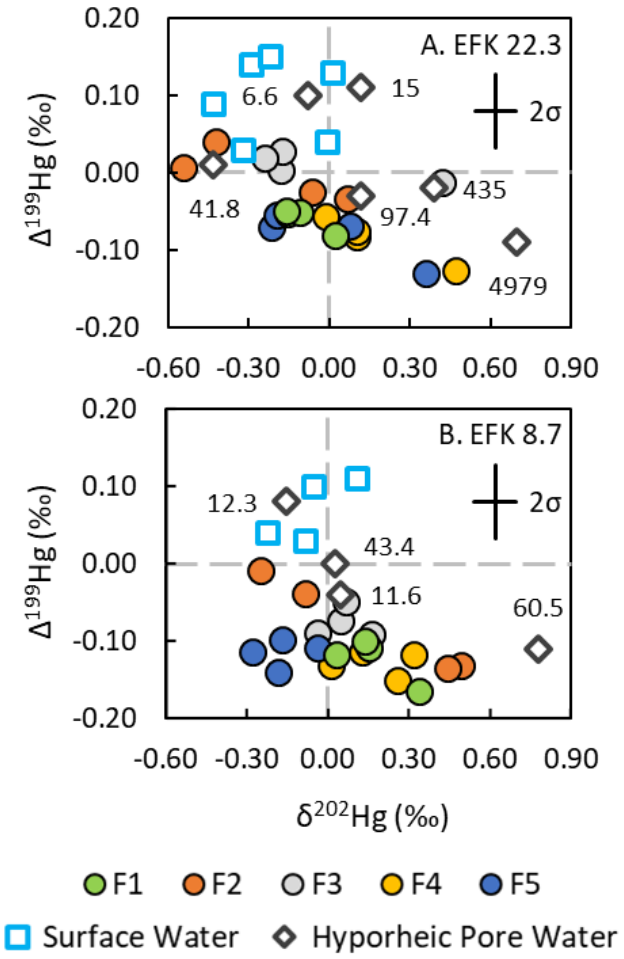

Figure 2.6. Mercury isotopic composition of sequential extractions of EFPC streambed sediment collected from (A) EFK 22.3 and (B) EFK 8.7, along with surface water and hyporheic pore water dissolved phase collected from (A) EFK 22.3 and (B) EFK 5.0 (Demers et al. 2018).

Dissolved Hg concentrations of the hyporheic pore water samples are shown as numbers on the plots (ng L^{-1}). One EFK 5.0 pore water sample is not shown because it plots off scale at 0.28‰ δ^{202}Hg and 0.37‰ Δ^{199}Hg, and has a dissolved Hg concentration of 6.7 ng L^{-1}. Analytical uncertainty in sequential extraction delta values is shown as the average uncertainty (2SD) across all UM-Almadén analyses (see Section 2.2.5). Analytical uncertainty for water samples is less than or equal to analytical uncertainty of sequential extraction samples (Demers et al. 2018).

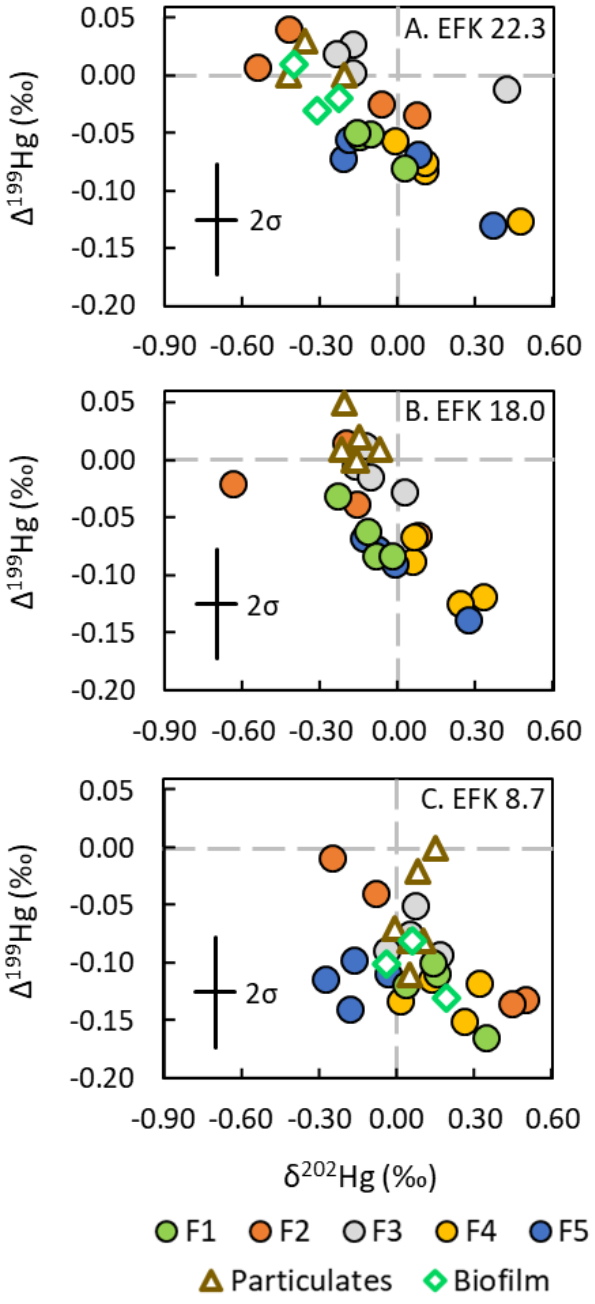

Figure 2.7. Mercury isotopic composition of sequential extractions of EFPC streambed sediment collected from (A) EFK 22.3, (B) EFK 18.0, and (C) EFK 8.7, along with biofilm collected from (A) EFK 22.3 and (C) EFK 5.0, and suspended particulates collected from (A) EFK 22.3, (B) EFK 18.2, EFK 17.8, (C) EFK 9.8, and EFK 5.0 (Demers et al. 2018).

Analytical uncertainty in sequential extraction delta values is shown as the average uncertainty (2SD) across all UM-Almadén analyses (see Section 2.2.5). Analytical uncertainty for biofilm and suspended particulate samples is less than or equal to analytical uncertainty of sequential extraction samples (Demers et al. 2018).

References

Barnett, Mark O., Lawerence A. Harris, Ralph R. Turner, Robert J. Stevenson, Thomas J. Henson, Ruben C. Melton, and Douglas P. Hoffman. 1997. "Formation of mercuric sulfide in soil." *Environmental Science & Technology* 31 (11):3037-3043. doi: 10.1021/es960389j.

Barnett, Mark O., Ralph R. Turner, and Philip C. Singer. 2001. "Oxidative dissolution of metacinnabar (β-HgS) by dissolved oxygen." *Applied Geochemistry* 16 (13):1499-1512. doi: 10.1016/S0883-2927(01)00026-9.

Bartov, Gideon. 2014. "Mercury Stable Isotope Geochemistry as a Tool for Tracing Sources and Chemical Transformations in the Environment."Ph.D. Thesis, Department of Geology, University of Illinois at Urbana-Champaign.

Bergquist, Bridget A., and Joel D. Blum. 2007. "Mass-dependent and -independent fractionation of Hg isotopes by photoreduction in aquatic systems." *Science* 318:417-420. doi: 10.1126/science.1148050.

Bloom, Nicolas S., Eve Preus, Jodie Katon, and Misti Hiltner. 2003. "Selective extractions to assess the biogeochemically relevant fractionation of inorganic mercury in sediments and soils." *Analytica Chimica Acta* 479 (2):233-248. doi: 10.1016/s0003-2670(02)01550-7.

Blum, Joel D., and Bridget A. Bergquist. 2007. "Reporting of variations in the natural isotopic composition of mercury." *Analytical and Bioanalytical Chemistry* 388:353-359. doi: 10.1007/s00216-007-1236-9.

Blum, Joel D., and Marcus W. Johnson. 2017. "Recent developments in mercury stable isotope analysis." *Reviews in Mineralogy and Geochemistry* 82:733-757. doi: 10.2138/rmg.2017.82.17.

Blum, Joel D., Laura S. Sherman, and Marcus W. Johnson. 2014. "Mercury isotopes in earth and environmental sciences." *Annual Review of Earth and Planetary Sciences* 42:249-269. doi: 10.1146/annurev-earth-050212-124107.

Brezonik, Patrick L., and William A. Arnold. 2011. *Water Chemistry: An Introduction to the Chemistry of Natural and Engineered Aquatic Systems*, 364-405. Oxford, New York: Oxford University Press, Inc.

Brocza, Flora M., Harald Biester, Jan-Helge Richard, Stephan M. Kraemer, and Jan G. Wiederhold. 2019. "Mercury isotope fractionation in the subsurface of a Hg(II) chloride-contaminated industrial legacy site." *Environmental Science & Technology* 53:7296-7305. doi: 10.1021/acs.est.9b00619.

Brooks, Scott C., and George R. Southworth. 2011. "History of mercury use and environmental contamination at the Oak Ridge Y-12 Plant." *Environmental Pollution* 159 (1):219-228. doi: 10.1016/j.envpol.2010.09.009.

Brooks, Scott, Virginia Eller, John Dickson, Jennifer Earles, Kenneth Lowe, Tonia Mehlhorn, Todd Olsen, Chris DeRolph, David Watson, Debra Phillips, and Mark Peterson. 2017. Mercury Content of Sediments in East Fork Poplar Creek: Current Assessment and Past Trends. Oak Ridge, TN: Oak Ridge National Laboratory.

Buchachenko, Anatolii L. 2009. "Mercury isotope effects in the environmental chemistry and biochemistry of mercury-containing compounds." *Russian Chemical Reviews* 78:319-328. doi: 10.1070/RC2009v078n04ABEH003904.

Chen, JiuBin, Holger Hintelmann, XinBin Feng, and Brian Dimock. 2012. "Unusual fractionation of both odd and even mercury isotopes in precipitation from Peterborough,

ON, Canada." *Geochimica et Cosmochimica Acta* 90:33-46. doi: 10.1016/j.gca.2012.05.005.

Chen, Ying, Yongguang Yin, Jianbo Shi, Guangliang Liu, Ligang Hu, Jing-Fu Liu, Yong Cai, and Guibin Jiang. 2017. "Analytical methods, formation, and dissolution of cinnabar and its impact on environmental cycle of mercury." *Critical Reviews in Environmental Science and Technology* 47 (24):2415-2447. doi: 10.1080/10643389.2018.1429764.

Choe, Key-Young, Gary A. Gill, Ronald D. Lehman, Seunghee Han, Wesley A. Heim, and Kenneth H. Coale. 2004. "Sediment-water exchange of total mercury and monomethyl mercury in the San Francisco Bay-Delta." *Limnology and Oceanography* 49 (5):1512-1527. doi: 10.4319/lo.2004.49.5.1512.

Demers, Jason D., Joel D. Blum, Scott C. Brooks, Patrick M. Donovan, Ami L. Riscassi, Carrie L. Miller, Wang Zheng, and Baohua Gu. 2018. "Hg isotopes reveal in-stream processing and legacy inputs in East Fork Poplar Creek, Oak Ridge, Tennessee, USA." *Environmental Science: Processes & Impacts* 20 (4):686-707. doi: 10.1039/c7em00538e.

Demers, Jason D., Joel D. Blum, and Donald R. Zak. 2013a. "Mercury isotopes in a forested ecosystem: Implications for air-surface exchange dynamics and the global mercury cycle." *Global Biogeochemical Cycles* 27:222-238. doi: 10.1002/gbc.20021.

Demers, Jason D., Joseph B. Yavitt, Charles T. Driscoll, and Mario R. Montesdeoca. 2013b. "Legacy mercury and stoichiometry with C, N, and S in soil, pore water, and stream water across the upland-wetland interface: The influence of hydrogeologic setting." *Journal of Geophysical Research: Biogeosciences* 118 (2):825-841. doi: 10.1002/jgrg.20066.

Dickson, Johnbull O., Melanie A. Mayes, Scott C. Brooks, Tonia L. Mehlhorn, Kenneth A. Lowe, Jennifer K. Earles, Leroy Goñez-Rodríguez, David B. Watson, and Mark J. Peterson. 2019. "Source relationships between streambank soils and streambed sediments in a mercury-contaminated stream." *Journal of Soils and Sediments* 19:2007-2019. doi: 10.1007/s11368-018-2183-0.

Donovan, Patrick M., Joel D. Blum, Jason D. Demers, Baohua Gu, Scott C. Brooks, and John Peryam. 2014. "Identification of multiple mercury sources to stream sediments near Oak Ridge, TN, USA." *Environmental Science & Technology* 48 (7):3666-3674. doi: 10.1021/es4046549.

Donovan, Patrick M., Joel D. Blum, Michael Bliss Singer, Mark Marvin-DiPasquale, and Martin T. K. Tsui. 2016. "Methylmercury degradation and exposure pathways in streams and wetlands impacted by historical mining." *Science of The Total Environment* 568:1192-1203. doi: 10.1016/j.scitotenv.2016.04.139.

Eganhouse, Robert P., David R. Young, and Joseph N. Johnson. 1978. "Geochemistry of mercury in Palos Verdes sediments." *Environmental Science & Technology* 12 (10):1151-1157. doi: 10.1021/es60146a004.

Estrade, Nicolas, Jean Carignan, Jeroen E. Sonke, and Olivier F. X. Donard. 2009. "Mercury isotope fractionation during liquid-vapor evaporation experiments." *Geochimica et Cosmochimica Acta* 73:2693-2711. doi: 10.1016/j.gca.2009.01.024.

Foucher, Delphine, Holger Hintelmann, Tom A. Al, and Kerry T. MacQuarrie. 2013. "Mercury isotope fractionation in waters and sediments of the Murray Brook mine watershed (New Brunswick, Canada): Tracing mercury contamination and transformation." *Chemical Geology* 336:87-95. doi: 10.1016/j.chemgeo.2012.04.014.

Ghosh, Sanghamitra, Edwin A. Schauble, Georges Lacrampe Couloume, Joel D. Blum, and Bridget A. Bergquist. 2013. "Estimation of nuclear volume dependent fractionation of mercury isotopes in equilibrium liquid-vapor evaporation experiments." *Chemical Geology* 336:5-12. doi: 10.1016/j.chemgeo.2012.01.008.

Gratz, Lynne E., Gerald J. Keeler, Joel D. Blum, and Laura S. Sherman. 2010. "Isotopic composition and fractionation of mercury in Great Lakes precipitation and ambient air." *Environmental Science and Technology* 44:7764-7770. doi: 10.1021/es100383w.

Grigg, Andrew R. C., Ruben Kretzschmar, Robin S. Gilli, and Jan G. Wiederhold. 2018. "Mercury isotope signatures of digests and sequential extracts from industrially contaminated soils and sediments." *Science of The Total Environment* 636:1344-1354. doi: 10.1016/j.scitotenv.2018.04.261.

Gu, B., B. Mishra, C. Miller, W. Wang, B. Lai, S. C. Brooks, K. M. Kemner, and L. Liang. 2014. "X-ray fluorescence mapping of mercury on suspended mineral particles and diatoms in a contaminated freshwater system." *Biogeosciences* 11:5259-5267. doi: 10.5194/bg-11-5259-2014.

Hall, Gwendy E. M., and Pierre Pelchat. 2005. "The design and application of sequential extractions for mercury, Part 2. Resorption of mercury onto the sample during leaching." *Geochemistry: Exploration, Environment, Analysis* 5 (2):115-121. doi: 10.1144/1467-7873/03-062.

Hall, Gwendy E. M., Pierre Pelchat, and Jeanne B. Percival. 2005. "The design and application of sequential extractions for mercury, Part 1. Optimization of HNO3 extraction for all non-sulphide forms of Hg." *Geochemistry: Exploration, Environment, Analysis* 5 (2):107-113. doi: 10.1144/1467-7873/03-061.

Hasany, Syed Moosa, Mohammad Mufazzal Saeed, and Munir Ahmed. 1999. "Retention of Hg(II) by solid mercury sulfide from acidic solution." *Separation Science and Technology* 34:487-499. doi: 10.1081/ss-100100662.

Holley, Elizabeth A., A. James McQuillan, Dave Craw, Jonathan P. Kim, and Sylvia G. Sander. 2007. "Mercury mobilization by oxidative dissolution of cinnabar (α-HgS) and metacinnabar (β-HgS)." *Chemical Geology* 240 (3-4):313-325. doi: 10.1016/j.chemgeo.2007.03.001.

Hong, Young-Seoub, Yu-Mi Kim, and Kyung-Eun Lee. 2012. "Methylmercury exposure and health effects." *Journal of Preventive Medicine and Public Health* 45 (6):353-363. doi: 10.3961/jpmph.2012.45.6.353.

Hsieh, Y. H., S. Tokunaga, and C. P. Huang. 1991. "Some chemical reactions at the HgS(s)-water interface as affected by photoirradiation." *Colloids and Surfaces* 53 (2):257-274. doi: 10.1016/0166-6622(91)80141-a.

Huang, Shuyuan, Yuhan Zhao, Supeng Lv, Weiguo Wang, Weili Wang, Yuanbiao Zhang, Yunlong Huo, Xiuwu Sun, and Yaojin Chen. 2021. "Distribution of mercury isotope signatures in Yundang Lagoon, Xiamen, China, after long-term interventions." *Chemosphere* 272:129716. doi: 10.1016/j.chemosphere.2021.129716.

Issaro, N., C. Abi-Ghanem, and A. Bermond. 2009. "Fractionation studies of mercury in soils and sediments: A review of the chemical reagents used for mercury extraction." *Analytica Chimica Acta* 631 (1):1-12. doi: 10.1016/j.aca.2008.10.020.

Janssen, Sarah E., Michael T. Tate, David P. Krabbenhoft, John F. DeWild, Jacob M. Ogorek, Christopher L. Babiarz, Anthony Sowers, and Peter L. Tuttle. 2020. "The influence of legacy contamination on the transport and bioaccumulation of mercury within the Mobile

River Basin." *Journal of Hazardous Materials* 404 A:124097. doi: 10.1016/j.jhazmat.2020.124097.
Jiang, Ping, Yanbin Li, Guangliang Liu, Guidi Yang, Leonel Lagos, Yongguang Yin, Baohua Gu, Guibin Jiang, and Yong Cai. 2016. "Evaluating the role of re-adsorption of dissolved Hg2+ during cinnabar dissolution using isotope tracer technique." *Journal of Hazardous Materials* 317:466-475. doi: 10.1016/j.jhazmat.2016.05.084.
Jiskra, Martin, Jan G. Wiederhold, Bernard Bourdon, and Ruben Kretzschmar. 2012. "Solution speciation controls mercury isotope fractionation of Hg(II) sorption to goethite." *Environmental Science & Technology* 46:6654-6662. doi: 10.1021/es3008112.
Kim, Christopher S., Nicolas S. Bloom, James J. Rytuba, and Gordon E. Brown Jr. 2003. "Mercury speciation by X-ray absorption fine structure spectroscopy and sequential chemical extractions: A comparison of speciation methods." *Environmental Science & Technology* 37 (22):5102-5108. doi: 10.1021/es0341485.
Lauretta, Dante S., Bjoern Klaue, Joel D. Blum, and Peter R. Buseck. 2001. "Mercury abundances and isotopic compositions in the Murchison (CM) and Allende (CV) carbonaceous chondrites." *Geochimica et Cosmochimica Acta* 65:2807-2818. doi: 10.1016/s0016-7037(01)00630-5.
Liu, Guangliang, Julio Cabrera, Marshall Allen, and Yong Cai. 2006. "Mercury characterization in a soil sample collected nearby the DOE Oak Ridge Reservation utilizing sequential extraction and thermal desorption method." *Science of The Total Environment* 369 (1-3):384-392. doi: 10.1016/j.scitotenv.2006.07.011.
Miller, Carrie L., David B. Watson, Brian P. Lester, Kenneth A. Lowe, Eric M. Pierce, and Liyuan Liang. 2013. "Characterization of soils from an industrial complex contaminated with elemental mercury." *Environmental Research* 125:20-29. doi: 10.1016/j.envres.2013.03.013.
Newbold, J. Denis, Jerry W. Elwood, Robert V. O'Neill, and Webster Van Winkle. 1981. "Measuring nutrient spiralling in streams." *Canadian Journal of Fisheries and Aquatic Sciences* 38:860-863. doi: 10.1139/f81-114.
Olsen, Todd A., Craig C. Brandt, and Scott C. Brooks. 2016. "Periphyton biofilms influence net methylmercury production in an industrially contaminated system." *Environmental Science & Technology* 50:10843-10850. doi: 10.1021/acs.est.6b01538.
Olson, M. L., L. B. Cleckner, J. P. Hurley, D. P. Krabbenhoft, and T. W. Heelan. 1997. "Resolution of matrix effects on analysis of total and methyl mercury in aqueous samples from the Florida Everglades." *Fresenius' Journal of Analytical Chemistry* 358:392-396. doi: 10.1007/s002160050435.
Pelcová, Pavlína, Jana Margetínová, Tomáš Vaculovič, Josef Komárek, and Vlastimil Kubáň. 2010. "Adsorption of mercury species on river sediments – effects of selected abiotic parameters." *Central European Journal of Chemistry* 8:116-125. doi: 10.2478/s11532-009-0128-6.
Peterson, Mark J., Scott C. Brooks, Teresa J. Mathews, Melanie A. Mayes, Alexander Johs, Ryan McManamay, David B. Watson, Katherine Muller, Leroy Goñez-Rodríguez, Chris DeRolph, and Sujith Nair. 2018a. Mercury Remediation Technology Development for Lower East Fork Poplar Creek–FY 2018 Update. Oak Ridge, TN: Oak Ridge National Laboratory.
Peterson, Mark J., Scott C. Brooks, Teresa J. Mathews, Melanie Mayes, Alexander Johs, David B. Watson, Monica D. Poteat, John G. Smith, Tonia Mehlhorn, Brian Lester, Jesse

Morris, Kenneth Lowe, Johnbull O. Dickson, Virginia Eller, and Christopher R. DeRolph. 2016. Mercury Remediation Technology Development for Lower East Fork Poplar Creek–FY 2015 Progress Report. Oak Ridge, TN: Oak Ridge National Laboratory.

Peterson, Mark J., Melanie Mayes, Scott Brooks, Teresa Mathews, Alex Johs, Leroy Goñez-Rodríguez, Christopher DeRolph, Eric Pierce, David Watson, Katherine Muller, Todd Olsen, Kenneth Lowe, Ryan McManamay, John Smith, Jesse Morris, and Michael Jones. 2018b. Mercury Remediation Technology Development for Lower East Fork Poplar Creek–2017 Progress Report. Oak Ridge, TN: Oak Ridge National Laboratory.

Pribyl, Douglas W. 2010. "A critical review of the conventional SOC to SOM conversion factor." *Geoderma* 156:75-83. doi: 10.1016/j.geoderma.2010.02.003.

Ravichandran, Mahalingam, George R. Aiken, Michael M. Reddy, and Joseph N. Ryan. 1998. "Enhanced dissolution of cinnabar (mercuric sulfide) by dissolved organic matter isolated from the Florida Everglades." *Environmental Science & Technology* 32 (21):3305-3311. doi: 10.1021/es9804058.

Revis, Nathaniel W., Tanya R. Osborne, Dawn Sedgley, and Adolf King. 1989. "Quantitative method for determining the concentration of mercury(II) sulphide in soils and sediments." *ANALYST* 114:823-825. doi: 10.1039/an9891400823.

Riscassi, Ami, Carrie Miller, and Scott Brooks. 2016. "Seasonal and flow-driven dynamics of particulate and dissolved mercury and methylmercury in a stream impacted by an industrial mercury source." *Environmental Toxicology and Chemistry* 35 (6):1386-1400. doi: 10.1002/etc.3310.

Rothschild, E. R., R. R. Turner, S. H. Stow, M. A. Bogle, L. K. Hyder, O. M. Sealand, and H. J. Wyrick. 1984. Investigation of Subsurface Mercury at the Oak Ridge Y-12 Plant. Oak Ridge, TN: Oak Ridge National Laboratory.

Rudd, John W. M., R. A. Bodaly, Nicholas S. Fisher, C. A. Kelly, Dianne Kopec, and Chris Whipple. 2018. "Fifty years after its discharge, methylation of legacy mercury trapped in the Penobscot Estuary sustains high mercury in biota." *Science of the Total Environment* 642:1340-1352. doi: 10.1016/j.scitotenv.2018.06.060.

Rytuba, James J. 2000. "Mercury mine drainage and processes that control its environmental impact." *Science of the Total Environment* 260:57-71. doi: 10.1016/S0048-9697(00)00541-6.

Schauble, Edwin A. 2007. "Role of nuclear volume in driving equilibrium stable isotope fractionation of mercury, thallium, and other very heavy elements." *Geochimica et Cosmochimica Acta* 71:2170-2189. doi: 10.1016/j.gca.2007.02.004.

Scheuhammer, Anton M., Michael W. Meyer, Mark B. Sandheinrich, and Michael W. Murray. 2007. "Effects of environmental methylmercury on the health of wild birds, mammals, and fish." *Ambio* 36 (1):12-18. doi: 10.1579/0044-7447(2007)36[12:eoemot]2.0.co;2.

Schnabel, Ed J., Steven Butler, Charles Ahlem, Jane Papazian, Craig Pedersen, William Porter, John Sharrah, Patricia M. Smith, Clifford C. Wisdom, and Gary M. Carlton. 1998. Mercury Concentrations and Loads from the Sacramento River and from Cache Creek to the Sacramento-San Joaquin Delta Estuary. Central Valley Region: California Regional Water Quality Control Board.

Smith, Robin S., Jan G. Wiederhold, and Ruben Kretzschmar. 2015. "Mercury isotope fractionation during precipitation of metacinnabar (β-HgS) and montroydite (HgO)." *Environmental Science & Technology* 49:4325-4334. doi: 10.1021/acs.est.5b00409.

Southworth, George, Mark Greeley, Mark Peterson, Kenneth Lowe, and Richard Ketelle. 2010. Sources of Mercury to East Fork Poplar Creek Downstream from the Y-12 National Security Complex: Inventories and Export Rates. Oak Ridge, TN: Oak Ridge National Laboratory.

Stetson, Sarah J., John E. Gray, Richard B. Wanty, and Donald L. Macalady. 2009. "Isotopic variability of mercury in ore, mine-waste calcine, and leachates of mine-waste calcine from areas mined for mercury." *Environmental Science & Technology* 43:7331-7336. doi: 10.1021/es9006993.

Sun, Ruoyu, David G. Streets, Hannah M. Horowitz, Helen M. Amos, Guijian Liu, Vincent Perrot, Jean-Paul Toutain, Holger Hintelmann, Elsie M. Sunderland, and Jeroen E. Sonke. 2016. "Historical (1850-2010) mercury stable isotope inventory from anthropogenic sources to the atmosphere." *Elementa: Science of the Anthropocene* 4:1-15. doi: 10.12952/journal.elementa.000091.

Turner, R. R., and G. R. Southworth. 1999. *Mercury Contaminated Sites–Characterization, Risk Assessment and Remediation*, edited by R. Ebinghaus, R. R. Turner, L. D. de Lacerda, O. Vasiliev and W. Salomons, 89-112. Springer-Verlag Berlin Heidelberg.

U.S. EPA. 2002. Method 1631, Revision E: Mercury in Water by Oxidation, Purge and Trap, and Cold Vapor Atomic Fluorescence Spectrometry. Washington, D.C.: U.S. Environmental Protection Agency, Office of Water.

UNEP. 2013. Global Mercury Assessment 2013: Sources, Emissions, Releases and Environmental Transport. Geneva, Switzerland: UNEP Chemicals Branch.

Vázquez-Rodríguez, Adiari I, Colleen M. Hansel, Tong Zhang, Carl H. Lamborg, Cara M. Santelli, Samuel M. Webb, and Scott C. Brooks. 2015. "Microbial- and thiosulfate-mediated dissolution of mercury sulfide minerals and transformation to gaseous mercury." *Frontiers in Microbiology* 6:1-11. doi: 10.3389/fmicb.2015.00596.

Vermeesch, Pieter. 2018. "IsoplotR: A free and open toolbox for geochronology." *Geoscience Frontiers* 9:1479-1493. doi: 10.1016/j.gsf.2018.04.001.

Wang, Qingren, Yuncong Li, and Y. Wang. 2011. "Optimizing the weight loss-on-ignition methodology to quantify organic and carbonate carbon of sediments from diverse sources." *Environmental Monitoring and Assessment* 174:241-257. doi: 10.1007/s10661-010-1454-z.

Waples, Jacob S., Kathryn L. Nagy, George R. Aiken, and Joseph N. Ryan. 2005. "Dissolution of cinnabar (HgS) in the presence of natural organic matter." *Geochimica et Cosmochimica Acta* 69 (6):1575-1588. doi: 10.1016/j.gca.2004.09.029.

Watson, David, Mark Bevelhimer, Craig Brandt, Chris DeRolph, Scott Brooks, Melanie Mayes, Todd Olsen, Johnbull Dickson, Mark Peterson, and Richard Ketelle. 2016a. Evaluation of Lower East Fork Poplar Creek Mercury Sources–Model Update. Oak Ridge, TN: Oak Ridge National Laboratory.

Watson, David, Scott Brooks, Teresa Mathews, Mark Bevelhimer, Chris DeRolph, Craig Brandt, Mark Peterson, and Richard Ketelle. 2016b. Evaluation of Lower East Fork Poplar Creek Mercury Sources. Oak Ridge, TN: Oak Ridge National Laboratory.

Wiederhold, Jan G. 2015. "Metal stable isotope signatures as tracers in environmental geochemistry." *Environmental Science & Technology* 49:2606-2624. doi: 10.1021/es504683e.

Wiederhold, Jan G., Christopher J. Cramer, Kelly Daniel, Ivan Infante, Bernard Bourdon, and Ruben Kretzschmar. 2010. "Equilibrium mercury isotope fractionation between dissolved

Hg(II) species and thiol-bound Hg." *Environmental Science & Technology* 44:4191-4197. doi: 10.1021/es100205t.

Wiederhold, Jan G., Stephan M. Kraemer, Nadya Teutsch, Paul M. Borer, Alex N. Halliday, and Ruben Kretzschmar. 2006. "Iron isotope fractionation during proton-promoted, ligand-controlled, and reductive dissolution of goethite." *Environmental Science and Technology* 40:3787-3793. doi: 10.1021/es052228y.

Wiederhold, Jan G., Ulf Skyllberg, Andreas Drott, Martin Jiskra, Sofi Jonsson, Erik Björn, Bernard Bourdon, and Ruben Kretzschmar. 2015. "Mercury isotope signatures in contaminated sediments as a tracer for local industrial pollution sources." *Environmental Science & Technology* 49:177-185. doi: 10.1021/es5044358.

Wiederhold, Jan G., Robin S. Smith, Hagar Siebner, Adam D. Jew, Gordon E. Brown Jr., Bernard Bourdon, and Ruben Kretzschmar. 2013. "Mercury isotope signatures as tracers for Hg cycling at the New Idria Hg Mine." *Environmental Science & Technology* 47:6137-6145. doi: 10.1021/es305245z.

WRRP, and UCOR. 2016. 2016 Remediation Effectiveness Report for the U.S. Department of Energy Oak Ridge Reservation, Oak Ridge, Tennessee: Data and Evaluations. prepared by the Water Resources Restoration Program and URS | CH2M Oak Ridge LLC.

WRRP, and UCOR. 2019. 2019 Remediation Effectiveness Report for the U.S. Department of Energy Oak Ridge Site, Oak Ridge, Tennessee: Data and Evaluations. prepared by the Water Resources Restoration Program and UCOR, an AECOM-led partnership with Jacobs.

Yang, Sha, and Yun Liu. 2015. "Nuclear volume effects in equilibrium stable isotope fractionations of mercury, thallium and lead." *Scientific Reports* 5:12626. doi: 10.1038/srep12626.

Yin, Runsheng, Xinbin Feng, Jianxu Wang, Zhengduo Bao, Ben Yu, and Jiubin Chen. 2013. "Mercury isotope variations between bioavailable mercury fractions and total mercury in mercury contaminated soil in Wanshan Mercury Mine, SW China." *Chemical Geology* 336:80-86. doi: 10.1016/j.chemgeo.2012.04.017.

Yin, Yujun, Herbert E. Allen, C. P. Huang, Donald L. Sparks, and Paul F. Sanders. 1997. "Kinetics of mercury(II) adsorption and desorption on soil." *Environmental Science & Technology* 31:496-503. doi: 10.1021/es9603214.

York, Derek. 1966. "Least-squares fitting of a straight line." *Canadian Journal of Physics* 44:1079-1086. doi: 10.1139/p66-090.

Zhang, Lijie, Xujun Liang, Quanying Wang, Yaoling Zhang, Xiangping Yin, Xia Lu, Eric M. Pierce, and Baohua Gu. 2021. "Isotope exchange between mercuric [Hg(II)] chloride and Hg(II) bound to minerals and thiolate ligands: Implications for enriched isotope tracer studies." *Geochimica et Cosmochimica Acta* 292:468-481. doi: 10.1016/j.gca.2020.10.013.

Zhang, Lijie, Shan Wu, Linduo Zhao, Xia Lu, Eric M. Pierce, and Baohua Gu. 2019. "Mercury sorption and desorption on organo-mineral particulates as a source for microbial methylation." *Environmental Science and Technology* 53:2426-2433. doi: 10.1021/acs.est.8b06020.

Zheng, Wang, Jason D. Demers, Xia Lu, Bridget A. Bergquist, Ariel D. Anbar, Joel D. Blum, and Baohua Gu. 2019. "Mercury stable isotope fractionation during abiotic dark oxidation in the presence of thiols and natural organic matter." *Environmental Science & Technology* 53:1853-1862. doi: 10.1021/acs.est.8b05047.

Zheng, Wang, and Holger Hintelmann. 2009. "Mercury isotope fractionation during photoreduction in natural water is controlled by its Hg/DOC ratio." *Geochimica et Cosmochimica Acta* 73:6704-6715. doi: 10.1016/j.gca.2009.08.016.
Zheng, Wang, and Holger Hintelmann. 2010a. "Isotope fractionation of mercury during its photochemical reduction by low-molecular-weight organic compounds." *Journal of Physical Chemistry A* 114 (12):4246-4253. doi: 10.1021/jp9111348.
Zheng, Wang, and Holger Hintelmann. 2010b. "Nuclear field shift effect in isotope fractionation of mercury during abiotic reduction in the absence of light." *J. Phys. Chem. A* 114:4238-4245. doi: 10.1021/jp910353y.

2.5 Supporting Information

2.5.1 Quality control for total mercury analyses

Cold vapor atomic fluorescence spectrometry (CVAFS) (U.S. EPA 2002) was used to measure total mercury (THg) concentrations of sequential extraction solutions and combustion 1% $KMnO_4$ trap solutions, as well as to determine percent recoveries after purge and trap and transfer procedures. Across all analytical sessions, the percent relative standard deviation (%RSD) of the mean calibration factor (CF_m) for calibration standards (2.5 to 500 pg Hg, or 0.5 to 100 ng L^{-1} on a volumetric basis) was 1.5% (SE = 0.2%, n=18). Average recovery of the lowest calibration standard relative to its expected value was 99.6% (SE = 0.7%, n=18). All initial and calibration verification blanks were below the reporting limit (i.e., the lowest calibration standard) (n=328). Initial calibration verification standards using a certified secondary Hg standard (100, 200, or 300 pg Hg) had an average recovery of 101.1% (SE = 0.3%, n=18). Instrument precision and recovery checks (25 pg Hg, or 5 ng L^{-1}) had an average recovery of 99.9% (SE = 0.3%, n=18). Continuing calibration verification standards (100, 200, or 300 pg Hg) had an average recovery of 101.2% (SE < 0.1%, n=268).

The method detection limit (MDL) was approximately 0.5 pg Hg, or 0.1 ng L^{-1}. The MDL was calculated using the equation MDL = t * SD, where t is the student's t-value appropriate for the single-tailed 99th percentile and a standard deviation estimate with n-1 degrees of freedom, and SD is the standard deviation associated with the average mass or concentration of Hg detected in replicate MDL check standards, which should be analyzed at a concentration ~5 times higher than the expected MDL value (U.S. EPA 2016). Our MDL check standards were analyzed at 2.5 pg Hg, or 0.5 ng L^{-1}. In our calculation of the MDL, the t-value was 2.57 (based on 17 degrees of freedom), and the SD value was 0.2 pg, or 0.04 ng L^{-1} (n=18).

To assess recovery for sequential extraction samples, matrix spike samples were analyzed, in which an aliquot of spiking solution was added to an aliquot of sample which had undergone UV treatment, which had an average recovery of 100.5% (SE = 0.1%, n=109). Additionally, aliquots of spiking solution were added to a subset of sequential extraction samples prior to undergoing UV treatment, which had an average recovery of 98.4% (SE = 0.5%, n=21). Relative percent difference among duplicate UV-treated sequential extraction sample analyses averaged 1.2% (SE=0.1%, n=17).

2.5.2 Sequential extraction reagents

Based on the sequential extraction procedure developed by Bloom *et al.* (2003), our reagents were made as follows. F1 (deionized water) was purged overnight with argon gas. F2 (0.1 M acetic acid + 0.01 M HCl) was made by diluting 6 mL glacial acetic acid + 0.8 mL trace metal grade HCl to 1000 mL with deionized water. F3 (1 M KOH) was made by diluting 86 mL of 45% (w/w) reagent grade KOH solution to 1000 mL with deionized water. F4 (12 M HNO_3) was made by diluting 750 mL trace metal grade HNO_3 to 1000 mL with deionized water. F5 (aqua regia) was made by adding 10 mL trace metal grade HCl, followed by 3 mL trace metal grade HNO_3, directly into centrifuge tubes. Reagents were diluted in trace metal clean glass volumetric flasks and stored in trace metal clean glass or Teflon bottles.

2.5.3 Comparison of sequential extractions of reference materials across multiple studies

Our study is one of three that has measured the isotopic composition of sequential extractions of NIST SRM 2711 (Montana Soil), each of which used different reagents to target organically-bound Hg. Wiederhold *et al.* (2015) performed a two-step extraction in which 6 M HNO_3 released 19% of the THg from NIST SRM 2711, and Grigg *et al.* (2018) performed a

four-step extraction in which 0.1 M $Na_4P_2O_7$ released 6.0% of the THg from NIST SRM 2711a. In our study, the 1 M KOH (F3) extraction step was used to target organically-bound Hg, which released 2.6 ± 0.2% (1SD, n=3) of the THg from NIST SRM 2711 and was isotopically similar to the residual Hg. For our analysis of NIST SRM 2711, δ^{202}Hg values of the F3 extraction and the weighted average of the F4 and F5 extractions were -0.25‰ and -0.19‰, respectively (± 0.08‰, 2SD) (Table S2.5). In the other two studies, the organically-bound fractions tended to be isotopically heavier than the residual Hg, although their delta values were also within analytical uncertainty. For Wiederhold *et al.* (2015), δ^{202}Hg values of the 6 M HNO_3 and aqua regia extractions of NIST SRM 2711 were 0.05‰ and -0.33‰, respectively (± 0.15‰, 2SD), and for Grigg *et al.* (2018), δ^{202}Hg values of the 0.1 M $Na_4P_2O_7$ and aqua regia extractions of NIST SRM 2711a were -0.01‰ and -0.13‰, respectively (± 0.11‰, 2SD). These differences among various study results are likely due to different reagents (6 M HNO_3, 0.1 M $Na_4P_2O_7$, and 1 M KOH) targeting different pools of Hg. Given the large range in the amount of Hg released by these various methods (2.6 to 19%), it seems plausible that different pools of organically-bound Hg with unique isotopic compositions could have been accessed. For example, soil and sediment are known to contain acid-soluble and base-soluble organic constituents (Aiken et al. 1985). Additionally, the 6 M HNO_3 step for Wiederhold *et al.* (2015) was isotopically more similar to our 12 M HNO_3 step (F4) and released ~7 times more Hg than to our 1 M KOH step (F3), further suggesting that the Hg species found in operationally-defined pools of organically-bound Hg likely differ slightly depending on which reagent is used. Alternatively, differences in the isotopic composition of organically-bound Hg may be due to differences between individual batches of NIST SRM 2711 and NIST SRM 2711a, as reported δ^{202}Hg values of individual batches of NRC MESS-3 have differed by as much as 0.38‰ (Blum and Johnson 2017),

although the bulk isotopic composition of individual batches of NIST SRM 2711 and NIST SRM 2711a has been shown to be fairly consistent (Wiederhold et al. 2015, Blum and Johnson 2017, Grigg et al. 2018).

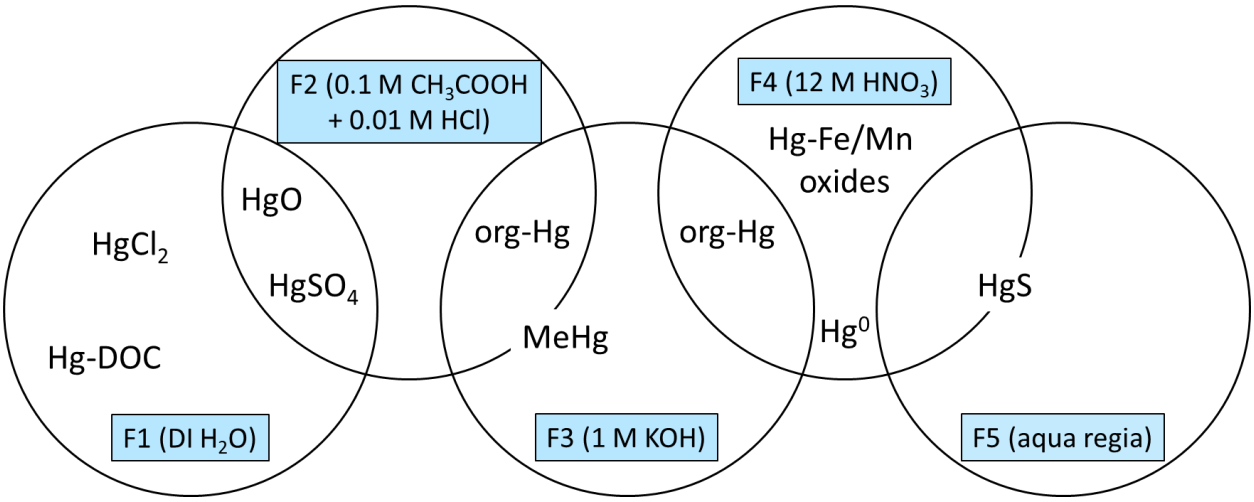

Figure S2.1. Schematic diagram showing Hg compounds that may be released during sequential extractions.

Blue boxes indicate the reagents used for the five-step sequential extraction procedure. Hg-DOC represents Hg bound to highly soluble or easily desorbable organic matter, while org-Hg represents Hg bound to less soluble or more strongly sorbed organic matter. Note that methylmercury (MeHg) makes up a small percentage (typically <0.05%) of THg in EFPC streambed sediment (Brooks et al. 2017). Also note that some Hg(0) may be released during earlier extraction steps. Placement of Hg compounds is approximate, and is based on information found in the literature (Eganhouse et al. 1978, Bloom et al. 2003, Hall et al. 2005, Brocza et al. 2019).

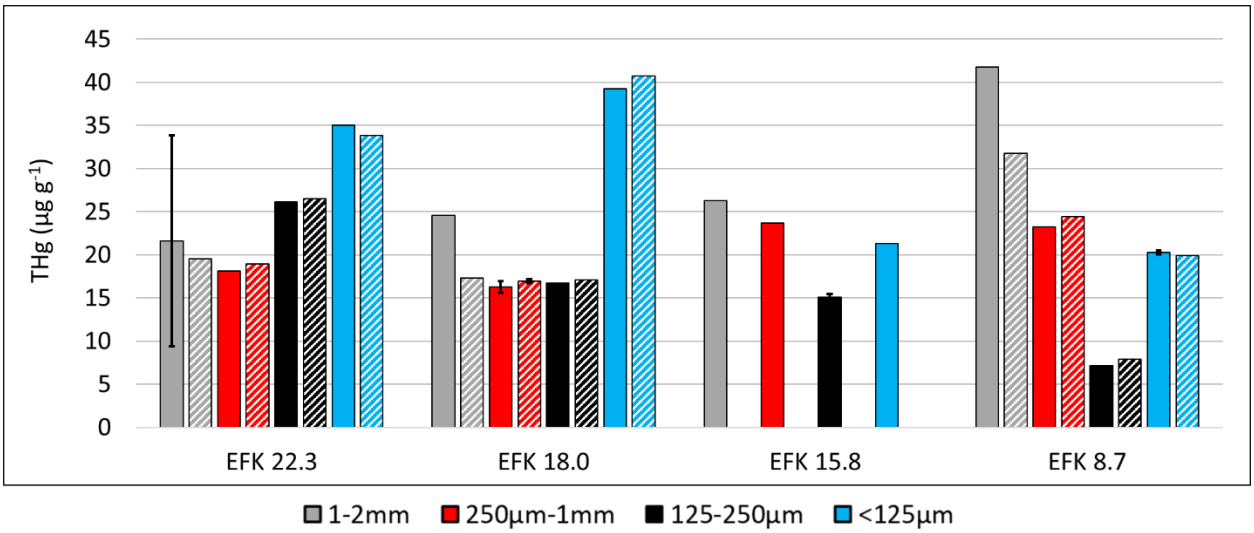

Figure S2.2. Total Hg concentration (µg g^{-1}) of EFPC streambed sediment, measured via combustion (solid bars) and the sum of sequential extractions (striped bars).

Error bars represent 1SD for combustion sample replicates (n=2) or sequential extraction replicates (n=2).

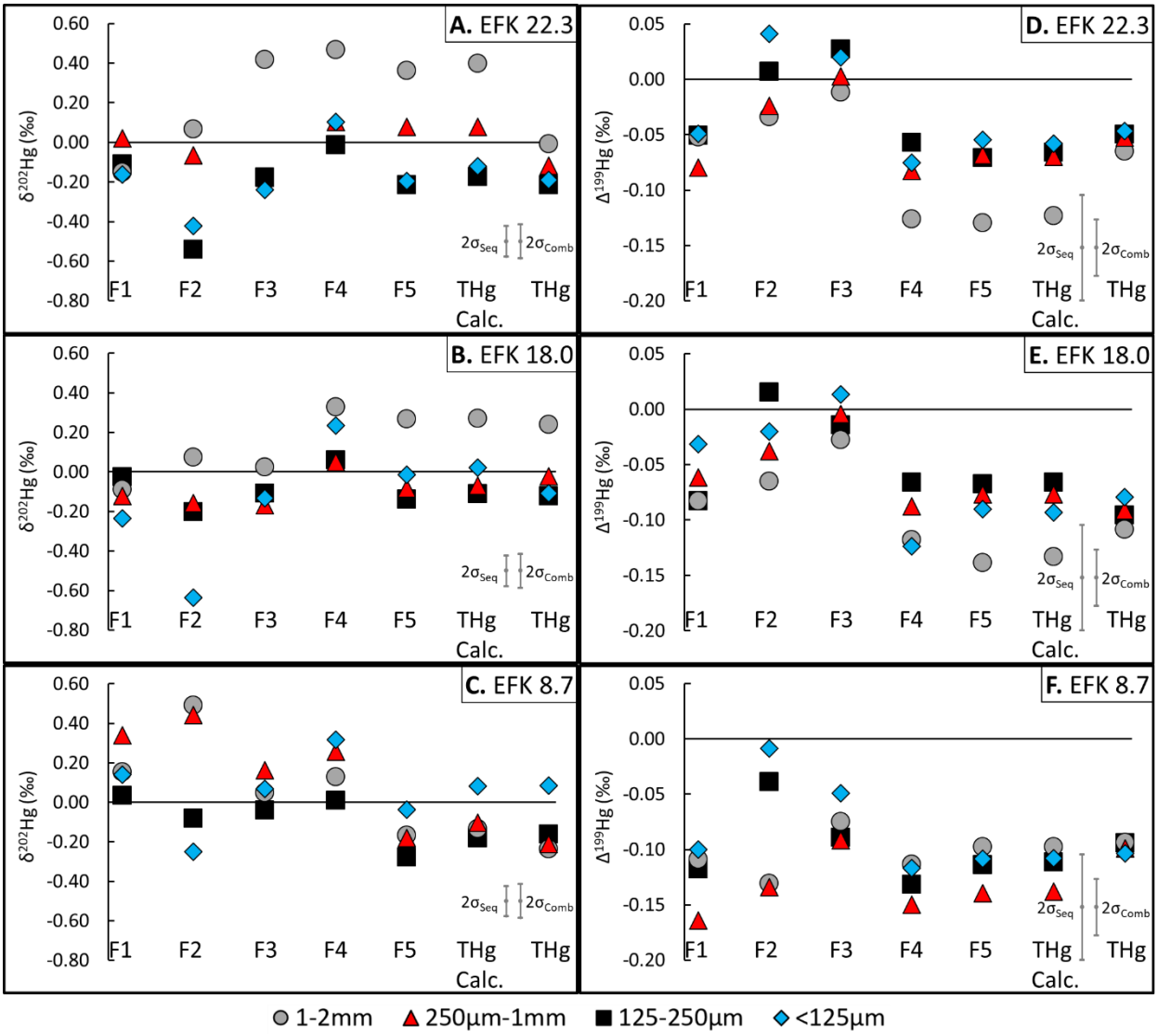

Figure S2.3. Mercury isotopic composition of sequential extractions of EFPC streambed sediment. Shown are (A-C) δ^{202}Hg and (D-F) Δ^{199}Hg of sequentially extracted Hg pools, the calculated total Hg based on the weighted average of sequential extraction concentrations (THg Calc.), and bulk sediment measured via combustion (THg).

Some of the THg points represent an average of combustion replicates (Table S2.3, Table S2.4). Analytical uncertainty in sequential extraction delta values is shown as the average uncertainty (2SD) across all UM-Almadén analyses ($2\sigma_{seq}$). Analytical uncertainty in combustion sample delta values is shown as the average uncertainty (2SD) across combustion reference material analyses ($2\sigma_{comb}$) (see Section 2.2.5).

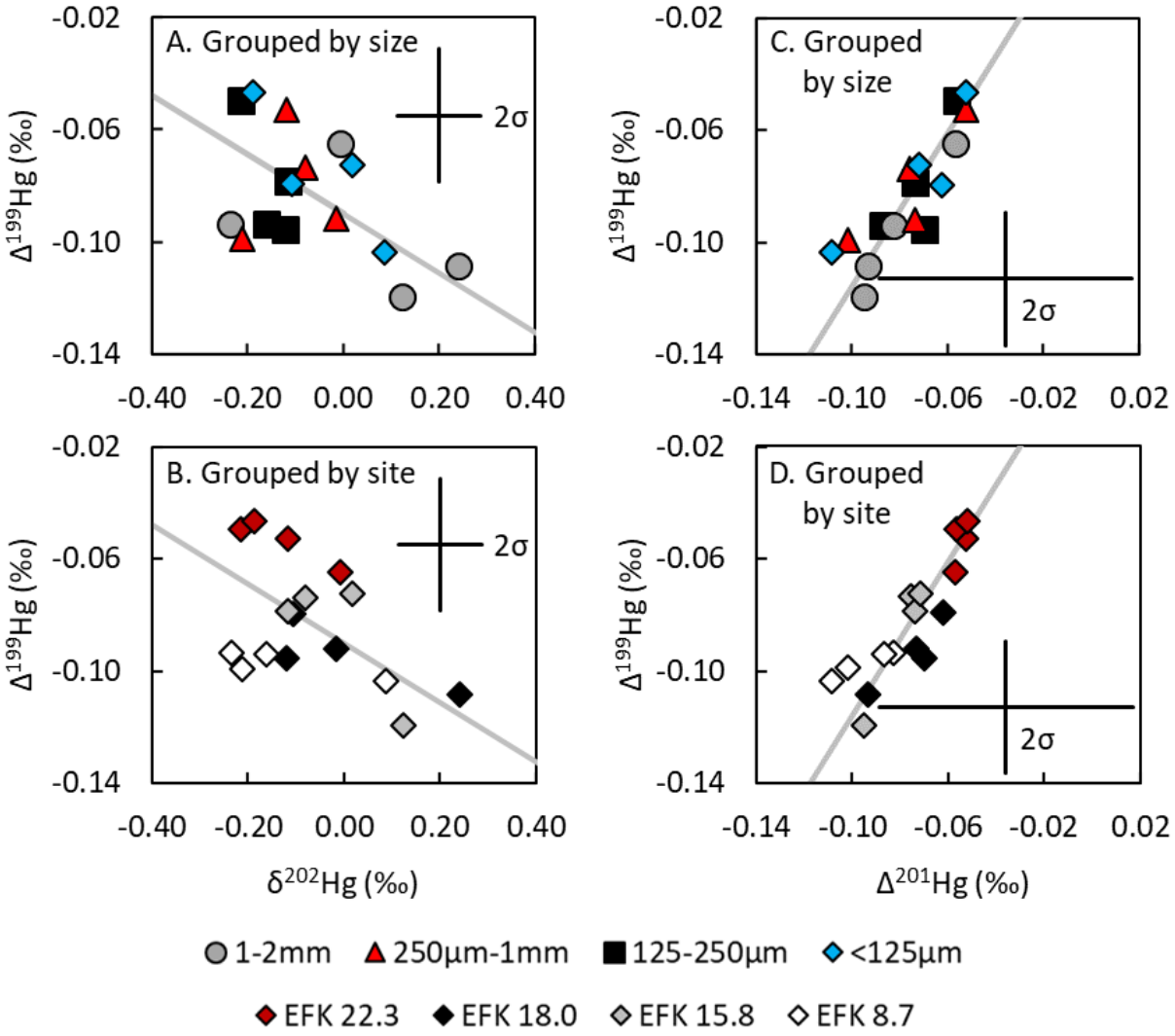

Figure S2.4. Mercury isotopic composition of EFPC streambed sediment, measured via combustion. Shown are (A and B) Δ^{199}Hg versus δ^{202}Hg and (C and D) Δ^{199}Hg versus Δ^{201}Hg for samples grouped by (A and C) sediment size fraction and (B and D) sampling site.

Analytical uncertainty in delta values is shown as the average uncertainty (2SD) across combustion reference material analyses (see Section 2.2.5). Using the York regression (York 1966), the Δ^{199}Hg/δ^{202}Hg slope is -0.11 (± 0.01, 1SE, n=16), and the Δ^{199}Hg/Δ^{201}Hg slope is 1.37 (± 0.21, 1SE, n=16). Slopes were generated using IsoplotR (Vermeesch 2018).

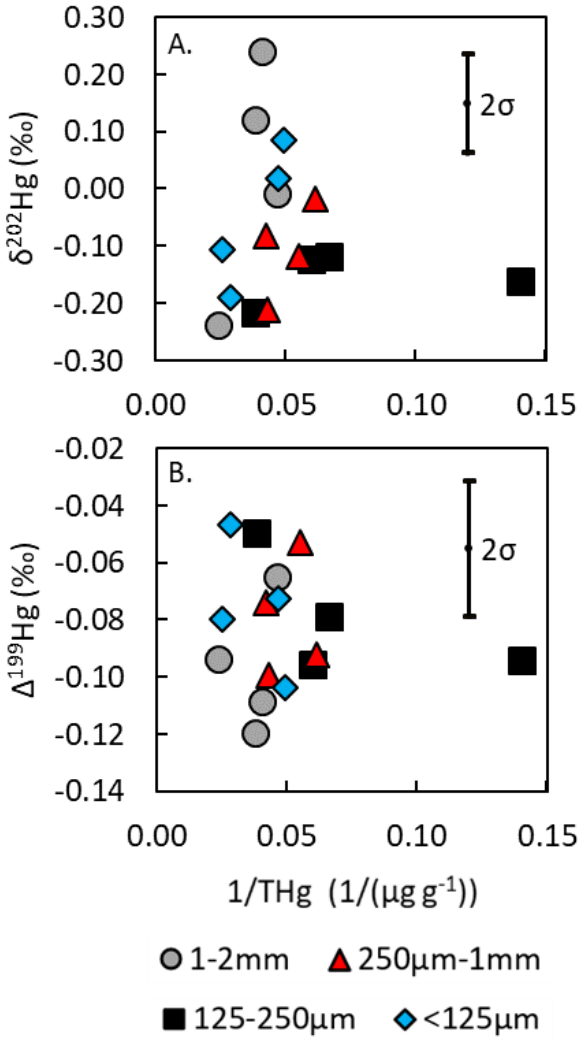

Figure S2.5. Mercury isotopic composition of EFPC streambed sediment, measured via combustion. Shown are (A) δ^{202}Hg and (B) Δ^{199}Hg versus inverse total Hg concentration.

Analytical uncertainty in delta values is shown as the average uncertainty (2SD) across combustion reference material analyses (see Section 2.2.5).

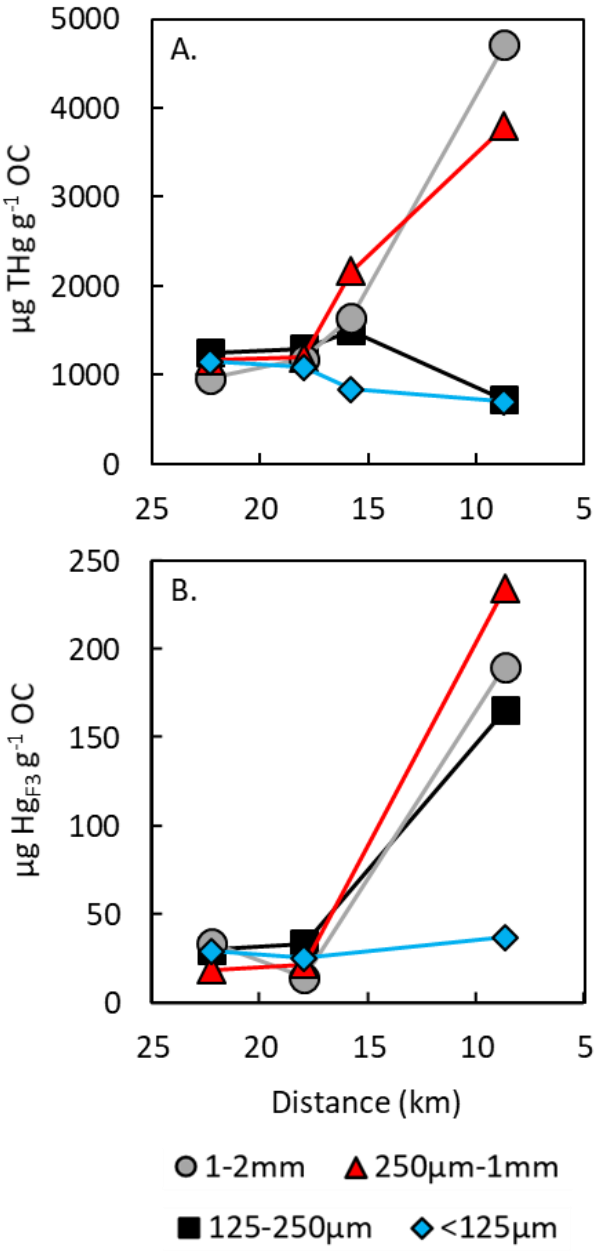

Figure S2.6. Concentrations of (A) total Hg and (B) F3-extracted Hg per mass of organic carbon for EFPC streambed sediment versus distance upstream of the confluence with Poplar Creek.

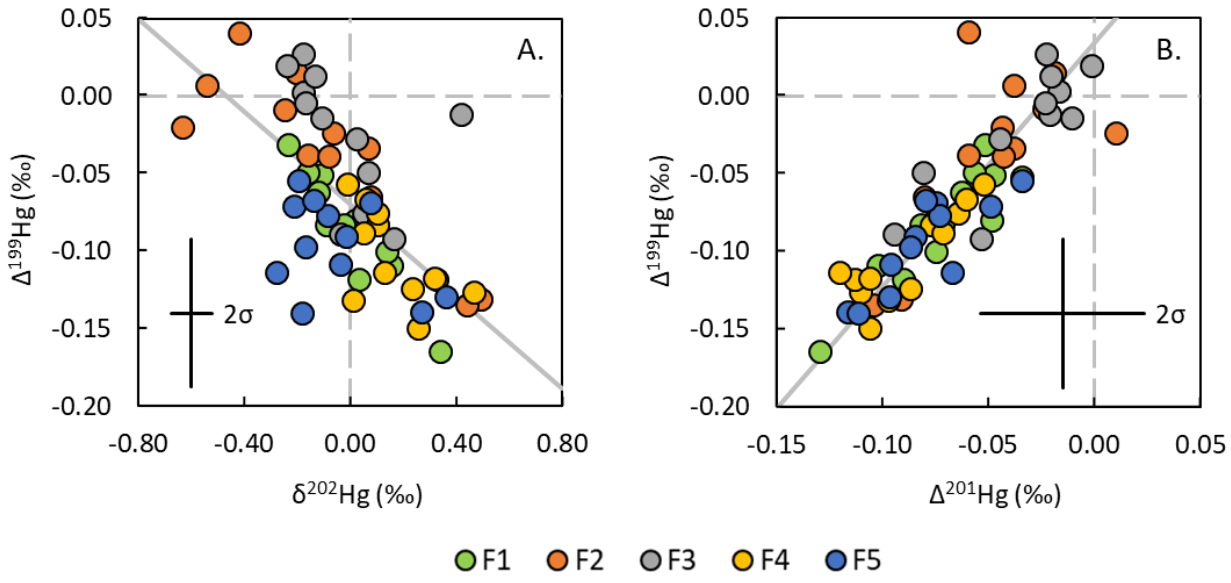

Figure S2.7. Mercury isotopic composition of sequential extractions of EFPC streambed sediment. Shown are (A) Δ^{199}Hg versus δ^{202}Hg and (B) Δ^{199}Hg versus Δ^{201}Hg across all sampling sites and size fractions.

Analytical uncertainty in delta values is shown as the average uncertainty (2SD) across all UM-Almadén analyses (see Section 2.2.5). Using the York regression (York 1966), the Δ^{199}Hg/δ^{202}Hg slope is -0.15 (± 0.01, 1SE, n=60), and the Δ^{199}Hg/Δ^{201}Hg slope is 1.57 (± 0.16, 1SE, n=60). Slopes were generated using IsoplotR (Vermeesch 2018).

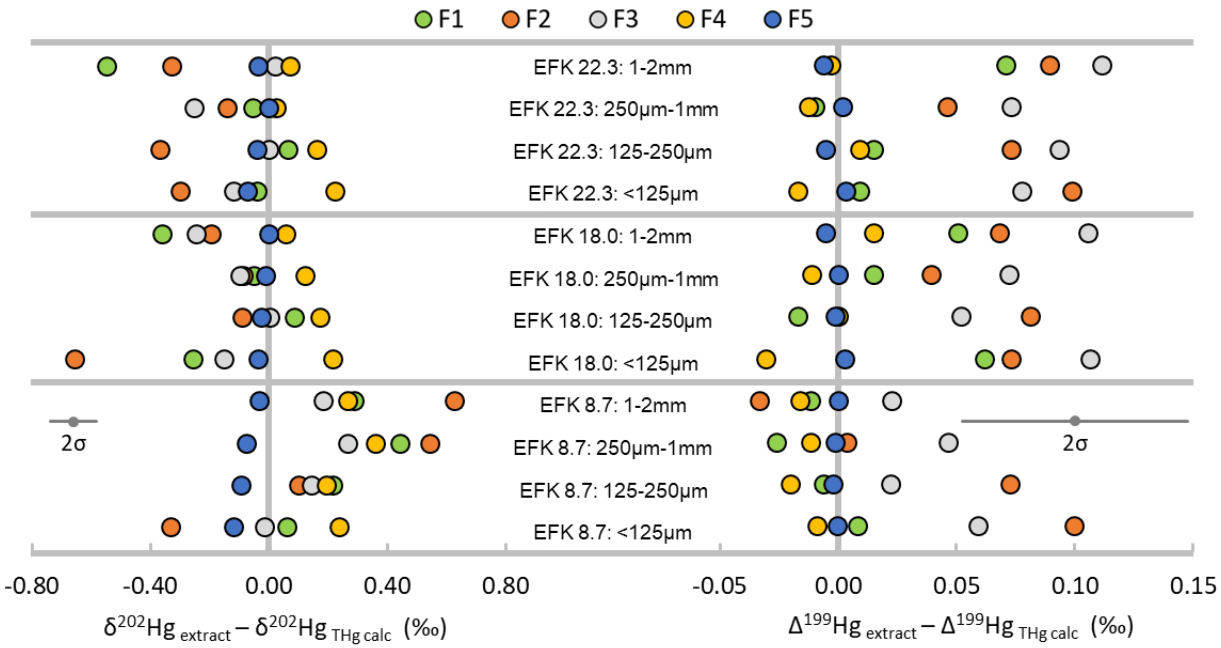

Figure S2.8. Offsets in isotopic composition ($\delta^{202}Hg$ and $\Delta^{199}Hg$) of sequential extractions relative to the isotopic composition of bulk sediment calculated via the weighted average of the five sequential extractions for each sediment size fraction.

Analytical uncertainty in delta values is shown as the average uncertainty (2SD) across all UM-Almadén analyses (see Section 2.2.5).

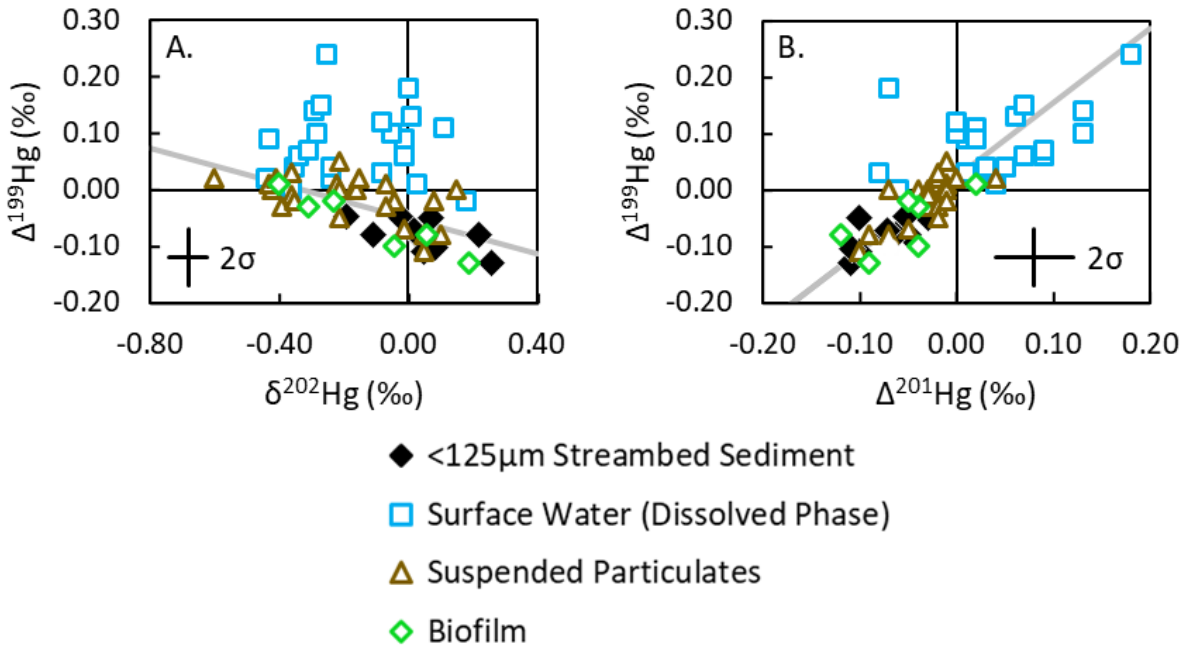

Figure S2.9. Mercury isotopic composition of <125µm streambed sediment (including sediment analyzed in this study as well as by Donovan *et al.* (2014)), along with EFPC surface water (dissolved phase), suspended particulates, and biofilm analyzed by Demers *et al.* (2018). Shown are (A) Δ^{199}Hg versus δ^{202}Hg and (B) Δ^{199}Hg versus Δ^{201}Hg.

Analytical uncertainty in delta values is shown as the average uncertainty (2SD) across all UM-Almadén analyses as defined by Demers *et al.* (2018), which is similar to this study, though the analytical uncertainty for sediment analyzed by Donovan *et al.* (2014) is somewhat larger. Using the York regression (York 1966), the Δ^{199}Hg/δ^{202}Hg slope for suspended particulates and <125µm streambed sediment combined is -0.16 (± 0.02, 1SE, n=34), and the Δ^{199}Hg/Δ^{201}Hg slope is 1.32 (± 0.20, 1SE, n=34). Slopes were generated using IsoplotR (Vermeesch 2018).

Table S2.1. Mass and Hg fractions of each grain size of EFPC streambed sediment within each sampling site.

Site ID	1-2mm		250µm-1mm		125-250µm		<125µm	
	Mass Fraction	Hg Fraction	Mass Fraction	Hg Fraction	Mass Fraction	Hg Fraction	Mass Fraction	Hg Fraction
EFK 22.3	42%	41%	40%	33%	4%	5%	14%	22%
EFK 18.0	42%	49%	50%	39%	3%	2%	5%	9%
EFK 15.8	40%	43%	53%	51%	2%	1%	5%	4%
EFK 8.7	43%	59%	45%	34%	3%	1%	9%	6%

Mass fraction is based on freeze dried masses of each sediment size fraction within each site. Hg fraction is based on THg concentrations (measured via combustion) normalized to the mass fraction of each sediment size fraction within each site. Excludes >2mm sediment.

Table S2.2. Mercury isotopic composition of UM-Almadén and procedural standards.

Standard Type	n	δ^{202}Hg (‰)	2σ (‰)	Δ^{204}Hg (‰)	2σ (‰)	Δ^{201}Hg (‰)	2σ (‰)	Δ^{200}Hg (‰)	2σ (‰)	Δ^{199}Hg (‰)	2σ (‰)
UM-Almadén	25	-0.55	0.01	-0.01	0.01	-0.04	0.00	0.01	0.00	-0.03	0.00
Purge & Trap NIST SRM 3133	21	0.00	0.02	0.00	0.01	0.00	0.01	0.00	0.01	0.00	0.01
NIST SRM 2711 (Montana Soil)	2	-0.21	0.02	0.04	0.05	-0.19	0.01	-0.01	0.01	-0.23	0.02
NIST SRM 2711 (Montana Soil) Long-term average	11	-0.18	0.05	-0.01	0.03	-0.19	0.02	-0.01	0.01	-0.24	0.01
NIST SRM 1944 (NY/NJ Sediment)	1	-0.43	-	-0.01	-	-0.01	-	0.01	-	0.00	-
NIST SRM 1944 (NY/NJ Sediment) Long-term average	62	-0.43	0.01	-0.01	0.01	-0.02	0.01	0.01	0.01	0.00	0.01

For UM-Almadén, n is the number of preparations (i.e. the number of session averages, with preparations at different concentrations counted separately). For procedural standards, n is the number of completely independent preparations of the material (via purge and trap or combustions). Isotope ratios represent the average value (± 2SE) across independent preparations for each standard type. Long-term average isotopic compositions are included for comparison (Blum and Johnson 2017).

Table S2.3. Mercury concentration and isotopic composition of EFPC streambed sediment measured via combustion.

Site ID	Size Fraction	THg ($\mu g\ g^{-1}$)	n_1	n_2	n_3	% Rec.	δ^{202}Hg (‰)	2σ (‰)	Δ^{204}Hg (‰)	2σ (‰)	Δ^{201}Hg (‰)	2σ (‰)	Δ^{200}Hg (‰)	2σ (‰)	Δ^{199}Hg (‰)	2σ (‰)
EFK 22.3	1-2mm	21.60	2	3	9	92.8	-0.01	0.09	0.01	0.01	-0.06	0.05	-0.01	0.02	-0.06	0.02
	250µm-1mm	18.14	1	1	3	93.5	-0.12	0.09	0.00	0.01	-0.05	0.05	0.01	0.02	-0.05	0.02
	125-250µm	26.15	1	1	2	97.2	-0.22	0.09	-0.01	0.01	-0.06	0.05	0.01	0.02	-0.05	0.02
	<125µm	35.00	1	1	2	95.5	-0.19	0.09	0.02	0.01	-0.05	0.05	0.01	0.02	-0.05	0.02
EFK 18.0	1-2mm	24.58	1	1	2	94.1	0.24	0.09	-0.02	0.01	-0.09	0.05	-0.02	0.02	-0.11	0.02
	250µm-1mm	16.28	2	3	7	96.6	-0.02	0.09	-0.01	0.01	-0.07	0.05	-0.01	0.02	-0.09	0.02
	125-250µm	16.75	1	1	2	97.4	-0.12	0.09	0.00	0.01	-0.07	0.05	0.00	0.02	-0.10	0.02
	<125µm	39.27	1	1	3	97.7	-0.11	0.09	0.02	0.01	-0.06	0.05	0.00	0.02	-0.08	0.02
EFK 15.8	1-2mm	26.30	1	1	3	96.1	0.12	0.09	-0.01	0.01	-0.10	0.05	0.00	0.02	-0.12	0.02
	250µm-1mm	23.68	1	1	2	96.9	-0.08	0.09	-0.01	0.01	-0.08	0.05	0.01	0.02	-0.07	0.02
	125-250µm	15.07	2	3	8	95.2	-0.12	0.09	0.00	0.01	-0.07	0.05	0.00	0.02	-0.08	0.02
	<125µm	21.32	1	1	2	97.3	0.02	0.09	-0.02	0.01	-0.07	0.05	0.00	0.02	-0.07	0.02
EFK 8.7	1-2mm	41.77	1	1	2	92.1	-0.24	0.09	0.01	0.01	-0.08	0.05	0.02	0.02	-0.09	0.02
	250µm-1mm	23.22	1	1	4	96.2	-0.21	0.09	0.03	0.01	-0.10	0.05	0.01	0.02	-0.10	0.02
	125-250µm	7.14	1	1	2	97.6	-0.16	0.09	0.01	0.01	-0.09	0.05	0.00	0.02	-0.09	0.02
	<125µm	20.26	2	3	6	96.2	0.09	0.09	0.01	0.01	-0.11	0.05	-0.01	0.02	-0.10	0.02

Sieved streambed sediment was collected from four sites along EFPC. Site ID refers to the sampling location identified by the number of kilometers upstream of the confluence of Poplar Creek and EFPC. Here, n_1 denotes the number of sample replicates that were ground independently prior to combustions, n_2 denotes the number of combustion preparations, and n_3 denotes the number of separate isotopic analyses on an individual preparation(s). The percent recovery (% Rec.) shows recovery of Hg during the transfer procedure for preparation of combustion samples for isotope analysis. The uncertainty in the isotopic composition of Hg in combustion samples is represented by the average uncertainty (2SD) across combustion reference material analyses.

Table S2.4. Comparison of combustion replicates.

Sample ID	Replicates	THg ($\mu g\ g^{-1}$)	n_1	% Rec.	δ^{202}Hg (‰)	2σ (‰)	Δ^{204}Hg (‰)	2σ (‰)	Δ^{201}Hg (‰)	2σ (‰)	Δ^{200}Hg (‰)	2σ (‰)	Δ^{199}Hg (‰)	2σ (‰)
EFK 22.3 1-2mm	Rep 1, C1	30.32	3	94.1	-0.14	0.09	0.01	0.01	-0.05	0.05	0.00	0.02	-0.05	0.02
	Rep 1, C2	30.20	3	92.7	-0.20	0.09	0.00	0.01	-0.05	0.05	0.00	0.02	-0.03	0.02
	Rep 2	12.94	3	92.2	0.15	0.09	0.02	0.01	-0.06	0.05	-0.01	0.02	-0.09	0.02
EFK 18.0 250µm-1mm	Rep 1, C1	15.98	2	99.3	0.04	0.09	0.01	0.01	-0.08	0.05	0.00	0.02	-0.10	0.02
	Rep 1, C2	15.65	3	96.2	-0.06	0.09	0.01	0.01	-0.07	0.05	0.00	0.02	-0.08	0.02
	Rep 2	16.75	2	95.4	-0.02	0.09	-0.03	0.01	-0.08	0.05	-0.01	0.02	-0.09	0.02
EFK 15.8 125-250µm	Rep 1, C1	14.90	3	97.6	-0.13	0.09	0.00	0.01	-0.06	0.05	0.00	0.02	-0.08	0.02
	Rep 1, C2	14.69	3	94.2	-0.12	0.09	-0.01	0.01	-0.08	0.05	0.01	0.02	-0.07	0.02
	Rep 2	15.35	2	94.6	-0.11	0.09	0.01	0.01	-0.07	0.05	0.01	0.02	-0.08	0.02
EFK 8.7 <125µm	Rep 1, C1	20.30	2	98.5	0.06	0.09	0.02	0.01	-0.09	0.05	0.01	0.02	-0.11	0.02
	Rep 1, C2	19.92	2	93.7	0.13	0.09	0.02	0.01	-0.08	0.05	-0.01	0.02	-0.10	0.02
	Rep 2	20.41	2	96.3	0.08	0.09	0.01	0.01	-0.13	0.05	-0.02	0.02	-0.11	0.02
NIST SRM 2711 (Montana Soil)	Rep 1	6.56	3	95.9	-0.22	0.09	0.06	0.01	-0.19	0.05	-0.02	0.02	-0.24	0.02
	Rep 2	6.57	3	92.7	-0.20	0.09	0.01	0.01	-0.19	0.05	-0.01	0.02	-0.22	0.02

Sieved streambed sediment was collected from four sites along EFPC. Sample ID refers to the sediment size fraction and the sampling location identified by the number of kilometers upstream of the confluence of Poplar Creek and EFPC. Rep 1 and Rep 2 refer to sample replicates that were ground independently prior to combustions. C1 and C2 refer to combustion process replicates, which used aliquots of ground sediment from the same vial. Here, n_1 denotes the number of separate isotopic analyses on an individual preparation. The percent recovery (% Rec.) shows recovery of Hg during the transfer procedure for preparation of combustion samples for isotope analysis. The uncertainty in the isotopic composition of Hg in combustion samples is represented by the average uncertainty (2SD) across combustion reference material analyses.

Table S2.5. Mercury concentration and isotopic composition of sequential extractions of standard reference materials.

Reference Material	Sequential Extraction	THg (μg g^{-1})	% of THg	n_1	n_2	n_3	% Rec.	δ^{202}Hg (‰)	2σ (‰)	Δ^{204}Hg (‰)	2σ (‰)	Δ^{201}Hg (‰)	2σ (‰)	Δ^{200}Hg (‰)	2σ (‰)	Δ^{199}Hg (‰)	2σ (‰)
NIST SRM 2711 (Montana Soil)	F1	0.07	1.2	3	4	5	98.4	-0.21	0.08	0.02	0.08	-0.16	0.04	0.00	0.04	-0.20	0.05
	F2	0.00	0.1	2	2	2	96.0	-0.81	0.08	0.03	0.08	-0.06	0.04	0.06	0.04	-0.10	0.05
	F3	0.15	2.6	3	5	9	97.5	-0.25	0.08	0.00	0.08	-0.15	0.04	-0.01	0.04	-0.19	0.05
	F4	4.07	68.3	3	4	7	97.7	-0.09	0.08	0.01	0.08	-0.20	0.04	0.00	0.04	-0.23	0.05
	F5	1.66	27.8	3	4	7	98.9	-0.43	0.08	0.02	0.08	-0.18	0.04	-0.01	0.04	-0.22	0.05
	Calc. THg	5.96					95.4	-0.19	0.08	0.01	0.08	-0.19	0.04	0.00	0.04	-0.22	0.05
NIST SRM 1944 (NY/NJ Waterway Sediment)	F1	0.02	0.4	1	1	1	95.1	-0.41	0.08	0.13	0.08	0.00	0.04	0.13	0.04	-0.09	0.05
	F2	0.00	<0.1	Insufficient mercury for isotopic analysis.													
	F3	0.31	8.8	1	2	3	95.7	-0.39	0.08	-0.02	0.08	0.01	0.04	0.00	0.04	0.04	0.05
	F4	2.77	79.6	1	3	4	97.5	-0.40	0.08	0.02	0.08	-0.01	0.04	-0.01	0.04	-0.01	0.05
	F5	0.39	11.1	1	2	3	95.6	-1.46	0.08	0.00	0.08	-0.10	0.04	0.01	0.04	-0.12	0.05
	Calc. THg	3.48					102.3	-0.52	0.08	0.02	0.08	-0.02	0.04	-0.01	0.04	-0.02	0.05

Five-step sequential extractions were performed on two standard reference materials. Calc. THg refers to the calculated THg concentration and isotopic composition of the material based on the weighted average of sequential extractions. Here, n_1 denotes the number of sequential extraction sets, n_2 denotes the number of purge and trap preparations, and n_3 denotes the number of separate isotopic analyses on an individual preparation(s). The percent recovery (% Rec.) for F1 – F5 shows recovery of Hg during the purge and trap procedure for preparation of sequential extraction samples for isotope analysis. The percent recovery for Calc. THg is based on the sum of sequential extractions relative to certified values. The uncertainty in the isotopic composition of Hg in sequential extraction samples is represented by the average uncertainty (2SD) across all UM-Almadén analyses.

Table S2.6a. Mercury concentration and isotopic composition of sequential extractions of EFPC streambed sediment at EFK 22.3.

Sample ID	Sequential Extraction	THg (μg g^{-1})	% of THg	n_1	n_2	n_3	% Rec.	δ^{202}Hg (‰)	2σ (‰)	Δ^{204}Hg (‰)	2σ (‰)	Δ^{201}Hg (‰)	2σ (‰)	Δ^{200}Hg (‰)	2σ (‰)	Δ^{199}Hg (‰)	2σ (‰)
EFK 22.3 1-2mm	F1	0.08	0.4	1	2	4	91.5	-0.15	0.08	0.00	0.08	-0.03	0.04	-0.01	0.04	-0.05	0.05
	F2	0.09	0.5	1	2	5	96.0	0.07	0.08	-0.03	0.08	-0.04	0.04	0.01	0.04	-0.03	0.05
	F3	0.75	3.8	1	1	2	101.5	0.42	0.08	-0.06	0.08	-0.02	0.04	0.01	0.04	-0.01	0.05
	F4	6.73	34.4	1	1	2	96.7	0.47	0.08	0.01	0.08	-0.11	0.04	-0.02	0.04	-0.13	0.05
	F5	11.92	60.9	1	1	2	93.7	0.36	0.08	0.01	0.08	-0.10	0.04	-0.01	0.04	-0.13	0.05
	Calc. THg	19.57					90.6	0.40	0.08	0.00	0.08	-0.10	0.04	-0.01	0.04	-0.12	0.05
EFK 22.3 250μm-1mm	F1	0.31	1.6	1	1	2	96.8	0.02	0.08	-0.02	0.08	-0.05	0.04	-0.01	0.04	-0.08	0.05
	F2	0.01	<0.1	1	1	1	97.2	-0.07	0.08	0.02	0.08	0.01	0.04	-0.01	0.04	-0.02	0.05
	F3	0.29	1.5	1	2	5	96.6	-0.18	0.08	-0.01	0.08	-0.02	0.04	0.02	0.04	0.00	0.05
	F4	3.49	18.4	1	1	2	95.8	0.10	0.08	-0.02	0.08	-0.08	0.04	-0.02	0.04	-0.08	0.05
	F5	14.83	78.4	1	1	2	99.5	0.08	0.08	0.00	0.08	-0.07	0.04	0.00	0.04	-0.07	0.05
	Calc. THg	18.92					104.3	0.08	0.08	-0.01	0.08	-0.07	0.04	-0.01	0.04	-0.07	0.05
EFK 22.3 125-250μm	F1	0.15	0.6	1	1	2	98.5	-0.11	0.08	-0.02	0.08	-0.05	0.04	0.01	0.04	-0.05	0.05
	F2	0.00	<0.1	1	1	1	98.9	-0.54	0.08	-0.01	0.08	-0.04	0.04	0.01	0.04	0.01	0.05
	F3	0.62	2.4	1	1	2	96.3	-0.18	0.08	-0.02	0.08	-0.02	0.04	0.03	0.04	0.03	0.05
	F4	5.22	19.7	1	1	2	97.6	-0.01	0.08	-0.02	0.08	-0.05	0.04	0.01	0.04	-0.06	0.05
	F5	20.48	77.3	1	2	5	95.3	-0.21	0.08	0.03	0.08	-0.05	0.04	0.01	0.04	-0.07	0.05
	Calc. THg	26.48					101.3	-0.17	0.08	0.02	0.08	-0.05	0.04	0.01	0.04	-0.07	0.05
EFK 22.3 <125μm	F1	0.07	0.2	1	2	4	97.5	-0.16	0.08	-0.01	0.08	-0.06	0.04	0.00	0.04	-0.05	0.05
	F2	0.01	<0.1	1	1	1	96.5	-0.42	0.08	-0.04	0.08	-0.06	0.04	0.02	0.04	0.04	0.05
	F3	0.89	2.6	1	1	2	102.5	-0.24	0.08	0.03	0.08	0.00	0.04	0.01	0.04	0.02	0.05
	F4	8.57	25.3	1	2	4	96.8	0.10	0.08	-0.02	0.08	-0.06	0.04	0.00	0.04	-0.08	0.05
	F5	24.31	71.8	1	1	2	95.9	-0.19	0.08	-0.01	0.08	-0.03	0.04	0.00	0.04	-0.05	0.05
	Calc. THg	33.85					96.7	-0.12	0.08	-0.01	0.08	-0.04	0.04	0.00	0.04	-0.06	0.05

See Table S2.6c for notes.

Table S2.6b. Mercury concentration and isotopic composition of sequential extractions of EFPC streambed sediment at EFK 18.0.

Sample ID	Sequential Extraction	THg (μg g^{-1})	% of THg	n_1	n_2	n_3	% Rec.	δ^{202}Hg (‰)	2σ (‰)	Δ^{204}Hg (‰)	2σ (‰)	Δ^{201}Hg (‰)	2σ (‰)	Δ^{200}Hg (‰)	2σ (‰)	Δ^{199}Hg (‰)	2σ (‰)
EFK 18.0 1-2mm	F1	0.10	0.6	1	1	2	99.6	-0.09	0.08	0.01	0.08	-0.08	0.04	-0.03	0.04	-0.08	0.05
	F2	0.02	0.1	1	2	2	96.6	0.08	0.08	-0.01	0.08	-0.08	0.04	0.00	0.04	-0.06	0.05
	F3	0.30	1.7	1	1	2	101.4	0.02	0.08	-0.01	0.08	-0.04	0.04	0.00	0.04	-0.03	0.05
	F4	2.70	15.6	1	1	2	101.0	0.33	0.08	-0.02	0.08	-0.11	0.04	-0.02	0.04	-0.12	0.05
	F5	14.19	82.0	1	1	2	104.0	0.27	0.08	-0.03	0.08	-0.12	0.04	-0.02	0.04	-0.14	0.05
	Calc. THg	17.31					70.4	0.27	0.08	-0.03	0.08	-0.11	0.04	-0.02	0.04	-0.13	0.05
EFK 18.0 250μm-1mm	F1	0.23	1.3	2	2	4	100.4	-0.12	0.08	0.02	0.08	-0.06	0.04	0.01	0.04	-0.06	0.05
	F2	0.01	0.1	2	2	2	97.2	-0.16	0.08	-0.01	0.08	-0.06	0.04	0.00	0.04	-0.04	0.05
	F3	0.29	1.7	2	2	4	99.9	-0.17	0.08	-0.01	0.08	-0.02	0.04	0.02	0.04	0.00	0.05
	F4	1.97	11.6	2	3	7	98.7	0.05	0.08	0.01	0.08	-0.07	0.04	0.00	0.04	-0.09	0.05
	F5	14.43	85.2	2	2	4	100.2	-0.08	0.08	-0.02	0.08	-0.07	0.04	0.00	0.04	-0.08	0.05
	Calc. THg	16.93					104.0	-0.07	0.08	-0.01	0.08	-0.07	0.04	0.00	0.04	-0.08	0.05
EFK 18.0 125-250μm	F1	0.11	0.7	1	2	5	99.5	-0.02	0.08	-0.01	0.08	-0.07	0.04	0.00	0.04	-0.08	0.05
	F2	0.00	<0.1	1	1	1	96.7	-0.20	0.08	-0.04	0.08	-0.02	0.04	0.00	0.04	0.02	0.05
	F3	0.43	2.5	1	1	2	99.0	-0.11	0.08	0.02	0.08	-0.01	0.04	0.02	0.04	-0.01	0.05
	F4	2.16	12.6	1	1	2	97.3	0.06	0.08	-0.01	0.08	-0.06	0.04	0.00	0.04	-0.07	0.05
	F5	14.40	84.2	1	1	2	100.0	-0.14	0.08	0.01	0.08	-0.08	0.04	-0.01	0.04	-0.07	0.05
	Calc. THg	17.11					102.1	-0.11	0.08	0.01	0.08	-0.08	0.04	-0.01	0.04	-0.07	0.05
EFK 18.0 <125μm	F1	0.04	0.1	1	1	2	99.2	-0.24	0.08	-0.02	0.08	-0.05	0.04	0.01	0.04	-0.03	0.05
	F2	0.01	<0.1	1	1	1	96.9	-0.64	0.08	-0.01	0.08	-0.04	0.04	-0.01	0.04	-0.02	0.05
	F3	0.91	2.2	1	1	2	98.7	-0.13	0.08	-0.03	0.08	-0.02	0.04	0.02	0.04	0.01	0.05
	F4	6.29	15.4	1	1	2	99.8	0.24	0.08	-0.01	0.08	-0.09	0.04	-0.01	0.04	-0.12	0.05
	F5	33.52	82.2	1	2	5	100.6	-0.01	0.08	-0.01	0.08	-0.08	0.04	-0.01	0.04	-0.09	0.05
	Calc. THg	40.76					103.8	0.02	0.08	-0.01	0.08	-0.08	0.04	-0.01	0.04	-0.09	0.05

See Table S2.6c for notes.

Table S2.6c. Mercury concentration and isotopic composition of sequential extractions of EFPC streambed sediment at EFK 8.7.

Sample ID	Sequential Extraction	THg (μg g^{-1})	% of THg	n_1	n_2	n_3	% Rec.	δ^{202}Hg (‰)	2σ (‰)	Δ^{204}Hg (‰)	2σ (‰)	Δ^{201}Hg (‰)	2σ (‰)	Δ^{200}Hg (‰)	2σ (‰)	Δ^{199}Hg (‰)	2σ (‰)
EFK 8.7 1-2mm	F1	0.20	0.6	1	2	4	104.8	0.15	0.08	0.00	0.08	-0.10	0.04	0.00	0.04	-0.11	0.05
	F2	0.04	0.1	1	2	2	101.0	0.49	0.08	0.05	0.08	-0.09	0.04	0.02	0.04	-0.13	0.05
	F3	1.68	5.3	1	1	2	105.1	0.05	0.08	-0.04	0.08	-0.07	0.04	0.01	0.04	-0.07	0.05
	F4	2.05	6.5	1	1	2	102.5	0.13	0.08	0.02	0.08	-0.12	0.04	0.00	0.04	-0.11	0.05
	F5	27.80	87.5	1	1	2	107.7	-0.17	0.08	-0.01	0.08	-0.09	0.04	-0.01	0.04	-0.10	0.05
	Calc. THg	31.77					76.1	-0.13	0.08	-0.01	0.08	-0.09	0.04	0.00	0.04	-0.10	0.05
EFK 8.7 250μm-1mm	F1	0.24	1.0	1	2	5	104.7	0.34	0.08	0.03	0.08	-0.13	0.04	-0.03	0.04	-0.16	0.05
	F2	0.02	0.1	1	1	1	101.0	0.44	0.08	0.08	0.08	-0.10	0.04	0.01	0.04	-0.13	0.05
	F3	1.43	5.9	1	1	2	105.6	0.16	0.08	0.01	0.08	-0.05	0.04	-0.01	0.04	-0.09	0.05
	F4	2.89	11.8	1	1	2	103.9	0.26	0.08	-0.02	0.08	-0.11	0.04	-0.02	0.04	-0.15	0.05
	F5	19.84	81.3	1	1	2	105.3	-0.18	0.08	0.00	0.08	-0.11	0.04	-0.03	0.04	-0.14	0.05
	Calc. THg	24.41					105.2	-0.10	0.08	0.00	0.08	-0.11	0.04	-0.02	0.04	-0.14	0.05
EFK 8.7 125-250μm	F1	0.05	0.6	1	1	2	103.8	0.03	0.08	0.03	0.08	-0.09	0.04	-0.02	0.04	-0.12	0.05
	F2	0.00	<0.1	1	1	1	93.9	-0.08	0.08	0.00	0.08	-0.04	0.04	-0.06	0.04	-0.04	0.05
	F3	1.62	20.5	1	1	2	103.9	-0.04	0.08	0.03	0.08	-0.09	0.04	0.00	0.04	-0.09	0.05
	F4	1.22	15.4	1	2	5	105.2	0.01	0.08	0.02	0.08	-0.10	0.04	0.00	0.04	-0.13	0.05
	F5	4.99	63.4	1	1	2	106.0	-0.28	0.08	0.05	0.08	-0.07	0.04	0.00	0.04	-0.11	0.05
	Calc. THg	7.88					110.4	-0.18	0.08	0.04	0.08	-0.08	0.04	0.00	0.04	-0.11	0.05
EFK 8.7 <125μm	F1	0.08	0.4	1	1	2	105.4	0.14	0.08	-0.01	0.08	-0.07	0.04	0.00	0.04	-0.10	0.05
	F2	0.01	<0.1	1	1	1	99.8	-0.25	0.08	0.02	0.08	-0.02	0.04	0.01	0.04	-0.01	0.05
	F3	1.07	5.4	1	1	2	105.3	0.07	0.08	0.02	0.08	-0.08	0.04	-0.01	0.04	-0.05	0.05
	F4	6.31	31.7	1	1	2	104.5	0.32	0.08	0.01	0.08	-0.11	0.04	0.00	0.04	-0.12	0.05
	F5	12.43	62.5	1	2	5	102.9	-0.04	0.08	0.02	0.08	-0.10	0.04	-0.01	0.04	-0.11	0.05
	Calc. THg	19.90					98.2	0.08	0.08	0.02	0.08	-0.10	0.04	-0.01	0.04	-0.11	0.05

Five-step sequential extractions were performed on sieved streambed sediment collected from three sites along EFPC. Sample ID refers to the sediment size fraction and the sampling location identified by the number of kilometers upstream of the confluence of Poplar Creek and EFPC. Calc. THg refers to the calculated THg concentration and isotopic composition of the sediment based on the weighted average of sequential extractions. Here, n_1 denotes the number of sequential extraction sets, n_2 denotes the number of purge and trap preparations, and n_3 denotes the number of separate isotopic analyses on an individual preparation(s). The percent recovery (% Rec.) for F1 – F5 shows recovery of Hg during the purge and trap procedure for preparation of sequential extraction samples for isotope analysis. The percent recovery for Calc. THg is based on the sum of sequential extractions relative to THg concentrations obtained by

combustions. The uncertainty in the isotopic composition of Hg in sequential extraction samples is represented by the average uncertainty (2SD) across all UM-Almadén analyses.

Table S2.7a. Comparison of sequential extraction replicates.

Sample ID	Sequential Extraction	Rep #	THg (µg g^{-1})	% of THg	n_1	n_2	% Rec.	δ^{202}Hg (‰)	2σ (‰)	Δ^{204}Hg (‰)	2σ (‰)	Δ^{201}Hg (‰)	2σ (‰)	Δ^{200}Hg (‰)	2σ (‰)	Δ^{199}Hg (‰)	2σ (‰)
EFK 18.0 250µm-1mm	F1	Rep 1	0.32	1.89	1	2	101.5	-0.18	0.08	0.03	0.08	-0.04	0.04	0.01	0.04	-0.04	0.05
	F2	Rep 1	0.01	0.04	1	1	98.0	-0.13	0.08	-0.02	0.08	-0.05	0.04	0.00	0.04	-0.03	0.05
	F3	Rep 1	0.29	1.71	1	2	99.0	-0.15	0.08	-0.02	0.08	-0.02	0.04	0.01	0.04	-0.01	0.05
	F4	Rep 1	2.13	12.4	2	5	98.9	-0.01	0.08	0.01	0.08	-0.08	0.04	0.00	0.04	-0.09	0.05
	F5	Rep 1	14.36	83.9	1	2	101.9	-0.14	0.08	-0.02	0.08	-0.06	0.04	0.00	0.04	-0.07	0.05
	Calc. THg	Rep 1	17.11				105.1	-0.12	0.08	-0.02	0.08	-0.06	0.04	0.00	0.04	-0.07	0.05
	F1	Rep 2	0.13	0.78	1	2	99.4	-0.07	0.08	0.01	0.08	-0.08	0.04	0.01	0.04	-0.08	0.05
	F2	Rep 2	0.02	0.11	1	1	96.4	-0.19	0.08	-0.01	0.08	-0.07	0.04	-0.01	0.04	-0.04	0.05
	F3	Rep 2	0.30	1.77	1	2	100.9	-0.19	0.08	-0.01	0.08	-0.02	0.04	0.03	0.04	0.00	0.05
	F4	Rep 2	1.82	10.8	1	2	98.4	0.11	0.08	0.00	0.08	-0.06	0.04	-0.01	0.04	-0.09	0.05
	F5	Rep 2	14.50	86.5	1	2	98.5	-0.03	0.08	-0.01	0.08	-0.09	0.04	0.00	0.04	-0.08	0.05
	Calc. THg	Rep 2	16.76				102.9	-0.02	0.08	-0.01	0.08	-0.08	0.04	0.00	0.04	-0.08	0.05
EFK 8.7 1-2mm	F1	Rep 1	0.20	0.6	2	4	104.8	0.15	0.08	0.00	0.08	-0.10	0.04	0.00	0.04	-0.11	0.05
	F2	Rep 1	0.04	0.1	2	2	101.0	0.49	0.08	0.05	0.08	-0.09	0.04	0.02	0.04	-0.13	0.05
	F1	Rep 2	0.34	-	1	2	105.6	0.15	0.08	0.01	0.08	-0.12	0.04	0.00	0.04	-0.14	0.05
	F2	Rep 2	0.14	-	1	2	105.3	0.35	0.08	0.02	0.08	-0.11	0.04	0.01	0.04	-0.13	0.05
EFK 8.7 250µm-1mm	F1	Rep 1	0.24	1.0	2	5	104.7	0.34	0.08	0.03	0.08	-0.13	0.04	-0.03	0.04	-0.16	0.05
	F2	Rep 1	0.02	0.1	1	1	101.0	0.44	0.08	0.08	0.08	-0.10	0.04	0.01	0.04	-0.13	0.05
	F1	Rep 2	0.34	-	1	2	102.8	-0.11	0.08	0.01	0.08	-0.08	0.04	-0.01	0.04	-0.11	0.05
	F2	Rep 2	0.04	-	1	1	104.8	0.40	0.08	0.07	0.08	-0.09	0.04	0.00	0.04	-0.14	0.05
EFK 8.7 125-250µm	F1	Rep 1	0.05	0.6	1	2	103.8	0.03	0.08	0.03	0.08	-0.09	0.04	-0.02	0.04	-0.12	0.05
	F1	Rep 2	0.04	-	1	1	103.0	0.09	0.08	0.04	0.08	-0.07	0.04	0.01	0.04	-0.11	0.05
EFK 8.7 <125µm	F1	Rep 1	0.08	0.4	1	2	105.4	0.14	0.08	-0.01	0.08	-0.07	0.04	0.00	0.04	-0.10	0.05
	F1	Rep 2	0.04	-	1	1	104.4	0.06	0.08	0.00	0.08	-0.11	0.04	-0.03	0.04	-0.12	0.05

See Table S2.7b for notes.

Table S2.7b. Comparison of sequential extraction replicates, cont.

Sample ID	Sequential Extraction	Rep #	THg (μg g^{-1})	% of THg	n_1	n_2	% Rec.	δ^{202}Hg (‰)	2σ (‰)	Δ^{204}Hg (‰)	2σ (‰)	Δ^{201}Hg (‰)	2σ (‰)	Δ^{200}Hg (‰)	2σ (‰)	Δ^{199}Hg (‰)	2σ (‰)
NIST SRM 2711 (Montana Soil)	F1	Rep 1	0.05	0.9	1	1	98.0	-0.28	0.08	0.07	0.08	-0.14	0.04	0.00	0.04	-0.19	0.05
	F2	Rep 1	0.00	0.1	Insufficient mercury for isotopic analysis.												
	F3	Rep 1	0.15	2.5	2	2	94.6	-0.22	0.08	0.04	0.08	-0.15	0.04	-0.01	0.04	-0.20	0.05
	F4	Rep 1	4.03	69.0	2	3	97.0	-0.05	0.08	0.01	0.08	-0.19	0.04	-0.01	0.04	-0.22	0.05
	F5	Rep 1	1.61	27.5	2	3	97.3	-0.42	0.08	0.01	0.08	-0.19	0.04	-0.01	0.04	-0.21	0.05
	Calc. THg	Rep 1	5.84				93.4	-0.16	0.08	0.02	0.08	-0.19	0.04	-0.01	0.04	-0.22	0.05
	F1	Rep 2	0.05	0.8	2	2	99.0	-0.21	0.08	-0.01	0.08	-0.17	0.04	0.00	0.04	-0.20	0.05
	F2	Rep 2	0.00	0.1	1	1	93.8	-0.94	0.08	-0.01	0.08	-0.04	0.04	0.05	0.04	-0.13	0.05
	F3	Rep 2	0.15	2.5	1	2	103.3	-0.28	0.08	-0.01	0.08	-0.14	0.04	-0.02	0.04	-0.18	0.05
	F4	Rep 2	4.25	70.5	1	2	95.3	-0.15	0.08	0.03	0.08	-0.21	0.04	0.00	0.04	-0.23	0.05
	F5	Rep 2	1.58	26.2	1	2	96.9	-0.46	0.08	0.04	0.08	-0.16	0.04	0.00	0.04	-0.22	0.05
	Calc. THg	Rep 2	6.03				96.5	-0.23	0.08	0.03	0.08	-0.19	0.04	0.00	0.04	-0.23	0.05
	F1	Rep 3	0.12	2.1	1	2	98.1	-0.15	0.08	-0.01	0.08	-0.19	0.04	0.02	0.04	-0.21	0.05
	F2	Rep 3	0.00	0.1	1	1	98.1	-0.68	0.08	0.07	0.08	-0.07	0.04	0.06	0.04	-0.08	0.05
	F3	Rep 3	0.17	2.8	2	5	94.6	-0.23	0.08	-0.02	0.08	-0.15	0.04	0.00	0.04	-0.19	0.05
	F4	Rep 3	3.92	65.3	1	2	100.9	-0.07	0.08	-0.02	0.08	-0.20	0.04	0.00	0.04	-0.23	0.05
	F5	Rep 3	1.79	29.8	1	2	102.5	-0.41	0.08	0.00	0.08	-0.19	0.04	-0.02	0.04	-0.22	0.05
	Calc. THg	Rep 3	6.01				96.1	-0.18	0.08	-0.02	0.08	-0.20	0.04	0.00	0.04	-0.23	0.05

Five-step sequential extractions were performed on standard reference materials and on sieved streambed sediment collected from three sites along EFPC. Sample ID refers to the sediment size fraction and the sampling location identified by the number of kilometers upstream of the confluence of Poplar Creek and EFPC. Calc. THg refers to the calculated THg concentration and isotopic composition of the sediment based on the weighted average of sequential extractions. Rep # refers to sequential extraction replicates on separate aliquots of sediment. Here, n_1 denotes the number of purge and trap preparations, and n_2 denotes the number of separate isotopic analyses on an individual preparation(s). The percent recovery (% Rec.) for F1 – F5 shows recovery of Hg during the purge and trap procedure for preparation of sequential extraction samples for isotope analysis. The percent recovery for Calc. THg of EFPC sediment is based on the sum of sequential extractions relative to THg concentrations obtained by combustions. The percent recovery for Calc. THg of reference materials is based on the sum of sequential extractions relative to certified values. The uncertainty in the isotopic composition of Hg in sequential extraction samples is represented by the average uncertainty (2SD) across all UM-Almadén analyses.

Table S2.8. Results of loss-on-ignition.

Site ID	Size Fraction	Percent mass loss after 500ºC (i.e., organic matter) (± 1SD, n=2)	Percent mass loss after 800ºC (i.e., carbonates) (± 1SD, n=2)	Calculated percent organic carbon (± 1SD, n=2)	Total Hg per mass of organic carbon, μg THg g^{-1} OC (± 1SD, n=2)	F3-extracted Hg per mass of organic matter carbon, μg Hg_{F3} g^{-1} OC (± 1SD, n=2)
EFK 22.3	1-2mm	4.39 ± 0.24	2.56 ± 0.65	2.19 ± 0.12	970 ± 504	34.2 ± 1.9
	250μm-1mm	3.09	2.78	1.54	1175	19.0
	125-250μm	4.15	2.28	2.08	1259	30.1
	<125μm	6.04	2.37	3.02	1159	29.4
EFK 18.0	1-2mm	4.14	3.70	2.07	1188	14.6
	250μm-1mm	2.71 ± 0.19	2.55 ± 0.07	1.36 ± 0.09	1205 ± 133	21.8 ± 1.5
	125-250μm	2.57	2.43	1.28	1306	33.6
	<125μm	7.15	2.81	3.57	1099	25.4
EFK 15.8	1-2mm	3.18	1.17	1.59	1656	-
	250μm-1mm	2.18	0.91	1.09	2174	-
	125-250μm	2.02 ± 0.27	0.87 ± 0.08	1.01 ± 0.13	1510 ± 238	-
	<125μm	5.04	1.61	2.52	846	-
EFK 8.7	1-2mm	1.77	0.50	0.89	4715	190
	250μm-1mm	1.22	0.24	0.61	3802	234
	125-250μm	1.95	0.13	0.98	731	166
	<125μm	5.74 ± 0.01	0.87 ± 0.04	2.87 ± 0.01	706 ± 5	37.2 ± 0.1
NIST SRM 1944 (NY/NJ Waterway Sediment)		8.77 ± 0.06	1.73 ± 0.14	4.38 ± 0.03	82 ± 1	7.0 ± 0.0

A loss-on-ignition procedure was performed on sieved streambed sediment collected from four sites along EFPC. Site ID refers to the sampling location identified by the number of kilometers upstream of the confluence of Poplar Creek and EFPC. Percentages of mass loss after 500ºC and 800ºC are thought to primarily represent percentages of organic matter and carbonates, respectively. Percentages of organic carbon were calculated by dividing the percentages of mass lost after 500ºC by 2. Concentrations of total Hg per mass of organic carbon (μg THg g^{-1} OC) were calculated using THg concentrations measured via combustion (Table S2.3, Table S2.4), and for values represented by an average ± 1SD, these averages were based on independently ground sediment samples which were each analyzed for THg and OC concentrations. Concentrations of F3-extracted Hg per mass of organic carbon (μg Hg_{F3} g^{-1} OC) were calculated using Hg concentrations of the F3 sequential extractions (Table S2.6a-c), and for values represented by an average ± 1SD, these averages were based on replicate OC concentrations.

Table S2.9. Results of two-tailed paired samples t-tests for EFPC sediment sequential extraction results.

Sampling site	Group 1[a]	Group 2[a]	Mean Offset in δ^{202}Hg (1SD)	Mean Offset in Δ^{199}Hg (1SD)	p-value[b] (δ^{202}Hg)	p-value[c] (Δ^{199}Hg)
EFK 22.3	F2	F3	-0.20 ± 0.22‰	-0.01 ± 0.02‰	0.175	0.361
EFK 18.0	F2	F3	-0.13 ± 0.25‰	-0.02 ± 0.03‰	0.366	0.331
EFK 8.7	F2	F3	0.09 ± 0.34‰	0.00 ± 0.06‰	0.631	0.952
EFK 22.3	F4	F5	0.16 ± 0.12‰	0.00 ± 0.02‰	0.075	0.629
EFK 18.0	F4	F5	0.16 ± 0.08‰	-0.01 ± 0.02‰	0.030*	0.651
EFK 8.7	F4	F5	0.34 ± 0.07‰	-0.01 ± 0.00‰	0.002*	0.010*

[a] Group 1 and Group 2 represent different pools of extracted Hg (n=4 for each group).
[b] Null hypothesis: The mean offset in δ^{202}Hg values of different pools of extracted Hg within individual sediment size fractions (i.e., paired samples) is zero.
[c] Null hypothesis: The mean offset in Δ^{199}Hg values of different pools of extracted Hg within individual sediment size fractions (i.e., paired samples) is zero.
* indicates that the mean offset in delta values of different pools of extracted Hg within individual sediment size fractions is significantly different from zero ($p < 0.05$).

Table S2.10. Results of two-tailed paired samples t-tests for EFPC sediment sequential extraction results using the Bonferroni correction for multiple comparisons.

Sampling site	Group 1[a]	Group 2[a]	Mean Offset in δ^{202}Hg (1SD)	Mean Offset in Δ^{199}Hg (1SD)	p-value$_{adjusted}$[b] (δ^{202}Hg)	p-value$_{adjusted}$[c] (Δ^{199}Hg)
EFK 22.3	F1	F2F3	0.04 ± 0.29‰	-0.06 ± 0.02‰	1.000	0.034*
EFK 22.3	F1	F4F5	-0.19 ± 0.26‰	0.03 ± 0.03‰	0.730	0.960
EFK 22.3	F2F3	F4F5	-0.23 ± 0.05‰	0.09 ± 0.02‰	0.007*	0.011*
EFK 18.0	F1	F2F3	0.04 ± 0.13‰	-0.05 ± 0.02‰	1.000	0.096
EFK 18.0	F1	F4F5	-0.21 ± 0.19‰	0.03 ± 0.04‰	0.354	0.611
EFK 18.0	F2F3	F4F5	-0.25 ± 0.17‰	0.08 ± 0.02‰	0.184	0.011*
EFK 8.7	F1	F2F3	0.06 ± 0.14‰	-0.05 ± 0.03‰	1.000	0.138
EFK 8.7	F1	F4F5	0.16 ± 0.12‰	0.00 ± 0.01‰	0.242	1.000
EFK 8.7	F2F3	F4F5	0.10 ± 0.24‰	0.04 ± 0.04‰	1.000	0.258

[a] Group 1 and Group 2 represent different pools of extracted Hg (n=4 for each group). The isotopic composition of groups F2F3 and F4F5 was calculated as the non-weighted average isotopic composition of the two pools of sequentially extracted Hg within the group.
[b] Null hypothesis: The mean offset in δ^{202}Hg values of different pools of extracted Hg within individual sediment size fractions (i.e., paired samples) is zero.
[c] Null hypothesis: The mean offset in Δ^{199}Hg values of different pools of extracted Hg within individual sediment size fractions (i.e., paired samples) is zero.
* indicates that the mean offset in delta values of different pools of extracted Hg within individual sediment size fractions is significantly different from zero ($p < 0.05$).

Table S2.11. Results of two-tailed paired samples t-tests for EFPC sediment sequential extraction results using the Bonferroni correction for multiple comparisons, excluding the F2 mercury pool.

Sampling site	Group 1[a]	Group 2[a]	Mean Offset in δ^{202}Hg (1SD)	Mean Offset in Δ^{199}Hg (1SD)	p-value$_{adjusted}$[b] (δ^{202}Hg)	p-value$_{adjusted}$[c] (Δ^{199}Hg)
EFK 22.3	F1	F3	-0.06 ± 0.35‰	-0.07 ± 0.02‰	1.000	0.017*
EFK 22.3	F1	F4F5	-0.19 ± 0.26‰	0.03 ± 0.03‰	0.730	0.960
EFK 22.3	F3	F4F5	-0.13 ± 0.12‰	0.09 ± 0.02‰	0.371	0.011*
EFK 18.0	F1	F3	-0.02 ± 0.10‰	-0.06 ± 0.01‰	1.000	0.004*
EFK 18.0	F1	F4F5	-0.21 ± 0.19‰	0.03 ± 0.04‰	0.364	0.611
EFK 18.0	F3	F4F5	-0.18 ± 0.09‰	0.09 ± 0.03‰	0.087	0.028*
EFK 8.7	F1	F3	0.11 ± 0.05‰	-0.05 ± 0.02‰	0.068	0.055
EFK 8.7	F1	F4F5	0.16 ± 0.12‰	0.00 ± 0.01‰	0.242	1.000
EFK 8.7	F3	F4F5	0.05 ± 0.09‰	0.05 ± 0.02‰	0.921	0.032*

[a] Group 1 and Group 2 represent different pools of extracted Hg (n=4 for each group). The isotopic composition of group F4F5 was calculated as the non-weighted average isotopic composition of the two pools of sequentially extracted Hg within the group.
[b] Null hypothesis: The mean offset in δ^{202}Hg values of different pools of extracted Hg within individual sediment size fractions (i.e., paired samples) is zero.
[c] Null hypothesis: The mean offset in Δ^{199}Hg values of different pools of extracted Hg within individual sediment size fractions (i.e., paired samples) is zero.
* indicates that the mean offset in delta values of different pools of extracted Hg within individual sediment size fractions is significantly different from zero ($p < 0.05$).

Table S2.12. Results of two-tailed independent samples t-tests for EFPC sediment sequential extraction results.

Sampling site	G1[a]	G2[a]	Mean δ^{202}Hg Group 1 (1SD)	Mean δ^{202}Hg Group 2 (1SD)	Mean Δ^{199}Hg Group 1 (1SD)	Mean Δ^{199}Hg Group 2 (1SD)	p-value[b] (δ^{202}Hg)	p-value[c] (Δ^{199}Hg)
EFK 22.3	F2	F3	-0.24 ± 0.29‰	-0.04 ± 0.31‰	0.00 ± 0.03‰	0.01 ± 0.02‰	0.389	0.553
EFK 18.0	F2	F3	-0.23 ± 0.30‰	-0.10 ± 0.08‰	-0.03 ± 0.03‰	-0.01± 0.02‰	0.416	0.362
EFK 8.7	F2	F3	0.15 ± 0.37‰	0.06 ± 0.08‰	-0.08 ± 0.06‰	-0.08 ± 0.02‰	0.653	0.959
EFK 22.3	F4	F5	0.17 ± 0.21‰	0.01 ± 0.27‰	-0.09 ± 0.03‰	-0.08 ± 0.03‰	0.392	0.853
EFK 18.0	F4	F5	0.17 ± 0.14‰	0.01 ± 0.18‰	-0.10 ± 0.03‰	-0.09 ± 0.03‰	0.207	0.362
EFK 8.7	F4	F5	0.18 ± 0.14‰	-0.17 ± 0.10‰	-0.13 ± 0.02‰	-0.11 ± 0.02‰	0.006*	0.317

[a] Group 1 (G1) and Group 2 (G2), representing different pools of extracted Hg (n=4 for each group).
[b] Null hypothesis: Across all sediment size fractions within a site (i.e., unpaired samples), the difference between mean δ^{202}Hg values of different pools of extracted Hg is zero.
[b] Null hypothesis: Across all sediment size fractions within a site (i.e., unpaired samples), the difference between mean Δ^{199}Hg values of different pools of extracted Hg is zero.
* indicates that the mean delta values of different pools of extracted Hg are significantly different from each other ($p < 0.05$).

Table S2.13. Results of independent samples Tukey honestly significant difference (HSD) tests for multiple comparisons for EFPC sediment sequential extraction results.

Sampling site	G1[a]	G2[a]	Mean δ^{202}Hg Group 1 (1SD)	Mean δ^{202}Hg Group 2 (1SD)	Mean Δ^{199}Hg Group 1 (1SD)	Mean Δ^{199}Hg Group 2 (1SD)	p-value$_{adj.}$[b] (δ^{202}Hg)	p-value$_{adj.}$[c] (Δ^{199}Hg)
EFK 22.3	F1	F2F3	-0.10 ± 0.08‰	-0.14 ± 0.30‰	-0.06 ± 0.01‰	0.00 ± 0.03‰	0.900	0.018*
EFK 22.3	F1	F4F5	-0.10 ± 0.08‰	0.09 ± 0.24‰	-0.06 ± 0.01‰	-0.08 ± 0.03‰	0.469	0.441
EFK 22.3	F2F3	F4F5	-0.14 ± 0.30‰	0.09 ± 0.24‰	0.00 ± 0.03‰	-0.08 ± 0.03‰	0.336	0.003*
EFK 18.0	F1	F2F3	-0.12 ± 0.09‰	-0.16 ± 0.21‰	-0.06 ± 0.02‰	-0.02 ± 0.03‰	0.900	0.055
EFK 18.0	F1	F4F5	-0.12 ± 0.09‰	0.09 ± 0.17‰	-0.06 ± 0.02‰	-0.10 ± 0.03‰	0.165	0.215
EFK 18.0	F2F3	F4F5	-0.16 ± 0.21‰	0.09 ± 0.17‰	-0.02 ± 0.03‰	-0.10 ± 0.03‰	0.085	0.004*
EFK 8.7	F1	F2F3	0.17 ± 0.13‰	0.11 ± 0.25‰	-0.12 ± 0.03‰	-0.08 ± 0.04‰	0.833	0.126
EFK 8.7	F1	F4F5	0.17 ± 0.13‰	0.01 ± 0.21‰	-0.12 ± 0.03‰	-0.12 ± 0.02‰	0.357	0.900
EFK 8.7	F2F3	F4F5	0.11 ± 0.25‰	0.01 ± 0.21‰	-0.08 ± 0.04‰	-0.12 ± 0.02‰	0.652	0.139

[a] Group 1 (G1) and Group 2 (G2), representing different pools of extracted Hg (n=4 for each group). The isotopic composition of groups F2F3 and F4F5 was calculated as the non-weighted average isotopic composition of the two pools of sequentially extracted Hg within the group.

[b] Null hypothesis: Across all sediment size fractions within a site (i.e., unpaired samples), the difference between mean δ^{202}Hg values of different pools of extracted Hg is zero.

[b] Null hypothesis: Across all sediment size fractions within a site (i.e., unpaired samples), the difference between mean Δ^{199}Hg values of different pools of extracted Hg is zero.

* indicates that the mean delta values of different pools of extracted Hg are significantly different from each other ($p < 0.05$).

References for Supporting Information

Aiken, G. R., D. M. McKnight, R. L. Wershaw, and P. MacCarthy. 1985. *Humic Substances in Soil, Sediment, and Water*. New York: Wiley-Interscience.

Bloom, Nicolas S., Eve Preus, Jodie Katon, and Misti Hiltner. 2003. "Selective extractions to assess the biogeochemically relevant fractionation of inorganic mercury in sediments and soils." *Analytica Chimica Acta* 479 (2):233-248. doi: 10.1016/s0003-2670(02)01550-7.

Blum, Joel D., and Marcus W. Johnson. 2017. "Recent developments in mercury stable isotope analysis." *Reviews in Mineralogy and Geochemistry* 82:733-757. doi: 10.2138/rmg.2017.82.17.

Brocza, Flora M., Harald Biester, Jan-Helge Richard, Stephan M. Kraemer, and Jan G. Wiederhold. 2019. "Mercury isotope fractionation in the subsurface of a Hg(II) chloride-contaminated industrial legacy site." *Environmental Science & Technology* 53:7296-7305. doi: 10.1021/acs.est.9b00619.

Brooks, Scott, Virginia Eller, John Dickson, Jennifer Earles, Kenneth Lowe, Tonia Mehlhorn, Todd Olsen, Chris DeRolph, David Watson, Debra Phillips, and Mark Peterson. 2017. Mercury Content of Sediments in East Fork Poplar Creek: Current Assessment and Past Trends. Oak Ridge, TN: Oak Ridge National Laboratory.

Demers, Jason D., Joel D. Blum, Scott C. Brooks, Patrick M. Donovan, Ami L. Riscassi, Carrie L. Miller, Wang Zheng, and Baohua Gu. 2018. "Hg isotopes reveal in-stream processing and legacy inputs in East Fork Poplar Creek, Oak Ridge, Tennessee, USA." *Environmental Science: Processes & Impacts* 20 (4):686-707. doi: 10.1039/c7em00538e.

Donovan, Patrick M., Joel D. Blum, Jason D. Demers, Baohua Gu, Scott C. Brooks, and John Peryam. 2014. "Identification of multiple mercury sources to stream sediments near Oak Ridge, TN, USA." *Environmental Science & Technology* 48 (7):3666-3674. doi: 10.1021/es4046549.

Eganhouse, Robert P., David R. Young, and Joseph N. Johnson. 1978. "Geochemistry of mercury in Palos Verdes sediments." *Environmental Science & Technology* 12 (10):1151-1157. doi: 10.1021/es60146a004.

Grigg, Andrew R. C., Ruben Kretzschmar, Robin S. Gilli, and Jan G. Wiederhold. 2018. "Mercury isotope signatures of digests and sequential extracts from industrially contaminated soils and sediments." *Science of The Total Environment* 636:1344-1354. doi: 10.1016/j.scitotenv.2018.04.261.

Hall, Gwendy E. M., Pierre Pelchat, and Jeanne B. Percival. 2005. "The design and application of sequential extractions for mercury, Part 1. Optimization of HNO3 extraction for all non-sulphide forms of Hg." *Geochemistry: Exploration, Environment, Analysis* 5 (2):107-113. doi: 10.1144/1467-7873/03-061.

U.S. EPA. 2002. Method 1631, Revision E: Mercury in Water by Oxidation, Purge and Trap, and Cold Vapor Atomic Fluorescence Spectrometry. Washington, D.C.: U.S. Environmental Protection Agency, Office of Water.

U.S. EPA. 2016. Definition and Procedure for the Determination of the Method Detection Limit, Revision 2. Washington, D.C.: U.S. Environmental Protection Agency, Office of Water.

Vermeesch, Pieter. 2018. "IsoplotR: A free and open toolbox for geochronology." *Geoscience Frontiers* 9:1479-1493. doi: 10.1016/j.gsf.2018.04.001.

Wiederhold, Jan G., Ulf Skyllberg, Andreas Drott, Martin Jiskra, Sofi Jonsson, Erik Björn, Bernard Bourdon, and Ruben Kretzschmar. 2015. "Mercury isotope signatures in contaminated sediments as a tracer for local industrial pollution sources." *Environmental Science & Technology* 49:177-185. doi: 10.1021/es5044358.

York, Derek. 1966. "Least-squares fitting of a straight line." *Canadian Journal of Physics* 44:1079-1086. doi: 10.1139/p66-090.

Chapter 3 Coupling of Nitric Acid Digestion and Anion-Exchange Resin Separation for the Determination of Methylmercury Isotopic Composition within Organisms

Co-authored with Jason D. Demers, Joel D. Blum, Scott C. Brooks, and Marcus W. Johnson. Coupling of nitric acid digestion and anion-exchange resin separation for the determination of methylmercury isotopic composition within organisms. *Analytical and Bioanalytical Chemistry*, 2022, DOI: 10.1007/s00216-022-04468-8

Abstract: Isotope ratios of methylmercury (MeHg) within organisms can be used to identify sources of MeHg that has accumulated in food webs, but these isotopic compositions are masked in organisms at lower-trophic-levels by the presence of inorganic mercury (iHg). To facilitate measurement of MeHg isotope ratios in organisms, we developed a method of extracting and isolating MeHg from fish and aquatic invertebrates for compound-specific isotopic analysis involving nitric acid digestion, batch anion-exchange resin separation, and pre-concentration by purge and trap. Recovery of MeHg was quantified after each step in the procedure, and the average cumulative recovery of MeHg was 93.4 ± 2.9% (1SD, n=28) for biological reference materials and natural biota samples and 96.9 ± 1.8% (1SD, n=5) for aqueous MeHgCl standards. The amount of iHg impurities was also quantified after each step, and the average MeHg purity was 97.8 ± 4.3% (1SD, n=28) across all reference materials and natural biota samples after the final separation step. Measured MeHg isotopic compositions of reference materials agreed with literature values obtained using other MeHg separation techniques, and MeHg isotope ratios of aqueous standards, reference materials, and natural biota samples were reproducible. On average, the reproducibility associated with reference material process replicates (2SD) was 0.10‰ for

δ^{202}MeHg and 0.04‰ for Δ^{199}MeHg. This new method provides a streamlined, reliable technique that utilizes a single sample aliquot for MeHg concentration and isotopic analysis. This promotes a tight coupling between MeHg concentration, %MeHg, and Hg isotopic composition, which may be especially beneficial for studying complex food webs with multiple isotopically distinct sources of iHg and/or MeHg.

3.1 Introduction

The speciation of mercury (Hg) influences its mobility, bioavailability, and toxicity. In natural environments, oxidized inorganic mercury (iHg) may be chemically reduced to elemental mercury (Hg(0)) by microbial, photochemical, or dark abiotic reactions, after which it may be evaded to the atmosphere (Selin 2009). A variety of microorganisms can also convert bioavailable iHg into methylmercury (MeHg), an organic form of mercury that is highly toxic and bioaccumulative (Regnell and Watras 2019). This MeHg may then be partially degraded by microbial and/or photochemical reactions (Barkay and Gu 2022) before bioaccumulating in organisms and biomagnifying in food webs. Each of these reactions and processes, along with many others, can induce mercury isotope fractionation, resulting in distinct isotopic compositions within various environmental compartments and between different mercury species. Mercury stable isotope ratios, which can be altered by both mass-dependent and mass-independent isotope fractionation (MDF and MIF) mechanisms (Blum et al. 2014), can be used to study the biogeochemical cycling of mercury in ecosystems and to aid in the identification of sources of mercury contamination.

Typically, isotopic measurements are made on total mercury (THg) within environmental samples, but recently, isotopic measurements on individual mercury pools or species within individual samples have become possible with the use of various sequential extraction (Stetson et

al. 2009, Wiederhold et al. 2013, Yin et al. 2013, Wiederhold et al. 2015, Brocza et al. 2019, Grigg et al. 2018, Crowther et al. 2021, Huang et al. 2021, McLagan et al. 2022) or compound-specific extraction (Epov et al. 2008, Masbou et al. 2013, Janssen et al. 2015, Li et al. 2017, Bouchet et al. 2018, Entwisle et al. 2018, Qin et al. 2018, Qin et al. 2020, Rosera et al. 2020, Manceau et al. 2021, Poulin et al. 2021, Yang et al. 2021, Zhang et al. 2021, Rosera et al. 2022) techniques. Various chemical species of mercury within a sample can have distinct isotopic compositions and when the specific mercury species of interest, often MeHg, makes up only a small fraction of the THg, its isotopic composition can be masked (Rosera et al. 2022). For example, while the MeHg fraction in fish occupying higher trophic levels often makes up the majority of the THg, the MeHg fraction in other environmental samples such as sediment, biofilm, and lower trophic level organisms is typically small, meaning that their MeHg isotopic compositions are masked when only the THg isotopic composition is measured. Estimation approaches using linear regression and mass balance techniques have been developed to approximate the isotopic composition of MeHg within a food web while only measuring the THg and MeHg concentration and the THg isotopic composition of each organism (Tsui et al. 2012, Kwon et al. 2014, Kwon et al. 2015). This approach works well when there is only one primary source of iHg and one primary source of MeHg to a food web, each with a narrow and consistent isotopic composition. However, in some ecosystems, there may be multiple isotopically distinct sources of iHg and/or MeHg, in which case the ability to directly analyze the MeHg isotopic composition within organisms and basal resources is especially beneficial. Assessing the isotopic composition(s) of MeHg within a food web, either directly or by estimation, is useful for identifying potential sources of MeHg to the organisms, as well as tracking biogeochemical transformations within bioavailable mercury prior to its incorporation into the food web.

A number of techniques have been developed to separate MeHg from iHg for isotopic analysis (Zhang et al. 2022). One example is the toluene extraction method (Masbou et al. 2013, Li et al. 2017, Qin et al. 2020, Rosera et al. 2020, Yang et al. 2021, Zhang et al. 2021), which has been used successfully for a wide variety of sample types including plant and animal tissue and human hair. However, this method has been found to be unsuitable for biota samples with a high lipid content, such as plankton and some fish samples, due to the formation of a thick emulsion layer during the extraction (Rosera et al. 2020, Zhang et al. 2021). Another recently developed method is an alkaline digestion followed by reduction and volatilization of iHg by stannous chloride ($SnCl_2$), which can be accomplished in a shorter amount of time compared to some of the other MeHg separation methods and has been shown to work well for fish and plankton reference materials (Zhang et al. 2021). However, dissolved organic matter (DOM) in a non-brominated sample matrix can potentially cause incomplete reduction and removal of iHg by $SnCl_2$ (Stoichev et al. 2002). Additionally, while $SnCl_2$ is generally considered to be nonreactive toward MeHg (Magos 1971, Gao et al. 2013, Balarama Krishna and Karunasagar 2015), a recent study found that MeHg can be reduced by $SnCl_2$ under conditions of low sulfate concentration (Li et al. 2018), though this issue was not observed when the alkaline digestion / $SnCl_2$ reduction method was applied to aqueous MeHg standards (Zhang et al. 2021). Other techniques for separating MeHg from iHg for isotopic analysis have involved the use of gas chromatography (GC), either offline (Janssen et al. 2015, Qin et al. 2018, Qin et al. 2020) or coupled directly to a multi-collector inductively coupled plasma mass spectrometer (Krupp and Donard 2005, Epov et al. 2008, Dzurko et al. 2009, Rodríguez-González et al. 2009, Epov et al. 2010, Bouchet et al. 2018). Variations of these GC separation methods have been used for sediment, soil, and animal tissue samples, as well as bacterial cultures and aqueous solutions with high MeHg

concentrations. However, incomplete recovery of MeHg by variable species derivatization (i.e., ethylation or propylation) efficiency can cause artificial shifts in the mercury isotopic composition, leading to inaccurate isotopic measurements and high uncertainty (Yang and Sturgeon 2009). Additional challenges for the online GC separation method involve drifting isotope ratios during transient peak elution (Krupp and Donard 2005, Epov et al. 2008, Dzurko et al. 2009), and even when sample pre-concentration strategies (extended elution times) and species-specific bracketing schemes are employed, reported uncertainty in isotopic measurements has remained high relative to other offline MeHg separation methods (Bouchet et al. 2018). Offline high performance liquid chromatography (HPLC) has also recently been used for MeHg separation for isotopic analysis (Entwisle et al. 2018). This method does not require species derivatization and has resulted in isotope data with lower levels of uncertainty. Other methods of separating MeHg have involved the use of anion-exchange chromatography, which has been used for MeHg isotopic analysis of aqueous solutions with high MeHg concentrations (Malinovsky et al. 2010, Malinovsky and Vanhaecke 2011). More recently, methods employed to separate MeHg for isotopic analysis have involved the use of distillation followed by either GC separation (Dzurko et al. 2009, Janssen et al. 2015) or anion-exchange chromatography (Rosera et al. 2020, Manceau et al. 2021, Poulin et al. 2021, Rosera et al. 2022), the latter of which has been used successfully for a wide variety of biological and abiotic sample types with both high and low levels of MeHg relative to iHg (%MeHg). Distillation can be a particularly useful pre-treatment method for samples with a high organic matter content, though this method requires careful optimization to achieve complete recovery of MeHg and prevent the artificial formation of MeHg during the process, which can be an issue for samples with low %MeHg (Bloom et al. 1997, Hintelmann et al. 1997).

In this study, we developed a method for extracting and isolating MeHg from biota samples for isotopic analysis that utilizes a widely used hot nitric acid digestion followed by a batch anion-exchange resin separation procedure (Figure 3.1). This new combination of procedures is relatively simple and avoids some of the challenges involved with optimizing distillation and GC separation methods. A nitric acid digestion may also be more suitable for certain sample types than a toluene extraction or alkaline digestion. Additionally, by using this method, the MeHg concentration and MeHg isotope ratios can be measured on the same sample aliquot, and both MeHg and THg concentrations can be measured at the end of the anion-exchange resin separation procedure to verify MeHg recovery and check for iHg impurities prior to isotopic analysis.

To assess accuracy and precision, we performed this new method on aqueous MeHg and iHg standards, four different biological reference materials, and five different natural biota samples. Each sample type was processed and analyzed multiple times. The MeHg isotopic compositions of the reference materials were compared to results from several other studies that used different MeHg separation techniques. In this paper, we also present the results of a holding test in which aqueous MeHgCl standards were exposed to different acidic matrices (with and without nitric acid) and to different bottle types (borosilicate glass and polyethylene terephthalate glycol (PETG)) to verify that the materials used throughout the procedure were sufficient for maintaining consistent MeHg concentrations.

3.2 Methods

3.2.1 Description of reference materials and biota samples

Standard reference materials used for THg and MeHg concentration and isotopic analysis included DORM-3 fish protein, TORT-2 lobster hepatopancreas, DOLT-2 dogfish liver, and

DOLT-5 dogfish liver (National Research Council Canada; DOLT-5 used for MeHg analyses only). Total Hg and MeHg concentration and isotopic analyses were also performed on five biota samples collected from East Fork Poplar Creek, a point-source contaminated stream in Oak Ridge, TN, USA. These samples, in order of increasing proportion of THg as MeHg (%MeHg), include Asian clams (soft tissue; 6.3% MeHg), megaloptera larvae (whole body; 12% MeHg), mayfly larvae (whole body; 13% MeHg), crayfish (muscle tissue; 62% MeHg), and shiner (skinless fillet; 104% MeHg). Except for the shiner fillets, all samples were multi-individual composites. All samples were placed in either clean plastic bags or clean centrifuge tubes, placed on dry ice in the field, and then frozen the same day upon arrival at the laboratory. Biota samples were later freeze-dried and ground using a SPEX 8000 Mixer/Mill with an alumina grinding cylinder and ball. To avoid cross contamination, Ottawa Sand (quartz, Fisher Scientific) was ground between each sample, and the grinding cylinder and ball were rinsed thoroughly with deionized water and isopropanol. Prepared samples were stored in trace-metal clean borosilicate glass vials in the dark.

3.2.2 Total mercury extraction by combustion

Standard reference materials (Table S3.1) and natural biota samples (Table S3.2) were prepared for analysis of THg concentration and isotopic composition following a previously-described combustion procedure (Demers et al. 2013). Sample aliquots (250 to 460 mg for reference materials; 25 to 100 mg for natural biota samples) were combusted in a two-stage furnace, and volatilized Hg(0) was trapped in a 24 g oxidizing solution of 1% $KMnO_4$ (w/w) in 10% H_2SO_4 (v/v) (hereafter, 1% $KMnO_4$). Trap solutions of 1% $KMnO_4$ were later reduced with hydroxylamine hydrochloride ($HONH_3Cl$), and a small aliquot was analyzed for THg concentration using cold vapor atomic fluorescence spectrometry (CVAFS; RA-3F, Nippon

Instruments) following EPA Method 1631 (U.S. EPA 2002). Samples were analyzed in batches with quality control that included analysis of calibration verification standards, secondary standards, and blanks (see Section 3.5.1 in the Supporting Information).

To eliminate matrix effects from combustion residues, aliquots of the 1% $KMnO_4$ combustion trap solutions were reduced with $SnCl_2$, and Hg(0) was transferred to secondary 1% $KMnO_4$ trap solutions (Demers et al. 2013). These secondary solutions were later reduced with $HONH_3Cl$, and a small aliquot was analyzed for THg concentration by CVAFS. This was done to assess the percent recovery of the transfer process and to allow matching of standard and sample concentrations for isotopic analysis. Recovery of mercury after the transfer process was 98.0 ± 2.7% (1SD, n=19 including reference materials and natural biota samples) (Table S3.1, Table S3.2).

Procedural blanks and standard reference materials were combusted to monitor combustion performance. Average procedural blank 1% $KMnO_4$ solutions yielded 0.12 ng Hg (± 0.10 ng Hg, 1SD, n=18) prior to transfer, and 0.10 ng Hg (± 0.08 ng Hg, 1SD, n=16) after transfer, representing <0.2% of the sample solution mercury mass. Standard reference materials (with certified THg concentrations provided in parentheses) included DORM-3 (382 ± 60 ng g^{-1} THg) with an average recovery of 97.5 ± 2.4% (1SD, n=7), TORT-2 (270 ± 60 ng g^{-1} THg) with an average recovery of 100.5 ± 1.7% (1SD, n=5), and DOLT-2 (1990 ± 100 ng g^{-1} THg) with an average recovery of 106.5 ± 3.0% (1SD, n=2) relative to certified values (Table S3.1).

3.2.3 Methylmercury extraction by nitric acid digestion

Standard reference materials and natural biota samples were prepared for analysis of MeHg concentration (Table S3.3) following a modified version of a previously-described 12-hour nitric acid digestion procedure (Hammerschmidt and Fitzgerald 2005, Brooks Rand

Instruments 2013). The digestion was done in a stainless steel water bath placed inside a drying oven (Fisher Scientific, Isotemp Oven, Model 625G) (Figure S3.1a). Two thermocouples were threaded through a hole in the top of the oven, one of which was also threaded through a small hole drilled through the lid of the water bath (Figure S3.1a-b). These thermocouples were used to monitor air and water temperature prior to and during the digestion.

On the morning of the digestion, sample aliquots (25 to 75 mg for reference materials; 40 to 60 mg for natural biota samples; aiming for a minimum of 6 ng MeHg) were weighed into pre-weighed 15-mL borosilicate glass centrifuge tubes, and then 7.5 mL of 30% (v/v) HNO_3 was added to each vial. Separate sample aliquots weighed for matrix spike tests were immersed in the nitric acid, as described above, and then dosed with small volumes (120 to 800 µL) of a 50 or 1000 ng g^{-1} MeHgCl spike solution in 0.5% (v/v) acetic acid + 0.2% (v/v) HCl. Additional centrifuge tubes for procedural blanks and aqueous MeHgCl standard tests, to which no dry sample material was added, were included with each digestion batch. Aqueous MeHgCl standard tests received 400 µL of a ~50-ng g^{-1} MeHgCl spike solution. Each tube was shaken by hand and then centrifuged for 15 min at 3300 revolutions per minute (1380 relative centrifugal force (RCF)) which helped prevent the sample material from floating to the top of the solution during the digestion. After centrifuging, the tubes were shaken vigorously either by hand or with a touch mixer (Fisher Scientific, Model 232) to dislodge the plug of sample material from the tip of the centrifuge tube and to thoroughly remix contents. Just before the centrifuge tubes were placed into the hot water bath, each tube was shaken again and then rolled while being held at an angle, which helped prevent the sample material from sticking to the glass in the top half of the tube. Each tube was then placed in a plastic vial rack in the hot water bath inside the oven. The air and water temperatures were monitored to maintain a water temperature of 59.5 to 60.5°C throughout

the 12-h digestion. At the end of the digestion, the sample tubes were removed from the water bath and shaken by hand, then the tube contents were diluted with 7.5 mL of deionized water (Brooks Rand Instruments 2013) and the sample tubes were shaken again. The sample tubes were placed in a refrigerator to lower the temperature of the digestion samples and stored there overnight (maximum of 2 days) prior to MeHg analysis, at which time they were brought to room temperature and weighed to determine the total solution mass for calculation of the solid-sample MeHg concentration.

Aliquots of the digestion samples were analyzed for their MeHg concentration by gas chromatography coupled with cold vapor atomic fluorescence spectroscopy (GC-CVAFS) (MERX-M, Brooks Rand Instruments) following a modified version of EPA Method 1630 (U.S. EPA 2001) (Table S3.3). Sample and standard aliquots were added to 40-mL amber glass vials containing deionized water and 300 µL of 2 M acetate buffer. The pH was adjusted to 4.5 using small amounts of 20% (w/v) KOH (Brooks Rand Instruments 2013) and the amber vials were inverted to mix. Freshly thawed 1% (w/v) sodium tetraethylborate ($NaBEt_4$) in 2% KOH was slowly inverted five times to gently mix the solution, and then 50 µL was added to each of the amber vials, which were then re-capped and shaken to mix before starting the analysis. After removing aliquots for MeHg concentration analysis, digestion samples in their original glass tubes were returned to a refrigerator overnight before performing the batch anion-exchange resin separation procedure.

Samples were analyzed for MeHg concentration in batches with quality control that included calibration verification standards, secondary standards, and blanks, and each digestion sample was analyzed in duplicate (see Section 3.5.2 in the Supporting Information). The exact concentration, or titer, of the aqueous MeHgCl standard (Brooks Rand) used for calibration

standards, digestion matrix spike tests, and aqueous standard tests was determined following EPA Method 1630 (U.S. EPA 2001). On average, the nitric acid digestion procedural blank solutions yielded 0.01 ng MeHg (± <0.01 ng MeHg, 1SD, n=13), representing <0.2% of the sample solution MeHg mass. Standard reference materials (with certified MeHg concentrations provided in parentheses) included DORM-3 (355 ± 56 ng g^{-1} MeHg; 93% MeHg), TORT-2 (152 ± 13 ng g^{-1} MeHg; 56% MeHg), DOLT-2 (693 ± 53 ng g^{-1} MeHg; 35% MeHg), and DOLT-5 (119 ± 58 ng g^{-1} MeHg; 27% MeHg). Duplicate nitric acid digestion matrix spike tests were performed on each of the reference materials and natural biota samples, with an average recovery of 101.4 ± 2.4% (1SD, n=22) (Table S3.3). Nitric acid digestion aqueous MeHgCl standard tests had an average recovery of 99.9 ± 2.7% (1SD, n=8).

3.2.4 Isolation of methylmercury by resin separation for isotopic analysis

The nitric acid digestion releases not only MeHg, but also a large portion of the iHg from biota samples. To isolate the MeHg from the iHg for isotopic analysis, we utilized an anion-exchange resin (Bio-Rad AG 1-X4 resin, analytical grade, 200-400 mesh, chloride form), which under acidic and chlorinated conditions removes negatively charged iHg species (e.g., $HgCl_3^-$ and $HgCl_4^{2-}$) while leaving neutral MeHg species (e.g., $MeHgCl^0$) in solution (Korkisch 1989, Alderighi et al. 2003, Powell et al. 2009). For this study, reference materials and natural biota samples with greater than ~60% of THg as MeHg underwent one resin separation step, and those with less than ~60% of THg as MeHg underwent two consecutive resin separation steps. This protocol was based on testing an initial set of reference materials.

Prior to the nitric acid digestion, resin was cleaned and conditioned (Štrok et al. 2014, Washburn et al. 2019) so that it was ready for use immediately after the MeHg concentration analysis. Approximately 2.5 g of resin was weighed into 20-mL glass vials, which were then

filled to the shoulder with 4 M HNO_3. Resin vials were loaded onto a tube rotator (Fisher Scientific), and rotated for 15 min at 25 rotations per minute (Figure S3.1c). Resin vials were then removed from the rotator, and after waiting ~10 min with them sitting upright, the liquid layer was pipetted out and discarded, and the vials were again filled with 4 M HNO_3. This HNO_3 cleaning process was repeated four times, except that after rotating the fourth time, the resin vials were not decanted, but rather they sat upright filled with HNO_3 overnight. The next day, this same process was used to condition the resin, first with one round of 4 M HNO_3, then three rounds of deionized water, then three rounds of 0.1 M HCl. After rotating a third time with HCl, the resin vials were not decanted, but rather they sat upright filled with HCl for a few days until it was time to perform the resin separation procedure.

After the MeHg concentration analysis was complete, acid digestion sample tubes were removed from the refrigerator, brought to room temperature, and weighed (total solution mass was required for calculating the syringe filtering percent recovery). Digested samples were syringe filtered using 50-mL polypropylene syringes (no rubber on plunger) that had been cleaned with 5% HCl, and 0.45 µm polypropylene syringe filters. Just before filtering each digestion sample, the filter was cleaned by pipetting 15 mL of 15% HNO_3 into the syringe barrel and filtering into a waste container. The digestion sample was then shaken and carefully poured into the syringe barrel and filtered into either a 125-mL PETG bottle containing 50 mL of 1.1% HCl, or a 250-mL PETG bottle containing 150 mL of 1.1% HCl. All PETG bottles were pre-weighed and had previously been filled completely with 1% HCl, which was discarded just prior to syringe filtering without rinsing the bottles. After each digestion sample was syringe filtered into its PETG bottle, 15 mL of 1.1% HCl was pipetted into the glass digestion sample tube, which was shaken and then poured into the syringe barrel and filtered into the PETG bottle. This

rinse step was repeated a total of four times. At this point, samples filtered into 125-mL PETG bottles would have an acid content of 1.8% HNO_3 + 1% HCl, and samples filtered into 250-mL PETG bottles would have an acid content of 1% HNO_3 + 1% HCl. The PETG bottles were weighed (total solution mass was required for calculating the syringe filtering percent recovery), then a small aliquot was transferred from each bottle into a pre-weighed trace-metal clean borosilicate vial for MeHg and THg concentration analysis, and then the PETG bottles were weighed again (total solution mass was required for calculating the resin separation recovery). Next, the 0.1 M HCl was pipetted out of each of the 20-mL resin conditioning vials and discarded, and the vials were filled with a 1% HNO_3 + 1% HCl solution, shaken by hand, and poured into each of the PETG bottles. The PETG bottle caps were secured with parafilm and attached to the tube rotator which was tilted backward to 129º to accommodate the height of the bottles (Figure S3.1d-e). The bottles were rotated for 2 h at 25 rotations per minute, based on the mixing time used previously by Štrok et al. (2014) for their batch resin mercury pre-concentration procedure.

At the end of the rotation period, the contents of the PETG bottles were filtered using 0.45 µm cellulose nitrate filter cups (Thermo Scientific, #130-4045) and a vacuum pump (Figure S3.1f). Each filter cup was first conditioned with ~150 mL of a 1% HNO_3 + 1% HCl solution, which was filtered and discarded. For samples undergoing one resin separation step, the contents of the PETG bottle were filtered into a 500-mL Pyrex glass bottle that had been previously trace-metal cleaned in a hot 10% HNO_3 bath for at least 8 h and then filled with 1% HCl at room temperature for at least 8 h, then rinsed and set to dry. For samples undergoing two consecutive resin separation steps, the contents of the PETG bottle were filtered into a secondary PETG bottle (either into a 250-mL bottle if the sample was originally in a 125-mL bottle, or into a 500-

mL bottle if the sample was originally in a 250-mL bottle). As with the first set of PETG bottles, these Pyrex and secondary PETG bottles were also pre-weighed and had previously been filled completely with 1% HCl, which was discarded just prior to filtering the samples. After each sample was filtered, 40 mL of a 1% HNO_3 + 1% HCl solution was poured into the original PETG bottle, which was shaken, filtered, and poured into the new Pyrex or PETG bottle. This rinse step was repeated with two rounds of 40 mL of 0.1 M HCl and then 40 mL of deionized water. The Pyrex and PETG sample bottles were weighed (total solution mass was required for calculating the resin separation recovery), then a small aliquot was transferred from each PETG bottle into a pre-weighed trace-metal clean borosilicate vial for MeHg and THg concentration analysis, and then the PETG bottles were weighed again (total solution mass was required for calculating the second resin separation recovery). The resin separation process was repeated a second time for those samples in PETG bottles. After the second resin separation step, the samples were filtered (using new filter cups) into 500-mL Pyrex bottles. Pyrex sample bottles were refrigerated for up to 2 days before MeHg concentration analysis.

After the resin separation procedure was complete, sample aliquots were analyzed for their MeHg concentration following EPA Method 1630 (U.S. EPA 2001) as described in the previous section. Samples representing the final resin step (in Pyrex bottles) were analyzed in duplicate, and sample aliquots used to calculate recovery of MeHg after syringe filtering and the first of two resin separation steps (in glass vials) were each analyzed once. Following the MeHg concentration analysis, all Pyrex bottles and glass vials containing samples were weighed, and then the samples were oxidized with 5% BrCl for the final resin step samples in Pyrex bottles, or 10% BrCl for sample aliquots in glass vials, and weighed again. It is important while performing the resin separation procedure to not expose samples to any BrCl, including fumes, as this could

inadvertently oxidize MeHg and convert it into iHg. Brominated sample bottles and vials were placed on a covered hot plate at 70°C for a minimum of 2 days, and then aliquots of syringe filtered and resin separation samples were transferred into 15-mL Teflon vials, after which the sample bottles were immediately returned to the hot plate. Teflon sample vials were exposed to ultraviolet (UV) light for 7 to 16 days to break down dissolved organic matter – this was a conservative approach based on convenience and previous experience, but was not specifically optimized to maximize efficiency. Sample aliquots were then analyzed for their THg concentration by CVAFS following EPA Method 1631 (U.S. EPA 2002). Samples were analyzed in batches with quality control including calibration verification standards, secondary standards, blanks, and matrix spike recovery tests (see Section 3.5.1 in the Supporting Information). The MeHg and THg concentrations were used to calculate MeHg recovery and purity after each of the syringe filtering and resin separation steps (Table S3.3).

Prior to isotopic analysis, each of the final resin separation samples was chemically reduced, and the resulting Hg(0) was purged from solution and re-oxidized in a 1% KMnO4 trapping solution following previously described methods (Demers et al. 2013). In preparation for the purge and trap procedure, brominated samples were placed on a covered hot plate for 2 weeks to break down dissolved organic matter – again, this was a conservative approach based on convenience and previous experience but was not specifically optimized to maximize efficiency. Samples were then diluted to 1 L with deionized water and then further acidified (0.5% HCl). Additional BrCl (to 1% BrCl) was typically not necessary, as the samples had already been brought to 5% BrCl prior to dilution. Samples were then pre-reduced with 2 mL $HONH_3Cl$ per 1 L of 5% BrCl solution and allowed to react for ~1 h. Within the closed purge and trap system, samples were reduced with ~100 mL of 10% $SnCl_2$ (in 10% HCl), and the

resulting Hg(0) was purged from solution with clean-laboratory air (passed through a gold filter) and subsequently trapped in a 5-10 g oxidizing solution of 1% $KMnO_4$. The 1% $KMnO_4$ trap solutions were later reduced with $HONH_3Cl$, and a small aliquot was analyzed for THg concentration using CVAFS following EPA Method 1631 (U.S. EPA 2002) as previously described for combustion solutions. Purge-and-trap recovery of mercury from resin separation samples was 101.4 ± 1.8% (1SD, n=30 including aqueous MeHgCl standards, biological reference materials, and natural biota samples) (Table S3.4). Purge and trap procedural blanks and standards (7.5, 15, and 35 ng Hg; NIST SRM 3133) were used to monitor analytical performance. Procedural blank 1% $KMnO_4$ solutions, yielding 0.03 ng Hg (± 0.01 ng Hg, 1SD, n=3), represented <0.5% of sample solution mercury mass. Procedural standard recovery was 98.5 ± 0.7% (1SD, n=3) and procedural standards were not significantly fractionated isotopically relative to NIST SRM 3133 bracketing standards (Table S3.1).

3.2.5 Mercury isotopic analysis

Following the transfer (for combustion analysis) and purge and trap (for resin separation) pre-concentration procedures, the mercury isotopic composition of each 1% $KMnO_4$ trap solution (Table S3.4) was measured using cold vapor multiple collector inductively coupled plasma mass spectrometry (CV-MC-ICP-MS; Nu Instruments) using previously described methods (Lauretta et al. 2001, Blum and Bergquist 2007). Thallium (NIST SRM 997) was used as an internal standard to correct for instrumental mass bias, along with sample-standard bracketing with mercury standard NIST SRM 3133. On-peak zero corrections were applied to all masses.

Mass-dependent isotope fractionation (MDF) is reported as the permil (‰) deviation from the average of NIST SRM 3133 bracketing standards (Blum and Bergquist 2007) using delta notation:

$$\delta^{xxx}Hg\ (‰) = ([(^{xxx}Hg/^{198}Hg)_{sample} / (^{xxx}Hg/^{198}Hg)_{NIST\ SRM\ 3133}] - 1) * 1000$$

where xxx is the mass of each mercury isotope between ^{199}Hg and ^{204}Hg. Mass-dependent fractionation is reported as $\delta^{202}Hg$ values. Mass-independent isotope fractionation (MIF) is reported as the difference between the measured $\delta^{xxx}Hg$ value and that which is theoretically predicted by the kinetic mass-dependent fractionation law (Blum and Bergquist 2007), using capital delta notation:

$$\Delta^{xxx}Hg\ (‰) \approx \delta^{xxx}Hg - (\delta^{202}Hg * \beta)$$

where xxx is the mass of each mercury isotope ^{199}Hg, ^{200}Hg, ^{201}Hg, and ^{204}Hg, and β is a constant for each isotope (0.252, 0.502, 0.752, 1.493, respectively) (Blum and Bergquist 2007).

To characterize the analytical uncertainty and reproducibility associated with isotope ratio measurements, each analytical session included 5 to 14 analyses of a secondary standard (UM-Almadén) at representative mercury concentrations (1 to 5 ng g^{-1}). We also measured the isotopic composition of each combustion reference material two to four times within an analytical session. To evaluate the accuracy and reproducibility of our results, we calculated the mean isotopic composition (± 2SE) for the collection of independent preparations of UM-Almadén and each reference material type (Table S3.1), and compared those means to the long-term average isotopic composition measured at the University of Michigan (Blum and Johnson 2017). We represent the analytical uncertainty in the THg isotopic composition of natural biota samples (via combustion) with the average uncertainty (2SD) across combustion reference material analyses (Table S3.1, Table S3.2). Because each reference material process replicate

was analyzed only once for MeHg isotopic composition, we represent the analytical uncertainty in the MeHg isotopic composition of reference materials and natural biota samples (via resin separation) with the average uncertainty (2SD) across UM-Almadén analyzed alongside resin separation materials within each session (Table S3.1, Table S3.4). Additionally, in order to provide a direct comparison of the MeHg isotopic composition of our reference materials to other published values, we also report the reproducibility associated with complete process replicates (reported as 2SD) for each of the four biological reference materials (each with 4 or 5 replicates), and also for each of the five natural biota samples (each with 2 replicates) (Table S3.4).

3.3 Results and Discussion

3.3.1 Nitric acid digestion validation

Standard reference materials were used to assess the performance of the nitric acid digestion procedure. Reference materials included DORM-3 with an average MeHg recovery of 94.7 ± 0.8% (1SD, n=4), TORT-2 with an average recovery of 108.1 ± 2.4% (1SD, n=4), DOLT-2 with an average recovery of 114.4 ± 1.6% (1SD, n=5), and DOLT-5 with an average recovery of 108.2 ± 0.9% (1SD, n=5) relative to certified values (Table S3.3). The average measured MeHg concentrations for three of the four reference materials were within the uncertainty of their certified values, with the exception of DOLT-2 for which the measured MeHg concentration was within two times the uncertainty of its certified value (Table S3). The exact concentration, or titer (U.S. EPA 2001), of the Brooks Rand 1 ppm aqueous MeHgCl standard solution was found to be 1.076 μg g^{-1} MeHg (as Hg). When this titer was accounted for in the calibration curve used for MeHg analyses, this resulted in sample concentrations that were 7.6% higher than if the MeHgCl standard was assumed to be exactly 1.000 μg g^{-1}. It is unknown

whether the titer of the MeHg standard solution was accounted for in the calibration curves of the analyses performed to certify each of the reference materials. If it was not, then this might explain why our nitric acid digestion recoveries were ≥108% for three of the standard reference materials. In general, a difference in measured MeHg concentrations of 7.6% would have a very small effect on interpreting the results of environmental samples; however, this difference has a relatively large effect on calculating the percent purity (MeHg / THg) of resin separation samples (Table S3.3). Overall, we believe that it is important to use the exact titer of the MeHgCl standard solution in the calibration curves of all MeHg concentration analyses, even though it shifts the nitric acid digestion percent recovery for one of the reference materials (DOLT-2) just beyond its certified range.

The average percent relative standard deviation (%RSD) associated with the measured MeHg concentration of the nitric acid digestion sample replicates for both reference materials and natural biota samples was 1.2 ± 0.8% (1SD, n=9), demonstrating consistency in the extraction of MeHg during the nitric acid digestion. Aqueous MeHgCl standard tests (containing no solid material) had an average recovery of 97.9 ± 3.1% (1SD, n=7) after the nitric acid digestion. Duplicate matrix spike tests were performed on each of the reference materials and natural biota samples, in which a small aliquot of the aqueous MeHgCl standard solution was added to the glass sample tube prior to the start of the nitric acid digestion. The MeHg concentration of each of the matrix spike tests was ~2 to 3 times higher than the background concentration of the sample, with the exception of the mayfly larvae samples in which the matrix spike tests were ~6 times higher. Across all reference materials and natural biota samples, the average recovery for the matrix spike tests was 101.4 ± 2.4% (1SD, n=22) (Table S3.3). Complete recovery of nitric acid digestion matrix spike tests suggested that our MeHg

concentrations were not influenced by matrix interferences, and therefore, we did not make independent measurements of MeHg concentrations of natural biota samples using another mercury extraction technique. As individual laboratories develop the use of this or other MeHg separation techniques, it will be important to evaluate QA/QC metrics to determine whether independent verification of MeHg concentrations in natural samples is warranted. Overall, complete recovery of MeHg for the reference materials and matrix spike tests in this study, along with small %RSD values for sample replicates, demonstrates that the nitric acid digestion procedure was reliable for extracting MeHg from biota samples, which could then be subsequently separated from iHg for isotopic analysis using the resin separation procedure.

3.3.2 Separation efficiency of methylmercury in aqueous standard solutions

In order to follow a nitric acid digestion with a resin separation procedure, samples need to be diluted to a lower nitric acid content because MeHg degrades over time under high nitric acid content (Horvat 2005, Parker and Bloom 2005). Additionally, high acidity prevents iHg from adsorbing to the resin (Chen et al. 2010). We aimed to dilute the digestion sample solutions to 1-2% HNO_3 based on other studies which showed that MeHg solutions maintained their concentration for at least 2 weeks in a 1% HNO_3 matrix (Leermakers et al. 1990) and demonstrated complete adsorption of iHg to the same anion-exchange resin used in our study in a 1% HNO_3 + seawater matrix (Štrok et al. 2014). We also added ~1% HCl to form negatively charged iHg species ($HgCl_3^-$ and $HgCl_4^{2-}$) (Powell et al. 2009) that would be retained on the resin (Korkisch 1989), and to prevent MeHg from adsorbing to the PETG and glass bottles and vials throughout the process (Parker and Bloom 2005).

To test whether a 1% HNO_3 + 1% HCl matrix was sufficient for maintaining consistent MeHg concentrations throughout the resin separation process without either degrading the MeHg

or allowing the MeHg to be adsorbed to the walls of the container, we conducted a long-term holding test. This involved the use of 13-, 45-, and 135-pg g^{-1} aqueous MeHgCl standards in either a 1% HCl or a 1% HNO_3 + 1% HCl matrix, in both PETG and glass bottles. Each of the solutions was analyzed for its MeHg concentration after 0, 7, 14, 28, 49, and 83 days (Table S3.5). Aqueous MeHgCl standards at all three solution concentrations in a 1% HCl matrix in glass bottles maintained >97% recovery over the entire testing period. For the other three matrix + bottle type combinations (1% HCl in PETG; 1% HNO_3 + 1% HCl in glass; and 1% HNO_3 + 1% HCl in PETG), MeHg recovery across all three solution concentrations declined to ≤95% either between 7 and 14 days, or between 14 and 28 days (Figure S3.2). For MeHgCl standards in a 1% HNO_3 + 1% HCl matrix, the 13-pg g^{-1} solutions were more susceptible to loss of MeHg than solutions at higher concentrations, reaching minimum recoveries of 90.4% and 88.6% in glass and PETG bottles, respectively, though this difference in recovery at lower concentrations was not observed for MeHgCl standards in a 1% HCl matrix (Figure S3.2). Despite the observed losses of MeHg over time, potentially due to degradation by nitric acid and/or adsorption to PETG bottles, as long as the nitric acid digestion, syringe filtering, and resin separation procedures are performed in less than a week, the use of PETG bottles and a 1% HNO_3 + 1% HCl matrix should not influence MeHg recoveries.

We tested the syringe filtering and resin separation procedures using 3, 10, and 30 ng aqueous MeHgCl standards (~200, 670, and 2000 pg g^{-1} in 15 mL of 15% HNO_3 in glass centrifuge tubes prior to syringe filtering and dilution with 1.1% HCl). The average recovery of MeHg after syringe filtering was 98.3 ± 1.1% (1SD, n=5) and the average recovery of the resin separation was 98.6 ± 1.3% (1SD, n=5), resulting in an average cumulative recovery of 96.9 ± 1.8% (1SD, n=5) (Table S3.3). The average isotopic composition of the post-resin separation

aqueous MeHgCl standards (Table S3.4) was within error of the average THg isotopic composition of the source MeHgCl (Table S3.1). Note that different batches of Brooks Rand MeHgCl standards may be isotopically unique, as they are not certified for mercury isotopic composition, with recorded δ^{202}Hg values of different batches ranging from -1.21‰ to -0.48‰ (Janssen et al. 2015, Qin et al. 2018, Rosera et al. 2020, Zhang et al. 2021, Rosera et al. 2022). Average nitric acid digestion procedural blank solutions yielded 0.01 ng MeHg (± 0.02 ng MeHg, 1SD, n=3) after syringe filtering, and 0.03 ng MeHg (± 0.03 ng MeHg, 1SD, n=3) after the resin separation, representing <0.6% of the sample solution MeHg mass.

We also tested the resin separation procedure using 10, 100, and 250 ng aqueous iHg standards (NIST 3133 in 2% BrCl reduced with $HONH_3Cl$) and found that on average, 98.6 ± 0.5% (1SD, n=4) of the iHg had adsorbed to the resin. We found that using 5 g of resin only had a slightly higher iHg adsorption efficiency (99.4%, n=1) compared to using 2.5 g of resin (98.6%, n=1) for 250 ng aqueous iHg standards, and so we opted to use 2.5 g of resin for all resin separations to minimize resin usage. Average nitric acid digestion procedural blank solutions yielded 0.03 ng THg (± <0.01 ng THg, 1SD, n=3) after syringe filtering, and 0.06 (± 0.03 ng THg, 1SD, n=3) after the resin separation, representing <1.2% of the sample solution THg mass.

Overall, nearly complete recovery of MeHg and adsorption of iHg to the resin from aqueous standard solutions, along with the apparent lack of procedurally induced isotope fractionation, suggests that the batch resin separation procedure is a reliable method of separating MeHg from iHg in a 1-2% HNO_3 + 1% HCl matrix following a nitric acid digestion.

3.3.3 Separation efficiency of methylmercury for biological standard reference materials and natural biota samples

Across all four standard reference materials (DORM-3, TORT-2, DOLT-2, and DOLT-5), the average recovery of MeHg after syringe filtering the nitric acid digestion samples was 95.5 ± 2.3% (1SD, n=18). Similarly, across all five natural biota samples (shiner fillet, crayfish, megaloptera larvae, mayfly larvae, and Asian clams), the average recovery of MeHg after syringe filtering the nitric acid digestion samples was 96.9 ± 1.1% (1SD, n=10). The small losses of MeHg during syringe filtering could be explained by several factors, such as degradation and conversion into iHg by the ~15% HNO_3, re-adsorption to solid particles, or adsorption to the glass centrifuge tube after the initial MeHg concentration analysis but before syringe filtering, which were typically done 1 day apart. Other possible explanations include physical losses while filtering, adsorption to the 0.45 µm polypropylene syringe filter, or adsorption to the PETG bottle after filtering but before removing an aliquot for analysis and beginning the resin separation procedure, which was typically done the day after syringe filtering. To determine which of these potential explanations were more likely, we performed a test using replicate nitric acid digestion samples for DOLT-2, the shiner fillet, and the megaloptera larvae. We found that after 3 days in a refrigerator, the unfiltered nitric acid digestion samples still had an average MeHg recovery of 100.2 ± 0.4% (1SD, n=3), suggesting that the MeHg was not degraded by the ~15% HNO_3, nor had it re-adsorbed to solid particles or adsorbed to the glass centrifuge tubes over a 3-day holding time. These digestion samples were syringe filtered into PETG bottles, and aliquots were transferred into trace-metal clean glass vials immediately after filtering and again after ~12 and ~60 h, which were then analyzed for their MeHg concentration. Across these three samples, recovery of MeHg immediately after syringe filtering was 98.1 ± 0.7% (1SD, n=3), suggesting that ~2% of the MeHg was lost due to either physical losses or adsorption to the 0.45 µm polypropylene syringe filter. This result aligns with the MeHg recovery of 98.3 ± 1.1%

(1SD, n=5) after syringe filtering the aqueous MeHgCl standards (Table S3.3). For DOLT-2 and the megaloptera larvae, recovery of MeHg after ~12 and ~60 hours in a PETG bottle was 96.0 ± 1.2% (1SD, n=4), suggesting that another ~2% of the MeHg in these samples had adsorbed to the PETG bottles. For the shiner fillet, recovery of MeHg after ~12 and ~60 h was 98.4 ± 1.1% (1SD, n=2), suggesting that the shiner fillet sample did not experience a significant amount of MeHg adsorption to the PETG bottle. It should be noted that the DOLT-2 and megaloptera larvae digestion samples each contained ~20 ng MeHg, whereas the shiner fillet digestion sample contained ~70 ng MeHg, and so a larger mass of MeHg in the shiner fillet sample would need to be adsorbed to reflect a 2% adsorption loss. Thus, samples containing lower masses of MeHg may be more susceptible to decreases in recovery by adsorption. Overall, to minimize the loss of MeHg during and after syringe filtering, care must be taken to avoid physical losses, and it may be beneficial to use a different type of filter (e.g., 0.45 µm polyethersulfone filters). It is also important to begin the resin separation procedure as soon as possible after syringe filtering into PETG bottles, which is more easily achieved by working with smaller sample sets so that syringe filtering and the resin separation can be done on the same day.

Across the four standard reference materials, average recovery of MeHg after the first and second resin separation steps was 98.6 ± 2.5% (1SD, n=18) and 99.7 ± 2.3% (1SD, n=14), respectively. The average cumulative recovery of MeHg after syringe filtering and the resin separation procedure was 94.0 ± 2.6% (1SD, n=18) (Table S3.3). The resin separation recoveries of MeHg were similar among the four reference materials, but for the natural biota samples, recovery of MeHg after the first resin step was lower for the Asian clams than for the other four sample types. For the clam sample (6.3% MeHg in the solid material), the average recovery of MeHg was 90.1 ± 3.1% (1SD, n=2), and for the other four sample types (12, 13, 62, and 104%

MeHg in the solid material), the average recovery of MeHg was 98.7 ± 1.3% (1SD, n=8) after the first resin separation step. Unlike the first resin step, there was not a significant difference in MeHg recovery between natural biota sample types for the second resin separation step, with an average recovery of 97.9 ± 1.2% (1SD, n=8 excluding shiner fillets which only underwent one resin step). The average cumulative recovery of MeHg after syringe filtering and the resin separation procedure was 87.1 ± 1.2% (1SD, n=2) for clams and 93.7 ± 2.1% (1SD, n=8) for the other four sample types (Table S3.3). The reason for the lower MeHg recovery for the clam samples after the first resin separation step is unclear. It is possible that lower recovery during the first resin step for Asian clams could have been due to losses of MeHg by adsorption to the resin or binding to DOM or other compounds in the digestion sample matrix that were retained by the resin, which would have the greatest impact on recovery for samples containing the lowest mass of MeHg. However, the TORT-2, DOLT-5, and mayfly larvae digestion samples, as well as the 3 and 10 ng MeHgCl standard tests, each contained less MeHg than the clam digestion samples, but none of those other samples had major losses of MeHg to the resin or other surfaces, as demonstrated by their high recovery after the first resin step. Additionally, since high levels of DOM would be ubiquitous across all nitric acid digestion samples of biological material, the lower MeHg recovery for the clam samples alone, relative to all other biological reference materials and natural biota samples, is unlikely to have uniquely resulted from binding to DOM retained on the resin. While the explanation remains unclear, the lower MeHg recovery for the clam samples after the first resin separation step may be more related to the high level of iHg relative to MeHg within the digestion samples. Additional study is required to further explain the reason for lower MeHg recovery after the first resin separation for the clam samples

and to potentially modify the MeHg separation procedure to achieve higher cumulative MeHg recovery for samples with low %MeHg.

Based on measured MeHg concentrations relative to THg concentrations, MeHg purity was calculated for each of the standard reference materials and natural biota samples after syringe filtering and after each of the resin separation steps. These values indicate how much iHg remained in the samples after each step. For both the reference materials and natural biota samples, materials with >60% MeHg (DORM-3, shiner fillet, and crayfish) had ~100% MeHg purity after the first resin separation step, whereas materials with ≤60% MeHg had ~53-93% MeHg purity after the first resin step (Table S3.3). Although our aqueous iHg standard tests, which were not in the presence of DOM, demonstrated that 250 ng iHg could be adsorbed in a single resin step, this was not reflected in our reference materials and natural biota samples. For example, TORT-2, DOLT-2, and DOLT-5 each contained ~8-30 ng iHg, but these samples had ~85-93% MeHg purity after the first resin step and required a second resin separation step to further diminish the iHg impurities, bringing their MeHg purity up to ~94-99% (Table S3.3). Likewise, the megaloptera larvae, mayfly larvae, and Asian clam samples each contained ~85 to 240 ng iHg, and had ~53-69% MeHg purity after the first resin step and ~91-98% MeHg purity after the second resin step. Across all reference materials and natural biota samples, the average MeHg purity at the end of the resin separation procedure (whether they underwent one or two resin separation steps) was 97.8 ± 4.3% (1SD, n=28), with Asian clams having the lowest MeHg purity of 91.2 ± <0.1% (1SD, n=2) (Table S3.3). These high purity values demonstrate that a majority of the iHg was removed from each of the sample solutions by the resin.

For reference materials and natural biota samples that underwent two resin separation steps, the solid material left in the cellulose nitrate filter cup was typically a darker yellow color

after the first resin step than after the second resin step, and the aqueous solution became clearer and less foamy each time it was filtered. This could be due to negatively charged DOM within the digestion sample adsorbing to the anion-exchange resin along with the iHg. Though the exact mechanism is unknown, the presence of DOM may be the reason why iHg in the reference material and natural biota digestion samples was not adsorbing to the resin to the same extent as the aqueous iHg standard tests. Washburn et al. (2019) similarly found that for surface water samples with high levels of DOM, only 4.1 to 58.8% of the THg (n=3) was adsorbed when the samples were passed through a column containing the same anion-exchange resin used in our study, compared to an average of 91.6 ± 3.1% (1SD, n=7) for other surface water samples with lower levels of DOM. For our samples, once a substantial amount of the DOM was apparently removed from solution during the first resin step, the remaining iHg was more easily adsorbed to the resin during the second step. The slightly lower MeHg purity (91.2%) for the clam sample after the second resin separation step (Table S3.3) may have been due to both its low %MeHg (6.3%) as well as its organic-rich sample matrix. For samples with <10% MeHg and those with complex organic-rich matrices, additional modifications to this MeHg separation procedure may be necessary to achieve higher MeHg purity, such as utilizing a third resin separation step, using a larger amount of resin, or employing a resin column separation method rather than a batch resin separation method.

One strength of this study is our rigorous analysis of both MeHg and THg concentrations after each step in the process. The ability to calculate not only MeHg recovery, but also MeHg purity after syringe filtering and after each of the resin separation steps, provides validation that each of the resin-separated mercury samples truly represents MeHg in the organism and allows for the quantification of iHg impurities. Some previous studies using other MeHg separation

methods describe measuring both the MeHg and THg concentration after the final separation step so that both MeHg recovery and purity can be determined (Masbou et al. 2013, Li et al. 2017, Qin et al. 2020, Yang et al. 2021). Other studies describe measuring only the THg concentration after the final separation step (Rosera et al. 2020, Manceau et al. 2021, Poulin et al. 2021, Zhang et al. 2021, Rosera et al. 2022) and assume that this is equal to the MeHg concentration because, theoretically, all of the iHg should have been removed. However, THg concentration analysis alone could be misleading if MeHg recovery is low and if iHg impurities are present after the final separation step. A good example of this scenario involves the Asian clam sample in our study. Based on the MeHg concentration after the second resin separation step, the calculated cumulative recovery of MeHg was only 87.1% (Table S3.3). However, because there were iHg impurities in the sample at the end of the procedure, the apparent cumulative recovery of MeHg based on the THg concentration alone after the second resin step would have been 95.5%, making it seem like the procedure performed much better on the clam sample than it actually did. Achieving high MeHg recovery and purity is important for ensuring accurate measurements of MeHg isotopic composition, as losses of MeHg during the separation procedure could potentially lead to isotope fractionation, and the presence of iHg impurities would shift the measured MeHg isotopic composition toward that of the iHg. Therefore, regardless of which MeHg separation procedure is used, we recommend measuring both the MeHg and THg concentration after the final separation step, prior to isotopic analysis, to verify the actual MeHg recovery and purity for each sample.

For this method of isolating MeHg from biological samples involving nitric acid extraction coupled with batch anion-exchange resin separation, we recommend acceptable separation thresholds of ≥90% cumulative MeHg recovery and ≥90% MeHg purity, and suggest

that recovery and purity values are clearly reported for each sample. We note that the impact of iHg impurities on the measured isotopic composition of a resin-separated mercury sample depends not only on the amount of impurities, but also on the offset in isotopic composition between iHg and MeHg within the organism. For example, if the iHg and MeHg isotopic compositions are ~1‰ apart from one another, as is the case for TORT-2 and DOLT-2 (with δ^{202}iHg values calculated via mass balance using measured δ^{202}THg and δ^{202}MeHg values), then the isotopic composition of a resin-separated mercury sample with 90% MeHg purity would theoretically be shifted toward that of the iHg by ~0.1‰. In this study, the offsets in δ^{202}Hg and Δ^{199}Hg values of iHg and MeHg within the natural biota samples were never more than ~0.3‰, and so the measured MeHg isotope ratios of even the Asian clam samples with only ~91% MeHg purity (Table S3.3) would theoretically be shifted by only ~0.03‰. Shifts in the measured MeHg isotopic composition caused by the presence of <10% iHg impurities are unlikely to influence interpretations based on these measured values, though this in part would depend on the overall range in measured MeHg and THg isotopic compositions of organisms (and basal resources) within the study.

Based on high MeHg recovery and purity (Table S3.3), nitric acid digestion paired with a batch resin separation procedure is a reliable method for isolating MeHg from iHg for compound-specific isotopic analysis. We recommend using two batch resin separation steps (each with 2.5 g of resin) for biota samples with less than ~60% MeHg in the solid material, and only one resin separation step for biota samples with greater than ~60% MeHg. However, for biota samples near this ~60% MeHg threshold, sample type may also be an important variable to consider when deciding whether to use one or two resin separation steps. For example, TORT-2 lobster hepatopancreas and the natural crayfish muscle tissue sample both had 56-62% MeHg,

but only TORT-2 benefitted from a second resin separation step whereas the crayfish had already reached ~100% MeHg purity after the first step (Table S3.3). This suggests that protein-rich samples (e.g., muscle tissue) with moderate %MeHg values may require only one resin step, whereas more complex sample matrices (e.g., organ tissue or whole-body homogenates) with moderate %MeHg values may require two resin steps, potentially due to the quantity and/or quality of organic matter within different sample types. Further investigation may be needed to address differing results for different sample matrices.

3.3.4 Methylmercury isotopic composition of biological standard reference materials and natural biota samples

The MeHg isotopic compositions of the biological reference materials in our study are similar to the values obtained in other studies for the same materials (Figure 3.2). Because the reference materials are not certified for their MeHg isotopic composition, we do not know the "true" isotopic composition or whether there are slight differences between batches. The reproducibility associated with complete process replicates (2SD, n=4 or 5) for each of the four types of reference materials ranged from 0.04 to 0.15‰ for δ^{202}MeHg and from 0.03 to 0.04‰ for Δ^{199}MeHg (Table S3.4). S4). These values showed better reproducibility than those associated with the online GC method (Bouchet et al. 2018) and were comparable to those associated with offline GC separation (Qin et al. 2018), toluene extraction (Masbou et al. 2013, Li et al. 2017, Qin et al. 2020, Rosera et al. 2020, Yang et al. 2021, Zhang et al. 2021), distillation and resin separation (Rosera et al. 2020, Manceau et al. 2021, Poulin et al. 2021, Rosera et al. 2022), and KOH digestion and purge and trap (Zhang et al. 2021) methods (Figure 3.2). Similarly, the reproducibility of the MeHg isotopic composition associated with complete process replicates (2SD, n=2) for each of the five natural biota samples ranged from <0.01 to

0.15‰ for δ^{202}MeHg and from 0.01 to 0.03‰ for Δ^{199}MeHg (Figure 3.3a, Table S3.4), also indicating high reproducibility for our nitric acid digestion and resin separation method. Note that the analytical uncertainty in the isotopic composition of MeHg in resin separation samples is represented by the average uncertainty (2SD) across UM-Almadén analyses (0.05‰ for δ^{202}MeHg and 0.04‰ for Δ^{199}MeHg) (Table S3.1, Table S3.4).

The MeHg isotopic compositions of TORT-2 (56% MeHg) and DOLT-2 (35% MeHg) differed from their THg isotopic composition, both having δ^{202}MeHg and Δ^{199}MeHg values that were higher than their respective δ^{202}THg and Δ^{199}THg values (Table S3.1, Table S3.4). The MeHg isotopic composition of DORM-3 (93% MeHg) was more similar to its THg isotopic composition, as expected. Additionally, some natural biota samples had MeHg isotopic compositions that differed from their THg isotopic compositions, while others had isotopically similar MeHg and THg isotopic compositions. In comparison to the THg isotopic composition of each of the biota samples, mayfly larvae (13% MeHg) and clams (6.3% MeHg) had δ^{202}MeHg values that were lower than their respective δ^{202}THg values, whereas the shiner fillet (104% MeHg), crayfish (62% MeHg), and megaloptera larvae (12% MeHg) each had δ^{202}MeHg and δ^{202}THg values that were similar (Figure 3.3a). Each of the biota samples had Δ^{199}MeHg values that were higher than their respective Δ^{199}THg values, with the exception of the shiner fillet for which the Δ^{199}MeHg and Δ^{199}THg values were similar (Figure 3.3a).

One previously developed method of estimating the isotopic compositions of iHg and MeHg within a food web involves performing linear regressions for δ^{202}THg vs. %MeHg and Δ^{199}THg vs. %MeHg (Kwon et al. 2015, Xu et al. 2016, Meng et al. 2020). The points at which δ^{202}THg and Δ^{199}THg intercept with 100% MeHg indicate the approximate MeHg isotopic composition, and the points at which δ^{202}THg and Δ^{199}THg intercept with 0% MeHg indicate the

approximate iHg isotopic composition of the food web. Although the five natural biota samples used in this study were collected from the same stream, their δ^{202}THg and %MeHg results do not conform to a linear relationship (Figure 3.3c). Three of the natural biota samples have relatively low %MeHg (6.3 to 13%) but have a wide range in δ^{202}THg (-0.76 to -0.14‰) (Figure 3.3c), potentially due to the presence of multiple isotopically distinct sources of iHg to the food web. Without a linear relationship between δ^{202}THg and %MeHg, the MeHg isotopic composition of each of these three samples could not be estimated using the regression method. Additionally, although there appears to be a relatively linear relationship between Δ^{199}THg and %MeHg for these five natural biota samples (Figure 3.3b), the extracted MeHg isotopic compositions revealed a range in Δ^{199}MeHg values (0.13 to 0.33‰), whereas an ordinary least-squares regression provides only a single value for Δ^{199}MeHg (0.25 ± 0.04‰, 1SE).

Another previously developed method of estimating the MeHg isotopic composition of organisms involves assigning a consistent iHg isotopic composition to all organisms in a food web, and then calculating the MeHg isotopic composition of each organism using mass balance (Tsui et al. 2012). However, this approach relies on the assumption that there is only one primary source of iHg to the food web, and that the iHg source has been correctly identified. While linear regression and isotopic mass balance approaches for estimating MeHg isotopic compositions of organisms may work well for food webs with only one primary source of iHg and one source of MeHg (Xu et al. 2016), the ability to extract and isolate MeHg for direct isotopic analysis is especially beneficial for food webs with multiple isotopically distinct sources of iHg and/or MeHg.

3.4 Conclusion

In this study, the use of a nitric acid digestion combined with a batch anion-exchange resin separation procedure has been shown to successfully separate MeHg from iHg within fish and aquatic invertebrate samples, allowing for accurate and precise measurements of MeHg isotopic composition that compare well with other offline separation methods. This new method has some distinct advantages over other MeHg separation methods. For example, nitric acid digestion and batch resin separation procedures are relatively simple methods that can be done without investing in the set-up and careful optimization of distillation procedures, which can be an obstacle for labs that do not already have experience with this technique. Nitric acid digestion is a well-established, widely used method of determining MeHg concentrations of biological samples, and the resin separation procedure can be added as a secondary step without repeating or performing a different mercury extraction technique on a separate sample aliquot. Not only does this eliminate additional procedures for independently measuring MeHg concentrations, but it also conserves sample mass, which is often limited. Moreover, this streamlining of MeHg concentration and separation techniques promotes a tight coupling between MeHg concentration, %MeHg, and isotopic composition, which will likely benefit studies of complex food webs. Additionally, for certain sample types, a nitric acid digestion may be a more suitable method than an alkaline digestion or a toluene extraction. Alkaline digestions can sometimes cause excessive foaming during the MeHg concentration analysis (Brooks Rand Instruments 2013), and toluene extractions have been shown to produce a lipid emulsion for some fish (Maggi et al. 2009, Watanabe et al. 2015, Valsecchi et al. 2021) and plankton (Rosera et al. 2020) samples, and is also more toxic. However, the nitric acid digestion and resin separation procedure also has some limitations, such as the total amount of time elapsed between digestion and isotopic

analysis, as well as the apparent challenges of achieving high MeHg purity in the presence of organic-rich matrices with low %MeHg, as demonstrated with Asian clams. With additional optimization of UV treatment and hot plate digestion steps, it is likely that the amount of time required for the nitric acid digestion and resin separation method could be substantially decreased. Also, given the success of this method with biological samples ranging from 6 to 100% MeHg, follow-up studies that extend the use of nitric acid digestion and resin separation procedures to isolate MeHg from basal resources with <10% MeHg are warranted.

By measuring both the MeHg and THg concentration at several points throughout the MeHg separation process, we were able to independently calculate MeHg recovery and purity for each sample prior to isotopic analysis. We recommend adopting this practice regardless of which MeHg separation method is chosen, because measuring the THg concentrations alone at the end of the procedure has the potential to mask incomplete MeHg recovery if iHg impurities are present. This may be especially important for unknown samples that have low %MeHg, a high organic matter content, and/or a particularly complex matrix, as these types of samples may have an increased risk of being affected by loss of MeHg and incomplete removal of iHg.

We have also shown that for some of the biological standard reference materials and natural biota samples, the isotopic composition of MeHg within the organism can be different from its THg isotopic composition, and that these MeHg isotopic compositions may not be accurately estimated by the regression method when the relationship between THg isotope ratios and %MeHg is not linear. In such cases, directly measuring the isotopic composition of MeHg within organisms, as well as within basal resources, will aid in determining the sources of MeHg production within the ecosystem.

Acknowledgements

We would like to thank Teresa Mathews, senior scientist and group leader of the Biodiversity and Ecosystem Health Group within the Environmental Sciences Division at Oak Ridge National Laboratory, for helping facilitate our collection of aquatic invertebrate samples from East Fork Poplar Creek, and for supplying the fish tissue sample used in this study. Patrick Donovan, Spencer Washburn, and Aaron Kurz also provided valuable assistance with the collection of benthic invertebrates used in this study. We would also like to thank Paul Drevnick for the use of the Brooks Rand automated MERX MeHg analyzer. This manuscript was improved substantially thanks to the thoughtful comments of two anonymous reviewers.

This research was supported by the U.S. Department of Energy (DOE), Office of Science, Biological and Environmental Research (BER), Subsurface Biogeochemical Research (SBR) program under Award No. DE-SC0016489 and is also a product of the Critical Interfaces Science Focus Area (SFA) at Oak Ridge National Laboratory (ORNL). ORNL is managed by UT-Battelle, LLC for the DOE under Contract No. DE-AC05-00OR22725. Additional funding was provided by the Geological Society of America Graduate Student Research Grant (2019), the University of Michigan (UM) Rackham Graduate Student Research Grant (2019), the UM Scott Turner Award (2020 and 2021), the Anchor QEA Scholarship (2021), and the John D. MacArthur Professorship.

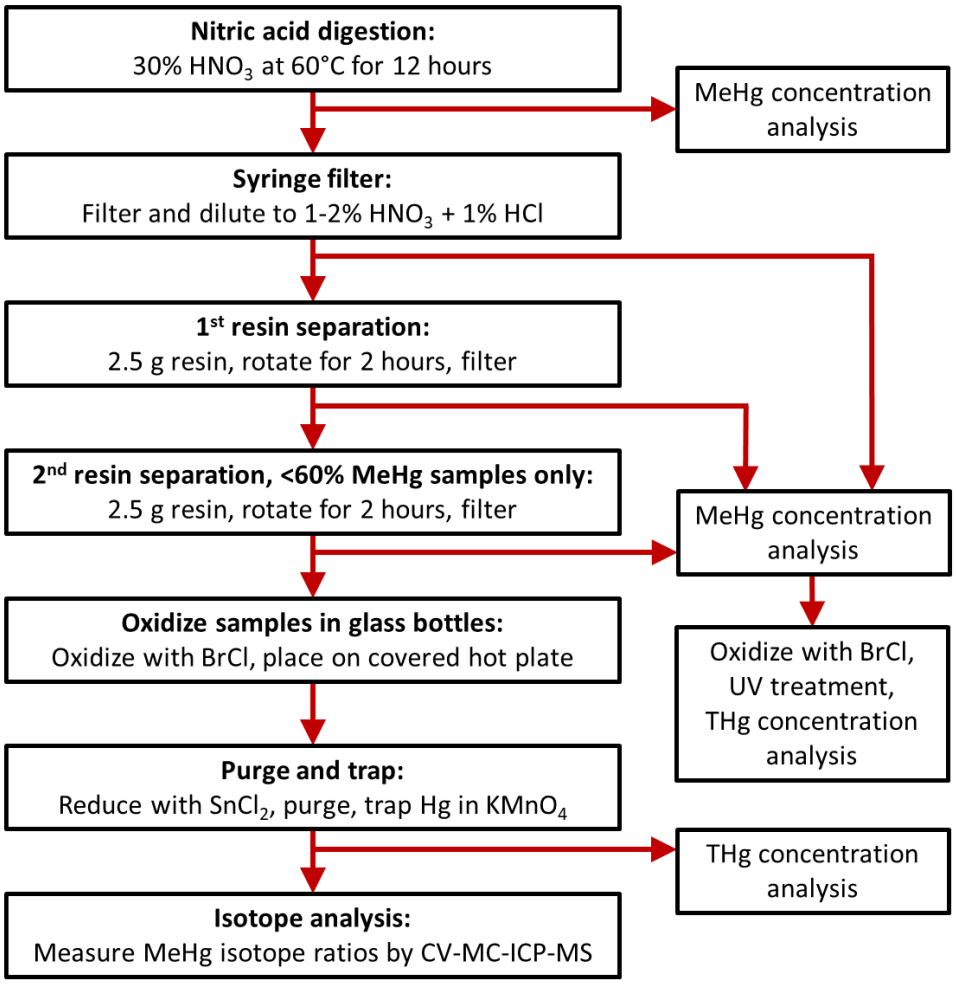

Figure 3.1. Schematic of MeHg extraction, quantification, separation from iHg, pre-concentration, and isotopic analysis, along with THg and MeHg concentration analyses to quantify MeHg recovery and purity.

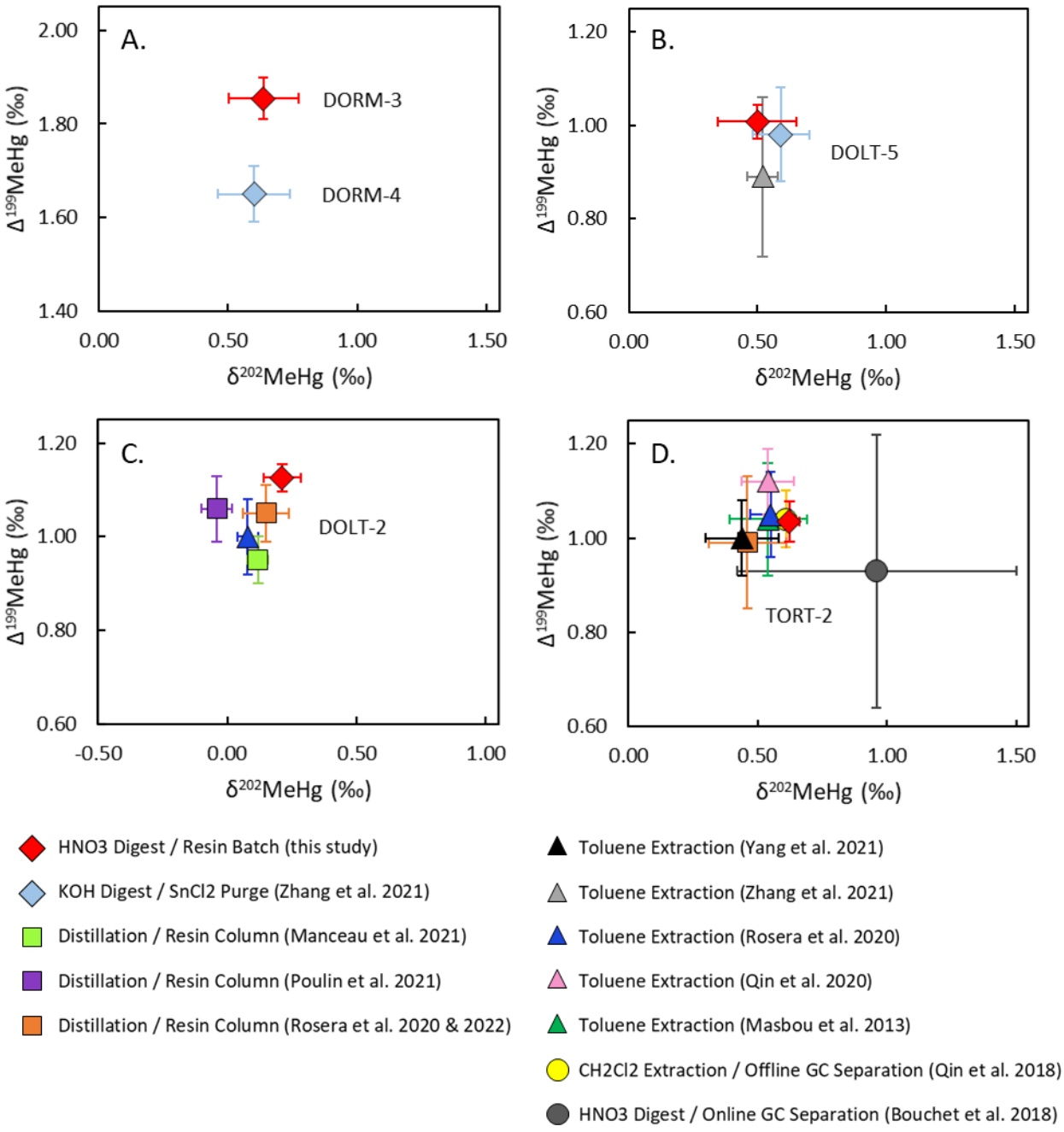

Figure 3.2. Methylmercury isotopic compositions of biological reference materials including (A) DORM-3 and DORM-4, (B) DOLT-5, (C) DOLT-2, and (D) TORT-2, as reported for this study and in the literature using other MeHg separation techniques (Masbou et al. 2013, Bouchet et al. 2018, Qin et al. 2018, Qin et al. 2020, Rosera et al. 2020, Manceau et al. 2021, Poulin et al. 2021, Yang et al. 2021, Zhang et al. 2021, Rosera et al. 2022).

Note that for (D), partially obscured symbols include an orange square, green triangle, and yellow circle. In order to compare our data with previously published values, the error bars in this figure show the reproducibility associated with complete process replicates (2SD) for each reference material (Table S3.4).

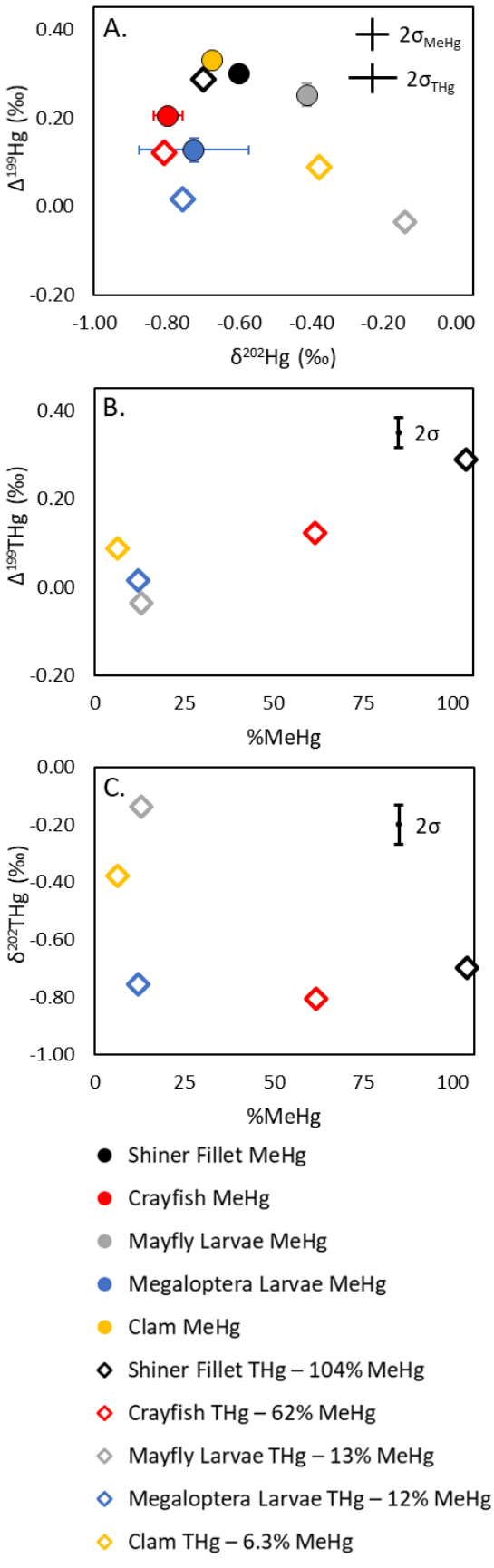
A.
2σMeHg
2σTHg
Δ199Hg (‰)
δ202Hg (‰)
B.
2σ
Δ199THg (‰)
%MeHg
C.
2σ
δ202THg (‰)
%MeHg
Shiner Fillet MeHg
Crayfish MeHg
Mayfly Larvae MeHg
Megaloptera Larvae MeHg
Clam MeHg
Shiner Fillet THg – 104% MeHg
Crayfish THg – 62% MeHg
Mayfly Larvae THg – 13% MeHg
Megaloptera Larvae THg – 12% MeHg
Clam THg – 6.3% MeHg

Figure 3.3. THg (open symbols) and MeHg (filled symbols) isotopic compositions of natural biota samples. Shown are (A) Δ^{199}Hg vs. δ^{202}Hg for both THg and MeHg, (B) Δ^{199}THg vs. %MeHg, and (C) δ^{202}THg vs. %MeHg.

Error bars on each of the filled symbols (MeHg) show the reproducibility associated with complete process replicates (2SD, n=2 for each sample type) (Table S3.4), which in most cases are the same size or smaller than the size of the symbol. Analytical uncertainty in THg delta values is shown as the average uncertainty (2SD) across combustion reference material analyses (Table S3.2). Analytical uncertainty in MeHg delta values is shown as the average uncertainty (2SD) across UM-Almadén analyses (Table S3.4).

References

Alderighi, Lucia, Peter Gans, Stefano Midollini, and Alberto Vacca. 2003. "Co-ordination chemistry of the methylmercury(II) ion in aqueous solution: a thermodynamic investigation." *Inorganica Chimica Acta* 356:8-18. doi: 10.1016/S0020-1693(03)00317-7.

Balarama Krishna, M. V., and D. Karunasagar. 2015. "Robust ultrasound assisted extraction approach using dilute TMAH solutions for the speciation of mercury in fish and plant materials by cold vapor atomic absorption spectrometry (CVAAS)." *Analytical Methods* 7:1997-2005. doi: 10.1039/C4AY02114B.

Barkay, Tamar, and Baohua Gu. 2022. "Demethylation–the other side of the mercury methylation coin: A critical review." *ACS Environmental Au* 2:77-97. doi: 10.1021/acsenvironau.1c00022.

Bloom, Nicolas S., John A. Colman, and Lee Barber. 1997. "Artifact formation of methyl mercury during aqueous distillation and alternative techniques for the extraction of methyl mercury from environmental samples." *Fresenius J Anal Chem* 358:371-377.

Blum, Joel D., and Bridget A. Bergquist. 2007. "Reporting of variations in the natural isotopic composition of mercury." *Analytical and Bioanalytical Chemistry* 388:353-359. doi: 10.1007/s00216-007-1236-9.

Blum, Joel D., and Marcus W. Johnson. 2017. "Recent developments in mercury stable isotope analysis." *Reviews in Mineralogy and Geochemistry* 82:733-757. doi: 10.2138/rmg.2017.82.17.

Blum, Joel D., Laura S. Sherman, and Marcus W. Johnson. 2014. "Mercury isotopes in earth and environmental sciences." *Annual Review of Earth and Planetary Sciences* 42:249-269. doi: 10.1146/annurev-earth-050212-124107.

Bouchet, Sylvain, Sylvain Bérail, and David Amouroux. 2018. "Hg compound-specific isotope analysis at ultratrace levels using an on line gas chromatographic preconcentration and separation strategy coupled to multicollector-inductively coupled plasma mass spectrometry." *Analytical Chemistry* 90:7809-7816. doi: 10.1021/acs.analchem.7b04555.

Brocza, Flora M., Harald Biester, Jan-Helge Richard, Stephan M. Kraemer, and Jan G. Wiederhold. 2019. "Mercury isotope fractionation in the subsurface of a Hg(II) chloride-contaminated industrial legacy site." *Environmental Science & Technology* 53:7296-7305. doi: 10.1021/acs.est.9b00619.

Brooks Rand Instruments. 2013. Application Note: Nitric acid digestion of biological tissue for methylmercury analysis.

Chen, Jiubin, Holger Hintelmann, and Brian Dimock. 2010. "Chromatographic pre-concentration of Hg from dilute aqueous solutions for isotopic measurement by MC-ICP-MS." *Journal of Analytical Atomic Spectrometry* 25:1402-1409. doi: 10.1039/c0ja00014k.

Crowther, Elizabeth R., Jason D. Demers, Joel D. Blum, Scott C. Brooks, and Marcus W. Johnson. 2021. "Use of sequential extraction and mercury stable isotope analysis to assess remobilization of sediment-bound legacy mercury." *Environmental Science: Processes & Impacts* 23:756-775. doi: 10.1039/d1em00019e.

Demers, Jason D., Joel D. Blum, and Donald R. Zak. 2013. "Mercury isotopes in a forested ecosystem: Implications for air-surface exchange dynamics and the global mercury cycle." *Global Biogeochemical Cycles* 27:222-238. doi: 10.1002/gbc.20021.

Dzurko, Mark, Delphine Foucher, and Holger Hintelmann. 2009. "Determination of compound-specific Hg isotope ratios from transient signals using gas chromatography coupled to multicollector inductively coupled plasma mass spectrometry (MC-ICP/MS)." *Analytical and Bioanalytical Chemistry* 393:345-355. doi: 10.1007/s00216-008-2165-y.

Entwisle, John, Dmitriy Malinovsky, Philip J. H. Dunn, and Heidi Goenaga-Infante. 2018. "Hg isotope ratio measurements of methylmercury in fish tissues using HPLC with off line cold vapour generation MC-ICPMS." *Journal of Analytical Atomic Spectrometry* 33:1645-1654. doi: 10.1039/c8ja00099a.

Epov, Vladimir N., Sylvain Bérail, María Jiménez-Moreno, Vincent Perrot, Christophe Pecheyran, David Amouroux, and Olivier F. X. Donard. 2010. "Approach to measure isotopic ratios in species using multicollector-ICPMS coupled with chromatography." *Analytical Chemistry* 82:5652-5662. doi: 10.1021/ac100648f.

Epov, Vladimir N., Pablo Rodríguez-González, Jeroen E. Sonke, Emmanuel Tessier, David Amouroux, Laurence Maurice Bourgoin, and Olivier F. X. Donard. 2008. "Simultaneous determination of species-specific isotopic composition of Hg by gas chromatography coupled to multicollector ICPMS." *Analytical Chemistry* 80:3530-3538. doi: 10.1021/ac800384b.

Gao, Ying, Rui Liu, and Lu Yang. 2013. "Application of chemical vapor generation in ICP-MS: A review." *Chinese Science Bulletin* 58:1980-1991. doi: 10.1007/s11434-013-5751-0.

Grigg, Andrew R. C., Ruben Kretzschmar, Robin S. Gilli, and Jan G. Wiederhold. 2018. "Mercury isotope signatures of digests and sequential extracts from industrially contaminated soils and sediments." *Science of The Total Environment* 636:1344-1354. doi: 10.1016/j.scitotenv.2018.04.261.

Hammerschmidt, Chad R., and William F. Fitzgerald. 2005. "Methylmercury in mosquitoes related to atmospheric mercury deposition and contamination." *Environmental Science & Technology* 39:3034-3039. doi: 10.1021/es0485107.

Hintelmann, H., R. Falter, G. Ilgen, and R. D. Evans. 1997. "Determination of artifactual formation of monomethylmercury (CH_3Hg^+) in environmental samples using stable Hg^{2+} isotopes with ICP-MS detection: Calculation of contents applying species specific isotope addition." *Fresenius' Journal of Analytical Chemistry* 358:363-370. doi: 10.1007/s002160050431.

Horvat, Milena. 2005. "Determination of mercury and its compounds in water, sediment, soil and biological samples." In *Dynamics of Mercury Pollution on Regional and Global Scales: Atmospheric Processes and Human Exposures Around the World*, edited by Nicola Pirrone and Kathryn R. Mahaffey, 153-190. New York, NY: Springer Science+Business Media Inc.

Huang, Shuyuan, Yuhan Zhao, Supeng Lv, Weiguo Wang, Weili Wang, Yuanbiao Zhang, Yunlong Huo, Xiuwu Sun, and Yaojin Chen. 2021. "Distribution of mercury isotope signatures in Yundang Lagoon, Xiamen, China, after long-term interventions." *Chemosphere* 272:129716. doi: 10.1016/j.chemosphere.2021.129716.

Janssen, Sarah E., Marcus W. Johnson, Joel D. Blum, Tamar Barkay, and John R. Reinfelder. 2015. "Separation of monomethylmercury from estuarine sediments for mercury isotope analysis." *Chemical Geology* 411:19-25. doi: 10.1016/j.chemgeo.2015.06.017.

Korkisch, Johann. 1989. *Handbook of Ion Exchange Resins: Their Application to Inorganic Analytical Chemistry*. Vol. 4. Boca Raton, FL: CRC Press.

Krupp, Eva M., and Olivier F. X. Donard. 2005. "Isotope ratios on transient signals with GC-MC-ICP-MS." *International Journal of Mass Spectrometry* 242:233-242. doi: 10.1016/j.ijms.2004.11.026.

Kwon, Sae Yun, Joel D. Blum, Celia Y. Chen, Dustin E. Meattey, and Robert P. Mason. 2014. "Mercury isotope study of sources and exposure pathways of methylmercury in estuarine food webs in the northeastern U.S." *Environmental Science & Technology* 48:10089-10097. doi: 10.1021/es5020554.

Kwon, Sae Yun, Joel D. Blum, Knute J. Nadelhoffer, J. Timothy Dvonch, and Martin Tsz-Ki Tsui. 2015. "Isotopic study of mercury sources and transfer between a freshwater lake and adjacent forest food web." *Science of The Total Environment* 532:220-229. doi: 10.1016/J.SCITOTENV.2015.06.012.

Lauretta, Dante S., Bjoern Klaue, Joel D. Blum, and Peter R. Buseck. 2001. "Mercury abundances and isotopic compositions in the Murchison (CM) and Allende (CV) carbonaceous chondrites." *Geochimica et Cosmochimica Acta* 65:2807-2818. doi: 10.1016/s0016-7037(01)00630-5.

Leermakers, M., P. Lansens, and W. Baeyens. 1990. "Storage and stability of inorganic and methylmercury solutions." *Fresenius' Journal of Analytical Chemistry* 336:655-662.

Li, Dan, Yanbin Li, and Xiulin Wang. 2018. "Study on the simultaneous reduction of methylmercury by $SnCl_2$ when analyzing inorganic Hg in aqueous samples." *Journal of Environmental Sciences* 68:177-184. doi: 10.1016/j.jes.2018.02.017.

Li, Ping, Buyun Du, Laurence Maurice, Laure Laffont, Christelle Lagane, David Point, Jeroen E. Sonke, Runsheng Yin, Che-Jen Lin, and Xinbin Feng. 2017. "Mercury isotope signatures of methylmercury in rice samples from the Wanshan mercury mining area, China: Environmental implications." *Environmental Science & Technology* 51:12321-12328. doi: 10.1021/acs.est.7b03510.

Maggi, Chiara, Maria Teresa Berducci, Jessica Bianchi, Michele Giani, and Luigi Campanella. 2009. "Methylmercury determination in marine sediment and organisms by Direct Mercury Analyser." *Analytica Chimica Acta* 641:32-36. doi: 10.1016/j.aca.2009.03.033.

Magos, L. 1971. "Selective atomic-adsorption determination of inorganic mercury and methylmercury in undigested bioogical samples." *Analyst* 96:847-853. doi: 10.1039/AN9719600847.

Malinovsky, D., and F. Vanhaecke. 2011. "Mercury isotope fractionation during abiotic transmethylation reactions." *International Journal of Mass Spectrometry* 307:214-224. doi: 10.1016/j.ijms.2011.01.020.

Malinovsky, Dmitriy, Kris Latruwe, Luc Moens, and Frank Vanhaecke. 2010. "Experimental study of mass-independence of Hg isotope fractionation during photodecomposition of dissolved methylmercury." *Journal of Analytical Atomic Spectrometry* 25:950-956. doi: 10.1039/B926650J.

Manceau, Alain, Romain Brossier, Sarah E. Janssen, Tylor J. Rosera, David P. Krabbenhoft, Yves Cherel, Paco Bustamante, and Brett A. Poulin. 2021. "Mercury isotope fractionation by internal demethylation and biomineralization reactions in seabirds: Implications for environmental mercury science." *Environmental Science & Technology* 55:13942-13952. doi: 10.1021/acs.est.1c04388.

Masbou, Jeremy, David Point, and Jeroen E. Sonke. 2013. "Application of a selective extraction method for methylmercury compound specific stable isotope analysis (MeHg-CSIA) in

biological materials." *Journal of Analytical Atomic Spectrometry* 28:1620-1628. doi: 10.1039/c3ja50185j.

McLagan, D. S., L. Schwab, J. G. Wiederhold, L. Chen, J. Pietrucha, S. M. Kraemer, and H. Biester. 2022. "Demystifying mercury geochemistry in contaminated soil-groundwater systems with complementary mercury stable isotope, concentration, and speciation analyses." *Environmental Science: Processes & Impacts*. doi: 10.1039/d1em00368b.

Meng, Mei, Ruo-Yu Sun, Hong-Wei Liu, Ben Yu, Yong-Guang Yin, Li-Gang Hu, Jiu-Bin Chen, Jian-Bo Shi, and Gui-Bin Jiang. 2020. "Mercury isotope variations within the marine food web of Chinese Bohai Sea: Implications for mercury sources and biogeochemical cycling." *Journal of Hazardous Materials* 384:121379. doi: 10.1016/j.jhazmat.2019.121379.

Parker, Jennifer L., and Nicolas S. Bloom. 2005. "Preservation and storage techniques for low-level aqueous mercury speciation." *Science of the Total Environment* 337:253-263. doi: 10.1016/j.scitotenv.2004.07.006.

Poulin, Brett A., Sarah E. Janssen, Tylor J. Rosera, David P. Krabbenhoft, Collin A. Eagles-Smith, Joshua T. Ackerman, A. Robin Stewart, Eunhee Kim, Zofia Baumann, Jeong-Hoon Kim, and Alain Manceau. 2021. "Isotope fractionation from *in vivo* methylmercury detoxification in waterbirds." *ACS Earth and Space Chemistry* 5:990-997. doi: 10.1021/acsearthspacechem.1c00051.

Powell, Kipton J., Paul L. Brown, Robert H. Byrne, Tamás Gajda, Glenn Hefter, Staffan Sjöberg, and Hans Wanner. 2009. "Chemical speciation of environmentally significant heavy metals with inorganic ligands. Part 1: The Hg^{2+}– Cl^{-}, OH^{-}, CO_3^{2-}, SO_4^{2-}, and PO_4^{3-} aqueous systems." *Pure and Applied Chemistry* 77:739-800. doi: 10.1351/pac200577040739.

Qin, Chongyang, Min Chen, Haiyu Yan, Lihai Shang, Heng Yao, Ping Li, and Xinbin Feng. 2018. "Compound specific stable isotope determination of methylmercury in contaminated soil." *Science of the Total Environment* 644:406-412. doi: 10.1016/j.scitotenv.2018.06.328.

Qin, Chongyang, Buyun Du, Runsheng Yin, Bo Meng, Xuewu Fu, Ping Li, Leiming Zhang, and Xinbin Feng. 2020. "Isotopic fractionation and source appointment of methylmercury and inorganic mercury in a paddy ecosystem." *Environmental Science & Technology* 54:14334-14342. doi: 10.1021/acs.est.0c03341.

Regnell, Olof, and Carl J. Watras. 2019. "Microbial mercury methylation in aquatic environments: A critical review of published field and laboratory studies." *Environmental Science & Technology* 53:4-19. doi: 10.1021/acs.est.8b02709.

Rodríguez-González, Pablo, Vladimir N. Epov, Romain Bridou, Emmanuel Tessier, Remy Guyoneaud, Mathilde Monperrus, and David Amouroux. 2009. "Species-specific stable isotope fractionation of mercury during Hg(II) methylation by an anaerobic bacteria (*Desulfobulbus propionicu*s) under dark conditions." *Environmental Science & Technology* 43:9183-9188. doi: 10.1021/es902206j.

Rosera, Tylor J., Sarah E. Janssen, Michael T. Tate, Ryan F. Lepak, Jacob M. Ogorek, John F. DeWild, Christopher L. Babiarz, David P. Krabbenhoft, and James P. Hurley. 2020. "Isolation of methylmercury using distillation and anion-exchange chromatography for isotopic analyses in natural matrices." *Analytical and Bioanalytical Chemistry* 412:681-690. doi: 10.1007/s00216-019-02277-0.

Rosera, Tylor J., Sarah E. Janssen, Michael T. Tate, Ryan F. Lepak, Jacob M. Ogorek, John F. DeWild, David P. Krabbenhoft, and James P. Hurley. 2022. "Methylmercury stable isotopes: New insights on assessing aquatic food web bioaccumulation in legacy impacted regions." *ACS ES&T Water* 2:701-709. doi: 10.1021/acsestwater.1c00285.

Selin, Noelle E. 2009. "Global biogeochemical cycling of mercury: A review." *Annual Review of Environment and Resources* 34:43-63. doi: 10.1146/annurev.environ.051308.084314.

Stetson, Sarah J., John E. Gray, Richard B. Wanty, and Donald L. Macalady. 2009. "Isotopic variability of mercury in ore, mine-waste calcine, and leachates of mine-waste calcine from areas mined for mercury." *Environmental Science & Technology* 43:7331-7336. doi: 10.1021/es9006993.

Stoichev, T., R. C Rodríguez Martín-Doimeadios, D. Amouroux, N. Molenat, and O. F. X. Donard. 2002. "Application of cryofocusing hydride generation and atomic fluorescence detection for dissolved mercury species determination in natural water samples." *Journal of Environmental Monitoring* 4:517-521. doi: 10.1039/b204233a.

Štrok, Marko, Holger Hintelmann, and Brian Dimock. 2014. "Development of pre-concentration procedure for the determination of Hg isotope ratios in seawater samples." *Analytica Chimica Acta* 851:57-63. doi: 10.1016/j.aca.2014.09.005.

Tsui, Martin Tsz Ki, Joel D. Blum, Sae Yun Kwon, Jacques C. Finlay, Steven J. Balogh, and Yabing H. Nollet. 2012. "Sources and transfers of methylmercury in adjacent river and forest food webs." *Environmental Science & Technology* 46:10957-10964. doi: 10.1021/es3019836.

U.S. EPA. 2001. Method 1630, Methyl Mercury in Water by Distillation, Aqueous Ethylation, Purge and Trap, and CVAFS. Washington, D.C.: U.S. Environmental Protection Agency Office of Water.

U.S. EPA. 2002. Method 1631, Revision E: Mercury in Water by Oxidation, Purge and Trap, and Cold Vapor Atomic Fluorescence Spectrometry. Washington, D.C.: U.S. Environmental Protection Agency, Office of Water.

Valsecchi, Lucia, Claudio Roscioli, Alfredo Schiavon, and Laura Marziali. 2021. "Methylmercury determinatino in freshwater biota and sediments: Static headspace GC-MS compared to direct mercury analyzer." *MethodsX* 8:101581. doi: 10.1016/j.mex.2021.101581.

Washburn, Spencer J., Joel D. Blum, Patrick M. Donovan, and Michael Bliss Singer. 2019. "Isotopic evidence for mercury photoreduction and retention on particles in surface waters of Central California, USA." *Science of the Total Environment* 674:451-461. doi: 10.1016/j.scitotenv.2019.04.145.

Watanabe, Takahiro, Hiroyuki Kikuchi, Rieko Matsuda, Tomoko Hayashi, Koichi Akaki, and Reiko Teshima. 2015. "Performance evaluation of an improved GC-MS method to quantify methylmercury in fish." *Food Hygiene and Safety Science* 56:69-76. doi: 10.3358/shokueishi.56.69.

Wiederhold, Jan G., Ulf Skyllberg, Andreas Drott, Martin Jiskra, Sofi Jonsson, Erik Björn, Bernard Bourdon, and Ruben Kretzschmar. 2015. "Mercury isotope signatures in contaminated sediments as a tracer for local industrial pollution sources." *Environmental Science & Technology* 49:177-185. doi: 10.1021/es5044358.

Wiederhold, Jan G., Robin S. Smith, Hagar Siebner, Adam D. Jew, Gordon E. Brown Jr., Bernard Bourdon, and Ruben Kretzschmar. 2013. "Mercury isotope signatures as tracers

for Hg cycling at the New Idria Hg Mine." *Environmental Science & Technology* 47:6137-6145. doi: 10.1021/es305245z.

Xu, Xiaoyu, Qianggong Zhang, and Wen-Xiong Wang. 2016. "Linking mercury, carbon, and nitrogen stable isotopes in Tibetan biota: Implications for using mercury stable isotopes as source tracers." *Scientific Reports* 6:25394. doi: 10.1038/srep25394.

Yang, Lu, and Ralph E. Sturgeon. 2009. "Isotopic fractionation of mercury induced by reduction and ethylation." *Analytical and Bioanalytical Chemistry* 393:377-385. doi: 10.1007/s00216-008-2348-6.

Yang, Shaochen, Bo Wang, Chongyang Qin, Runsheng Yin, Ping Li, Jinling Liu, David Point, Laurence Maurice, Jeroen E. Sonke, Leiming Zhang, and Xinbin Feng. 2021. "Compound-specific stable isotope analysis provides new insights for tracking human monomethylmercury exposure sources." *Environmental Science & Technology* 55:12493-12503. doi: 10.1021/acs.est.1c01771.

Yin, Runsheng, Xinbin Feng, Jianxu Wang, Zhengduo Bao, Ben Yu, and Jiubin Chen. 2013. "Mercury isotope variations between bioavailable mercury fractions and total mercury in mercury contaminated soil in Wanshan Mercury Mine, SW China." *Chemical Geology* 336:80-86. doi: 10.1016/j.chemgeo.2012.04.017.

Zhang, Lian, Yongguang Yin, Yanbin Li, and Yong Cai. 2022. "Mercury isotope fractionation during methylmercury transport and transformation: A review focusing on analytical method, fractionation characteristics, and its application." *Science of the Total Environment* 841:156558. doi: 10.1016/j.scitotenv.2022.156558.

Zhang, Wei, Guangyi Sun, Runsheng Yin, Xinbin Feng, Zuxiu Yao, Xuewu Fu, and Lihai Shang. 2021. "Separation of methylmercury from biological samples for stable isotopic analysis." *Journal of Analytical Atomic Spectrometry* 36:2415-2422. doi: 10.1039/d1ja00236h.

3.5 Supporting Information

3.5.1 Quality control for total mercury concentration analysis

Cold vapor atomic fluorescence spectrometry (CVAFS) (U.S. EPA 2002) was used to measure total mercury (THg) concentrations of syringe filtered nitric acid digestion solutions, resin separation sample solutions, and 1% $KMnO_4$ trap solutions associated with purge and trap, combustion, and transfer procedures. Across all analytical sessions, the percent relative standard deviation (%RSD) of the mean calibration factor (CF_m) for calibration standards (NIST SRM 3133; 2.5 to 500 pg Hg, or 0.5 to 100 ng L^{-1} on a volumetric basis) was 0.9% (SE = 0.1%, n=16). Average recovery of the lowest calibration standard relative to its expected value was 99.5% (SE = 0.4%, n=16). All initial and calibration verification blanks were below the reporting limit of 2.5 pg (i.e., the lowest calibration standard) (n=202). Initial calibration verification standards using a certified secondary mercury standard (Inorganic Ventures; 100, 200, or 300 pg Hg) had an average recovery of 100.8% (SE = 0.4%, n=16). Instrument precision and recovery checks (25 pg Hg, or 5 ng L^{-1}) had an average recovery of 99.9% (SE = 0.3%, n=16). Continuing calibration verification standards (100, 200, or 300 pg Hg) had an average recovery of 100.8% (SE = 0.1%, n=166).

The method detection limit (MDL) was approximately 0.33 pg Hg, or 0.07 ng L^{-1}. The MDL was calculated using the equation MDL = t * SD, where t is the student's t-value appropriate for the single-tailed 99th percentile and a standard deviation estimate with n-1 degrees of freedom, and SD is the standard deviation associated with the average mass or concentration of mercury detected in replicate MDL check standards, which should be analyzed at a concentration ~5 times higher than the expected MDL value (U.S. EPA 2016). Our MDL check standards were analyzed at 2.5 pg Hg, or 0.5 ng L^{-1}. In our calculation of the MDL, the t-

value was 2.60 (based on 15 degrees of freedom), and the SD value was 0.13 pg, or 0.03 ng L^{-1} (n=16).

To assess recovery for resin separation samples, matrix spike samples were analyzed, in which an aliquot of spiking solution was added to an aliquot of sample which had undergone UV treatment, which had an average recovery of 100.3% (SE = 0.2%, n=31). Additionally, aliquots of spiking solution were added to a subset of resin separation samples prior to undergoing UV treatment, which had an average recovery of 99.0% (SE = 0.4%, n=5).

3.5.2 Quality control for methylmercury concentration analysis

Gas chromatography coupled with cold vapor atomic fluorescence spectroscopy (GC-CVAFS) (U.S. EPA 2001) was used to measure methylmercury (MeHg) concentrations of pre- and post-syringe filtered nitric acid digestion solutions, resin separation sample solutions, and holding test solutions. Across all analytical sessions, the percent relative standard deviation (%RSD) of the mean calibration factor (CF_m) for calibration standards (MeHgCl, Brooks Rand; 2 to 800 pg Hg, or 0.05 to 20 ng L^{-1} on a volumetric basis) was 1.6% (SE = 0.2%, n=12). Average recovery of the lowest calibration standard relative to its expected value was 98.1% (SE = 0.3%, n=12). Initial and calibration verification blanks, which were analyzed in sets of three or six to assess the blank on each of the three Tenax traps, were below the reporting limit of 2 pg (i.e., the lowest calibration standard) (n=255), with the exception of the first blank following the calibration curve which typically had ~2.4 pg. Initial calibration verification standards using a certified secondary MeHg standard (MeHgOH, Brooks Rand; 200 pg Hg) had an average recovery of 99.7% (SE = 0.3%, n=12). Instrument precision and recovery checks (25 pg Hg, or 0.6 ng L^{-1}) had an average recovery of 100.9% (SE = 0.3%, n=12). Continuing calibration verification standards (200 pg Hg) had an average recovery of 100.8% (SE = 0.1%, n=123).

The method detection limit (MDL) was approximately 0.07 pg Hg, or 0.002 ng L^{-1}. The MDL was calculated using the equation MDL = t * SD, where t is the student's t-value appropriate for the single-tailed 99th percentile and a standard deviation estimate with n-1 degrees of freedom, and SD is the standard deviation associated with the average mass or concentration of Hg detected in replicate MDL check standards, which should be analyzed at a concentration ~5 times higher than the expected MDL value (U.S. EPA 2016). Our MDL check standards were analyzed at 2 pg Hg, or 0.05 ng L^{-1}. In our calculation of the MDL, the t-value was 2.72 (based on 11 degrees of freedom), and the SD value was 0.03 pg, or 0.001 ng L^{-1} (n=12).

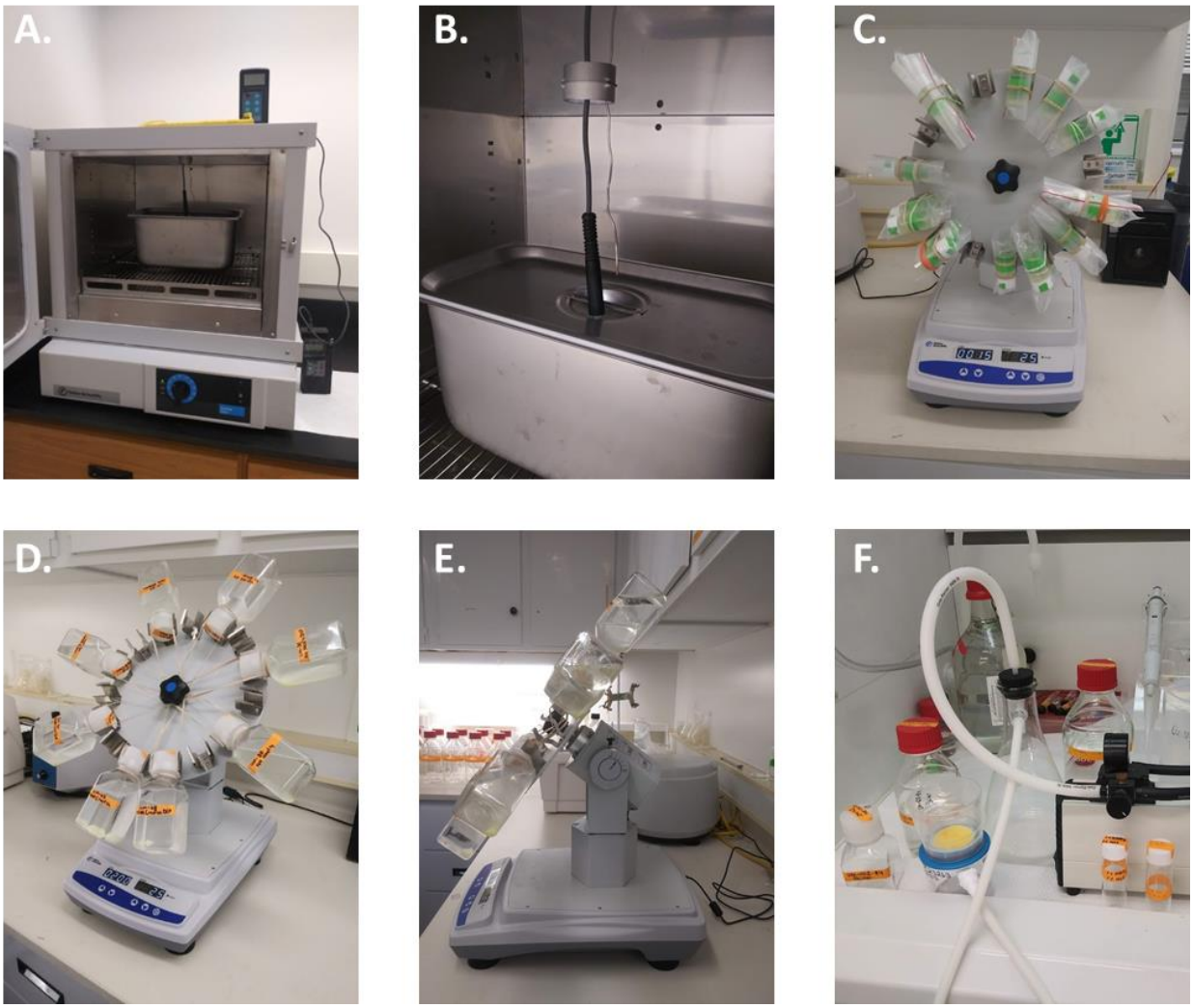

Figure S3.1. Photos taken during the nitric acid digestion and resin separation procedure.

Shown are (A) a water bath inside of an oven along with two thermocouples, (B) a close-up view of the two thermocouples, one to measure air temperature and one threaded through a hole in the lid of the water bath to measure water temperature, (C) a tube rotator being used for cleaning resin in 20 mL glass vials, (D) a set of 250 mL PETG sample bottles attached to a tube rotator for the resin separation procedure, (E) a side view of the tube rotator tilted on an angle for the resin separation procedure, (F) and the resin sample filtering setup including a cellulose nitrate filter cup, an overflow flask, a vacuum pump, sample bottles, and reagent bottles / vials.

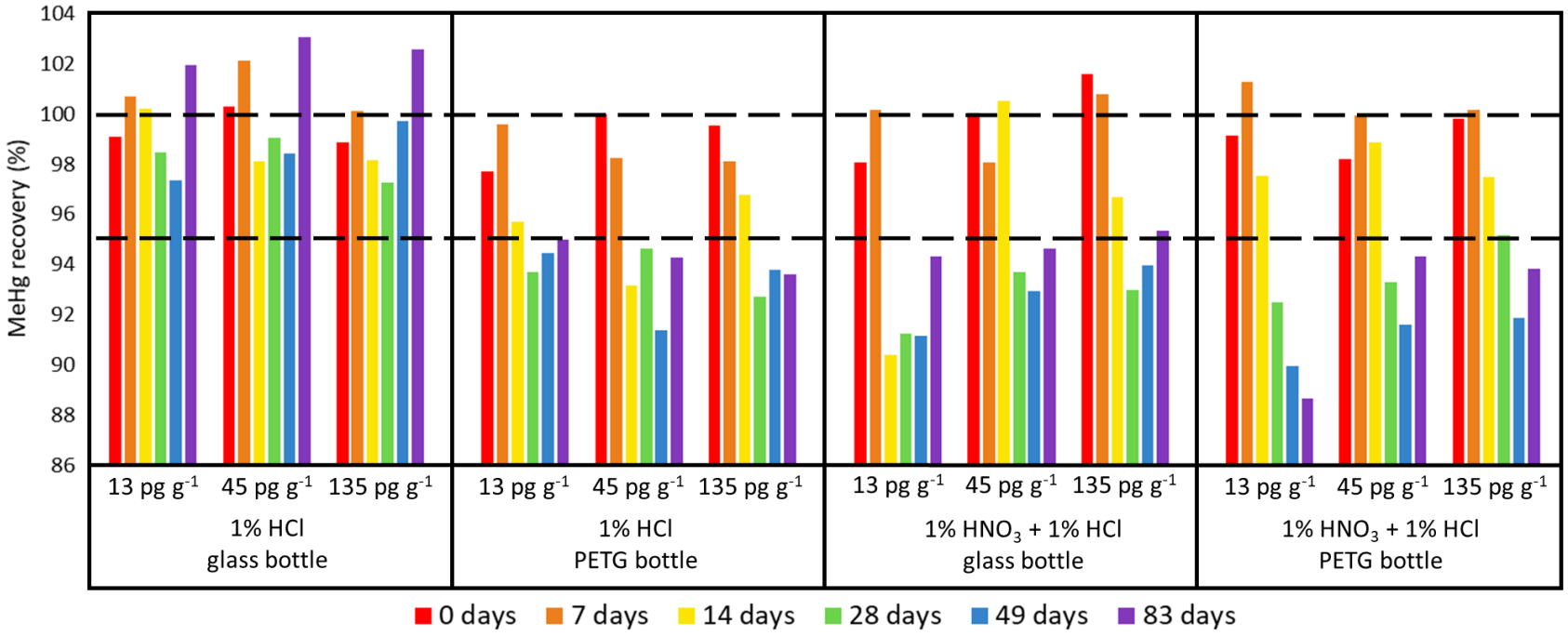

Figure S3.2. Results of the aqueous standard holding test using 13, 45, and 135 pg g^{-1} MeHgCl diluted in either a 1% HCl matrix or a 1% HNO_3 + 1% HCl matrix within either a glass or PETG bottle.

The upper dashed line marks 100% recovery, and the lower dashed line marks 95% recovery of MeHg. Note that the lowest MeHg recovery shown here is 88.6% for a 13 pg g^{-1} solution after 83 days in a 1% HNO_3 + 1% HCl matrix in a PETG bottle. Glass bottles were initially trace-metal cleaned in a hot 10% HNO_3 bath for at least 8 hours and then filled with 1% HCl at room temperature for at least 8 hours, then rinsed and set to dry. New PETG bottles were not cleaned or rinsed prior to use. Standard test bottle caps were secured with parafilm, stored in plastic zip bags, and refrigerated in the dark between analyses.

Table S3.1. THg isotopic composition of UM-Almadén, aqueous MeHgCl stock, and procedural standards.

Standard Type	THg (ng g^{-1})	n_1	n_2	Combustion %Rec. of THg (± 1SD)	Transfer or P+T %Rec. of THg (± 1SD)	δ^{202}Hg (‰)	2σ (‰)	Δ^{204}Hg (‰)	2σ (‰)	Δ^{201}Hg (‰)	2σ (‰)	Δ^{200}Hg (‰)	2σ (‰)	Δ^{199}Hg (‰)	2σ (‰)
UM-Almadén (analyzed alongside combustion samples)	–	17	130	–	–	-0.56	0.01 *0.08*	0.01	0.01 *0.09*	-0.04	0.00 *0.05*	0.01	0.01 *0.04*	-0.02	0.00 *0.06*
UM-Almadén (analyzed alongside resin separation samples)	–	4	22	–	–	-0.55	0.02 *0.05*	0.01	0.03 *0.07*	-0.03	0.00 *0.04*	0.01	0.01 *0.03*	-0.02	0.01 *0.04*
Aqueous MeHgCl Stock (Brooks Rand)	–	3	6	–	–	-1.21	0.02 *0.04*	-0.01	0.02 *0.03*	0.05	0.01 *0.03*	0.02	0.02 *0.03*	0.10	0.02 *0.02*
Purge & Trap NIST SRM 3133	–	3	3	–	98.5 ± 0.7	0.01	0.03	-0.02	0.01	0.00	0.02	0.03	0.04	-0.01	0.02
DORM-3 (Fish Protein)	372 ± 9 (382 ± 60)	7	24	97.5 ± 2.4	99.0 ± 1.7	0.47	0.02 *0.08*	-0.09	0.02 *0.08*	1.48	0.01 *0.04*	0.07	0.01 *0.02*	1.80	0.01 *0.03*
DORM-3 (Fish Protein) Long-term average	(382 ± 60)	32	–	–	–	0.48	0.02	-0.09	0.01	1.48	0.01	0.06	0.01	1.80	0.01
TORT-2 (Lobster Hepatopancreas)	271 ± 5 (270 ± 60)	5	16	100.5 ± 1.7	96.7 ± 4.5	0.04	0.03 *0.05*	-0.09	0.01 *0.06*	0.61	0.01 *0.05*	0.06	0.01 *0.02*	0.75	0.01 *0.03*
TORT-2 (Lobster Hepatopancreas) Long-term average	(270 ± 60)	89	–	–	–	0.06	0.02	-0.09	0.02	0.59	0.01	0.06	0.01	0.75	0.01
DOLT-2 (Dogfish Liver)	2119 ± 60 (1990 ± 100)	2	6	106.5 ± 3.0	98.4 ± 2.7	-0.52	0.03 *0.05*	-0.02	0.02 *0.04*	0.62	0.04 *0.06*	0.02	0.05 *0.03*	0.72	0.05 *0.06*
DOLT-2 (Dogfish Liver) Long-term average	(1990 ± 100)	17	–	–	–	-0.51	0.01	-0.03	0.02	0.60	0.01	0.03	0.01	0.73	0.01

For UM-Almadén and the brominated aqueous MeHgCl stock, n_1 denotes the number of preparations (i.e., the number of session averages, with preparations at different concentrations counted separately). For the purge and trap procedural standard and combustion reference materials, n_1 denotes the number of independent preparations of the material. For all standards and reference materials, n_2 denotes the number of separate isotopic analyses on an individual

preparation(s). Certified THg concentrations of the biological reference materials are provided in parentheses below our measured THg concentrations. Recovery of THg after combustion is relative to the certified THg concentration for each of the biological reference materials. Transfer or purge and trap (P+T) %Rec indicates the recovery of Hg during the transfer (for biological reference materials) or purge and trap pre-concentration step. Isotope ratios show the average value (± 2SE) across independent preparations for each standard type. For UM-Almadén, the aqueous MeHgCl stock, and biological reference materials, the average uncertainty (2SD) across all analyses is also provided in italics. Long-term average isotopic compositions (± 2SE) are included for comparison (Blum and Johnson 2017).

Table S3.2. THg isotopic composition of natural biota samples.

Natural Biota Sample Type	THg (ng g^{-1})	n_1	n_2	Transfer %Rec. of THg	δ^{202}Hg (‰)	2σ (‰)	Δ^{204}Hg (‰)	2σ (‰)	Δ^{201}Hg (‰)	2σ (‰)	Δ^{200}Hg (‰)	2σ (‰)	Δ^{199}Hg (‰)	2σ (‰)
Shiner Fillet	1604	1	2	98.8	-0.70	0.07	-0.04	0.07	0.21	0.05	0.02	0.03	0.29	0.03
Crayfish	1698	1	2	98.0	-0.81	0.07	-0.06	0.07	0.08	0.05	0.02	0.03	0.12	0.03
Mayfly Larvae	1633	1	2	96.2	-0.14	0.07	0.00	0.07	-0.05	0.05	-0.01	0.03	-0.04	0.03
Megaloptera Larvae	3569	1	3	99.4	-0.76	0.07	0.01	0.07	0.00	0.05	0.00	0.03	0.02	0.03
Asian Clams	6195	1	3	96.7	-0.38	0.07	0.01	0.07	0.05	0.05	0.01	0.03	0.09	0.03

Natural biota samples were collected from East Fork Poplar Creek. Here, n_1 denotes the number of independent preparations of the material (via combustion) and n_2 denotes the number of separate isotopic analyses on an individual preparation. The analytical uncertainty in the isotopic composition of THg in combustion samples is represented by the average uncertainty (2SD) across combustion reference material analyses.

Table S3.3. MeHg recovery and purity at various points throughout the MeHg separation procedure.

Standard or Natural Biota Sample Type	MeHg (ng g^{-1})	%MeHg in Solid Material	n_1	n_2	HNO_3 Digest %Rec. of MeHg (±1SD)	HNO_3 Digest Matrix Spike %Rec. of MeHg (±1SD)	Syringe Filtering %Rec. of MeHg (±1SD)	1st Resin Step %Rec. of MeHg (±1SD)	2nd Resin Step %Rec. of MeHg (±1SD)	Cumulative Syringe Filtering Resin %Rec. of MeHg (±1SD)	%Purity after Syringe Filtering (±1SD)	%Purity after 1st Resin Step (±1SD)	%Purity after 2nd Resin Step (±1SD)
Aqueous MeHgCl Stock (Brooks Rand)	–	–	5	–	–	–	98.3 ± 1.1	98.6 ± 1.3	–	96.9 ± 1.8	102.9 ± 2.5	102.3 ± 0.7	–
DORM-3 (Fish Protein)	332 ± 6 (355 ± 56)	89 (93)	4	4	94.7 ± 0.8	100.5 ± 2.3	95.9 ± 1.7	99.3 ± 1.1	–	95.3 ± 2.3	84.8 ± 2.7	100.7 ± 4.6	–
TORT-2 (Lobster Hepatopancreas)	163 ± 4 (152 ± 13)	60 (56)	4	4	108.1 ± 2.4	99.4 ± 2.4	94.8 ± 2.5	99.0 ± 1.5	99.6 ± 0.1	93.5 ± 3.5	54.2 ± 0.7	87.4 ± 4.2	94.3 ± 3.2
DOLT-2 (Dogfish Liver)	791 ± 12 (693 ± 53)	37 (35)	5	2	114.4 ± 1.6	102.4 ± 0.5	94.9 ± 3.3	99.0 ± 1.3	98.7 ± 0.5	93.2 ± 2.9	34.8 ± 0.9	93.3 ± 6.9	98.5 ± 2.9
DOLT-5 (Dogfish Liver)	129 ± 1 (119 ± 58)	– (27)	5	2	108.2 ± 0.9	97.7 ± 0.3	96.4 ± 1.5	97.2 ± 4.5	100.7 ± 4.5	94.0 ± 2.2	33.8 ± 0.2	85.4 ± 9.0	96.5 ± 1.3
Shiner Fillet	1668 ± 34	104	2	2	–	102.4 ± 0.1	96.7 ± 0.5	99.5 ± 0.1	–	96.2 ± 0.4	94.8 ± 1.1	103.1 ± 2.1	–
Crayfish	1047 ± 21	62	2	2	–	103.3 ± 1.4	96.7 ± 0.1	100.1 ± <0.1	97.8 ± 0.3	94.7 ± 0.4	62.8 ± 2.9	101.2 ± 0.9	104.3 ± 0.2
Mayfly Larvae	212 ± <1	13	2	2	–	103.7 ± 0.4	96.2 ± <0.1	98.1 ± 1.0	97.1 ± 1.1	91.7 ± 0.1	12.7 ± 0.1	68.7 ± 1.1	96.3 ± 0.4
Megaloptera Larvae	437 ± <1	12	2	2	–	102.1 ± 0.3	96.5 ± 0.1	97.2 ± 0.7	98.4 ± 1.1	92.2 ± 1.6	12.0 ± 0.3	65.4 ± 5.2	97.8 ± 0.3
Asian Clams	391 ± 1	6.3	2	2	–	103.8 ± 0.4	98.3 ± 2.4	90.1 ± 3.1	98.4 ± 2.3	87.1 ± 1.2	6.1 ± 0.2	52.9 ± 2.4	91.2 ± <0.1

Natural biota samples were collected from East Fork Poplar Creek. For the aqueous MeHgCl stock, n_1 is the number of preparations at ~200, 670, and 2000 pg g^{-1}. For the biological reference materials and natural biota samples, n_1 is the number of independent nitric acid digestion samples that underwent resin separation, and n_2 is the number of independent nitric acid digestion matrix spike tests for that material. Certified MeHg concentrations of the biological reference materials are provided in parentheses below our measured MeHg concentrations. Percent MeHg in the solid material was calculated by dividing the

measured MeHg concentration (via nitric acid digestion) by the measured THg concentration (via combustion), with the same calculation using certified MeHg and THg concentrations provided in parentheses (note that DOLT-5 was not analyzed for its THg concentration via combustion). Recovery of MeHg after the nitric acid digestion was calculated based on the certified MeHg concentrations of the biological reference materials. Recovery of MeHg for matrix spike tests is relative to doses of MeHgCl added into nitric acid digestion sample tubes. Recovery of MeHg after syringe filtering is relative to the measured MeHg concentration of the nitric acid digestion samples. Recovery of MeHg after the first resin separation step is relative to the measured MeHg concentration of the syringe filtered samples. Recovery of MeHg after the second resin separation step is relative to the measured MeHg concentration of the first resin separation samples. Cumulative MeHg recovery after the final resin separation step is relative to the measured MeHg concentration of the nitric acid digestion samples. Percent purity was calculated by dividing the measured MeHg concentration by the measured THg concentration of each of the syringe filtered and resin separation samples.

Table S3.4. MeHg isotopic composition of aqueous MeHgCl stock, biological reference materials, and natural biota samples.

Standard or Sample Type	n_1	n_2	P+T %Rec. (± 1SD)	δ^{202}MeHg (‰)	2σ (‰)	Δ^{204}MeHg (‰)	2σ (‰)	Δ^{201}MeHg (‰)	2σ (‰)	Δ^{200}MeHg (‰)	2σ (‰)	Δ^{199}MeHg (‰)	2σ (‰)
Aqueous MeHgCl Stock (Brooks Rand)	3	3	100.9 ± 1.9	-1.24	0.05 *0.03*	-0.02	0.07 *0.04*	0.05	0.04 *0.02*	0.01	0.03 *0.04*	0.08	0.04 *0.03*
DORM-3 (Fish Protein)	4	4	101.8 ± 1.7	0.64	0.05 *0.13*	-0.12	0.07 *0.10*	1.52	0.04 *0.04*	0.08	0.03 *0.03*	1.85	0.04 *0.04*
TORT-2 (Lobster Hepatopancreas)	4	4	101.1 ± 1.3	0.62	0.05 *0.04*	-0.11	0.07 *0.07*	0.85	0.04 *0.05*	0.07	0.03 *0.03*	1.04	0.04 *0.04*
DOLT-2 (Dogfish Liver)	5	5	101.4 ± 3.8	0.21	0.05 *0.07*	-0.07	0.07 *0.07*	0.93	0.04 *0.05*	0.05	0.03 *0.04*	1.13	0.04 *0.03*
DOLT-5 (Dogfish Liver)	4	4	101.9 ± 0.6	0.50	0.05 *0.15*	-0.03	0.07 *0.18*	0.85	0.04 *0.06*	0.08	0.03 *0.14*	1.01	0.04 *0.04*
Shiner Fillet	2	4	101.4 ± 1.6	-0.60	0.05 *0.00*	-0.02	0.07 *0.02*	0.24	0.04 *0.01*	0.01	0.03 *0.00*	0.30	0.04 *0.01*
Crayfish	2	2	101.7 ± 0.4	-0.80	0.05 *0.04*	-0.02	0.07 *0.02*	0.14	0.04 *0.00*	0.03	0.03 *0.01*	0.21	0.04 *0.01*
Mayfly Larvae	2	2	100.4 ± 0.4	-0.41	0.05 *0.01*	-0.07	0.07 *0.05*	0.19	0.04 *0.02*	0.04	0.03 *0.02*	0.25	0.04 *0.03*
Megaloptera Larvae	2	2	101.8 ± 2.3	-0.72	0.05 *0.15*	0.00	0.07 *0.05*	0.06	0.04 *0.10*	0.02	0.03 *0.01*	0.13	0.04 *0.03*
Asian Clams	2	2	101.2 ± 0.7	-0.67	0.05 *0.01*	-0.01	0.07 *0.03*	0.24	0.04 *0.02*	0.04	0.03 *0.04*	0.33	0.04 *0.02*

Natural biota samples were collected from East Fork Poplar Creek. Here, n_1 denotes the number of resin separation samples and n_2 denotes the number of separate isotopic analyses on an individual preparation(s). Note that for DOLT-5 and the aqueous MeHgCl stock, some of the resin separation samples were combined prior to isotopic analysis. Purge and trap (P+T) %Rec indicates the recovery of Hg during the purge and trap pre-concentration step. The analytical uncertainty in the isotopic composition of MeHg in resin separation samples is represented by the average uncertainty (2SD) across UM-Almadén analyses, which were analyzed alongside resin separation samples. Reproducibility associated with complete process replicates (reported as 2SD) is also provided in italics.

Table S3.5. Results of the aqueous MeHgCl standard holding test.

	MeHg concentration (pg g^{-1})	MeHg recovery (%)					
		0 days	7 days	14 days	28 days	49 days	83 days
1%HCl glass bottle	13	99.1	100.7	100.2	98.4	97.3	101.9
	45	100.3	102.1	98.1	99.0	98.4	103.0
	135	98.9	100.1	98.2	97.2	99.7	102.6
1% HCl PETG bottle	13	97.7	99.6	95.7	93.7	94.4	95.0
	45	100.0	98.2	93.2	94.6	91.4	94.3
	135	99.5	98.1	96.8	92.7	93.8	93.6
1% HNO_3 + 1% HCl glass bottle	13	98.1	100.1	90.4	91.2	91.1	94.3
	45	100.0	98.0	100.5	93.7	92.9	94.6
	135	101.6	100.8	96.7	93.0	94.0	95.3
1% HNO_3 + 1% HCl PETG bottle	13	99.1	101.3	97.5	92.5	89.9	88.6
	45	98.2	99.9	98.8	93.3	91.6	94.3
	135	99.8	100.1	97.5	95.2	91.9	93.8

Results of the aqueous standard holding test using 13, 45, and 135 pg g^{-1} MeHgCl diluted in either a 1% HCl matrix or a 1% HNO_3 + 1% HCl matrix within either a borosilicate glass or polyethylene terephthalate glycol (PETG) bottle. Glass bottles were initially trace-metal cleaned in a hot 10% HNO_3 bath for at least 8 hours and then filled with 1% HCl at room temperature for at least 8 hours, then rinsed and set to dry. New PETG bottles were not cleaned or rinsed prior to use. Standard test bottle caps were secured with parafilm, stored in plastic zip bags, and refrigerated in the dark between analyses.

References for Supporting Information

Blum, Joel D., and Marcus W. Johnson. 2017. "Recent developments in mercury stable isotope analysis." *Reviews in Mineralogy and Geochemistry* 82:733-757. doi: 10.2138/rmg.2017.82.17.

U.S. EPA. 2001. Method 1630, Methyl Mercury in Water by Distillation, Aqueous Ethylation, Purge and Trap, and CVAFS. Washington, D.C.: U.S. Environmental Protection Agency Office of Water.

U.S. EPA. 2002. Method 1631, Revision E: Mercury in Water by Oxidation, Purge and Trap, and Cold Vapor Atomic Fluorescence Spectrometry. Washington, D.C.: U.S. Environmental Protection Agency, Office of Water.

U.S. EPA. 2016. Definition and Procedure for the Determination of the Method Detection Limit, Revision 2. Washington, D.C.: U.S. Environmental Protection Agency, Office of Water.

Chapter 4 Food Web Mercury Isotopes Suggest Similarities and Differences in Sources and In-Stream Processes Influencing Biological Accumulation of Methylmercury in Natural Background vs. Point Source Contaminated Stream Ecosystems

Co-authored with Jason D. Demers and Joel D. Blum.

Abstract: The goal of this project was to identify sources of inorganic mercury (iHg) and methylmercury (MeHg) to the aquatic food webs of East Fork Poplar Creek (EFPC), an industrial point source impacted stream, and Hinds Creek (HC), a regional reference stream in eastern Tennessee, USA. Additionally, we compared the types and relative amounts of biogeochemical reactions influencing MeHg within the two streams. We measured total mercury (THg) and methylmercury (MeHg) concentrations, THg isotopic compositions, and compound-specific MeHg isotopic compositions of several different types of fish and aquatic invertebrates collected from each stream. We found that for HC, aquatic organisms had primarily obtained inorganic mercury (iHg) from streambed sediment, which is ultimately derived from a combination of precipitation and dry deposition. In contrast, for EFPC, aquatic organisms appear to have obtained iHg from multiple basal resources containing variable proportions of legacy mercury and newly released mercury from the point source. Organisms from both streams have also obtained MeHg from multiple basal resources including biofilm, suspended particulates, and streambed sediment. MeHg obtained from different basal resources can be isotopically distinguished from one another due to differences in the amount of isotope fractionation imparted by photochemical demethylation prior to bioaccumulation in the food web. Additionally, isotope fractionation imparted by microbial demethylation appears to be important

in terms of influencing the isotopic composition of MeHg within the HC reference site, whereas isotope fractionation induced by microbial methylation dominates over that induced by microbial demethylation within the highly contaminated EFPC sites. This aligns with the results of previous studies on other waterbodies.

4.1 Introduction

Mercury is a toxic metal that occurs naturally in the environment, and which has a long history of extraction from the earth for human use. Aquatic ecosystems can be contaminated through the release of mercury from industrial point sources, though many other nonpoint source aquatic ecosystems contain mercury from geogenic and long-range transport of atmospheric sources. Within the environment, oxidized inorganic mercury (iHg) can undergo several different types of biogeochemical processes, such as microbial, photochemical, and dark abiotic reduction, and microbial methylation (Selin 2009). Through microbial methylation, iHg is converted into methylmercury (MeHg), a more toxic and bioaccumulative form of mercury. Once produced, MeHg can undergo further biogeochemical processing, such as microbial and photochemical demethylation (Selin 2009). Both iHg and MeHg can be taken up by organisms, though MeHg bioaccumulates in the tissues of organisms more readily than iHg (Zhang et al. 2009) and generally only MeHg biomagnifies through an aquatic food web (Baeyens et al. 2003, Kehrig et al. 2010, Seixas et al. 2014). This results in higher MeHg concentrations and higher proportions of THg as MeHg (%MeHg) for predator species at higher trophic levels.

Biogeochemical transformations of both iHg and MeHg result in mass-dependent fractionation (MDF) and, in some cases, mass-independent fractionation (MIF) of mercury isotopes (Blum et al. 2014). Biogeochemical processes such as microbial reduction of iHg (Kritee et al. 2007, Kritee et al. 2009) and uptake of gaseous mercury into foliage (Demers et al.

2013) result in MDF, influencing the isotopic composition of iHg in ecosystems. Other biogeochemical processes such as photochemical reduction (Bergquist and Blum 2007, Zheng and Hintelmann 2009, 2010a, Rose et al. 2015) and dark abiotic reduction (Zheng and Hintelmann 2009, 2010b) of iHg result in both MDF and MIF, which can also influence the isotopic composition of iHg. The production of MeHg from a pool of iHg via microbial methylation (Rodríguez-González et al. 2009), as well as subsequent microbial demethylation (Kritee et al. 2009), results in additional MDF which influences the isotopic composition of MeHg. Degradation of MeHg via photochemical demethylation additionally results in both MDF and MIF, which can further influence the isotopic composition of MeHg prior to its incorporation into aquatic organisms. Because different mercury pools within various environmental compartments experience variable types and degrees of biogeochemical processing, this can lead to multiple iHg and MeHg isotopic compositions within an ecosystem. These differences, as well as the general lack of MeHg isotope fractionation during bioaccumulation and trophic transfer in aquatic food webs (Kwon et al. 2012), enable mercury isotopic measurements to be used for tracking biogeochemical cycling of mercury as well as identifying sources of iHg and MeHg to food webs.

Aquatic organisms contain a wide range of MeHg relative to iHg depending on their position in the food web. Due to biomagnification of MeHg, a majority of mercury within organisms at high trophic levels is in the form of MeHg, while organisms at lower trophic levels contain a high proportion of iHg. The THg isotopic composition of an organism represents the weighted average isotopic composition of iHg and MeHg within the organism. Measurements of THg isotopic composition of higher trophic level organisms containing high %MeHg are largely reflective of the isotopic composition of MeHg within the food web, whereas those of lower

trophic level organisms containing low %MeHg are largely influenced by the isotopic composition of iHg that enters the food web. The isotopic compositions of iHg and MeHg within an aquatic food web can sometimes be estimated using linear regression (Kwon et al. 2015) or mass balance (Tsui et al. 2012). These approaches rely on the relationships between THg isotope ratios and %MeHg across organisms with variable %MeHg values.

Offsets between the estimated isotopic compositions of iHg and MeHg within a food web can be used to determine the biogeochemical reactions that are influencing the isotopic fractionation of MeHg prior to uptake and accumulation in the food web. Additionally, these estimated isotopic compositions can be compared to the THg (and/or MeHg) isotopic compositions of co-located basal resources or other potential mercury sources to determine the sources or uptake pathways of iHg and MeHg to the food web (Kwon et al. 2015, Donovan et al. 2016, Xu et al. 2016, Rosera et al. 2022). Linear regression and mass balance approaches of estimating MeHg isotope ratios within a food web both rely on the assumption that organisms at various trophic levels obtain iHg from a common source, and the linear regression approach additionally assumes that the organisms also obtain MeHg from a common source. These assumptions are largely based on previous studies demonstrating linear relationships between THg isotope ratios and %MeHg for aquatic food webs (Tsui et al. 2012, Kwon et al. 2015, Donovan et al. 2016, Xu et al. 2016). However, in some aquatic ecosystems, different organisms may obtain iHg and/or MeHg from different combinations of sources. This has been demonstrated in other previous studies, such as nonlinear relationships between THg isotope ratios and %MeHg (Kwon et al. 2014, Rosera et al. 2022), or offsets in THg isotopic composition between different types of fish with high %MeHg (Laffont et al. 2021). For example, sediment (~0.2% MeHg), mussels (~64% MeHg), crabs (~85% MeHg), and fish (~95%

MeHg) collected from the Providence River Estuary (RI, USA) displayed a nonlinear relationship between δ^{202}THg and %MeHg, with mussels having anomalously high δ^{202}THg values (Kwon et al. 2014). In that study, the δ^{202}Hg values of MeHg were presumed to be higher in the mussels than within crabs and fish, either due to additional biogeochemical processing of MeHg prior to bioaccumulation in the mussels, or due to an external source of MeHg to the mussels (Kwon et al. 2014). However, the anomalously high δ^{202}THg values of the mussels could also have been explained by an external source of iHg with higher δ^{202}Hg values than the sediment, or perhaps by external sources of both iHg and MeHg. In cases such as this, it can be difficult to ascertain the iHg and MeHg isotopic compositions of the various organisms within a food web, making it difficult to determine the sources of iHg and MeHg to the food web.

For cases in which different types of organisms within an aquatic food web may be obtaining iHg and/or MeHg from multiple combinations of isotopically distinct sources, it can be beneficial to extract and isolate MeHg from biological samples for mercury isotope analysis. This approach is useful for more confidently determining the isotopic composition of MeHg within lower trophic level organisms containing low %MeHg, as their THg isotopic compositions would be dominated by iHg within the sample. Directly measuring the MeHg isotopic composition of various types of aquatic organisms in a food web can demonstrate whether different types of organisms have obtained MeHg from a common source, or from different sources. As with MeHg isotopic compositions estimated using linear regression and mass balance approaches, directly measured MeHg isotopic compositions of biological samples can also be used to determine the most likely sources of MeHg to the food web and to investigate the biogeochemical reactions occurring within the waterbody. With direct MeHg isotopic measurements, the isotopic composition of MeHg within lower trophic level organisms can be

determined without relying on the assumption that these organisms obtain MeHg from the same sources as high trophic level organisms with ~100% MeHg. This allows for a more confident determination of the sources of MeHg not only to fish, but to lower trophic level organisms as well. For this study, we used a MeHg separation method involving hot nitric acid digestion, batch anion-exchange resin separation, and pre-concentration by purge and trap to isolate MeHg from iHg for isotopic analysis (Crowther et al. 2022).

In this study, we used THg, MeHg, carbon (C), and nitrogen (N) isotopic analyses of fish and aquatic invertebrates to assist in determining the dominant sources of iHg and MeHg to the aquatic food webs of a point source contaminated stream and a regional background reference stream. East Fork Poplar Creek (EFPC) in Oak Ridge, TN, the highly polluted stream in this study, was contaminated with mercury in the 1950s and early 1960s through losses of mercury from the Y-12 National Security Complex. These losses included direct discharge of dissolved and particulate-bound oxidized mercury at the headwaters of the stream, as well as releases of liquid elemental mercury to the soil surrounding the headwaters through spills and leaks (Brooks and Southworth 2011). Sediment and soil in and around EFPC remain contaminated with legacy mercury, with current sediment THg concentrations of ~30,000 to 60,000 ng g^{-1} near the headwaters within the first 2 km of the stream and ~10,000 to 30,000 ng g^{-1} over the next 19.6 km of the stream (Brooks et al. 2017). Discharge of mercury from the Y-12 facility has dramatically decreased since the 1960s, although for the past twenty years, the total mercury flux at the Y-12 boundary has continued to fluctuate between 2.7 and 24 kg per year (WRRP and UCOR 2019). Methylmercury within the EFPC food web is hypothesized to have been formed from iHg derived from the Y-12 point source, though whether it is formed predominantly from the largely recalcitrant legacy mercury in the watershed or from ongoing new releases of

mercury from Y-12 is unclear. In contrast with EFPC, Hinds Creek (HC) in Heiskell, TN, the regional background stream in this study located ~25 km northeast of the Y-12 facility, has much lower sediment THg concentrations of ~10 to 30 ng g^{-1} (Donovan et al. 2014). Methylmercury within the HC food web is hypothesized to have been formed from iHg derived from long-range atmospheric sources, although whether it is formed predominantly from mercury in precipitation or dry deposition has not previously been determined. This study aims to fill these knowledge gaps and to determine which basal resources (e.g., streambed sediment, biofilm, suspended particulates, leaf litter, etc.) serve as the sources of iHg and MeHg to the aquatic food webs of each stream. Additionally, the THg and MeHg isotopic compositions of aquatic organisms were used to gain insight into which biogeochemical reactions have the most influence the isotopic composition of iHg and MeHg prior to entering the HC and EFPC food webs. We further place these findings within a broader context by making comparisons between previous studies involving mercury isotopic measurements of aquatic organisms and basal resources within other point source contaminated and regional background waterbodies to identify any generalizable differences in MeHg sources and biogeochemical processes based on the level of mercury contamination across various freshwater ecosystems.

4.2 Methods

4.2.1 Biological sample collection

East Fork Poplar Creek (EFPC) is a 26-kilometer-long low order stream in eastern Tennessee, USA, and is highly contaminated by inputs from the Y-12 National Security Complex at its headwaters. EFPC flows into Poplar Creek, which flows into the Clinch River another 5 km downstream (Figure 4.1). Sampling sites along EFPC are denoted by their creek kilometer upstream of the confluence of EFPC and Poplar Creek (i.e., EFK #). Our nonpoint

source contaminated reference site was Hinds Creek (HC), which flows into the Clinch River ~97 km upstream of the confluence of Poplar Creek and the Clinch River. Sampling sites along Hinds Creek are denoted by their creek kilometer upstream of the confluence of Hinds Creek and the Clinch River (i.e., HCK #).

A variety of types of fish and aquatic invertebrates were collected at EFK 24.2 (n=3), EFK 23.4 (n=25), EFK 22.3 (n=17), EFK 18.2 (n=2), EFK 13.8 (n=2), EFK 6.3 (n=35), and HCK 20.6 (n=39) between 2010 and 2014, where "n" indicates the number of biological samples collected from each site, some of which were composites, that were analyzed for THg and MeHg concentration and THg isotopic composition. Sample types include rock bass (filleted, n=19), redbreast sunfish (filleted, n=9), shiners (filleted, n=9), stoneroller minnows (whole body, n=11, and filleted, n=5), crayfish (whole body, n=2, and soft tissue, n=27), clams (soft tissue, n=11), snails (soft tissue, n=8), megaloptera larvae (whole body, n=6), and other miscellaneous benthic invertebrates (e.g., aquatic earthworms, water penny beetles, and other various types of insect larvae, all whole body, n=16), where "n" again indicates the number of biological samples analyzed for THg and MeHg concentrations and THg isotopic composition. The numbers of individuals composited for each biological sample are provided in Table S4.1a-c. Fish were collected by electrofishing, benthic invertebrates were collected from stream riffles with a kick net, and clams and snails were collected by coarsely sieving streambed sediment (Peterson et al. 2013). Fish and invertebrate samples were freeze dried, ground, and stored according to Crowther et al. (2022). For ten of the fish samples, an additional aliquot was ground separately as a sample replicate, representing 1 in 12 of all biological samples or 1 in 5 of the fish samples (Table S4.2a-c). Invertebrate samples were not ground in duplicate due to the limited amount of

material available for invertebrate samples. Additional sample information, such as sample length, sex, and the sample collection date, is provided in Table S4.1a-c.

4.2.2 Carbon and nitrogen isotope analysis

Fish, invertebrate, and biofilm samples were weighed, encapsulated in tin foil, and analyzed for carbon (C) and nitrogen (N) stable isotope ratios and C and N concentrations (Table S4.2a-c, Table S4.3) at the University of California Santa Cruz Stable Isotope Laboratory. These analyses were made using a CE Instruments NC2500 elemental analyzer coupled to a Thermo Scientific DELTAplus XP isotope ratio mass spectrometer via a Thermo-Scientific Conflo III. Twelve of the biological and two of the biofilm samples were analyzed for their C and N isotopic compositions in duplicate, representing 1 in 10 of the samples and representing the full range of fish and invertebrate sample types in this study (Table S4.2a-c, Table S4.3). Additionally, separately ground sample replicates were each analyzed for C and N concentrations and isotope ratios separately. For high C content samples, automated in-line CO_2 trapping was used to remove interferences with N_2. Measurements were corrected to VPDB (Vienna PeeDee Belemnite) for $\delta^{13}C$ and AIR for $\delta^{15}N$ against an in-house gelatin standard reference material (PUGel), which was extensively calibrated against international standard reference materials. Measurements were corrected for size effects, blank-mixing effects, and drift effects. An externally-calibrated Acetanilide standard reference material obtained from A. Schimmelmann of Indiana University and USGS41 L-glutamic acid were measured as samples for independent quality control. Additional reference materials provided by the University of Michigan include USGS25 ammonium sulfate, IAEA-N-2 ammonium sulfate, IAEA-600 caffeine, and IAEA-CH-6 sucrose. For high C:N samples, an additional matrix-matched in-house standard reference material (Oak) was measured for quality control. We represent the analytical uncertainty in the C

and N isotopic composition of biological and biofilm samples with the average uncertainty (1SD) across reference material analyses (0.06‰ for $\delta^{13}C_{VPDB}$ and 0.63‰ for $\delta^{15}N_{AIR}$) (Table S4.3).

4.2.3 Total mercury extraction by combustion

Biological reference materials and fish and invertebrate samples collected from Hinds Creek and East Fork Poplar Creek were prepared for analysis of THg concentration (Table S4.2a-c, Table S4.4) and isotopic composition (Table S4.5, Table S4.6a-c) following a previously described combustion procedure (Demers et al. 2013). Aliquots of ground biological samples (10 to 1000 mg) were combusted in a two-stage furnace, and volatilized Hg(0) was trapped in a 24 g oxidizing solution of 1% $KMnO_4$ (w/w) in 10% H_2SO_4 (v/v) (hereafter, 1% KMnO4). The ten fish samples with separately ground aliquots were combusted separately. Additionally, for six of the invertebrate samples, a replicate aliquot of ground material from the same vial was combusted separately as an analytical process replicate, representing 1 in 20 of all biological samples or 1 in 12 invertebrate samples (Table S4.2a-c). Combustion trap solutions of 1% $KMnO_4$ were later reduced with hydroxylamine hydrochloride ($HONH_3Cl$), and a small aliquot was analyzed for THg concentration using cold vapor atomic fluorescence spectrometry (CVAFS; RA-3F, Nippon Instruments) following EPA Method 1631 (U.S. EPA 2002). These solutions were analyzed in batches with quality control including calibration verification standards, secondary standards, and blanks.

To reduce matrix interferences from combustion residues during isotopic analysis, aliquots of the 1% $KMnO_4$ combustion trap solutions were reduced with stannous chloride ($SnCl_2$), and Hg(0) was transferred to secondary 1% $KMnO_4$ trap solutions (Demers et al. 2013). These secondary solutions were later reduced with $HONH_3Cl$, and a small aliquot was analyzed

for THg concentration by CVAFS. This was done to assess the percent recovery of the transfer process and to allow matching of standard and sample concentrations for isotope analysis. Recovery of mercury after the transfer process ranged from 87.7 to 114.2%, with an average of 98.2 ± 4.2% (1SD, n=145 including biological samples and reference materials, and counting ground replicates separately). Isotope ratios were not reported for five samples with <85% transfer recovery.

Procedural blanks and standard reference materials were combusted to monitor combustion performance. Average procedural blank 1% $KMnO_4$ solutions yielded 0.12 ng Hg (± 0.10 ng Hg, 1SD, n=18) prior to transfer, and 0.10 ng Hg (± 0.08 ng Hg, 1SD, n=16) after transfer, representing <0.7% and <3.6% of sample solution mercury mass for EFPC and HC biological samples, respectively. Standard reference materials (with certified THg concentrations provided in parentheses) included DORM-3 (382 ± 60 ng g^{-1} THg) with an average recovery of 97.5 ± 2.4% (1SD, n=7), TORT-2 (270 ± 60 ng g^{-1} THg) with an average recovery of 100.5 ± 1.7% (1SD, n=5), and DOLT-2 (1990 ± 100 ng g^{-1} THg) with an average recovery of 106.5 ± 3.0% (1SD, n=2) relative to certified values (Table S4.4).

4.2.4 Methylmercury extraction by nitric acid digestion

Biological reference materials and fish and invertebrate samples collected from Hinds Creek and East Fork Poplar Creek were prepared for analysis of MeHg concentration (Table S4.2a-c, Table S4.4) following a previously described 12-h nitric acid digestion procedure (Hammerschmidt and Fitzgerald 2005, Brooks Rand Instruments 2013). Specific details of the procedure as it was performed in our lab are described elsewhere (Crowther et al. 2022). Briefly, sample aliquots (25 to 75 mg for reference materials; 20 to 60 mg for natural biological samples) were weighed into pre-weighed 15-mL borosilicate glass centrifuge tubes, and then 7.5 mL of

30% (v/v) HNO_3 was added to each vial. Separate sample aliquots weighed for matrix spike tests were immersed in the nitric acid, as described above, and then dosed with small volumes (80 to 900 µL) of a 10-, 50-, or 1000-ng g^{-1} MeHgCl spike solution in 0.5% (v/v) acetic acid + 0.2% (v/v) HCl. Additional centrifuge tubes for procedural blanks and aqueous MeHgCl standard tests were included with each digestion batch. Aqueous MeHgCl standard tests received 400 µL of a ~50-ng g^{-1} MeHgCl spike solution. Sample tubes were placed in a hot water bath maintained at 59.5 to 60.5ºC throughout the 12-h digestion. At the end of the digestion, the sample tubes were removed from the water bath and shaken by hand. The tube contents were then diluted to 7.5 mL of deionized water and the sample tubes were shaken again. The sample tubes were placed in a refrigerator for a maximum of 2 days prior to MeHg concentration analysis, at which time they were brought to room temperature and weighed to determine the total solution mass for calculation of the solid-sample MeHg concentration.

Aliquots of the digestion samples were analyzed for their MeHg concentration by gas chromatography coupled with cold vapor atomic fluorescence spectroscopy (GC-CVAFS) (MERX-M, Brooks Rand Instruments) following EPA Method 1630 (U.S. EPA 2001) (Table S4.2a-c, Table S4.4), as previously described (Crowther et al. 2022). After removing aliquots for MeHg concentration analysis, digestion samples used later for MeHg isotopic analysis were returned to a refrigerator overnight before performing the batch anion-exchange resin separation procedure. Samples were analyzed for MeHg concentration in batches with quality control that included calibration verification standards, secondary standards, and blanks, and each digestion sample was analyzed in duplicate. The exact concentration, or titer, of the aqueous MeHgCl standard (Brooks Rand) used for calibration standards, digestion matrix spike tests, and aqueous standard tests was determined following EPA Method 1630 (U.S. EPA 2001). On average, the

nitric acid digestion procedural blank solutions yielded 0.01 ng MeHg (± <0.01 ng MeHg, 1SD, n=27), representing <0.2% of the sample solution MeHg mass. Standard reference materials (with certified MeHg concentrations provided in parentheses) included DORM-3 (355 ± 56 ng g^{-1} MeHg; 93% MeHg), TORT-2 (152 ± 13 ng g^{-1} MeHg; 56% MeHg), DOLT-2 (693 ± 53 ng g^{-1} MeHg; 35% MeHg), and DOLT-5 (119 ± 58 ng g^{-1} MeHg; 27% MeHg). Duplicate nitric acid digestion matrix spike tests were performed on each of the reference materials (Table S4.4) and on 17 of the natural biological samples (Table S4.2a-c), representing approximately 1 in 7 biological samples, with an average recovery of 102.2 ± 3.5% (1SD, n=46). Nitric acid digestion aqueous MeHgCl standard tests had an average recovery of 99.9 ± 2.7% (1SD, n=27).

4.2.5 Isolation of methylmercury by anion-exchange resin separation

For a subset of the nitric acid digestion samples, MeHg was isolated from iHg for compound-specific isotopic analysis following a previously described batch anion-exchange resin separation procedure (Crowther et al. 2022). Briefly, nitric acid digestion sample tubes were syringe filtered into either a 125- or 250-mL pre-weighed PETG bottle as previously described (Crowther et al. 2022). Small sample aliquots were transferred from each bottle into pre-weighed glass vials for MeHg and THg concentration analysis, and then 2.5 g aliquots of pre-cleaned and conditioned resin (Bio-Rad AG 1-X4 resin, analytical grade, 200-400 mesh, chloride form) were poured into the PETG bottles. Samples bottles were then attached to a tube rotator (Fisher Scientific) and rotated for 2 h at 25 rotations per minute. At the end of the rotation period, the contents of the PETG bottles were filtered using 0.45-µm cellulose nitrate filter cups (Thermo Scientific, #130-4045), as previously described (Crowther et al. 2022). For fish and invertebrate samples containing greater than ~60% of THg as MeHg, filtered resin separation samples were poured into pre-weighed 500-mL Pyrex glass bottles, and for those containing less

than ~60% of THg as MeHg, filtered samples were poured into a secondary pre-weighed 250- or 500-mL PETG bottle for a second resin separation step. Small sample aliquots were transferred from each of the secondary PETG bottles into pre-weighed glass vials for MeHg and THg concentration analysis, and then 2.5 g aliquots of resin were poured into the PETG bottles, after which the resin separation process was repeated a second time. After the second resin separation step, the samples were filtered into 500-mL Pyrex bottles. Pyrex bottles were refrigerated for up to 2 days before MeHg concentration analysis.

After the resin separation procedure was complete, sample aliquots were analyzed for their MeHg concentration following EPA Method 1630 (U.S. EPA 2001) as described in the previous section. Samples representing the final resin step (in Pyrex bottles) were analyzed in duplicate, and sample aliquots used to calculate recovery of MeHg after syringe filtering and the first of two resin separation steps (in glass vials) were each analyzed once. Following the MeHg concentration analysis, samples were oxidized with BrCl and placed on a hot plate, and sample aliquots used for THg concentration analysis were exposed to ultraviolet light, as previously described (Crowther et al. 2022). Sample aliquots were then analyzed for their THg concentration by CVAFS following EPA Method 1631 (U.S. EPA 2002). Samples were analyzed in batches with quality control including calibration verification standards, secondary standards, blanks, and matrix spike recovery tests. The MeHg and THg concentrations were used to calculate MeHg recovery and purity after each of the syringe filtering and resin separation steps (Table S4.7a-b).

Prior to MeHg isotopic analysis (Table S4.8a-b), each of the final resin separation samples was chemically reduced, and the resulting Hg(0) was purged from solution and re-oxidized in a 1% $KMnO_4$ trapping solution following previously described methods (Demers et

al. 2013). Specific details of the procedure as it was performed for resin separation samples are described elsewhere (Crowther et al. 2022). The 1% $KMnO_4$ trap solutions were later reduced with $HONH_3Cl$, and a small aliquot was analyzed for THg concentration using CVAFS following EPA Method 1631 (U.S. EPA 2002) as previously described for combustion solutions. Purge-and-trap recovery of mercury from resin separation samples was 101.0 ± 1.7% (1SD, n=56 including aqueous MeHgCl standards, biological reference materials, and natural biological samples) (Table S4.8a-b). Purge-and-trap procedural blanks and standards (7.5, 15, and 35 ng Hg; NIST SRM 3133) were used to monitor analytical performance. Procedural blank 1% $KMnO_4$ solutions, yielding 0.03 ng Hg (± 0.01 ng Hg, 1SD, n=3), represented <0.5% of sample solution mercury mass. Procedural standard recovery was 98.5 ± 0.7% (1SD, n=3), and procedural standards were not significantly fractionated isotopically relative to NIST SRM 3133 bracketing standards (Table S4.5).

4.2.6 Mercury isotope analysis

Following combustion and transfer procedures, the mercury isotopic composition of each 1% $KMnO_4$ trap solution (Table S4.5, Table S4.6a-c, Table S4.8a-b) was measured using cold vapor multiple collector inductively coupled plasma mass spectrometry (CV-MC-ICP-MS; Nu Instruments) using previously described methods (Lauretta et al. 2001, Blum and Bergquist 2007). Thallium (NIST SRM 997) was used as an internal standard to correct for instrumental mass bias, along with sample-standard bracketing with mercury standard NIST SRM 3133. On-peak zero corrections were applied to all masses.

Mass-dependent isotope fractionation (MDF) is reported as the permil (‰) deviation from the average of NIST SRM 3133 bracketing standards (Blum and Bergquist 2007) using delta notation:

$$\delta^{xxx}Hg\ (‰) = ([(^{xxx}Hg/^{198}Hg)_{sample} / (^{xxx}Hg/^{198}Hg)_{NIST\ SRM\ 3133}] - 1) * 1000$$

where xxx is the mass of each mercury isotope between ^{199}Hg and ^{204}Hg. Mass-dependent fractionation is reported with $\delta^{202}Hg$ values. Mass-independent isotope fractionation (MIF) is reported as the difference between the measured $\delta^{xxx}Hg$ value and that which is theoretically predicted by the kinetic mass-dependent fractionation law (Blum and Bergquist 2007) using capital delta notation:

$$\Delta^{xxx}Hg\ (‰) \approx \delta^{xxx}Hg - (\delta^{202}Hg * \beta)$$

where xxx is the mass of each mercury isotope ^{199}Hg, ^{200}Hg, ^{201}Hg, and ^{204}Hg, and β is a constant for each isotope (0.252, 0.502, 0.752, 1.493, respectively) (Blum and Bergquist 2007).

To characterize the analytical uncertainty and reproducibility associated with isotope ratio measurements, each analytical session included 5 to 14 analyses of a secondary standard (UM-Almadén) at representative mercury concentrations (1 to 5 ng g^{-1}). We also measured the isotopic composition of each combustion reference material two to four times within an analytical session. To evaluate the accuracy and reproducibility of our results, we calculated the mean isotopic composition (± 2SE) for the collection of independent preparations of UM-Almadén and each reference material type (Table S4.5), and compared those means to the long-term average isotopic composition measured at the University of Michigan (Blum and Johnson 2017). We represent the analytical uncertainty in the THg isotopic composition of biological samples (via combustion) with the average uncertainty (2SD) across combustion reference material analyses (Table S4.5, Table S4.6a-c). Because each reference material process replicate was analyzed only once for MeHg isotopic composition, we represent the analytical uncertainty in the MeHg isotopic composition of biological samples (via resin separation) with the average

uncertainty (2SD) across UM-Almadén analyzed alongside resin separation materials within each session (Table S4.5, Table S4.8a-b).

4.3 Results

4.3.1 Total mercury and methylmercury concentrations

At the Hinds Creek reference site, THg concentrations across all fish and invertebrate sample types ranged from 21 to 1842 ng g^{-1}, and MeHg concentrations ranged from 10 to 1829 ng g^{-1} (Figure S4.1a, Table S4.2a). At East Fork Poplar Creek, THg and MeHg concentrations were higher, ranging from 687 to 10902 ng g^{-1} and 103 to 5681 ng g^{-1}, respectively (Figure S4.1a, Table S4.2b-c). Organisms collected from HC tended to have higher %MeHg values than those collected from EFPC, and for some organism types, most notably for clams, crayfish, and whole body stoneroller minnows, %MeHg values increased between upstream and downstream EFPC sites due to both a decrease in THg concentrations and an increase in MeHg concentrations (Figure S4.1b, Table S4.2a-c). For crayfish, there was a sharp increase in %MeHg between EFK 23.4 and EFK 22.3, followed by a more gradual increase in %MeHg between EFK 22.3 and EFK 6.3, largely driven by high THg concentrations at the most upstream site (Table S4.2b-c). These trends in THg concentration, MeHg concentration, and %MeHg align with previous observations (Peterson et al. 2017).

4.3.2 Total mercury stable isotope ratios

Based on combustion and THg isotope analysis, organisms collected from the Hinds Creek reference site had substantially more negative δ^{202}THg values than those collected from the highly contaminated East Fork Poplar Creek sites, averaging -1.21 ± 0.13‰ (1SD, n=35) for HC and -0.52 ± 0.23‰ (1SD, n=82) for EFPC (Figure 4.2a, Figure S4.2a-d, Table S4.6a-c).

Within EFPC, δ^{202}THg values increased slightly between upstream and downstream sites, averaging -0.61 ± 0.21‰ (1SD, n=45) at the upstream sites (EFK 24.2, EFK 23.4, and EFK 22.3) and -0.39 ± 0.18‰ (1SD, n=33) at the downstream site (EFK 6.3) (Figure S4.2c-d). Organisms collected from HC also tended to have more negative Δ^{199}THg values than those collected from EFPC, averaging -0.03 ± 0.08‰ (1SD, n=35) for HC and 0.10 ± 0.09‰ (1SD, n=82) for EFPC (Figure S4.2a-h, Table S4.6a-c). Within EFPC, average Δ^{199}THg values were not statistically different between the upstream and downstream sites. Additionally, Δ^{200}THg and Δ^{204}THg were near-zero for EFPC, averaging 0.01 ± 0.02‰ (1SD, n=82) and -0.01 ± 0.03‰ (1SD, n=82), respectively (Figure S4.2k-l, Table S4.6b-c). For HC, Δ^{200}THg and Δ^{204}THg values were small but shifted slightly away from zero, averaging 0.03 ± 0.03‰ (1SD, n=35) and -0.05 ± 0.05‰ (1SD, n=35), respectively (Figure S4.2i-j, Table S4.6a).

4.3.3 Methylmercury stable isotope ratios

The MeHg isotopic composition of organisms collected from Hinds Creek and East Fork Poplar Creek showed patterns similar to those described for THg isotopic composition, with the primary exception of having higher Δ^{199}Hg values. Organisms collected from the HC reference site had substantially lower δ^{202}MeHg values than those collected from the highly contaminated EFPC sites, averaging -0.93 ± 0.20‰ (1SD, n=7) for HC and -0.49 ± 0.24‰ (1SD, n=24) for EFPC (Figure S4.3a, Table S4.8a-b). Within EFPC, δ^{202}MeHg values also increased between upstream and downstream sites, averaging -0.68 ± 0.20‰ (1SD, n=11) at the upstream sites (EFK 23.4 and EFK 22.3) and -0.33 ± 0.15‰ (1SD, n=13) at the downstream site (EFK 6.3) (Figure S4.3a, Table S4.8b). Organisms collected from HC also tended to have lower Δ^{199}MeHg values than those collected from EFPC, averaging 0.07 ± 0.06‰ (1SD, n=7) for HC and 0.22 ± 0.08‰ (1SD, n=24) for EFPC (Figure S4.3a-b, Table S4.8a-b). In comparison, average Δ^{199}THg

values for HC and EFPC were -0.03 ± 0.08‰ (1SD, n=35) and 0.10 ± 0.09‰ (1SD, n=82), respectively. Within EFPC, average Δ^{199}MeHg values were not statistically different between the upstream and downstream sites. Additionally, Δ^{200}MeHg and Δ^{204}MeHg were near-zero for EFPC, averaging 0.02 ± 0.01‰ (1SD, n=24) and -0.01 ± 0.02‰ (1SD, n=24), respectively (Figure S4.3c, Table S4.8b). For HC, Δ^{200}MeHg and Δ^{204}MeHg values were small but significant, averaging 0.03 ± 0.01‰ (1SD, n=7) and -0.05 ± 0.03‰ (1SD, n=7), respectively (Figure S4.3c, Table S4.8a). These values are similar to the Δ^{200}THg and Δ^{204}THg values of biological samples from each of the two streams, but with slightly lower variability (Figure S4.2i).

4.3.4 Carbon and nitrogen stable isotope ratios

Organisms collected from the HC reference site, the upstream EFPC sites (EFK 24.2, EFK 23.4, and EFK 22.3), and the downstream EFPC site (EFK 6.3) had distinct δ^{13}C and δ^{15}N values (Figure S4.4a-d; Table S4.2a-c). In comparison to the EFPC sites, HC organisms had relatively low δ^{13}C and δ^{15}N values, averaging -28.59 ± 1.93‰ (1SD, n=38) and 9.47 ± 1.66‰ (1SD, n=38), respectively. Between the upstream and downstream sites of EFPC, δ^{13}C values decreased and δ^{15}N values increased, averaging -23.21 ± 1.33‰ (1SD, n=44) and 8.75 ± 1.33‰ (1SD, n=44), respectively, at the upstream EFPC sites, and -27.58 ± 1.87‰ (1SD, n=35) and 12.27 ± 1.16‰ (1SD, n=35), respectively, at the downstream EFPC site (Figure S4.4c-d). Within each of the sites, δ^{13}C and δ^{15}N values were not correlated with one another (r^2 values ranged from 0.03 to 0.09) (Figure S4.4b-d). However, there were some commonalities among sites, such as the rock bass fillet samples having relatively high δ^{15}N values, clam samples having relatively low δ^{15}N values, and whole body stoneroller minnow samples having relatively low δ^{13}C values. Additionally, within each of the sites, biofilm samples had relatively low δ^{15}N values compared

to the fish and invertebrate samples (Figure S4.4b-d). Similar to the aquatic organism samples, $\delta^{13}C$ values of biofilm generally decreased while $\delta^{15}N$ values increased between upstream and downstream EFPC sites (Figure S4.4c-d, Table S4.3). Positive relationships were observed between MeHg concentrations (log scale) and $\delta^{15}N$ values of aquatic organisms and biofilm samples at each of the three sites (Figure S4.5a-d). These results indicate that aquatic organisms with higher MeHg concentrations are generally from higher trophic levels, as expected.

4.4 Discussion

4.4.1 THg and MeHg isotopic compositions of aquatic organisms

4.4.1.1 Nonlinear relationships between THg isotope ratios and %MeHg of organisms suggest multiple sources of iHg and MeHg to aquatic food webs

In an aquatic ecosystem, different pools of mercury can have distinct isotopic compositions due to mixing of different sources and isotopic fractionation caused by various biogeochemical reactions. In particular, isotope fractionation that occurs during the formation and subsequent degradation of MeHg often contributes to isotopic distinctions between MeHg and the pool of iHg from which it originated. Isotopically distinct iHg and MeHg, either from a common source or from separate sources, may then be taken up by aquatic organisms, resulting in a THg isotopic composition equal to the weighted average isotopic composition of the iHg and MeHg within the organism. The measured THg isotope ratios of a high trophic level organism with a high %MeHg value, therefore, would generally reflect its MeHg isotopic composition, whereas the MeHg isotopic composition of a lower trophic level organism with low %MeHg could be masked by the abundance of iHg. In such cases, the isotopic composition of MeHg within lower trophic level organisms can sometimes be estimated using linear regression (Kwon et al. 2015) or mass balance (Tsui et al. 2012) techniques involving measurements of THg and

MeHg concentration and THg isotopic composition. These estimation approaches work well when all organisms in the food web obtain iHg and MeHg each from a single source. Under these conditions, the linear relationships between δ^{202}THg and %MeHg, as well as between Δ^{199}THg and %MeHg, for various types of organisms at different trophic levels within a food web can be used to calculate the isotopic composition of MeHg accumulated in the organisms, which can then be used to identify sources of MeHg to the food web. However, if different types of organisms within a food web have obtained iHg and/or MeHg from different sources, then the relationships between THg isotopic composition and %MeHg of the various types of organisms may not be linear, complicating these approaches for estimating the isotopic composition of MeHg within the food web. When complex food webs obtain iHg and/or MeHg from multiple isotopically distinct sources, direct measurements of the MeHg isotopic composition of various organisms are necessary to identify MeHg source(s) to those organisms.

In this study, we measured the THg isotopic composition of 82 fish and aquatic invertebrate samples collected from highly contaminated sites along the flow path of East Fork Poplar Creek and 35 from the Hinds Creek reference site. In plotting both δ^{202}THg and Δ^{199}THg against %MeHg for HC, upstream EFPC, and downstream EFPC organisms, we found generally increasing or decreasing trends across most biological sample types. However, for some organisms with either low or high %MeHg, their THg isotopic compositions did not follow the generally linear trends. Specifically, we found a relatively wide range in Δ^{199}THg values for HC organisms with high %MeHg (Figure 4.3b), wide ranges in both δ^{202}THg and Δ^{199}THg for upstream EFPC organisms with both low and high %MeHg (Figure 4.3c-d), and relatively wide ranges in both δ^{202}THg and Δ^{199}THg for downstream EFPC organisms with high %MeHg (Figure 4.3e-f). Due to the nonlinearity of these relationships, which is suggestive of multiple

isotopically distinct sources of iHg and/or MeHg to the food webs, it was not reasonable to estimate the isotopic composition of MeHg within the food webs using a linear regression (Kwon et al. 2015) or mass balance (Tsui et al. 2012) approach. Instead, we extracted and isolated MeHg from a subset of fish and aquatic invertebrate samples from EFPC and HC for direct isotope analysis (Crowther et al. 2022) (Figure 4.4a-c, Figure S4.3a).

4.4.1.2 Differences in isotopic composition of iHg and MeHg within organisms result in offsets in THg and MeHg isotopic compositions of organisms with lower %MeHg

For both East Fork Poplar Creek and Hinds Creek, aquatic organisms with high %MeHg values (greater than ~70%) had THg and MeHg isotopic compositions that were similar to one another, as expected based on mass balance. Organisms with lower %MeHg values, however, frequently had distinct THg and MeHg isotopic compositions. Organisms from EFPC and HC with lower %MeHg had Δ^{199}MeHg values that were consistently higher than their respective Δ^{199}THg values (by up to 0.31‰) (Figure S4.6b), which aligned with the generally positive relationships between Δ^{199}THg and %MeHg values for organisms from each of the sampling sites (Figure 4.3b,d,f). These offsets are due to differences in Δ^{199}Hg between iHg and MeHg within the organisms, with Δ^{199}Hg values of MeHg being higher than those of iHg, likely due to photochemical degradation of MeHg (Bergquist and Blum 2007, Chandan et al. 2015, Rose et al. 2015) prior to uptake into the EFPC and HC food webs.

Offsets between δ^{202}MeHg and δ^{202}THg values, however, were more variable. Several of the organisms from EFPC with lower %MeHg had near-zero offsets between their δ^{202}MeHg and δ^{202}THg values, indicating that they each contained iHg and MeHg with similar δ^{202}Hg values. Some organisms though, particularly from the HC reference site, had positive offsets between their δ^{202}MeHg and δ^{202}THg values (by up to 0.48‰), while others, particularly from the highly

contaminated EFPC sites, had negative offsets (by up to 0.39‰) (Figure S4.6a). The directions of these offsets align with the generally positive relationship between δ^{202}THg and %MeHg values for organisms from HC (Figure 4.3a), and the generally negative relationship for organisms from EFPC (Figure 4.3c,e). These offsets show that within the bodies of HC aquatic organisms, MeHg is generally isotopically heavier than iHg, likely largely due to microbial demethylation (Kritee et al. 2009) prior to uptake into the food web. Within EFPC aquatic organisms, however, MeHg is generally either isotopically lighter than or similar to iHg, likely largely due to a stronger dominance of isotope fractionation from microbial methylation (Rodríguez-González et al. 2009) compared to microbial demethylation (Kritee et al. 2009). However, offsets between δ^{202}MeHg and δ^{202}THg values of an organism may also be dependent on whether iHg and MeHg within the organism are derived from a common basal resource or from different sources. Offsets in isotopic composition between MeHg within aquatic organisms and iHg within aquatic organisms and basal resources from HC, EFPC, and other waterbodies will be further explored throughout the following Discussion sections.

4.4.1.3 Comparison of directly measured MeHg isotope ratios to those estimated via mass balance

For the fish and aquatic invertebrate samples used for direct MeHg isotope analysis, we also estimated their MeHg isotopic composition using a mass balance approach (Tsui et al. 2012) (Table S4.9) and then compared these estimated and directly measured values for each of the samples (Table S4.8a-b). The mass balance approach used the following equations for each of the biological samples:

$$\delta^{202}\text{THg} = f_{\text{MeHg}} * \delta^{202}\text{MeHg} + f_{\text{iHg}} * \delta^{202}\text{iHg}$$

$$\Delta^{199}\text{THg} = f_{\text{MeHg}} * \Delta^{199}\text{MeHg} + f_{\text{iHg}} * \Delta^{199}\text{iHg}$$

where f_{MeHg} and f_{iHg} are the fractions of MeHg and iHg within the organism (based on %MeHg). These equations include THg isotope ratios of the organism (which are directly measured), iHg isotope ratios of the organism (which are assumed to be approximately equal to the average measured THg isotopic composition of a potential iHg source such as sediment or biofilm within the sampling site), and MeHg isotope ratios of the organism (which are the variables of interest). These equations can be rearranged to solve for the MeHg isotope ratios of the biological samples:

$$\delta^{202}MeHg = (\delta^{202}THg - f_{iHg} * \delta^{202}iHg) / f_{MeHg}$$

$$\Delta^{199}MeHg = (\Delta^{199}THg - f_{iHg} * \Delta^{199}iHg) / f_{MeHg}$$

Values used for $\delta^{202}iHg$ and $\Delta^{199}iHg$ are provided in the caption of Table S4.9, which include the average THg isotopic composition of previously analyzed streambed sediment and biofilm from each of the HC, upstream EFPC, and downstream EFPC sampling sites. This mass balance approach was only used for fish and aquatic invertebrate samples containing ≥25% MeHg (n=24 of 31 samples), as calculations for samples with lower %MeHg values tended to produce anomalously low $\delta^{202}MeHg$ values and anomalously high $\Delta^{199}MeHg$ values. This is largely due to the relatively high uncertainty in the assumed iHg isotopic composition of each of the organisms, which may or may not be equal to the average THg isotopic composition across sediment or biofilm within the site, and which mathematically is more highly weighted in these calculations for biological samples with low %MeHg values.

For many of the fish and invertebrate samples, the MeHg isotopic composition estimated via mass balance aligned with the directly measured MeHg isotopic composition (Figure S4.7a-b, Table S4.9). However, the estimated $\delta^{202}MeHg$ values for some of the organisms, particularly those containing ~25 to 60% MeHg (e.g., snails, clams, and some crayfish), were

lower than their respective directly measured δ^{202}MeHg values. Offsets between directly measured and estimated δ^{202}MeHg values were up to ~1‰ when considering organisms with ≥25% MeHg, or up to ~0.5‰ when only considering organisms with ≥50% MeHg (Figure S4.7a-b, Table S4.9). Additionally, in comparison to biological samples with high %MeHg, estimated δ^{202}MeHg values of samples containing ~25 to 60% MeHg were more sensitive to whether the average THg isotopic composition of streambed sediment or biofilm was chosen to represent the isotopic composition of iHg within the food web (Figure S4.7a-b, Table S4.9). Thus, while this mass balance approach is useful for estimating the isotopic composition of MeHg within HC and EFPC organisms containing >60% MeHg (e.g., shiners, redbreast sunfish, and some stoneroller minnows and crayfish), the error associated with this estimation approach increases substantially with decreasing %MeHg. Importantly, this approach relies on the assumptions that an organism obtains iHg from a single source and that this source has been correctly identified. The fact that there is a substantial mismatch between directly measured and estimated MeHg isotope ratios for several of the biological samples containing <60% MeHg, regardless of whether sediment or biofilm is assumed to be the source of iHg to the organisms, strongly suggests that there are multiple isotopically distinct sources of iHg to the Hinds Creek and East Fork Poplar Creek food webs. Therefore, this mass balance estimation approach, which relies on a single and correctly assumed isotopic composition of iHg, is unreliable for estimating the MeHg isotopic compositions of lower-trophic-level aquatic organisms from the two streams in this study. Instead, this study employs compound-specific MeHg isotope analysis of a subset of fish and aquatic invertebrate samples to more confidently determine the range of MeHg isotopic compositions within the HC and EFPC food webs in order to identify sources of MeHg to the food webs and to investigate biogeochemical cycling of MeHg within the two streams.

4.4.1.4 Using THg, MeHg, and calculated iHg isotopic compositions of organisms to identify sources of iHg and MeHg to aquatic food webs.

The most likely sources of iHg and MeHg to the HC, upstream EFPC, and downstream EFPC aquatic food webs were determined using both THg and MeHg isotopic measurements. For fish and aquatic invertebrates analyzed for both THg and MeHg isotope ratios, the isotopic composition of iHg within the organism was calculated via mass balance using the equations in Section 4.4.1.3 (Table S4.10). In this case, however, the THg and MeHg isotope ratios of the organism are directly measured and the iHg isotope ratios of the organism are the variables of interest. These equations can be rearranged to solve for the iHg isotope ratios of the biological samples:

$$\delta^{202}iHg = (\delta^{202}THg - f_{MeHg} * \delta^{202}MeHg) / f_{iHg}$$

$$\Delta^{199}iHg = (\Delta^{199}THg - f_{MeHg} * \Delta^{199}MeHg) / f_{iHg}$$

This mass balance approach was only used for biological samples containing <85% MeHg, as calculations for samples with higher %MeHg values tended to produce unreasonable δ^{202}iHg and Δ^{199}iHg values. This is likely due to slight differences in MeHg isotopic composition between different sample aliquots used in the combustion and resin separation procedures, and MeHg isotopic compositions mathematically being more highly weighted in these calculations for biological samples with high %MeHg values.

These calculated iHg isotopic compositions (Figure 4.5a-c), as well as the THg isotopic compositions of organisms with low %MeHg values (Figure 4.5d-e), were compared to the THg isotopic compositions of potential iHg sources, which themselves had low %MeHg values, to determine the most likely sources of iHg to each of the food webs. In addition, directly measured MeHg isotopic compositions (Figure 4.4a-c), as well as the THg isotopic compositions of

organisms with high %MeHg values (Figure 4.4d-f), were used to determine the most likely sources of MeHg to the food webs. These isotope ratios were corrected to account for the isotope fractionation caused by photochemical demethylation using an experimentally derived $\Delta^{199}Hg/\delta^{202}Hg$ slope of 2.43 associated with an aqueous system containing 1 mg L^{-1} of dissolved organic carbon (DOC) (Bergquist and Blum 2007) (Figure 4.4a-f, Table S4.10). This slope value was chosen based on previous measurements of DOC concentrations (1.2 to 2.4 mg L^{-1}) in EFPC stream water (Demers et al. 2018). These corrected isotopic compositions were compared to the THg isotopic compositions of potential MeHg sources, with the assumption that offsets in $\delta^{202}Hg$ could be explained by the balance of microbial methylation and demethylation (Kritee et al. 2009, Rodríguez-González et al. 2009).

4.4.2 Hinds Creek: Regional reference site

4.4.2.1 Sources of iHg to the Hinds Creek food web

Multiple methods can be used to determine the isotopic composition of iHg within aquatic organisms, which can then be used to identify the source(s) of iHg to the food web. In some cases, THg isotopic compositions of organisms with low %MeHg (≤10%) are used as a proxy for iHg isotopic compositions accessed by the food web. However, all of the organisms collected from the Hinds Creek reference site had ≥34% MeHg (Table S4.2a), and so THg isotopic compositions of low %MeHg organisms could not be used. Additionally, while linear regression techniques involving THg isotopic compositions and %MeHg values of aquatic organisms could potentially be used to estimate the isotopic composition of iHg within a food web (Kwon et al. 2015), the nonlinear relationship between $\Delta^{199}THg$ and %MeHg values of HC organisms (Figure 4.3b) prevented the use of this method. Instead, we estimated iHg isotopic compositions via mass balance for organisms analyzed for both their THg and MeHg isotopic

composition and which contained <85% MeHg. For HC, this applied to three biological sample types with distinctly different feeding strategies, including snails (45% MeHg), clams (61% MeHg), and stoneroller minnows (82% MeHg) (n=1 of each sample type). Calculated δ^{202}iHg values for these organisms ranged from -1.77 to -1.29‰, and calculated Δ^{199}iHg values ranged from -0.30 to -0.19‰ (Table S4.10). These results were broadly similar to the Δ^{199}THg values of both HC streambed sediment (Donovan et al. 2014) and biofilm (sediment = -0.27 ± 0.01‰, 1SD, n=2; biofilm = -0.28 ± <0.01‰, 1SD, n=2), but aligned more closely with the δ^{202}THg values of streambed sediment (-1.37 ± 0.08‰ δ^{202}THg, 1SD, n=2) than of biofilm (-0.89 ± 0.17‰, 1SD, n=2). (Figure 4.5a). We note that the difference in δ^{202}THg between HC streambed sediment and biofilm may be due to microbial mercury reduction reactions within the biofilm that induce kinetic MDF (Kritee et al. 2007, Kritee et al. 2009). The similarity between measured THg isotopic compositions of HC streambed sediment and calculated iHg isotopic compositions of HC organisms suggests that streambed sediment is a more dominant source of iHg to the HC food web than biofilm. Similarly, this suggests that all of these organisms are accessing basal resources more closely aligned with sediment than with biofilm. This is somewhat surprising given that clams are filter feeders that consume suspended matter, and snails are grazers that tend to feed on biofilm. Stoneroller minnows, however, are bottom feeders and build nests in the sediment, so they are in direct contact with the streambed and ingest streambed sediment (Kraatz 1923, Miller 1962).

The range in calculated Δ^{200}iHg values for HC snails, clams, and stoneroller minnows (-0.01 to 0.03‰) also aligned with the measured Δ^{200}THg values of HC streambed sediment (0.02 ± 0.03‰, 1SD, n=2) (Donovan et al. 2014) and biofilm (0.01 ± 0.01‰, 1SD, n=2). Given the low THg concentrations of HC streambed sediment (~10 to 30 ng g^{-1}) (Donovan et al. 2014)

and the absence of any known point sources of contamination, these near-zero Δ^{200}Hg values suggest that iHg within HC streambed sediment and biofilm, as well as that which enters the HC food web, is derived from a mixture of atmospheric sources, including both dry and wet deposition. While mercury isotopic measurements have not been made for precipitation or gaseous atmospheric mercury in Tennessee, they have been made for samples collected from various other sites across the eastern United States (gaseous atmospheric mercury from MI, WI, and FL; rainfall from MI, WI, and SC, excluding samples collected near the Crystal River coal-fired utility boiler in SC). Based on the average Δ^{200}Hg values of these gaseous atmospheric mercury (-0.06 ± 0.05‰, 1SD, n=39) (Gratz et al. 2010, Demers et al. 2013, Demers et al. 2015) and rainfall (0.15 ± 0.06‰, 1SD, n=35) (Gratz et al. 2010, Sherman et al. 2012, Demers et al. 2013) samples, iHg within HC streambed sediment, biofilm, and aquatic organisms appears to be approximately two-thirds derived from gaseous atmospheric mercury and one-third derived from mercury in rainfall.

Even-MIF (i.e., shifts in Δ^{200}Hg and Δ^{204}Hg values) is thought to occur primarily through photochemical oxidation reactions in the upper atmosphere (Yin et al. 2014, Blum and Johnson 2017), and so once mercury has entered a stream ecosystem through dry and/or wet deposition, its Δ^{200}Hg and Δ^{204}Hg values are conserved as the mercury undergoes further biogeochemical processing and subsequently enters the food web. However, δ^{202}Hg and Δ^{199}Hg values can be influenced by several other types of biogeochemical reactions, which explains why the δ^{202}THg and Δ^{199}THg values of HC streambed sediment, as well as calculated δ^{202}iHg and Δ^{199}iHg values of HC organisms, were each lower than a two-to-one mixture of gaseous atmospheric and precipitation mercury sources with no additional processing. Gaseous atmospheric mercury and rainfall samples from the eastern United States have average δ^{202}Hg values of 0.74 ± 0.34‰

(1SD, n=39) (Gratz et al. 2010, Demers et al. 2013, Demers et al. 2015) and -0.15 ± 0.27‰ (1SD, n=35) (Gratz et al. 2010, Sherman et al. 2012, Demers et al. 2013), respectively. Hypothetically, a two-to-one mixture of these atmospheric mercury sources with no additional biogeochemical processing would have a δ^{202}Hg value of approximately 0.44 ± 0.24‰ (1SD). Lower δ^{202}THg values of HC streambed sediment (-1.37 ± 0.08, 1SD, n=2) (Donovan et al. 2014), biofilm (-0.89 ± 0.17‰, 1SD, n=2), and calculated δ^{202}iHg values of HC aquatic organisms (-1.77 to -1.29‰) (Figure 4.5a, Table S4.10) have likely been influenced by kinetic MDF during uptake of gaseous atmospheric mercury into foliage (Demers et al. 2013), followed by physical incorporation of leaf litter into the streambed sediment over time. Additionally, gaseous atmospheric mercury and rainfall samples from the eastern United States have average Δ^{199}Hg values of -0.21 ± 0.07‰ (1SD, n=39) (Gratz et al. 2010, Demers et al. 2013, Demers et al. 2015) and 0.24 ± 0.24‰ (1SD, n=35) (Gratz et al. 2010, Sherman et al. 2012, Demers et al. 2013), respectively. A hypothetical two-to-one mixture of these atmospheric mercury sources with no additional biogeochemical processing would have a Δ^{199}Hg value of approximately -0.06 ± 0.09‰ (1SD). Lower Δ^{199}THg values of HC streambed sediment (-0.27 ± 0.01‰, 1SD, n=2) (Donovan et al. 2014) and biofilm (-0.28 ± <0.01‰, 1SD, n=2), as well as calculated Δ^{199}iHg values of HC aquatic organisms (-0.30 to -0.19‰) (Figure 4.5a, Table S4.10), may be due to photochemical reduction of thiol-bound mercury (Zheng and Hintelmann 2010a) within the stream ecosystem.

Overall, iHg within the Hinds Creek ecosystem appears to be ultimately derived from a mixture of precipitation, which delivers iHg to the stream through runoff, and dry deposition, which delivers iHg to the stream through uptake into foliage and subsequent incorporation of leaf litter into the streambed. Once in the stream, iHg appears to undergo additional biogeochemical

processing, including photochemical reduction of thiol-bound mercury, decreasing the Δ^{199}THg values and increasing the δ^{202}THg values of streambed sediment and biofilm, as well as microbial reduction of iHg within biofilm, further increasing its δ^{202}THg value. Organisms then take up iHg predominantly from streambed sediment, though smaller proportions of iHg within the food web may also be obtained from other basal resources.

4.4.2.2 Sources of MeHg to the Hinds Creek food web

The range in isotopic composition of MeHg within the Hinds Creek food web can be characterized using directly measured MeHg isotopic compositions of aquatic organisms, as well as THg isotopic compositions of organisms with high %MeHg. Biological samples with high %MeHg values (≥90% MeHg) include dragonfly larvae (n=1), crayfish (n=4), stoneroller minnows (n=1), redbreast sunfish (n=3), and rock bass (n=4) (Table S4.2a). These organisms had a relatively narrow range in δ^{202}THg values (-1.28 to -1.03‰) and a relatively wide range in Δ^{199}THg values (-0.13 to 0.11‰) (Figure 4.3, Figure 4.4d, Table S4.6a). Biological samples directly analyzed for their MeHg isotopic composition include snipe fly larvae, megaloptera larvae, snails, Asian clams, crayfish, stoneroller minnows, and redbreast sunfish (n=1 for each sample type). These organisms had MeHg isotope ratios that extended beyond the range in THg isotopic composition of high %MeHg biological samples (up to -0.55‰ δ^{202}MeHg, and up to 0.15‰ Δ^{199}MeHg) (Figure 4.4a, Table S4.8a). For this site, direct MeHg isotopic measurements revealed a wider range in MeHg isotopic composition than would have been estimated by THg isotopic measurements alone, particularly due to the high δ^{202}MeHg value of the clams. These relatively wide ranges in MeHg isotopic composition suggest that aquatic organisms within the HC reference site accumulate MeHg from multiple isotopically distinct basal resources.

The Δ^{200}Hg values of MeHg within the HC food web suggest that the bioaccumulated MeHg was formed from iHg derived from a combination of dry and wet deposition. Aquatic organisms directly analyzed for their MeHg isotopic composition had an average Δ^{200}MeHg of 0.03 ± 0.01‰ (1SD, n=7) (Figure S4.3c, Table S4.8a). Similarly, HC aquatic organisms with high %MeHg values (≥90% MeHg) had an average Δ^{200}THg of 0.02 ± 0.03‰ (1SD, n=13) (Table S4.6a). These values are reflective of MeHg formed from iHg derived from a mixture of gaseous atmospheric (-0.06 ± 0.04‰ Δ^{200}THg, 1SD, n=39) (Gratz et al. 2010, Demers et al. 2013, Demers et al. 2015) and precipitation (0.15 ± 0.06 Δ^{200}THg, 1SD, n=35) (Gratz et al. 2010, Sherman et al. 2012, Demers et al. 2013) sources, with between a one-to-one and two-to-one ratio. As described in Section 4.4.2.1, the iHg accumulated within the HC food web also appears to have been derived from a mixture of these same atmospheric sources (at an approximate two-to-one ratio), as does iHg within HC streambed sediment (0.02 ± 0.03‰ Δ^{200}THg, 1SD, n=2) (Donovan et al. 2014) and biofilm (0.01 ± 0.01‰ Δ^{200}THg, 1SD, n=2). Additionally, similar to the δ^{202}Hg values of iHg within the HC food web (Table S4.10) and basal resources, δ^{202}MeHg values of HC aquatic organisms (-0.93 ± 0.20‰, 1SD, n=7) (Table S4.8a) were also lower than the δ^{202}Hg value of a hypothetical two-to-one mixture of atmospheric gaseous mercury and precipitation (0.44 ± 0.24‰, 1SD). This supports the idea that a portion of the iHg that was methylated and subsequently accumulated in the HC food web was derived from atmospheric gaseous mercury, which was isotopically fractionated during uptake into foliage prior to entering the stream via leaf litter and subsequently being converted into MeHg and accumulating in the food web.

The directly measured Δ^{199}MeHg values of HC aquatic organisms (0.07 ± 0.06‰, 1SD, n=7) (Figure 4.4a, Table S4.8a), as well as the Δ^{199}THg values of organisms with ≥90% MeHg

(0.00 ± 0.08‰, 1SD, n=13) (Figure 4.4d, Table S4.6a), were consistently higher than their calculated Δ^{199}iHg values (-0.26 ± 0.07‰, 1SD, n=3) (Figure 4.5a, Table S4.10). These MeHg isotopic values were also consistently higher than the Δ^{199}THg values of HC streambed sediment (-0.27 ± 0.01‰, 1SD, n=2) (Donovan et al. 2014) and HC biofilm (-0.28 ± <0.01‰, 1SD, n=2) (Figure 4.4a,d). This positive offset in Δ^{199}Hg between MeHg in the food web and iHg in the food web and basal resources can potentially be explained by photochemical demethylation (Bergquist and Blum 2007, Chandan et al. 2015, Rose et al. 2015) prior to uptake of MeHg into the food web. The Δ^{199}Hg values of MeHg within the food web may also be influenced by photochemical reduction of iHg, either by sulfurless ligands, causing increasing Δ^{199}Hg values (Bergquist and Blum 2007, Rose et al. 2015, Zheng and Hintelmann 2009, 2010a), or by thiol ligands, causing decreasing Δ^{199}Hg values (Zheng and Hintelmann 2010a), prior to the formation of MeHg and uptake into the food web. Photochemical demethylation and photochemical reduction of iHg can be differentiated by their Δ^{199}Hg / Δ^{201}Hg slopes. Using directly measured MeHg isotopic compositions, the Δ^{199}MeHg / Δ^{201}MeHg slope of HC aquatic organisms was calculated to be 1.27 ± 0.11 (1SE, n=7) (Figure S4.3b). This slope value closely aligns with the characteristic Δ^{199}Hg / Δ^{201}Hg slope of photochemical demethylation (~1.3) (Bergquist and Blum 2007, Chandan et al. 2015, Rose et al. 2015), but also overlaps with that of photochemical reduction of iHg (~1.0 to 1.2) (Blum and Bergquist 2007, Zheng and Hintelmann 2009, 2010a, Rose et al. 2015, Kritee et al. 2018). It is likely that the Δ^{199}Hg values of MeHg within the HC food web have been influenced by both photochemical reduction of iHg and photochemical demethylation. As described in Section 4.4.2.1, iHg within HC streambed sediment and biofilm has likely undergone photochemical reduction by thiol ligands, based on their low Δ^{199}THg values relative to a hypothetical two-to-one mixture of mercury from gaseous atmospheric and

precipitation sources. While MeHg produced from iHg within sediment and/or biofilm would initially have an equally low Δ^{199}Hg value, subsequent photochemical demethylation would increase its Δ^{199}Hg value before it entered the food web. This combination of reactions could explain the relatively high Δ^{199}Hg values, as well as the Δ^{199}Hg / Δ^{201}Hg slope value, of MeHg within the HC food web.

The directly measured δ^{202}MeHg values of HC aquatic organisms (-0.93 ± 0.20‰, 1SD, n=7) (Figure 4.4a, Table S4.8a), as well as the δ^{202}THg values of organisms with ≥90% MeHg (-1.16 ± 0.08‰, 1SD, n=13) (Figure 4.4d, Table S4.6a), were slightly higher than their calculated δ^{202}iHg values (-1.52 ± 0.24‰, 1SD, n=3) (Figure 4.5a, Table S4.10). These MeHg isotopic values were also slightly higher than the δ^{202}THg values of HC streambed sediment (-1.37 ± 0.08, 1SD, n=2) (Donovan et al. 2014), which appears to be the primary source of iHg accumulated in the food web, but overlapped with the δ^{202}THg values of HC biofilm (-0.89 ± 0.17‰, 1SD, n=2) (Figure 4.4a). The MeHg isotopic compositions of aquatic organisms were corrected to account for the isotope fractionation caused by photochemical demethylation, as described in Section 4.4.1.4, using an assumed initial Δ^{199}MeHg value equal to the average Δ^{199}THg value across HC streambed sediment and biofilm (-0.28‰). These corrected δ^{202}MeHg values (-1.07 ± 0.18‰, 1SD, n=7) (Table S4.10) were slightly higher than the δ^{202}THg values of streambed sediment and overlapped with the δ^{202}THg values of biofilm (Figure 4.4a). Photochemical demethylation-corrected δ^{202}THg values of HC organisms with ≥90% MeHg, however, were slightly lower (-1.28 ± 0.06‰, 1SD, n=13) and overlapped with the δ^{202}THg values of streambed sediment and were slightly lower than the δ^{202}THg values of biofilm (Figure S4.4d). Together, these ranges in photochemical demethylation-corrected δ^{202}Hg values of MeHg in the HC food web overlapped with the δ^{202}THg values of both streambed sediment and biofilm,

but on average were higher than the calculated δ^{202}Hg values of iHg in the food web. Multiple combinations of biogeochemical reactions can potentially explain this slight positive offset in δ^{202}Hg between MeHg and iHg in the HC food web, depending on whether the MeHg in the food web was produced from iHg in the sediment or biofilm. If iHg and MeHg in the HC food web were both primarily sourced from streambed sediment, then the slight positive offset in δ^{202}Hg could be explained by high amounts of microbial demethylation relative to microbial methylation within the sediment. In this case, relatively large positive shifts in δ^{202}MeHg due to microbial demethylation (Kritee et al. 2009) could overprint smaller negative shifts in δ^{202}MeHg due to microbial methylation (Rodríguez-González et al. 2009) within the sediment. On the other hand, while iHg in the food web appears to be primarily sourced from streambed sediment, MeHg in the food web could be primarily sourced from biofilm, which itself has higher δ^{202}THg values than the sediment (Figure 4.5a), possibly due to microbial reduction of iHg within the biofilm (Kritee et al. 2007, Kritee et al. 2009). In this case, the positive offset in δ^{202}Hg between MeHg and iHg within the HC food web could be explained by the difference in THg isotopic composition between these source materials, rather than by relatively large amounts of microbial demethylation. Because the δ^{202}MeHg value of a basal resource may be either lower, higher, or the same as its δ^{202}THg value – largely based on the relative amounts of microbial methylation and microbial demethylation occurring within the material – it is difficult to differentiate between streambed sediment and biofilm as potential sources of MeHg to the HC food web using δ^{202}Hg values alone. However, the relatively wide range in Δ^{199}MeHg values of HC aquatic organisms can be used to differentiate between these basal resources as potential sources of MeHg to the food web.

The relatively wide range in Δ^{199}Hg values of MeHg within the HC food web, based on both directly measured Δ^{199}MeHg values of aquatic organisms (Figure 4.4a, Table S4.8a) as well as Δ^{199}THg values of high %MeHg organisms (Figure 4.4d, Table S4.6a), suggests that different types of organisms obtained MeHg from different mixtures of sources containing isotopically distinct MeHg. Differences in Δ^{199}MeHg values between different basal resources within HC would likely be the result of differing degrees of photochemical demethylation. The MeHg within materials such as biofilm and suspended particulates may be more susceptible to isotope fractionation via photochemical demethylation than MeHg within streambed sediment, which would result in higher Δ^{199}MeHg values (Bergquist and Blum 2007, Chandan et al. 2015, Rose et al. 2015). This could be due to higher amounts of sunlight exposure, as well as suspended particulates and biofilm each containing a smaller pool of MeHg compared to streambed sediment, which would be more easily isotopically fractionated. Relatively large offsets in Δ^{199}MeHg values between different basal resources have been observed previously in other stream ecosystems. For example, for the Fox River (WI, USA), Rosera et al. (2022) found that while the Δ^{199}THg values of streambed sediment and seston, as well as the directly measured Δ^{199}MeHg values of streambed sediment, were all near-zero, the Δ^{199}MeHg values of seston were >0.5‰. This suggested that MeHg within seston had undergone a relatively high degree of photochemical processing while MeHg within streambed sediment had not. Similarly, for the South Fork Eel River (CA, USA), although the MeHg isotopic compositions of basal resources were not measured, Tsui et al. (2013) found that scrapers that exclusively feed on algae had higher estimated Δ^{199}MeHg values than other types of benthic invertebrates. Likewise, for the Oyapock River (French Guiana), Laffont et al. (2021) found that periphytophagous fish consistently had slightly higher Δ^{199}THg values than piscivorous fish. These observations made

in two different studies were proposed to have been due to increased photochemical demethylation associated with biofilm compared to other basal resources, and suggested that different types of organisms within each of the rivers were obtaining MeHg from different combinations of sources. While the MeHg isotopic compositions of HC basal resources were not measured in this study, based on the findings of these previous studies, it is plausible that despite having similar Δ^{199}THg values, HC suspended particulates and biofilm may have higher Δ^{199}MeHg values than streambed sediment due to increased photochemical demethylation and smaller MeHg pool sizes. If this is true, then lower trophic level consumers from HC with relatively high Δ^{199}MeHg values may have obtained a majority of their MeHg from consuming suspended particulates and/or biofilm, which would then be passed to higher trophic level consumers, maintaining its isotopic composition as it biomagnifies. This could explain the relatively high Δ^{199}MeHg values of HC snails, clams, snipe fly larvae, megaloptera larvae, crayfish, and stoneroller minnows (Figure 4.4a, Table S4.8a). Other lower trophic level consumers from HC may have obtained a portion of their MeHg from suspended particulates and/or biofilm and another portion from streambed sediment, resulting in lower Δ^{199}MeHg values due to mixing of sources, which are maintained as the MeHg is passed to higher trophic level consumers. This could explain the slightly lower Δ^{199}MeHg values of redbreast sunfish (Figure 4.4a, Table S4.8a) as well as the slightly lower Δ^{199}THg values of dragonfly larvae, redbreast sunfish, and rock bass, all of which contained ~100% MeHg (Figure 4.3b, Figure 4.4d, Table S4.6a). It is likely that some of the lower trophic level organisms from HC also had relatively low Δ^{199}MeHg values, although none were identified in this study. Aquatic organisms across all trophic levels may also obtain a portion of their MeHg directly from the surface water dissolved phase, which could potentially have elevated Δ^{199}MeHg values due to photochemical

demethylation within the water column. Fish and benthic invertebrates obtain a majority of their MeHg from dietary sources, though previous studies have suggested that up to ~10-15% of MeHg in fish is obtained directly from water as it passes across the gills during respiration (Hall et al. 1997, Wang et al. 2010, Hrenchuk et al. 2012). Thus, elevated Δ^{199}MeHg values of HC organisms may be partially explained by uptake of dissolved MeHg from the surface water, though this would only be a minor source of MeHg to the food web.

As with iHg, MeHg within the Hinds Creek food web also appears to be ultimately derived from a mixture of precipitation and dry deposition, both of which contribute iHg to various basal resources within HC. Streambed sediment, biofilm, and suspended particulates each may be sources of MeHg production, but MeHg produced in biofilm and suspended particulates likely experiences a higher degree of photochemical demethylation than MeHg in streambed sediment, which would result in higher Δ^{199}MeHg values within these materials. Each of the aquatic organisms collected from HC in this study likely obtained a significant amount of their MeHg from biofilm and/or suspended particulates, based on the elevated Δ^{199}MeHg values across several different biological sample types, though organisms with slightly lower Δ^{199}MeHg values also likely obtained some of their MeHg from streambed sediment. If high and low Δ^{199}MeHg values of organisms are reflective of different proportions of their MeHg being obtained from different basal resources, then we may expect these Δ^{199}MeHg values to correlate with the δ^{13}C values of the organisms. However, these values are not correlated for HC aquatic organisms (Figure S4.8b), suggesting that the primary sources of MeHg to the organisms are not necessarily the same as their primary carbon source. Overall, these results suggest that iHg and MeHg within the HC food web are largely derived from different basal resources, with much of the iHg originating from streambed sediment and much of the MeHg originating from biofilm

and/or suspended particulates. Additionally, this suggests that positive offsets in δ^{202}Hg between MeHg and iHg in the HC food web may be directly related to the positive offset in δ^{202}THg between biofilm and streambed sediment (Figure S4.5a), which could potentially be largely explained by microbial reduction of iHg within biofilm prior to the formation of MeHg. While microbial demethylation is also likely occurring within streambed sediment and other basal resources, large amounts of microbial demethylation within streambed sediment relative to microbial methylation would not be required to explain the positive offsets in δ^{202}Hg between MeHg and iHg if much of the MeHg is produced in biofilm.

4.4.3 East Fork Poplar Creek: Point source impacted site

4.4.3.1 Sources of iHg to the East Fork Poplar Creek food web

Similar to Hinds Creek, estimates of iHg isotopic compositions within the upstream and downstream East Fork Poplar Creek food webs can be used to identify sources of iHg to the aquatic organisms. For the highly contaminated EFPC sites, as was the case for HC, regression techniques involving THg isotopic compositions and %MeHg values of aquatic organisms could not be used to estimate the isotopic composition of iHg within the food web because the relationships between δ^{202}THg and %MeHg and between Δ^{199}THg and %MeHg values of EFPC organisms were not linear (Figure 4.3c-f). However, THg isotopic compositions of organisms with low %MeHg (≤10%) could be used as a proxy for iHg isotopic compositions within the food web. Additionally, iHg isotopic compositions could be calculated via mass balance for organisms analyzed for both their THg and MeHg isotopic composition and which contained <85% MeHg. For upstream EFPC (EFK 24.2 to EFK 22.3), biological samples with ≤10% MeHg included aquatic earthworms (n=1), mayfly larvae (n=2), caddisfly larvae (n=1), megaloptera larvae (n=1), clams (n=5), and stoneroller minnows (n=1) (Table S4.2b). Among

these samples, δ^{202}THg values ranged from -0.90 to -0.22‰ and Δ^{199}THg values ranged from -0.10 to 0.12‰ (Figure 4.3c-d, Figure 4.5d, Table S4.6b). These relatively wide ranges in THg isotopic composition of low %MeHg biological samples suggest that upstream EFPC aquatic organisms obtain iHg from multiple isotopically distinct sources. Additionally, the range in THg isotopic composition of low %MeHg organisms was similar to the range in calculated iHg isotopic compositions of megaloptera larvae (n=2), clams (n=1), crayfish (n=3), and stoneroller minnows (n=1) from upstream EFPC (Figure 4.5b, Table S4.10). This suggests that both the measured THg isotopic compositions of organisms with ≤10% MeHg, as well as the calculated iHg isotopic compositions of organisms with <85% MeHg, can be used to characterize the isotopic composition of iHg within various organism types.

For downstream EFPC (EFK 8.7 to EFK 5.0), biological samples with ≤10% MeHg include only caddisfly larvae (n=1) (Table S4.2c) with a δ^{202}THg value of -0.06‰ and Δ^{199}THg value of -0.05‰ (Figure 4.3e-f, Figure 4.5e, Table S4.6c). This value falls near the range of calculated iHg isotopic compositions of mayfly larvae (n=1), snails (n=2), clams (n=2), and stoneroller minnows (n=2) from downstream EFPC (-0.31 to -0.10‰ δ^{202}iHg and -0.10 to 0.01‰ Δ^{199}iHg), which is narrower than that of upstream EFPC (Figure 4.5c, Table S4.10). This narrower range in isotopic composition may be partially explained by the absence of megaloptera larvae samples, which for upstream EFPC had strongly negative δ^{202}THg values and slightly positive Δ^{199}THg values. Therefore, this suggests that the makeup of the community of organisms within the food web influences the sources of iHg that are accessed, which in turn suggests that thorough sampling of lower trophic levels of the food web may be required to fully assess sources of iHg that are being accessed and accumulated within the food web.

Individual biological sample types with relatively low %MeHg collected from upstream EFPC were generally isotopically distinct from one another (Figure 4.3c-d, Figure 4.5d), suggesting that different types of organisms within EFPC obtain iHg from distinct sources based on their individual living and feeding habits. For example, the THg isotopic composition of upstream EFPC stoneroller minnows with 10-13% MeHg (-0.22 ± 0.08‰ δ^{202}THg and -0.08 ± 0.02‰ Δ^{199}THg, 1SD, n=3) (Figure 4.3c-d, Figure 4.5d, Table S4.6b), as well as its calculated iHg isotopic composition (Figure 4.5b, Table S4.10), was similar to that of upstream EFPC streambed sediment (-0.09 ± 0.17‰ δ^{202}THg and -0.05 ± 0.02‰ Δ^{199}THg, 1SD, n=6) (Donovan et al. 2014, Crowther et al. 2021) (Figure 4.3c-d, Figure 4.5b,d). This suggests that these fish derive much of their iHg from legacy mercury within streambed sediment derived from historical contamination from the Y-12 facility, which is further supported by their bottom-feeding and nest-building behaviors, through which they are in direct contact with the streambed and ingest streambed sediment (Kraatz 1923, Miller 1962).

The THg and calculated iHg isotopic compositions of EFPC Asian clams can also be used to identify the most likely sources of iHg to these organisms. Upstream EFPC clams with 4-7% MeHg had slightly lower δ^{202}THg values (-0.40 ± 0.05‰, 1SD, n=5) and higher Δ^{199}THg values (0.08 ± 0.02‰, 1SD, n=5) than stoneroller minnows from the same site (Figure 4.3d, Figure 4.5d, Table S4.6b), and their calculated iHg isotopic compositions were similar (Figure 4.5b, Table S4.10). These isotopic compositions generally aligned with the THg isotopic compositions of upstream EFPC biofilm (-0.31 ± 0.09‰ δ^{202}THg and -0.01 ± 0.02‰ Δ^{199}THg, 1SD, n=3), suspended particulates (-0.32 ± 0.10‰ δ^{202}THg and 0.01 ± 0.01‰ Δ^{199}THg, 1SD, n=9), and surface water dissolved phase (-0.23 ± 0.17‰ δ^{202}THg and 0.09 ± 0.06‰ Δ^{199}THg, 1SD, n=9) (Demers et al. 2018) more so than that of streambed sediment (-0.09 ± 0.17‰

δ^{202}THg and -0.05 ± 0.02‰ Δ^{199}THg, 1SD, n=6) (Figure 4.3c-d, Figure 4.5b,d). These observations align with previous studies showing that filter-feeding clams and other bivalves are capable of accumulating iHg from both the dissolved and particulate phases (King and Davies 1987, Inza et al. 1997), and that Asian clams have a preference for feeding on very small organic particles and phytoplankton (Atkinson et al. 2011). At the downstream EFPC site, Asian clams with 16-25% MeHg had slightly higher δ^{202}THg values (-0.20 ± 0.01‰, 1SD, n=2) and slightly lower Δ^{199}THg values (0.01 ± 0.01‰, 1SD, n=2) relative those from upstream sites (Figure 4.3e-f, Figure 4.5e, Table S4.6c). Calculated iHg isotopic compositions of these samples had similar δ^{202}Hg values but even lower Δ^{199}Hg values (-0.06 to -0.05‰ Δ^{199}iHg, n=2) (Figure 4.5c, Table S4.10) due to the influence of MeHg on their THg isotopic compositions. The iHg isotopic composition of downstream EFPC clams closely aligned with the THg isotopic composition of downstream EFPC streambed sediment (-0.13 ± 0.16‰ δ^{202}THg and -0.10 ± 0.01‰ Δ^{199}THg, 1SD, n=6) (Donovan et al. 2014, Crowther et al. 2021) and was dissimilar to the THg isotopic composition of the downstream EFPC surface water dissolved phase (-0.06 ± 0.14‰ δ^{202}THg and 0.07 ± 0.04‰ Δ^{199}THg, 1SD, n=4) (Figure 4.5c). Additionally, these offsets in iHg isotopic composition of Asian clams between upstream and downstream sites were in the same direction as the shifts in δ^{202}THg and Δ^{199}THg values along the flow path for biofilm (0.07 ± 0.12‰ δ^{202}THg and -0.10 ± 0.03‰ Δ^{199}THg, 1SD, n=3 at the downstream site) and suspended particulates (0.08 ± 0.05‰ δ^{202}THg and -0.06 ± 0.05‰ Δ^{199}THg, 1SD, n=4 at the downstream site) (Demers et al. 2018) (Figure S4.3c-f). These shifts in THg isotopic composition of biofilm and suspended particulates along the flow path have been hypothesized to be partially due to physical mixing with fine-grained streambed sediment (Crowther et al. 2021). Altogether, these observations suggest that EFPC Asian clams derive much of their iHg from biofilm and/or

suspended particulates, which themselves likely contain newly released iHg from the Y-12 facility and are influenced by the incorporation of sediment-bound legacy mercury along the flow path. Additionally, it is possible that upstream EFPC clams may obtain a higher proportion of their iHg from the surface water dissolved phase than those from the downstream site, which has been shown to largely contain newly released mercury from the Y-12 facility (Demers et al. 2018). Similar observations have been made previously for a contaminated estuary in which mussels collected from a more contaminated upstream site appeared to accumulate more iHg from the dissolved phase, as evidenced by the high proportion of iHg in the gills relative to the digestive glands, whereas mussels collected from a less contaminated downstream site appeared to accumulate more iHg from the particulate phase (King and Davies 1987). The relative importance of dissolved and particulate-bound iHg sources to Asian clams could be influenced by the higher concentrations of dissolved mercury at upstream EFPC sites, as well as higher ratio of particulate-bound THg concentration (ng L^{-1}) to dissolved THg concentration (ng L^{-1}) at the downstream site (4.6 ± 2.1, 1SD, n=4) relative to the upstream sites (2.9 ± 0.5, 1SD, n=9) (Demers et al. 2018). Additional analysis of mercury concentrations within individual organs would be beneficial for identifying the dominant iHg uptake route for EFPC clams as well as the relative importance of the dissolved and particulate phases as sources of iHg to clams within EFPC.

Megaloptera larvae with 9-17% MeHg collected from the upstream EFPC sites had uniquely low δ^{202}THg values (-0.89 ± 0.09‰, 1SD, n=4) and had Δ^{199}THg which were similar to those of upstream EFPC clams (0.08 ± 0.06‰, 1SD, n=4) (Figure 4.3c-d, Figure 4.5d, Table S4.6b). The calculated iHg isotopic compositions of upstream megaloptera larvae were similar to their THg isotopic compositions (Figure 4.5b, Table S4.10). Crayfish from the upstream EFPC

sites similarly had relatively low calculated δ^{202}iHg values (-0.82 to -0.65‰, n=3) (Figure 4.5b, Table S4.10). The δ^{202}Hg values of iHg within megaloptera larvae and crayfish were much lower than those of previously analyzed EFPC streambed sediment, biofilm, surface water dissolved phase, and suspended particulates (Figure 4.3c,e, Figure 4.5d) (Donovan et al. 2014, Demers et al. 2018, Crowther et al. 2021). These low δ^{202}Hg values are likely reflective of iHg originating from an isotopically unique source, rather than isotope fractionation within the organism's body through excretion. Although there have so far been no studies on internal mercury isotope fractionation within invertebrates (Li et al. 2022), previous studies on marine fish (Kwon et al. 2013) and humans (Sherman and Blum 2013, Sherman et al. 2015) with variable diets have found that lighter mercury isotopes are more readily excreted from the body than heavier isotopes, which would drive the isotopic composition of the organism toward higher δ^{202}THg values, not lower. Isotopically light iHg in EFPC megaloptera larvae and crayfish could partially have originated from vegetation, as uptake of gaseous atmospheric mercury by foliage has been shown to cause kinetic MDF as lighter mercury isotopes are preferentially bound within foliage (Demers et al. 2013). Foliage from EFPC has not been isotopically characterized, but foliage collected from various sites across the contiguous United States (ME, WI, CO, CA, WA) has an average δ^{202}THg value of -2.22 ± 0.22‰ (1SD, n=27) as well as an average Δ^{199}Hg value of -0.28 ± 0.10‰ (1SD, n=27) (Demers et al. 2013, Zheng et al. 2016). These strongly negative values suggest that EFPC megaloptera larvae and crayfish may each derive about one-third and one-fourth of their iHg from foliage, respectively. The rest of their iHg is likely derived from in-stream sources with higher δ^{202}THg and Δ^{199}Hg values, such as biofilm, suspended particulates, and/or the surface water dissolved phase.

Overall, different types of aquatic organisms within East Fork Poplar Creek obtain iHg from multiple isotopically distinct sources. For example, stoneroller minnows appear to obtain a majority of their iHg from streambed sediment. Asian clams appear to obtain much of their iHg from biofilm and/or suspended particulates, and may also obtain a portion of their iHg from the surface water dissolved phase, particularly at upstream sites. Megaloptera larvae and crayfish appear to obtain much of their iHg from in-stream sources such as biofilm, suspended particulates, and/or the surface water dissolved phase, and a smaller portion from foliage that has entered the stream as leaf litter. Most of the iHg within EFPC streambed sediment is legacy mercury derived from historical releases of mercury from the Y-12 facility, though much of the iHg within biofilm, suspended particulates, and the surface water dissolved phase is derived from ongoing releases from Y-12, which mixes with legacy mercury sources along the flow path (Demers et al. 2018). Thus, organisms that obtain most of their iHg from streambed sediment are largely deriving iHg from legacy contamination, while organisms that obtain most of their iHg from biofilm, suspended particulates, and/or the surface water dissolved phase are deriving iHg from a mixture of legacy contamination and ongoing inputs from Y-12.

4.4.3.2 Sources of MeHg to the East Fork Poplar Creek food web

As with Hinds Creek, the range in isotopic composition of MeHg within the East Fork Poplar Creek food web can be characterized using directly measured MeHg isotopic compositions of aquatic organisms, as well as THg isotopic compositions of organisms with high %MeHg. From the highly contaminated upstream EFPC sites (EFK 24.2 to EFK 22.3), biological samples with high %MeHg values (≥90% MeHg) include shiners (n=4), redbreast sunfish (n=2), and rock bass (n=6) (Table S4.2b). These organisms had relatively wide ranges in both δ^{202}THg values (-0.87 to -0.13‰) and Δ^{199}THg values (-0.05 to 0.30‰) (Figure 4.3c-d,

Figure 4.4e, Table S4.6b). Upstream EFPC biological samples directly analyzed for their MeHg isotopic composition include megaloptera larvae (n=2), Asian clams (n=1), crayfish (n=3), shiners (n=2), stoneroller minnows (n=1), and redbreast sunfish (n=2). These organisms had MeHg isotope ratios that were similar in δ^{202}Hg, but slightly narrower in Δ^{199}Hg relative to the range in THg isotopic composition of high %MeHg biological samples (Figure 4.4b, Table S4.8b), largely because MeHg was not extracted from rock bass which had particularly low Δ^{199}THg values. From the highly contaminated downstream EFPC site (EFK 6.3), biological samples with high %MeHg values (≥90% MeHg) include crayfish (n=6), shiners (n=4), stoneroller minnows (n=5), redbreast sunfish (n=3), and rock bass (n=2) (Table S4.2c). These organisms also had relatively wide ranges in both δ^{202}THg values (-0.70 to -0.18‰) and Δ^{199}THg values (0.11 to 0.30‰) (Figure 4.3e-f, Figure 4.4f, Table S4.6c). Downstream EFPC biological samples directly analyzed for their MeHg isotopic composition include mayfly larvae (n=1), snails (n=2), clams (n=2), crayfish (n=2), shiners (n=2), stoneroller minnows (n=2), and redbreast sunfish (n=2). These organisms had MeHg isotope ratios that were similar in δ^{202}Hg and Δ^{199}Hg relative to the range in THg isotopic composition of high %MeHg biological samples (Figure 4.4c, Table S4.8b). From the midstream EFPC sites (EFK 18.2 to EFK 13.8), only rock bass were collected (n=4), which had a relatively wide range in δ^{202}THg values (-1.01 to -0.36‰) and a narrow range in Δ^{199}THg values (0.00 to 0.09‰) (Table S4.6c).

The near-zero Δ^{200}Hg and Δ^{204}Hg values of MeHg within the EFPC food web are consistent with the bioaccumulated MeHg being formed from iHg derived from an industrial source. Across both upstream and downstream EFPC sites, aquatic organisms directly analyzed for their MeHg isotopic composition had average Δ^{200}MeHg and Δ^{204}MeHg values of 0.02 ± 0.01‰ (1SD, n=24) and -0.01 ± 0.02‰ (1SD, n=24), respectively (Figure S4.3c, Table S4.8b).

Similarly, EFPC aquatic organisms with high %MeHg values (≥90% MeHg) had average Δ^{200}THg and Δ^{204}THg values of 0.02 ± 0.02‰ (1SD, n=32) and -0.01 ± 0.03‰ (1SD, n=32), respectively (Table S4.6b-c). These values align with the near-zero Δ^{200}THg and Δ^{204}THg values of streambed sediment (0.01 ± 0.02‰ Δ^{200}THg, 1SD, n=12 and 0.00 ± 0.01‰ Δ^{204}THg, 1SD, n=12) (Donovan et al. 2014, Crowther et al. 2021) collected from upstream (EFK 24.2 to EFK 22.3) and downstream (EFK 8.7 to EFK 5.0) EFPC sites, which contains large amounts of legacy mercury that was historically released from the industrial point-source, Y-12. These values also align with the near-zero Δ^{200}THg and Δ^{204}THg values of biofilm (0.00 ± 0.03‰ Δ^{200}THg, 1SD, n=6 and 0.05 ± 0.05‰ Δ^{204}THg, 1SD, n=6) and suspended particulates (0.01 ± 0.02‰ Δ^{200}THg, 1SD, n=13 and 0.01 ± 0.03‰ Δ^{204}THg, 1SD, n=13) collected at these sites (Demers et al. 2018), which also likely contain a mixture of legacy mercury and newly released mercury from Y-12. Overall, these near-zero Δ^{200}MeHg and Δ^{204}MeHg values for EFPC aquatic organisms, along with their high THg and MeHg concentrations relative to the HC reference site, suggest that much of the MeHg that has bioaccumulated within the EFPC food web was formed from iHg derived from Y-12. This could include sediment-bound and/or remobilized legacy mercury, as well as ongoing releases of dissolved and particulate-bound mercury from Y-12. The δ^{202}MeHg and Δ^{199}MeHg values of EFPC aquatic organisms may be used to differentiate between these potential sources of MeHg to the food web.

Similar to Hinds Creek, the directly measured Δ^{199}MeHg values of EFPC aquatic organisms (0.22 ± 0.08‰, 1SD, n=24) (Figure 4.4b-c, Table S4.8b), as well as the Δ^{199}THg values of organisms with ≥90% MeHg (0.15 ± 0.09‰, 1SD, n=35) (Figure 4.4e-f, Table S4.6b-c), were generally higher than their calculated Δ^{199}iHg values (-0.02 ± 0.07‰, 1SD, n=14) (Figure 4.5b-c, Table S4.10). These MeHg isotopic values were also generally higher than the

Δ^{199}THg values of streambed sediment (-0.08 ± 0.03‰, 1SD, n=12) (Donovan et al. 2014, Crowther et al. 2021), biofilm (-0.06 ± 0.05‰, 1SD, n=6) (Demers et al. 2018), and suspended particulates (-0.01 ± 0.04‰, 1SD, n=13) (Demers et al. 2018) collected from the upstream and downstream EFPC sites (Figure 4.3d,f, Figure 4.4b-c). These MeHg isotopic values did, however, overlap with the slightly elevated Δ^{199}THg values of the surface water dissolved phase at these sites (0.08 ± 0.05‰, 1SD, n=13) (Figure 4.4b-c), which have previously been proposed to reflect the release of dissolved gaseous mercury from biofilm and/or suspended particulates via photochemical reduction of thiol-bound iHg (Demers et al. 2018). However, for this Δ^{199}Hg signature of the dissolved phase to be directly transferred to the accumulated MeHg within organisms, this dissolved iHg would need to be methylated and incorporated into the food web without undergoing significant amounts of photochemical demethylation. Typically, positive offsets in Δ^{199}Hg between MeHg in the food web and iHg in the food web and basal resources are explained by photochemical demethylation (Bergquist and Blum 2007, Chandan et al. 2015, Rose et al. 2015) prior to uptake of MeHg into the food web. However, the Δ^{199}Hg values of MeHg within the food web may also be influenced by photochemical reduction of iHg, either by sulfurless ligands, causing increasing Δ^{199}Hg values (Bergquist and Blum 2007, Rose et al. 2015, Zheng and Hintelmann 2009, 2010a), or by thiol ligands, causing decreasing Δ^{199}Hg values (Zheng and Hintelmann 2010a), prior to the formation of MeHg and uptake into the food web. Photochemical demethylation and photochemical reduction of iHg can be differentiated by their Δ^{199}Hg / Δ^{201}Hg slopes. Using directly measured MeHg isotopic compositions, the Δ^{199}MeHg / Δ^{201}MeHg slope of EFPC aquatic organisms was 1.12 ± 0.04 (1SE, n=24) (Figure S4.3b), which is lower than that of HC organisms. In contrast with HC, this slope value aligns more closely with the characteristic Δ^{199}Hg / Δ^{201}Hg slope of photochemical reduction of iHg (~1.0 to 1.2)

(Bergquist and Blum 2007, Zheng and Hintelmann 2009, 2010a, Rose et al. 2015, Kritee et al. 2018), and differs from that of photochemical demethylation (~1.3) (Bergquist and Blum 2007, Chandan et al. 2015, Rose et al. 2015). However, the Δ^{199}THg / Δ^{201}THg slope of EFPC organisms containing ≥90% MeHg was 1.26 ± 0.11 (1SE, n=35), which better aligns with the Δ^{199}Hg / Δ^{201}Hg slope of photochemical demethylation. This difference between slope values appears to be largely driven by differences in biological sample types represented in each of the regression analyses, suggesting that different slope values may be associated with different types of organisms which obtained MeHg from different combinations of basal resources. To test this, we determined the Δ^{199}THg / Δ^{201}THg slope value for EFPC shiners and stoneroller minnows with ≥90% MeHg separately from EFPC crayfish, redbreast sunfish, and rock bass with ≥90% MeHg. These biological sample types were separated because shiners and stoneroller minnows consistently had higher Δ^{199}THg values, and therefore the MeHg within these organisms may have undergone more photochemical demethylation relative to photochemical reduction in comparison to MeHg within other organism types. The Δ^{199}THg / Δ^{201}THg slope of EFPC shiners and stoneroller minnows with ≥90% MeHg was 1.41 ± 0.35 (1SE, n=13), which aligns more closely with that of photochemical demethylation, and the Δ^{199}THg / Δ^{201}THg slope of EFPC crayfish, redbreast sunfish, and rock bass with ≥90% MeHg was 1.13 ± 0.18 (1SE, n=23), which aligns more closely with that of photochemical reduction of iHg prior to methylation. The steeper slope associated with organisms containing MeHg with higher Δ^{199}Hg values suggests that before being bioaccumulated, the isotopic composition of MeHg within these organisms was more strongly influenced by photochemical demethylation than by photochemical reduction of iHg prior to methylation. In contrast, the shallower slope associated with organisms containing MeHg with lower Δ^{199}Hg values suggests the isotopic composition of MeHg within these

organisms was more strongly influenced by photochemical reduction of iHg prior to methylation than by photochemical demethylation.

The directly measured δ^{202}MeHg values of aquatic organisms from upstream EFPC sites (-0.68 ± 0.20‰, 1SD, n=11) (Figure 4.4b, Table S4.8b), as well as the δ^{202}THg values of organisms with ≥90% MeHg from these sites (-0.64 ± 0.20‰, 1SD, n=12) (Figure 4.4e, Table S4.6b), largely overlapped with their calculated δ^{202}iHg values (-0.65 ± 0.27‰, 1SD, n=7) (Figure 4.5b, Table S4.10) and with the δ^{202}THg values of upstream EFPC organisms with ≤10% MeHg (-0.44 ± 0.17‰, 1SD, n=11) (Figure 4.5d, Table S4.6b). These MeHg isotopic values were, however, generally lower than the δ^{202}THg values of streambed sediment (-0.09 ± 0.17‰, 1SD, n=6) (Donovan et al. 2014, Crowther et al. 2021), biofilm (-0.31 ± 0.09‰, 1SD, n=3) (Demers et al. 2018), suspended particulates (-0.32 ± 0.10‰, 1SD, n=9) (Demers et al. 2018), and the surface water dissolved phase (-0.23 ± 0.17‰, 1SD, n=9) collected from upstream EFPC sites (Figure 4.4b,e). Similarly, the directly measured δ^{202}MeHg values of aquatic organisms from the downstream EFPC site (-0.33 ± 0.15‰, 1SD, n=13) (Figure 4.4c, Table S4.8b) overlapped with their calculated δ^{202}iHg values (-0.21 ± 0.07‰, 1SD, n=7) (Figure 4.5c, Table S4.10), though the δ^{202}THg values of organisms with ≥90% MeHg from this site (-0.48 ± 0.14‰, 1SD, n=20) (Figure 4.4f, Table S4.6c) were slightly lower due to the different distribution of sample types. These MeHg isotopic values overlapped slightly with the δ^{202}THg values of streambed sediment (-0.13 ± 0.16‰, 1SD, n=6) (Donovan et al. 2014, Crowther et al. 2021), but were generally lower than those of biofilm (0.07 ± 0.12‰, 1SD, n=3) (Demers et al. 2018), suspended particulates (0.08 ± 0.05‰, 1SD, n=4) (Demers et al. 2018), and the surface water dissolved phase (-0.06 ± 0.14‰, 1SD, n=4) (Demers et al. 2018) collected from downstream EFPC sites (Figure 4.4c,f). The MeHg isotopic compositions of aquatic organisms were

corrected to account for the isotope fractionation caused by photochemical demethylation, as described in Section 4.4.1.4, using an assumed initial Δ^{199}MeHg value equal to the average Δ^{199}THg value across streambed sediment, biofilm, and suspended particulates for the upstream (-0.01‰) and downstream (-0.09‰) EFPC sites. These corrected δ^{202}MeHg values associated with the upstream (-0.79 ± 0.22‰, 1SD, n=11) and downstream (-0.45 ± 0.16‰, 1SD, n=13) EFPC sites were each slightly lower than their non-corrected values, and were both lower than the δ^{202}Hg values of iHg within the food web and in basal resources at these sites (Figure 4.4b-c, Table S4.10). This negative offset in δ^{202}Hg can be explained by high amounts of microbial methylation (Rodríguez-González et al. 2009) relative to microbial demethylation (Kritee et al. 2009) within the basal resources of EFPC at both upstream and downstream sites. However, it is difficult to differentiate between streambed sediment, biofilm, suspended particulates, and the surface water dissolved phase as potential sources of MeHg to the EFPC food web using δ^{202}Hg values alone. Instead, the relatively wide range in Δ^{199}MeHg values of EFPC aquatic organisms can be used to differentiate between these basal resources as potential sources of MeHg to the food web.

Similar to HC, the relatively wide range in Δ^{199}Hg values of MeHg within the EFPC food web, based on both directly measured Δ^{199}MeHg values of aquatic organisms (Figure 4.4b-c, Table S4.8b) as well as Δ^{199}THg values of high %MeHg organisms (Figure 4.4e-f, Table S4.6b-c), suggests that different types of organisms obtained MeHg from different mixtures of sources containing isotopically distinct MeHg. Differences in Δ^{199}MeHg values between different basal resources within EFPC would likely be the result of differing degrees of photochemical demethylation. As explained in Section 4.4.2.2, materials such as biofilm and suspended particulates may be more susceptible to isotope fractionation via photochemical

demethylation than MeHg within streambed sediment, which would result in higher Δ^{199}MeHg values within biofilm and suspended particulates (Bergquist and Blum 2007, Chandan et al. 2015, Rose et al. 2015). While the MeHg isotopic compositions of EFPC basal resources were not measured in this study, it is possible that EFPC suspended particulates and biofilm have higher Δ^{199}MeHg values than streambed sediment due to increased photochemical demethylation and smaller MeHg pool sizes. If this is true, then lower trophic level consumers from EFPC with relatively high Δ^{199}MeHg values may have obtained a majority of their MeHg from consuming suspended particulates and/or biofilm, which would then be passed to higher trophic level consumers, maintaining its isotopic composition as it biomagnifies. This could explain the relatively high Δ^{199}MeHg values of EFPC snails, clams, mayfly larvae, megaloptera larvae (one of the two samples), stoneroller minnows, and shiners (Figure 4.4b-c, Table S4.8b), as well as the relatively high Δ^{199}THg values of stoneroller minnows and shiners containing ~100% MeHg (Figure 4.3d,f, Figure 4.4e-f, Table S4.6b-c). Other lower trophic level consumers from EFPC may have obtained a portion of their MeHg from suspended particulates and/or biofilm and another portion from streambed sediment, resulting in lower Δ^{199}MeHg values due to mixing of sources, which are maintained as the MeHg is passed to higher trophic level consumers. This could explain the relatively low Δ^{199}MeHg values of megaloptera larvae (one of two samples), crayfish, and redbreast sunfish (Figure 4.4b-c, Table S4.8b), as well as the relatively low Δ^{199}THg values of crayfish, redbreast sunfish, and rock bass containing ~100% MeHg (Figure 4.3d,f, Figure 4.4e-f, Table S4.6b-c). Further evidence for multiple MeHg sources to the EFPC food web is provided by the previously mentioned Δ^{199}THg / Δ^{201}THg slope values associated with high trophic level organisms with higher Δ^{199}THg values (1.41 ± 0.35, 1SE, n=13) and those with lower Δ^{199}THg values (1.13 ± 0.18, 1SE, n=23). These different slope values further

support the idea that EFPC organisms with higher Δ^{199}MeHg values likely obtained a majority of their MeHg from biofilm and/or suspended particulates which had undergone a relatively large amount of photochemical demethylation, while organisms with lower Δ^{199}MeHg values likely obtained a portion of their MeHg from streambed sediment which had not undergone much photochemical demethylation. Aquatic organisms across all trophic levels may also obtain a portion of their MeHg directly from the surface water dissolved phase, which could potentially have elevated Δ^{199}MeHg values due to photochemical demethylation within the water column. Elevated Δ^{199}MeHg values of EFPC organisms may be partially explained by uptake of MeHg from the surface water, though, as explained in Section 4.4.2.2, this would only be a minor source of MeHg to the food web.

Overall, similar to the Hinds Creek food web, different types of aquatic organisms within East Fork Poplar Creek appear to obtain MeHg from different basal resources, which likely have distinct MeHg isotopic compositions due to higher amounts of photochemical demethylation in biofilm and suspended particulates relative to streambed sediment, resulting in higher Δ^{199}MeHg values. As mentioned in Section 4.4.2.2, if high and low Δ^{199}MeHg values of organisms are reflective of different proportions of their MeHg being obtained from different basal resources, then we may expect these Δ^{199}MeHg values to correlate with the δ^{13}C values of the organisms. However, these values are not correlated for EFPC aquatic organisms (Figure S4.8c-d), suggesting that the primary sources of MeHg to the organisms are not necessarily the same as their primary carbon source. For the upstream site, while the iHg isotopic composition of megaloptera larvae and crayfish appeared to have been influenced by the contribution of iHg from foliage, this was not observed for the MeHg isotopic compositions of these organisms. The directly measured δ^{202}MeHg values of megaloptera larvae, crayfish, clams, and stoneroller

minnows were all similar to one another, despite the wide range in calculated δ^{202}iHg values between these organism types. This suggests that iHg and MeHg within a particular organism may be derived from different combinations of sources, as iHg within megaloptera larvae and crayfish appears to have been partially obtained from foliage, while MeHg within these organisms does not. Additionally, in contrast with HC, photochemical demethylation-corrected δ^{202}Hg values of MeHg within the EFPC food web were consistently lower than the δ^{202}THg values of both streambed sediment and biofilm, suggesting that isotope fractionation induced by microbial methylation is dominant over that induced by microbial demethylation within EFPC basal resources.

4.4.4 Broader picture: Mercury cycling in natural background vs. point source contaminated waterbodies

4.4.4.1 Comparison of mercury biogeochemical cycling within Hinds Creek and East Fork Poplar Creek

This study, along with previous studies of mercury isotope ratios in environmental samples from Hinds Creek and East Fork Poplar Creek (Donovan et al. 2014, Demers et al. 2018, Crowther et al. 2021), has revealed both similarities and differences in the biogeochemical cycling of mercury within the two streams. Inorganic mercury within HC basal resources is largely derived from atmospheric sources, including precipitation and gaseous atmospheric mercury, which is taken up by foliage and deposited into the stream via leaf litter. In contrast, iHg within EFPC basal resources is predominantly derived from large historical releases and smaller ongoing releases of mercury from an industrial point source (Brooks and Southworth 2011). Despite this major difference in mercury sources to the two streams, iHg within both HC and EFPC has undergone similar biogeochemical reactions, which have influenced the THg

isotopic composition of basal resources. For HC, a portion of the iHg within streambed sediment and biofilm has likely undergone photochemical reduction by thiol ligands, based on the low Δ^{199}THg values of both of these basal resources, and a portion of the iHg within biofilm has likely additionally undergone microbial reduction, based on the positive offset in δ^{202}THg values between biofilm and streambed sediment. Similarly, for EFPC, a portion of the iHg within suspended particulates and biofilm may have undergone both photochemical reduction by thiol ligands and microbial reduction, based on the shift in isotopic composition of these basal resources toward higher δ^{202}THg and slightly lower Δ^{199}THg values along the flow path, as well as the transient increases in Δ^{199}THg values of the surface water dissolved phase along the flow path (Demers et al. 2018). While photochemical and microbial reduction reactions may be occurring within both HC and EFPC, these reactions are much less likely to influence THg concentrations of basal resources from EFPC than those from HC due to the large amount of mercury stored within the EFPC streambed and floodplain.

In addition to similarities in biogeochemical transformations of iHg within HC and EFPC, the basal resources that contribute iHg to the HC and EFPC food webs also have similarities, though relatively high %MeHg values for lower trophic level organisms from HC limited our assessment of the sources of iHg to the HC food web. For HC, streambed sediment appears to be a more dominant source of iHg to the food web than biofilm, based on the approximately matching δ^{202}Hg values of THg in sediment and of iHg within the food web. However, this does not exclude other potential sources of iHg to the food web, such as suspended particulates or foliage, since THg isotopic analyses were not performed on HC suspended particulates nor on HC biological samples with ≤10% MeHg, and since iHg isotopic compositions could only be calculated for three biological samples. In particular, iHg isotopic

compositions could not be calculated for HC megaloptera larvae, which for upstream EFPC were isotopically distinct from other organism types. For EFPC, streambed sediment and suspended particulates appear to be dominant sources of iHg to the food web, and foliage could be an additional source of iHg to certain types of organisms, including megaloptera larvae and crayfish. This was somewhat surprising, as mercury in foliage is largely derived from atmospheric gaseous mercury. However, a portion of this mercury may have been sourced from gaseous mercury released via photochemical and microbial reduction reactions occurring within the stream, which may represent a mechanism by which iHg is removed and subsequently re-deposited into the stream. Overall, while only the upstream EFPC food web was found to contain multiple distinct iHg isotopic compositions (in part because of the particular biological sample types collected from each site and their %MeHg values), it is likely that different types of aquatic organisms in both HC and EFPC obtain iHg from different combinations of basal resources.

For both HC and EFPC, relatively small proportions of the iHg within various basal resources is converted into MeHg via microbial methylation, after which it may be partially degraded by photochemical and/or microbial demethylation reactions before being bioaccumulated in the food web. Photochemcial demethylation appears to be an important reaction within both HC and EFPC basal resources, based on the elevated Δ^{199}MeHg values of aquatic organisms relative to the Δ^{199}THg values of basal resources. Additionally, it is likely that for both streams, MeHg within shallow streambed surface biofilm and suspended particulates likely undergoes a higher degree of photochemical demethylation than MeHg within streambed sediment, which would result in contrasting Δ^{199}MeHg values among different basal resources within each of the streams. This phenomenon appears to be reflected in the relatively wide ranges in Δ^{199}MeHg values of aquatic organisms collected from both HC and EFPC, as some

types of organisms may have obtained a majority of their MeHg from biofilm and/or suspended particulates while others may have obtained a larger proportion of their MeHg from streambed sediment. Although photochemical demethylation within biofilm and suspended particulates appears to be common to both HC and EFPC, the relative amount of microbial methylation and microbial demethylation within basal resources differs between the two streams. For the HC reference site, isotope fractionation resulting from microbial methylation and microbial demethylation appear to occur in roughly equal proportions, based on the similarity between the photochemical demethylation-corrected δ^{202}MeHg values of aquatic organisms and the δ^{202}THg values of biofilm from HC. In contrast, for the highly contaminated EFPC sites, isotope fractionation induced by microbial methylation appears to outweigh that of microbial demethylation at both the upstream and downstream sites, based on the consistently negative offsets between the photochemical demethylation-corrected δ^{202}MeHg values of aquatic organisms and the δ^{202}THg values of streambed sediment, biofilm, and suspended particulates from EFPC. Greater net MeHg production provides a mechanism for maintaining relatively higher MeHg concentrations in EFPC biofilm, surface water, and the food web.

4.4.4.2 Comparison of mercury biogeochemical cycling within other natural background and point source contaminated waterbodies

Measurements of mercury stable isotope ratios in aquatic organisms and basal resources have been used in several previous studies to identify sources of MeHg to aquatic food webs and to understand mercury biogeochemical cycling within a number of different freshwater streams and lakes. Some of these studies have been done on natural background streams and lakes, in which the sediment and other basal resources contain low THg concentrations (less than ~100 ng g^{-1}), while others have been done on point source contaminated waterbodies with high

mercury concentrations. Comparisons of these studies show both similarities and differences in the types of biogeochemical reactions and extent of processing undergone by MeHg in natural background and point source contaminated waterbodies. These comparisons also reveal general trends in whether MeHg in an aquatic food web tends to be derived from one or multiple sources, which may in part relate to the type of waterbody and/or level of contamination, among other factors.

As commonly suggested by previous studies involving measurements of THg isotopic composition of aquatic organisms, photochemical demethylation is an important reaction in both natural background and point source contaminated freshwater streams and lakes, based on elevated Δ^{199}THg values of fish and other high %MeHg aquatic organisms relative to sediment and other basal resources. This interpretation is supported by several examples of Δ^{199}THg/Δ^{201}THg slopes between 1.22 and 1.37 for aquatic organisms from several natural background sites (Tsui et al. 2012, Kwon et al. 2014, Kwon et al. 2015, Li et al. 2016, Xu et al. 2016, Laffont et al. 2021) and point source contaminated waterbodies (Gehrke et al. 2011, Donovan et al. 2016, Feng et al. 2019, Madenjian et al. 2019, Pribil et al. 2020, Rosera et al. 2022), including the two streams in our study. A smaller number of studies have reported lower Δ^{199}THg/Δ^{201}THg slopes between 0.84 and 1.18 for freshwater fish from natural background (Janssen et al. 2019) and point source contaminated (Laffont et al. 2021) waterbodies, suggesting that for these sites, the isotopic composition of the accumulated MeHg had been more strongly influenced by photochemical reduction of iHg prior to methylation. Overall, photochemical demethylation is likely nearly ubiquitous across both natural background and point source contaminated waterbodies, though sometimes, isotope fractionation resulting from

photochemical reduction of iHg can outweigh that resulting from subsequent photochemical demethylation.

In contrast with the consistent occurrence of photochemical demethylation across waterbodies containing both low and high mercury concentrations, the relative importance of microbial demethylation relative to microbial methylation within basal resources appears to be at least partially related to levels of mercury contamination within sediment and other basal resources. In several previous studies, photochemical demethylation-corrected δ^{202}Hg values of MeHg within an aquatic food web were found to be similar to or higher than the δ^{202}THg values of sediment and other basal resources. This applied to many different natural background sites, including Hinds Creek, with sediment THg concentrations of less than ~100 ng g^{-1} (Tsui et al. 2012, Sherman and Blum 2013, Kwon et al. 2014, Kwon et al. 2015, Li et al. 2016, Xu et al. 2016, Janssen et al. 2019, Laffont et al. 2021), as well as several point source contaminated sites with sediment THg concentrations of ~100 to 1000 ng g^{-1} (Sherman and Blum 2013, Kwon et al. 2014, Gehrke et al. 2011, Janssen et al. 2019, Madenjian et al. 2019, Laffont et al. 2021, Rosera et al. 2022). Additionally, in a study involving THg isotopic measurements of sediment and various types of fish across 23 streams in the northeastern United States, 78% of the 69 fish samples had photochemical demethylation-corrected δ^{202}THg values that were higher than the δ^{202}THg values of co-located sediment (Janssen et al. 2019). In that study, consistent negative offsets were only observed at three of the 23 streams, each of which were natural background sites, and positive offsets tended to be of higher magnitude than negative offsets (Janssen et al. 2019). Positive offsets in δ^{202}THg observed across many different waterbodies suggest that isotope fractionation resulting from microbial demethylation usually outweighs that resulting from microbial methylation within basal resources, prior to uptake of MeHg into the food web.

For studies on more highly contaminated waterbodies with sediment THg concentrations of greater than ~1000 ng g^{-1}, including East Fork Poplar Creek, photochemical demethylation-corrected δ^{202}Hg values of MeHg within the aquatic food web tended to be lower than the δ^{202}THg values of sediment and other basal resources (Donovan et al. 2016, Feng et al. 2019, Pribil et al. 2020). Such negative offsets were observed during two separate sampling campaigns in a study on the aquatic food web of the Yuba River downstream of a historical gold mining region in California, USA (Donovan et al. 2016), as well as in a study on fish in the Sagua la Grande River in Cuba downstream from a chlor-alkali plant (Feng et al. 2019). These offsets were proposed to have been due to low levels of microbial demethylation relative to microbial methylation within streambed sediment and/or algae, possibly due to the continuous transport of MeHg downstream, preventing pools of MeHg from being sufficiently demethylated in comparison to non-flowing waterbodies (Donovan et al. 2016, Feng et al. 2019). However, this was not observed for various other rivers with lower mercury concentrations (Tsui et al. 2012, Li et al. 2016, Laffont et al. 2021, Rosera et al. 2022), and so lower levels of microbial demethylation may instead be more strongly related to the effect of high mercury concentrations on microbial activity rather than physical transport of MeHg. It was noted for the Yuba River, however, that bioaccumulation of MeHg derived from an external iHg source with low δ^{202}THg values, such as soil or foliage, could not be ruled out (Donovan et al. 2016). This suggests that the observed negative offsets in δ^{202}THg between high %MeHg organisms and sediment could potentially be explained by mixing of multiple MeHg sources with distinct δ^{202}Hg values, and not necessarily by a dominance of microbial methylation, though it is difficult to distinguish between these two scenarios without knowing the isotopic composition of MeHg within various basal resources. In another study on the highly contaminated Paglia River in Italy, fish and

streambed sediment just downstream of a historical mercury mine had overlapping δ^{202}THg values, but further downstream, fish had lower δ^{202}THg values, which were negatively offset from those of sediment (Pribil et al. 2020). In this case, these negative offsets further downstream were proposed to have been explained by contributions of MeHg derived from soil and/or geothermal waters with low δ^{202}THg values (Pribil et al. 2020), rather than by relatively low levels of microbial demethylation. Comparisons across each of these studies demonstrate that negative offsets between photochemical demethylation-corrected δ^{202}Hg values of MeHg within an aquatic food web and δ^{202}THg values of sediment and other basal resources appear to be largely unique to highly contaminated waterbodies with sediment THg concentrations of greater than ~1000 ng g^{-1}. The results of our study on the aquatic food webs of Hinds Creek and East Fork Poplar Creek follow this trend, which we attribute to differing amounts of microbial methylation and microbial demethylation between the two streams, which is likely influenced by the level of mercury contamination in the watershed.

4.4.4.3 Organisms within an aquatic food web may obtain MeHg from either a single or multiple sources

In addition to identifying trends in biogeochemical reactions as they relate to levels of contamination, comparisons of studies involving THg isotopic measurements of aquatic organisms and basal resources can also demonstrate whether different types of aquatic organisms in natural background and point source contaminated waterbodies tend to derive MeHg from the same source or from multiple isotopically distinct sources. Among previous studies on natural background sites, some found that aquatic organisms appear to have obtained a majority of their MeHg from a single source or single combination of sources, resulting in a narrow range of MeHg isotopic compositions within the food web. For example, in studies on the aquatic food

webs of the upper South Fork Eel River in California, USA (Tsui et al. 2012), Douglas Lake in Michigan, USA (Kwon et al. 2015), and Nam Co Lake and Yamdork Lake in Tibet, China (Xu et al. 2016), linear relationships between THg isotope ratios and %MeHg of various types of fish, invertebrates, and basal resources were observed. These observations suggest that various types of aquatic organisms within each of the waterbodies obtained MeHg from a common source with a distinct and consistent MeHg isotopic composition.

In other studies on natural background sites, however, relatively wide ranges in THg isotopic composition of fish containing high %MeHg have been observed. This could be the result of differing types and/or degrees of biogeochemical reactions between different basal resources, as was proposed for Hinds Creek, or alternatively could be the result of variable degrees of biogeochemical reactions within a particular basal resource. For example, fish collected from the lower Churchill River in Manitoba, Canada had a relatively wide range in Δ^{199}THg values, suggesting that different fish samples (both within and across species) had obtained MeHg that had undergone variable degrees of photochemical demethylation (Li et al. 2016). In that study, the isotopically variable freshwater fish were proposed to have obtained MeHg from a common source that was sensitive to differing degrees of photochemical demethylation, likely as a function of variable levels of turbidity, water depth, and/or canopy cover in different areas surrounding the sampling site (Li et al. 2016). This was supported by the within-species variability in fish THg isotopic composition, as well as the overlapping THg isotopic compositions among each of the different fish species. Other examples can be found in a study involving THg isotopic measurements of sediment and various types of fish across 23 streams in the northeastern United States (Janssen et al. 2019). In that study, fish from many of the streams had relatively narrow within-stream ranges in photochemical demethylation-

corrected δ^{202}THg values, suggesting a single MeHg source. However, fish from a few of the streams had relatively wide ranges, including the Saxtons River in Vermont, Ley Creek in New York, and Allen Creek in New York (Janssen et al. 2019). In addition to having wide ranges, the photochemical demethylation-corrected δ^{202}THg values of fish from each of these three streams extended both above and below the δ^{202}THg values of streambed sediment at each site. This suggests that different fish within each of these three streams may have obtained MeHg from different combinations of basal resources with distinct MeHg isotopic compositions. Overall, based on these studies, it appears that for freshwater streams and lakes containing natural background mercury concentrations, various types of aquatic organisms often obtain their MeHg from a single source with a consistent MeHg isotopic composition. Sometimes, though, different organisms within a food web may accumulate MeHg with variable isotopic compositions, either due to consumption of different basal resources, or due to consumption of a single basal resource that is sensitive to differing degrees of biogeochemical reactions.

Similar types of studies involving THg isotopic measurements of various types of aquatic organisms and basal resources have also been done for point source contaminated waterbodies with high sediment THg concentrations (greater than ~100 ng g^{-1}). As with the natural background sites, these studies suggest that various aquatic organisms in some contaminated waterbodies obtain MeHg from a single source or single combination of sources, while those in other contaminated waterbodies obtain MeHg from multiple isotopically distinct sources. For example, in a study on the aquatic food web of the Yuba River downstream of a historical gold mining region in California, USA, linear relationships between THg isotope ratios and %MeHg of various types of fish, invertebrates, and algae were observed for each of the sampling campaigns (Donovan et al. 2016). These observations suggest that various types of aquatic

organisms within this river likely obtained MeHg from a common source. Additionally, in a study involving THg isotopic measurements of sediment and two types of fish in the San Francisco Bay in California, which became contaminated largely through historical mercury and gold mining, spatial shifts in δ^{202}THg values of fish were observed throughout the bay, which closely correlated with δ^{202}THg values of sediment (Gehrke et al. 2011). This suggested that sediment was the primary source of MeHg to the food web, but that the source signature shifted spatially.

In contrast, evidence of multiple isotopically distinct sources of MeHg to the aquatic food web of a point source contaminated waterbody can be found in another study involving THg isotopic measurements of sediment, mussels, crabs, and fish across five estuaries on the northeastern coast of the United States (three natural background, two contaminated) (Kwon et al. 2014). In that study, most of the aquatic organisms across all five sites were proposed to have obtained a majority of their MeHg from sediment, based on generally linear relationships between THg isotopic composition and %MeHg, with the exception of mussels from Bold Point in Rhode Island, USA, which had anomalously high δ^{202}THg values. The isotopic composition of MeHg within mussels from this industrially contaminated site was proposed to have been either shifted by microbial demethylation within suspended sediment, or influenced by mixing with an external MeHg source (Kwon et al. 2014). Another example of isotopically variable MeHg being accumulated into different organisms within a contaminated waterbody is found in a study on fish from Green Bay in Wisconsin, USA, which was largely contaminated by several paper mills along the Fox River, the major tributary of the bay. In that study, adult walleye had a wide range in Δ^{199}THg values, which was proposed to have been due to variable spatial ranges of where individual fish lived in the bay, with Δ^{199}Hg values of MeHg likely increasing with distance

away from the mouth of the Fox River due to increased amounts of photochemical demethylation with higher water clarity (Madenjian et al. 2019). In this case, the within-species variability in fish THg isotopic composition did not appear to be driven by uptake of MeHg from different basal resources, but rather were likely driven by spatially variable degrees of photochemical demethylation occurring within a basal resource. However, in another study of fish in a contaminated waterbody, a wide range in Δ^{199}THg values was again observed, but was explained by differences in diet between different types of fish. In that study on the Oyapock River in French Guiana, which became contaminated with mercury through small-scale gold mining activities, periphytophagous fish consistently had slightly higher Δ^{199}THg values than piscivorous fish (Laffont et al. 2021). Periphytophagous fish primarily consume biofilm, which may contain MeHg with elevated Δ^{199}Hg values due to enhanced photochemical demethylation, while piscivorous fish consume a variety of smaller prey fish and may obtain MeHg from multiple isotopically distinct sources, potentially resulting in lower Δ^{199}THg values (Laffont et al. 2021). Ultimately, whether aquatic organisms within a contaminated waterbody accumulate MeHg from multiple isotopically unique sources appears to be site specific. These studies also highlight the idea that isotopically variable MeHg within different aquatic organisms may either have originated from different basal resources, or may be due to variable degrees of photochemical reactions within a basal resource. This second explanation is more likely to be the case for a larger waterbody with spatially variable levels of water clarity, rather than a particular reach of a stream, such as our sampling sites in East Fork Poplar Creek.

Overall, this study and previous studies involving measurements of THg isotope ratios in aquatic organisms and basal resources reveal both similarities and differences in biogeochemical processing of MeHg within natural background and point source contaminated sites.

Photochemical demethylation is likely ubiquitous across waterbodies containing both low and high concentrations of mercury. Microbial demethylation is also typically an important reaction within freshwater ecosystems containing a wide range of mercury concentrations, though for sites with sediment THg concentrations of greater than ~1000 ng g^{-1}, isotope fractionation induced by microbial methylation is more likely to be dominant over that induced by microbial demethylation. Previous studies have shown inconsistent results with regard to whether organisms in an aquatic food web are likely to accumulate MeHg from a common source or from multiple different sources. This appears to be site-specific for both natural background and point source contaminated waterbodies.

4.5 Conclusions and Implications

In this study, we measured THg and MeHg concentrations and isotopic compositions of several types of fish and aquatic invertebrates collected from upstream and downstream sites within an industrial point source impacted stream (EFPC), and from a regional reference stream (HC). The δ^{202}Hg and Δ^{199}Hg values of iHg and MeHg within HC organisms were generally lower than the those of iHg and MeHg within EFPC organisms, suggesting that aquatic organisms within each of the streams obtained mercury from different sources. Additionally, within-site variability in iHg and MeHg isotopic compositions of organisms suggests that different types of organisms within an individual site may obtain iHg and/or MeHg from different basal resources. These differences point toward a decoupling of iHg and MeHg biogeochemical cycling within an aquatic ecosystem. Both iHg and MeHg within HC aquatic organisms was ultimately derived from a mixture of precipitation and dry deposition, though these forms of mercury appeared to have been taken up into the food web through different basal resources. The organisms of this stream appeared to have obtained iHg primarily from streambed

sediment, and MeHg largely from biofilm and/or suspended particulates, along with smaller contributions of MeHg from streambed sediment to certain types of organisms such as redbreast sunfish. In contrast, most of the iHg and MeHg within EFPC aquatic organisms was ultimately derived from mercury released from an upstream industrial point source, including both legacy mercury contamination which dominates the streambed sediment as well as recent releases of mercury which is present in higher proportions in biofilm, suspended particulates, and the surface water dissolved phase (Demers et al. 2018). Unlike the HC food web, which largely seems to take up iHg from a single basal resource (streambed sediment), different types of organisms within the EFPC food web appear to have taken up iHg from different combinations of basal resources according to the feeding and living habits of different types of organisms. Additionally, similar to the HC food web, several types of organisms within EFPC appear to have obtained MeHg from biofilm and/or suspended particulates, but some, such as crayfish, redbreast sunfish, and rock bass, appear to have obtained a portion of their MeHg from streambed sediment. Some types of organisms within EFPC appear to have taken up iHg and MeHg from a common source, while others appear to have taken up iHg and MeHg from different sources or combinations of sources. For example, EFPC clams seem to have taken up both iHg and MeHg from biofilm and/or suspended particulates. Megaloptera larvae and crayfish, however, appear to have obtained a portion of their iHg from foliage, based on their low δ^{202}iHg values relative to basal resources and other organism types, but this was not the case for MeHg within these organisms. Overall, these results demonstrate that aquatic organisms may obtain iHg and MeHg from multiple sources, not only between point source impacted and regional reference streams, but within sampling sites as well.

Isotopic compositions of MeHg within aquatic organisms from HC and EFPC additionally demonstrate both similarities and differences in biogeochemical processing of mercury between the two streams. Photochemical demethylation was ubiquitous across the HC, upstream EFPC, and downstream EFPC sites, and likely influenced the isotopic composition of MeHg within biofilm and suspended particulates more so than MeHg within streambed sediment. Microbial demethylation, however, seemed to be a more important process within HC basal resources than within EFPC basal resources, which is likely related to the large difference in sediment THg concentrations between the two streams. Additionally, the general increase in δ^{202}MeHg values of organisms between the upstream and downstream EFPC sites is similar to the previously observed increasing δ^{202}THg values of biofilm and suspended particulates along the flow path of EFPC (Demers et al. 2018). Each of these shifts in isotopic composition are likely due to mixing between newly released mercury from Y-12 and legacy mercury in fine grained sediment along the flow path (Demers et al. 2018, Crowther et al. 2021), though they could each also be due to microbial reduction of iHg along the flow path (Demers et al. 2018). A third potential explanation for the difference in δ^{202}MeHg values of organisms between upstream and downstream sites involves a higher degree of microbial methylation relative to microbial demethylation at the upstream EFPC sites compared to the downstream site. However, because much of the MeHg within EFPC organisms seems to be derived from biofilm and/or suspended particulates, it is likely that the processes influencing the shift in THg isotopic composition of these materials along the flow path is also at least partially responsible for the shift in MeHg isotopic composition of aquatic organisms between the upstream and downstream sites.

Compound specific isotopic analysis of aquatic organisms in this study was beneficial for multiple reasons. First, using THg isotopic measurements alone, only the MeHg isotopic

compositions of organisms containing high %MeHg, including fish and in some cases crayfish, could be approximated with confidence. Direct MeHg isotopic measurements allowed for the determination of the isotopic composition of MeHg within lower trophic level organisms, including mayfly larvae, snails, and clams. These MeHg isotopic compositions could not have been confidently estimated using a linear regression approach (Kwon et al. 2015) due to the nonlinear relationships between THg isotope ratios and %MeHg of aquatic organisms at each of the sampling sites (Figure 4.3a-f). These values also could not be confidently estimated using a mass balance approach (Tsui et al. 2012) due to either containing <25% MeHg or due to the presence of multiple isotopically distinct sources of iHg to the food web within a sampling site. Inaccurate estimates of MeHg isotopic composition of organisms containing ~25-60% MeHg using a mass balance approach can be visualized in Figure S4.7a-b, in which the estimated δ^{202}MeHg values of multiple biological samples across each of the sampling sites were artificially low compared to direct measurements. In fact, direct measurements of MeHg isotopic compositions of snails and clams revealed higher δ^{202}MeHg values within the HC food web (Figure 4.4a) than would have been estimated via linear regression based on THg isotopic measurements alone (Figure 4.3a). This finding was important, as it demonstrated that the δ^{202}Hg values of MeHg within the HC food web overlapped with the δ^{202}THg values of both streambed sediment and biofilm, not just sediment (Figure 4.4a,d). That being said, it is also beneficial to rely on both MeHg and THg isotopic measurements to understand the full range in MeHg isotopic compositions within a food web. Compound-specific isotopic analysis requires more time, effort, and resources than THg isotopic analysis, as well as a larger sample mass, which is why in this study, only a subset of fish and aquatic invertebrate samples were analyzed for their MeHg isotopic analysis, and not all biological sample types were represented. For upstream

EFPC, direct measurements of MeHg isotopic composition of a subset of fish and aquatic invertebrate samples resulted in a narrower range in Δ^{199}MeHg values (Figure 4.4b) than was determined by THg isotopic analysis of various types of fish with high %MeHg (Figure 4.4e), due to the lack of representation of rock bass with particularly low Δ^{199}THg values.

Overall, compound specific MeHg isotopic analysis of biological samples is especially beneficial for determining the isotopic composition of MeHg within lower trophic level organisms when linear regression and mass balance approaches are not viable, while THg isotopic analysis of additional high %MeHg organisms increases the likelihood that the full range in MeHg isotopic composition within the food web is represented. Another benefit to measuring both the THg and MeHg isotopic compositions of biological samples is that for organisms containing <85% MeHg, these values can be used together to calculate the iHg isotopic composition of the sample. As was done in this study, these calculated iHg isotopic compositions, as well as THg isotopic compositions of low %MeHg organisms, can be used to identify sources of iHg to a food web. Ultimately, measurements of both THg and MeHg isotopic compositions of various types of fish and aquatic invertebrates containing a wide range of %MeHg values can be useful, and is sometimes necessary, for identifying sources of mercury to a food web, as well as for investigating the biogeochemical processing of mercury prior to bioaccumulation in organisms.

Acknowledgements

We would like to thank Teresa Mathews, senior scientist and group leader of the Biodiversity and Ecosystem Health Group within the Environmental Sciences Division at Oak Ridge National Laboratory for helping facilitate our collection of aquatic invertebrates from Hinds Creek and East Fork Poplar Creek, and for supplying the fish tissue samples used in this

study. Patrick Donovan, Spencer Washburn, and Aaron Kurz also provided valuable assistance with the collection of benthic invertebrates used in this study. Renee Veresh provided invaluable help processing invertebrate samples, and Hanna von Bernthal assisted with sample preparation for total mercury isotopic analysis. We would also like to thank Paul Drevnick for the use of the Brooks Rand automated MERX MeHg analyzer, and Marcus Johnson for his assistance in operating the CV-MC-ICP-MS. Thank you also to Colin Carney for performing the carbon and nitrogen stable isotope analyses for this study.

This research was supported by the U.S. Department of Energy (DOE), Office of Science, Biological and Environmental Research (BER), Subsurface Biogeochemical Research (SBR) program under Award No. DE-SC0016489 and is also a product of the Critical Interfaces Science Focus Area (SFA) at Oak Ridge National Laboratory (ORNL). ORNL is managed by UT-Battelle, LLC for the DOE under Contract No. DE-AC05-00OR22725. Additional funding was provided by the Geological Society of America Graduate Student Research Grant (2019), the University of Michigan (UM) Rackham Graduate Student Research Grant (2019), the UM Scott Turner Award (2020 and 2021), the Anchor QEA Scholarship (2021), and the John D. MacArthur Professorship.

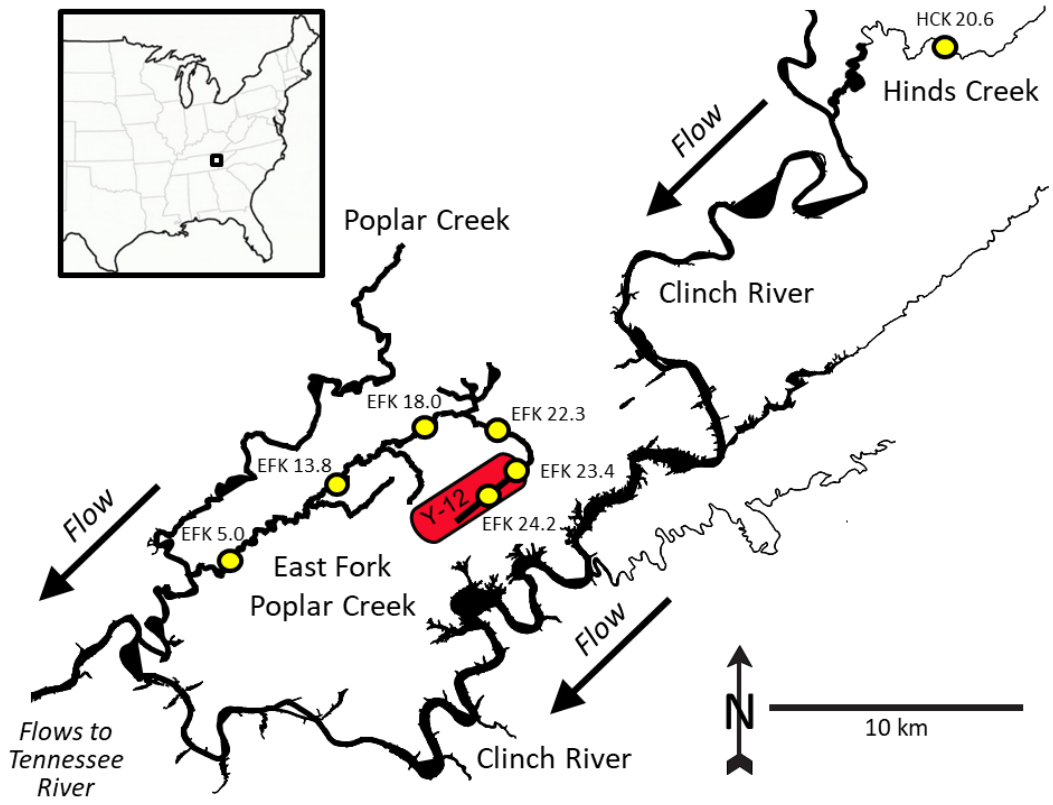

Figure 4.1. Map of Hinds Creek, East Fork Poplar Creek (EFPC), Poplar Creek, and the Clinch River in eastern Tennessee, USA.

Highlighted are the Y-12 National Security Complex (red oval) and seven aquatic organism sampling sites within Hinds Creek (HCK 20.6), upstream EFPC (EFK 24.2, EFK 23.4, and EFK 22.3), midstream EFPC (EFK 18.0 and EFK 13.8), and downstream EFPC (EFK 5.0) (yellow circles).

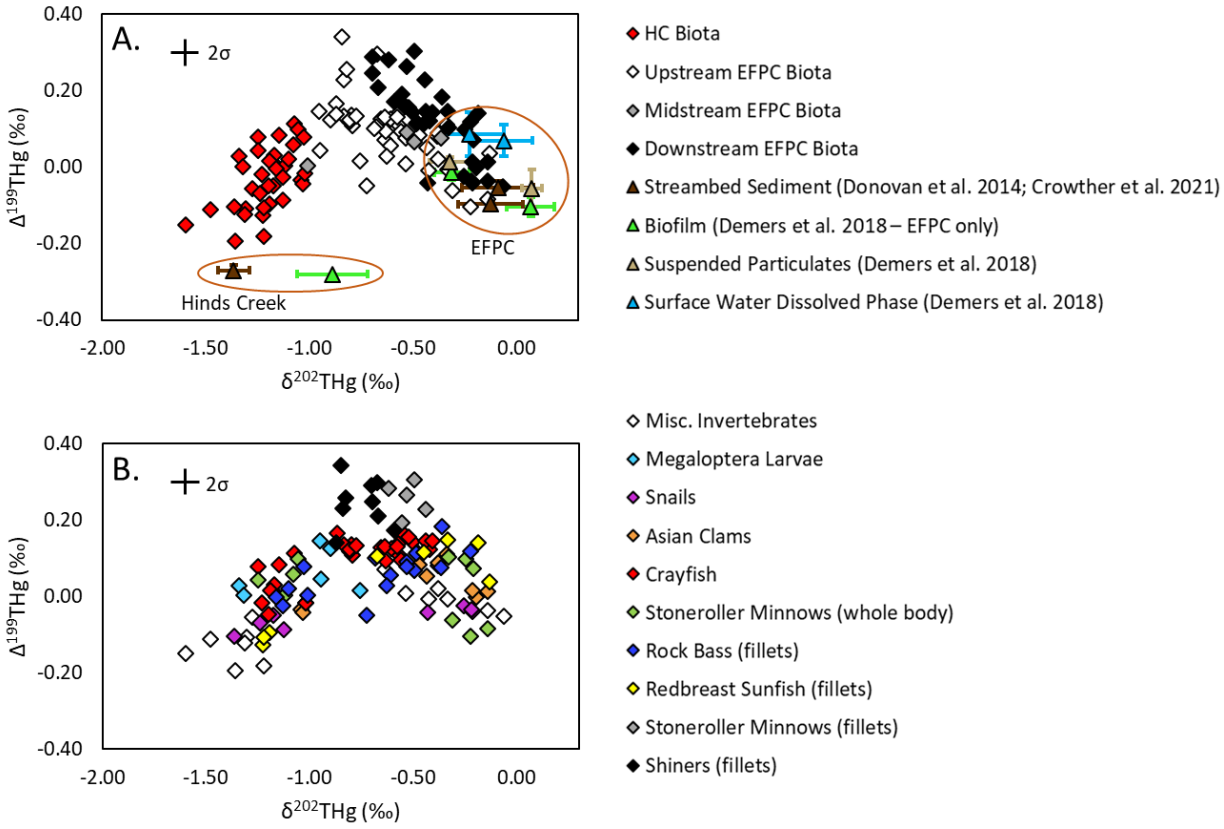

Figure 4.2. THg isotopic composition of HC and EFPC biological samples (diamonds), measured via combustion, grouped by (A) sampling site and (B) biological sample type.

Also shown are average THg isotopic compositions of streambed sediment and biofilm from HC, and streambed sediment, biofilm, suspended particulates, and surface water dissolved phase from upstream (EFK 24.2 to EFK 22.3) and downstream (EFK 8.7 to EFK 5.0) EFPC sites (triangles), with error bars representing variability (1SD) (Donovan et al. 2014; Demers et al. 2018; Crowther et al. 2021). Symbols for HC and EFPC basal resources are differentiated by brown ovals. Analytical uncertainty in delta values for biological samples is shown as the average uncertainty (2SD) across combustion reference material analyses.

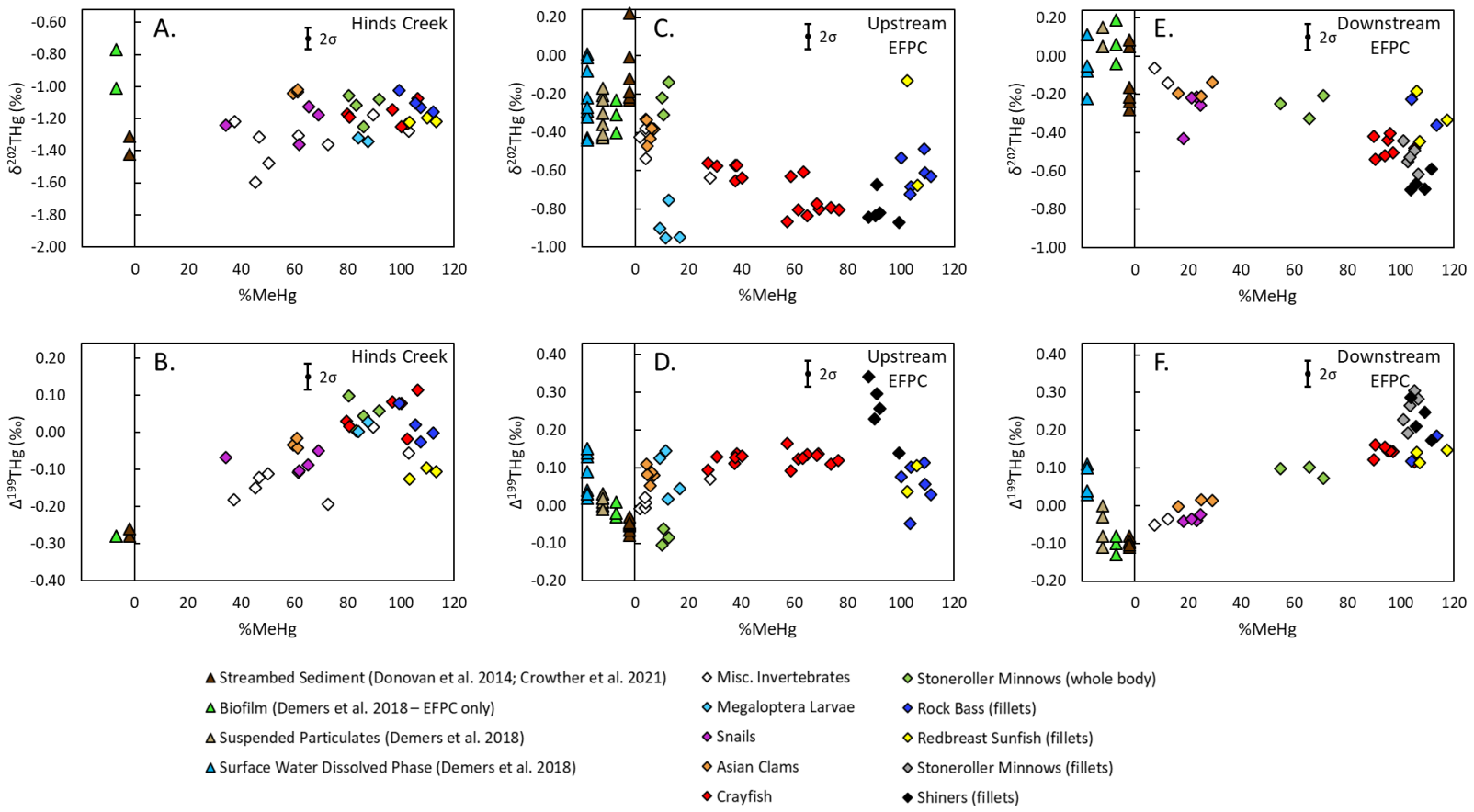

Figure 4.3. THg isotopic composition of (A and B) HC, (C and D) upstream EFPC, and (E and F) downstream EFPC biological samples (diamonds) measured via combustion. Shown are (A, C, and E) δ^{202}THg versus %MeHg and (B, D, and F) Δ^{199}THg versus %MeHg for each sampling site.

Also shown are THg isotopic compositions of streambed sediment and biofilm from HC, and streambed sediment, biofilm, suspended particulates, and surface water dissolved phase from upstream (EFK 24.2 to EFK 22.3) and downstream (EFK 8.7 to EFK 5.0) EFPC sites (triangles) (Donovan et al. 2014; Demers et al. 2018; Crowther et al. 2021). Note that basal resources each contain <1% MeHg and are positioned to the left of the vertical axes for easier visualization. Analytical uncertainty in delta values for biological samples is shown as the average uncertainty (2SD) across combustion reference material analyses

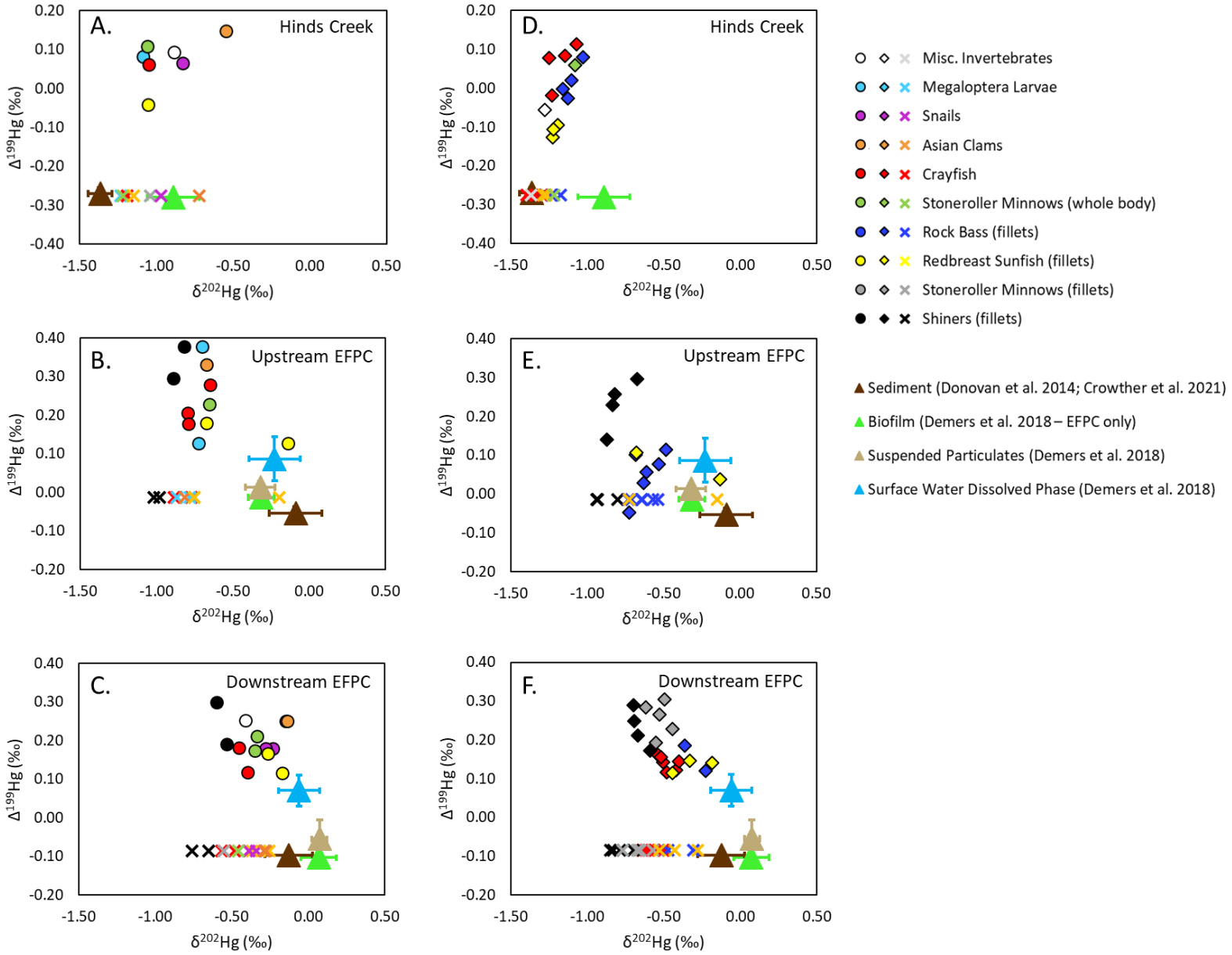
A.
Hinds Creek
B.
Upstream EFPC
C.
Downstream EFPC
D.
Hinds Creek
E.
Upstream EFPC
F.
Downstream EFPC
Δ199Hg (‰)
δ202Hg (‰)
0.20
0.10
0.00
-0.10
-0.20
-0.30
-0.40
0.40
0.30
-1.50
-1.00
-0.50
0.00
0.50
Misc. Invertebrates
Megaloptera Larvae
Snails
Asian Clams
Crayfish
Stoneroller Minnows (whole body)
Rock Bass (fillets)
Redbreast Sunfish (fillets)
Stoneroller Minnows (fillets)
Shiners (fillets)
Sediment (Donovan et al. 2014; Crowther et al. 2021)
Biofilm (Demers et al. 2018 – EFPC only)
Suspended Particulates (Demers et al. 2018)
Surface Water Dissolved Phase (Demers et al. 2018)

Figure 4.4. Isotopic composition of MeHg within the HC and EFPC food webs. Shown are direct measurements of MeHg isotopic compositions of aquatic organisms (circles) from (A) HC, (B) upstream EFPC, and (C) downstream EFPC, measured by resin separation, grouped by biological sample type. Also shown are THg isotopic compositions of aquatic organisms containing ≥90% MeHg (diamonds) from (D) HC, (E) upstream EFPC, and (F) downstream EFPC.

Photochemical demethylation corrected isotopic compositions (X's) are also shown. Each plot also includes THg isotopic compositions of streambed sediment and biofilm from HC, and streambed sediment, biofilm, suspended particulates, and surface water dissolved phase from upstream (EFK 24.2 to EFK 22.3) and downstream (EFK 8.7 to EFK 5.0) EFPC sites (triangles) (Donovan et al. 2014, Demers et al. 2018, Crowther et al. 2021).

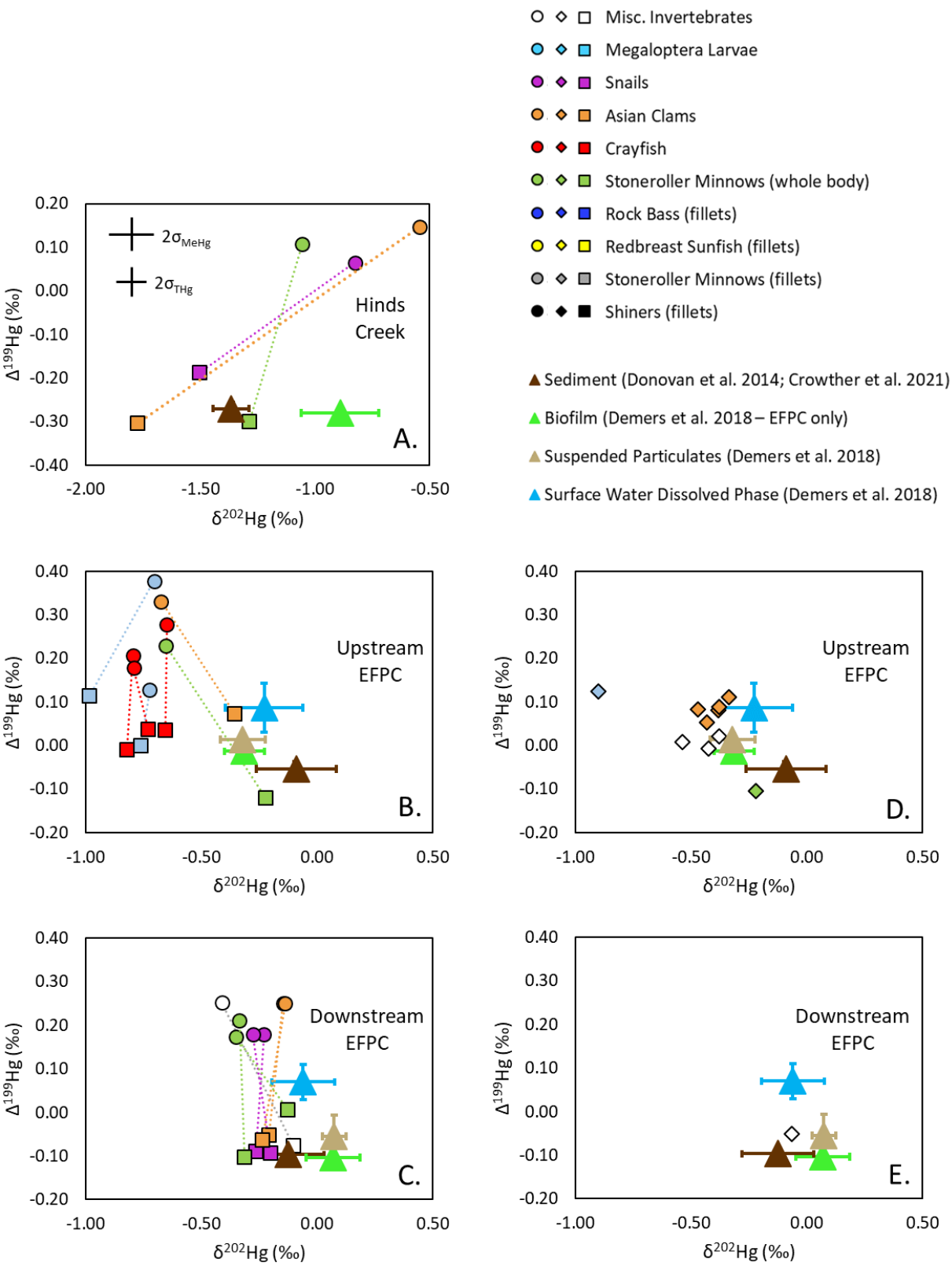
Misc. Invertebrates
Megaloptera Larvae
Snails
Asian Clams
Crayfish
Stoneroller Minnows (whole body)
Rock Bass (fillets)
Redbreast Sunfish (fillets)
Stoneroller Minnows (fillets)
Shiners (fillets)
Sediment (Donovan et al. 2014; Crowther et al. 2021)
Biofilm (Demers et al. 2018 – EFPC only)
Suspended Particulates (Demers et al. 2018)
Surface Water Dissolved Phase (Demers et al. 2018)
2σMeHg
2σTHg
Hinds Creek
A.
Upstream EFPC
B.
Upstream EFPC
D.
Downstream EFPC
C.
Downstream EFPC
E.
Δ199Hg (‰)
δ202Hg (‰)
0.20
0.10
0.00
-0.10
-0.20
-0.30
-0.40
-2.00
-1.50
-1.00
-0.50
0.40
0.30
0.20
0.10
0.00
-0.10
-0.20
-1.00
-0.50
0.00
0.50

Figure 4.5. Isotopic composition of iHg within the HC and EFPC food webs. Shown are (A, B, and C) iHg isotopic compositions of aquatic organisms (squares) calculated via mass balance using THg and MeHg isotopic compositions, along with directly measured MeHg isotopic compositions associated with each organism (circles) from (A) HC, (B) upstream EFPC, and (C) downstream EFPC. Also shown are THg isotopic compositions of aquatic organisms containing ≤10% MeHg (diamonds) from (D) upstream EFPC, and (E) downstream EFPC. Note that none of the biological samples collected from HC had ≤10% MeHg.

Each plot also includes THg isotopic compositions of streambed sediment and biofilm from HC, and streambed sediment, biofilm, suspended particulates, and surface water dissolved phase from upstream (EFK 24.2 to EFK 22.3) and downstream (EFK 8.7 to EFK 5.0) EFPC sites (triangles) (Donovan et al. 2014, Demers et al. 2018, Crowther et al. 2021).

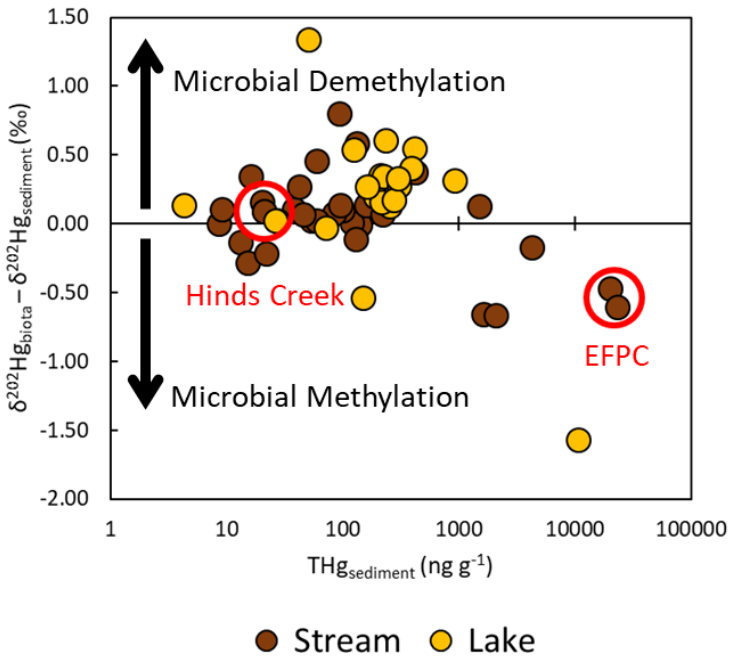

Figure 4.6. Offsets between photochemical demethylation corrected δ^{202}THg values of aquatic organisms with >90% MeHg and δ^{202}THg values of sediment versus THg concentration of sediment for various freshwater streams and lakes.

These values were obtained from the literature (Gehrke et al. 2011a, Gehrke et al. 2011b, Sherman and Blum 2013, Kwon et al. 2015, Donovan et al. 2014, Donovan et al. 2016, Xu et al. 2016, Goix et al. 2019, Janssen et al. 2019, Madenjian et al. 2019, Pribil et al. 2020, Crowther et al. 2021, Janssen et al. 2021, Laffont et al. 2021, Rosera et al. 2022). Corrections for photochemical demethylation were made using a Δ^{199}Hg/δ^{202}Hg slope of 2.43 (Bergquist and Blum 2007). For cases in which MeHg concentrations of biological samples were measured, organisms with <90% MeHg were excluded. For cases in which MeHg concentrations of only a select number of biological samples were measured, organisms with <90% MeHg and those without MeHg concentration measurements were excluded. For cases in which MeHg concentrations of biological samples were not measured, fish were assumed to contain >90% MeHg and other organism types were excluded.

References

Atkinson, Carla L., Matt R. First, Alan P. Covich, Stephen P. Opsahl, and Stephen W. Golladay. 2011. "Suspended material availability and filtration-biodeposition processes performed by a native and invasive bivalve species in streams." *Hydrobiologia* 667:191-204. doi: 10.1007/s10750-011-0640-5.

Baeyens, W., M. Leermakers, T. Papina, A. Saprykin, N. Brion, J. Noyen, M. De Gieter, M. Elskens, and L. Goeyens. 2003. "Bioconcentration and biomagnification of mercury and methylmercury in North Sea and Scheldt Estuary fish." *Archives of Environmental Contamination and Toxicology* 45:498-508. doi: 10.1007/s00244-003-2136-4.

Bergquist, Bridget A., and Joel D. Blum. 2007. "Mass-dependent and -independent fractionation of Hg isotopes by photoreduction in aquatic systems." *Science* 318:417-420. doi: 10.1126/science.1148050.

Blum, Joel D., and Bridget A. Bergquist. 2007. "Reporting of variations in the natural isotopic composition of mercury." *Analytical and Bioanalytical Chemistry* 388:353-359. doi: 10.1007/s00216-007-1236-9.

Blum, Joel D., and Marcus W. Johnson. 2017. "Recent developments in mercury stable isotope analysis." *Reviews in Mineralogy and Geochemistry* 82:733-757. doi: 10.2138/rmg.2017.82.17.

Blum, Joel D., Laura S. Sherman, and Marcus W. Johnson. 2014. "Mercury isotopes in earth and environmental sciences." *Annual Review of Earth and Planetary Sciences* 42:249-269. doi: 10.1146/annurev-earth-050212-124107.

Brooks Rand Instruments. 2013. Application Note: Nitric acid digestion of biological tissue for methylmercury analysis.

Brooks, Scott C., and George R. Southworth. 2011. "History of mercury use and environmental contamination at the Oak Ridge Y-12 Plant." *Environmental Pollution* 159 (1):219-228. doi: 10.1016/j.envpol.2010.09.009.

Brooks, Scott, Virginia Eller, John Dickson, Jennifer Earles, Kenneth Lowe, Tonia Mehlhorn, Todd Olsen, Chris DeRolph, David Watson, Debra Phillips, and Mark Peterson. 2017. Mercury Content of Sediments in East Fork Poplar Creek: Current Assessment and Past Trends. Oak Ridge, TN: Oak Ridge National Laboratory.

Chandan, Priyanka, Sanghamitra Ghosh, and Bridget A. Bergquist. 2015. "Mercury isotope fractionation during aqueous photoreduction of monomethylmercury in the presence of dissolved organic matter." *Environmental Science and Technology* 49 (1):259-267. doi: 10.1021/es5034553.

Crowther, Elizabeth R., Jason D. Demers, Joel D. Blum, Scott C. Brooks, and Marcus W. Johnson. 2021. "Use of sequential extraction and mercury stable isotope analysis to assess remobilization of sediment-bound legacy mercury." *Environmental Science: Processes & Impacts* 23:756-775. doi: 10.1039/d1em00019e.

Crowther, Elizabeth R., Jason D. Demers, Joel D. Blum, Scott C. Brooks, and Marcus W. Johnson. 2022. "Coupling of nitric acid digestion and anion-exchange resin separation for the determination of methylmercury isotopic composition within organisms." *Analytical and Bioanalytical Chemistry*. doi: 10.1007/s00216-022-04468-8.

Demers, Jason D., Joel D. Blum, Scott C. Brooks, Patrick M. Donovan, Ami L. Riscassi, Carrie L. Miller, Wang Zheng, and Baohua Gu. 2018. "Hg isotopes reveal in-stream processing

and legacy inputs in East Fork Poplar Creek, Oak Ridge, Tennessee, USA." *Environmental Science: Processes & Impacts* 20 (4):686-707. doi: 10.1039/c7em00538e.

Demers, Jason D., Joel D. Blum, and Donald R. Zak. 2013. "Mercury isotopes in a forested ecosystem: Implications for air-surface exchange dynamics and the global mercury cycle." *Global Biogeochemical Cycles* 27:222-238. doi: 10.1002/gbc.20021.

Demers, Jason D., Laura S. Sherman, Joel D. Blum, Frank J. Marsik, and J. Timothy Dvonch. 2015. "Coupling atmospheric mercury isotope ratios and meteorology to identify sources of mercury impacting a coastal urban-industrial region near Pensacola, Florida, USA." *Global Biogeochemical Cycles* 29:1689-1705. doi: 10.1002/2015GB005146.

Donovan, Patrick M., Joel D. Blum, Michael Bliss Singer, Mark Marvin-DiPasquale, and Martin T. K. Tsui. 2016. "Isotopic composition of inorganic mercury and methylmercury downstream of a historical gold mining region." *Environmental Science & Technology* 50:1691-1702. doi: 10.1021/acs.est.5b04413.

Donovan, Patrick M., Joel D. Blum, Jason D. Demers, Baohua Gu, Scott C. Brooks, and John Peryam. 2014. "Identification of multiple mercury sources to stream sediments near Oak Ridge, TN, USA." *Environmental Science & Technology* 48 (7):3666-3674. doi: 10.1021/es4046549.

Feng, Caiyan, Zoyne Pedrero, Lázaro Lima, Susana Olivares, Daniel de la Rosa, Sylvain Berail, Emmanuel Tessier, Florence Pannier, and David Amouroux. 2019. "Assessment of Hg contamination by a Chlor-Alkali Plant in riverine and coastal sites combining Hg speciation and isotopic signature (Sagua la Grande River, Cuba)." *Journal of Hazardous Materials* 371:558-565. doi: 10.1016/j.jhazmat.2019.02.092.

Gehrke, Gretchen E., Joel D. Blum, and Mark Marvin-DiPasquale. 2011a. "Sources of mercury to San Francisco Bay surface sediment as revealed by mercury stable isotopes." *Geochimica et Cosmochimica Acta* 75 (3):691-705. doi: 10.1016/J.GCA.2010.11.012.

Gehrke, Gretchen E., Joel D. Blum, Darell G. Slotton, and Ben K. Greenfield. 2011. "Mercury isotopes link mercury in San Francisco Bay forage fish to surface sediments." *Environmental Science & Technology* 45 (4):1264-1270. doi: 10.1021/es103053y.

Goix, Sylvaine, Laurence Maurice, Laure Laffont, Raphaelle Rinaldo, Christelle Lagane, Jerome Chmeleff, Johanna Menges, Lars-Eric Heimbürger, Régine Maury-Brachet, and Jeroen E. Sonke. 2019. "Quantifying the impacts of artisanal gold mining on a tropical river system using mercury isotopes." *Chemosphere* 219:684-694. doi: 10.1016/j.chemosphere.2018.12.036.

Gratz, Lynne E., Gerald J. Keeler, Joel D. Blum, and Laura S. Sherman. 2010. "Isotopic composition and fractionation of mercury in Great Lakes precipitation and ambient air." *Environmental Science and Technology* 44:7764-7770. doi: 10.1021/es100383w.

Hall, B. D., R. A. Bodaly, R. J. P. Fudge, J. W. M. Rudd, and D. M. Rosenberg. 1997. "Food as the dominant pathway of methylmercury uptake by fish." *Water, Air, and Soil Pollution* 100:13-24. doi: 10.1023/A:1018071406537.

Hammerschmidt, Chad R., and William F. Fitzgerald. 2005. "Methylmercury in mosquitoes related to atmospheric mercury deposition and contamination." *Environmental Science & Technology* 39:3034-3039. doi: 10.1021/es0485107.

Hrenchuk, Lee E., Paul J. Blanchfield, Michael J. Paterson, and Holger H. Hintelmann. 2012. "Dietary and waterborne mercury accumulation by yellow perch: A field experiment." *Environmental Science & Technology* 46:509-516. doi: 10.1021/es202759q.

Inza, B., F. Ribeyre, R. Maury-Brachet, and A. Boudou. 1997. "Tissue distribution of inorganic mercury, methylmercury and cadmium in the Asiatic clam (*Corbicula fluminea*) in relation to the contamination levels of the water column and sediment." *Chemosphere* 35:2817-2836. doi: 10.1016/S0045-6535(97)00342-1.

Janssen, Sarah E., Karen Riva-Murray, John F. Dewild, Jacob M. Ogorek, Michael T. Tate, Peter C. Van Metre, David P. Krabbenhoft, and James F. Coles. 2019. "Chemical and physical controls on mercury source signatures in stream fish from the northeastern United States." *Environmental Science and Technology* 53:10110-10119. doi: 10.1021/acs.est.9b03394.

Janssen, Sarah E., Michael T. Tate, David P. Krabbenhoft, John F. DeWild, Jacob M. Ogorek, Christopher L. Babiarz, Anthony D. Sowers, and Peter L. Tuttle. 2021. "The influence of legacy contamination on the transport and bioaccumulation of mercury within the Mobile River Basin." *Journal of Hazardous Materials* 404 Part A:124097. doi: 10.1016/j.jhazmat.2020.124097.

Kehrig, Helena A., Tércia G. Seixas, Aída P. Baêta, Olaf Malm, and Isabel Moreira. 2010. "Inorganic and methylmercury: Do they transfer along a tropical coastal food web?" *Marine Pollution Bulletin* 60:2350-2356. doi: 10.1016/j.marpolbul.2010.08.010.

King, D. G., and I. M. Davies. 1987. "Laboratory and field studies of the accumulation of inorganic mercury by the mussel *Mytilus edulis* (L.)." *Marine Pollution Bulletin* 18:40-45. doi: 10.1016/0025-326X(87)90657-6.

Kraatz, Walter C. 1923. "A study of the food of the minnow *Campostoma anomalum*." *The Ohio Journal of Science* 23:265-283.

Kritee, K., Tamar Barkay, and Joel D. Blum. 2009. "Mass dependent stable isotope fractionation of mercury during mer mediated microbial degradation of monomethylmercury." *Geochimica et Cosmochimica Acta* 73:1285-1296. doi: 10.1016/j.gca.2008.11.038.

Kritee, K., Joel D. Blum, Marcus W. Johnson, Bridget A. Bergquist, and Tamar Barkay. 2007. "Mercury stable isotope fractionation during reduction of Hg(II) to Hg(0) by mercury resistant microorganisms." *Environmental Science and Technology* 41 (6):1889-1895. doi: 10.1021/ES062019T.

Kritee, K., Laura C. Motta, Joel D. Blum, Martin Tsz Ki Tsui, and John R. Reinfelder. 2018. "Photomicrobial Visible Light-Induced Magnetic Mass Independent Fractionation of Mercury in a Marine Microalga." *ACS Earth and Space Chemistry* 2 (5):432-440. doi: 10.1021/acsearthspacechem.7b00056.

Kwon, Sae Yun, Joel D. Blum, Michael J. Carvan, Niladri Basu, Jessica A. Head, Charles P. Madenjian, and Solomon R. David. 2012. "Absence of fractionation of mercury isotopes during trophic transfer of methylmercury to freshwater fish in captivity." *Environmental Science & Technology* 46:7527-7534. doi: 10.1021/es300794q.

Kwon, Sae Yun, Joel D. Blum, Celia Y. Chen, Dustin E. Meattey, and Robert P. Mason. 2014. "Mercury isotope study of sources and exposure pathways of methylmercury in estuarine food webs in the northeastern U.S." *Environmental Science & Technology* 48:10089-10097. doi: 10.1021/es5020554.

Kwon, Sae Yun, Joel D. Blum, Michelle A. Chirby, and Edward J. Chesney. 2013. "Application of mercury isotopes for tracing trophic transfer and internal distribution of mercury in marine fish feeding experiments." *Environmental Toxicology* 32:2322-2330. doi: 10.1002/etc.2313.

Kwon, Sae Yun, Joel D. Blum, Knute J. Nadelhoffer, J. Timothy Dvonch, and Martin Tsz-Ki Tsui. 2015. "Isotopic study of mercury sources and transfer between a freshwater lake and adjacent forest food web." *Science of The Total Environment* 532:220-229. doi: 10.1016/J.SCITOTENV.2015.06.012.

Laffont, Laure, Johanna Megnes, Sylvaine Goix, Sophie Gentès, Régine Maury-Brachet, Jeroen E. Sonke, Alexia Legeay, Patrice Gonzalez, Raphaëlle Rinaldo, and Laurence Maurice. 2021. "Hg concentrations and stable isotope variations in tropical fish species of a gold-mining-impacted watershed in French Guiana." *Environmental Science and Pollution Research* 28:60609-60621. doi: 10.1007/s11356-021-14858-7.

Lauretta, Dante S., Bjoern Klaue, Joel D. Blum, and Peter R. Buseck. 2001. "Mercury abundances and isotopic compositions in the Murchison (CM) and Allende (CV) carbonaceous chondrites." *Geochimica et Cosmochimica Acta* 65:2807-2818. doi: 10.1016/s0016-7037(01)00630-5.

Li, Mi-Ling, Sae Yun Kwon, Brett A. Poulin, Martin Tsz-Ki Tsui, Laura C. Motta, and Moonkyoung Cho. 2022. "Internal dynamics and metabolism of mercury in biota: A review of insights from mercury stable isotopes." *Environmental Science & Technology* 56:9182-9195. doi: 10.1021/acs.est.1c08631.

Li, Miling, Amina T. Schartup, Amelia P. Valberg, Jessica D. Ewald, David P. Krabbenhoft, Runsheng Yin, Prentiss H. Balcom, and Elsie M. Sunderland. 2016. "Environmental origins of methylmercury accumulated in subarctic estuarine fish indicated by mercury stable isotopes." *Environmental Science & Technology* 50 (21):11559-11568. doi: 10.1021/acs.est.6b03206.

Madenjian, Charles P., Sarah E. Janssen, Ryan F. Lepak, Jacob M. Ogorek, Tylor J. Rosera, John F. Dewild, David P. Krabbenhoft, Stewart F. Cogswell, and Mark E. Holey. 2019. "Mercury isotopes reveal an ontogenetic shift in habitat use by walleye in lower Green Bay of Lake Michigan." *Environmental Science & Technology Letters* 6:8-13. doi: 10.1021/acs.estlett.8b00592.

Miller, Rudolph J. 1962. "Reproductive behavior of the stoneroller minnow, *Campostoma anomalum pullum*." *Copeia* 1962:407-417. doi: 10.2307/1440909.

Peterson, M. J., T. J. Mathews, M. G. Ryon, J. G. Smith, S. W. Christensen, Jr. Greely, M. S., W. K. Roy, C. C. Brandt, and K. A. Sabo. 2013. Y-12 National Security Complex Biological Monitoring and Abatement Program Plan. Oak Ridge, TN: Oak Ridge National Laboratory.

Peterson, Mark J., Melanie Mayes, Scott Brooks, Teresa Mathews, Alex Johs, Johnbull Dickson, Tonia Mehlhorn, Leroy Goñez-Rodríguez, Christopher DeRolph, David Watson, Virginia Eller, Todd Olsen, Kenneth Lowe, Ryan McManamay, John Smith, Jesse Morris, and Monica Poteat. 2017. Mercury Remediation Technology Development for Lower East Fork Poplar Creek–FY 2016 Progress Report.

Pribil, Michael J., Valentina Rimondi, Pilario Costagliola, Piefranco Lattanzi, and Danny L. Rutherford. 2020. "Assessing mercury distribution using isotopic fractionation of mercury processes and sources adjacent and downstream of a legacy mine district in Tuscany, Italy." *Applied Geochemistry* 117:104600. doi: 10.1016/j.apgeochem.2020.104600G.

Rodríguez-González, Pablo, Vladimir N. Epov, Romain Bridou, Emmanuel Tessier, Remy Guyoneaud, Mathilde Monperrus, and David Amouroux. 2009. "Species-specific stable isotope fractionation of mercury during Hg(II) methylation by an anaerobic bacteria

(*Desulfobulbus propionicu*s) under dark conditions." *Environmental Science & Technology* 43:9183-9188. doi: 10.1021/es902206j.

Rose, Carla H., Sanghamitra Ghosh, Joel D. Blum, and Bridget A. Bergquist. 2015. "Effects of ultraviolet radiation on mercury isotope fractionation during photo-reduction for inorganic and organic mercury species." *Chemical Geology* 405:102-111. doi: 10.1016/j.chemgeo.2015.02.025.

Rosera, Tylor J., Sarah E. Janssen, Michael T. Tate, Ryan F. Lepak, Jacob M. Ogorek, John F. DeWild, David P. Krabbenhoft, and James P. Hurley. 2022. "Methylmercury stable isotopes: New insights on assessing aquatic food web bioaccumulation in legacy impacted regions." *ACS ES&T Water* 2:701-709. doi: 10.1021/acsestwater.1c00285.

Seixas, Tércia G., Isabel Moreira, Salvatore Siciliano, Olaf Malm, and Helena A. Kehrig. 2014. "Differences in methylmercury and inorganic mercury biomagnification in a tropical marine food web." *Bulletin of Environmental Contamination and Toxicology* 92:274-278. doi: 10.1007/s00128-014-1208-7.

Selin, Noelle E. 2009. "Global biogeochemical cycling of mercury: A review." *Annual Review of Environment and Resources* 34:43-63. doi: 10.1146/annurev.environ.051308.084314.

Sherman, Laura S., and Joel D. Blum. 2013. "Mercury stable isotopes in sediments and largemouth bass from Florida lakes, USA." *Science of The Total Environment* 448:163-175. doi: 10.1016/J.SCITOTENV.2012.09.038.

Sherman, Laura S., Joel D. Blum, J. Timothy Dvonch, Lynne E. Gratz, and Matthew S. Landis. 2015. "The use of Pb, Sr, and Hg isotopes in Great Lakes precipitation as a tool for pollution source attribution." *Science of The Total Environment* 502:362-374. doi: 10.1016/J.SCITOTENV.2014.09.034.

Sherman, Laura S., Joel D. Blum, Gerald J. Keeler, Jason D. Demers, and J. Timothy Dvonch. 2012. "Investigation of local mercury deposition from a coal-fired power plant using mercury isotopes." *Environmental Science & Technology* 46:382-390. doi: 10.1021/es202793c.

Tsui, Martin Tsz Ki, Joel D. Blum, Jacques C. Finlay, Steven J. Balogh, Sae Yun Kwon, and Yabing H. Nollet. 2013. "Photodegradation of methylmercury in stream ecosystems." *Limnology and Oceanography* 58 (1):13-22. doi: 10.4319/lo.2013.58.1.0013.

Tsui, Martin Tsz Ki, Joel D. Blum, Sae Yun Kwon, Jacques C. Finlay, Steven J. Balogh, and Yabing H. Nollet. 2012. "Sources and transfers of methylmercury in adjacent river and forest food webs." *Environmental Science & Technology* 46:10957-10964. doi: 10.1021/es3019836.

U.S. EPA. 2001. Method 1630, Methyl Mercury in Water by Distillation, Aqueous Ethylation, Purge and Trap, and CVAFS. Washington, D.C.: U.S. Environmental Protection Agency Office of Water.

U.S. EPA. 2002. Method 1631, Revision E: Mercury in Water by Oxidation, Purge and Trap, and Cold Vapor Atomic Fluorescence Spectrometry. Washington, D.C.: U.S. Environmental Protection Agency, Office of Water.

Wang, Rui, Ming-Hung Wong, and Wen-Xiong Wang. 2010. "Mercury exposure in the freshwater tilapia *Oreochromis niloticus*." *Environmental Pollution* 158:2694-2701. doi: 10.1016/j.envpol.2010.04.019.

WRRP, and UCOR. 2019. 2019 Remediation Effectiveness Report for the U.S. Department of Energy Oak Ridge Site, Oak Ridge, Tennessee: Data and Evaluations. prepared by the

Water Resources Restoration Program and UCOR, an AECOM-led partnership with Jacobs.

Xu, Xiaoyu, Qianggong Zhang, and Wen-Xiong Wang. 2016. "Linking mercury, carbon, and nitrogen stable isotopes in Tibetan biota: Implications for using mercury stable isotopes as source tracers." *Scientific Reports* 6:25394. doi: 10.1038/srep25394.

Yin, Runsheng, Xinbin Feng, Xiangdong Li, Ben Yu, and Buyun Du. 2014. "Trends and advances in mercury stable isotopes as a geochemical tracer." *Trends in Environmental Analytical Chemistry* 2:1-10. doi: 10.1016/j.teac.2014.03.001.

Zhang, Zhong Sheng, Dong Mei Zheng, Qi Chao Wang, and Xian Guo Lv. 2009. "Bioaccumulation of total and methyl mercury in three earthworm species (*Drawida* sp., *Allolobophora* sp., and *Limnodrilus* sp.)." *Bulletin of Environmental Contamination and Toxicology* 83:937-942. doi: 10.1007/s00128-009-9872-8.

Zheng, Wang, and Holger Hintelmann. 2009. "Mercury isotope fractionation during photoreduction in natural water is controlled by its Hg/DOC ratio." *Geochimica et Cosmochimica Acta* 73:6704-6715. doi: 10.1016/j.gca.2009.08.016.

Zheng, Wang, and Holger Hintelmann. 2010a. "Isotope fractionation of mercury during its photochemical reduction by low-molecular-weight organic compounds." *Journal of Physical Chemistry A* 114 (12):4246-4253. doi: 10.1021/jp9111348.

Zheng, Wang, and Holger Hintelmann. 2010b. "Nuclear field shift effect in isotope fractionation of mercury during abiotic reduction in the absence of light." *J. Phys. Chem. A* 114:4238-4245. doi: 10.1021/jp910353y.

Zheng, Wang, Daniel Obrist, Dominique Weis, and Bridget A. Bergquist. 2016. "Mercury isotope compositions across North American forests." *Global Biogeochemical Cycles* 30:1475-1492. doi: 10.1002/2015GB005323.

4.6 Supporting Information

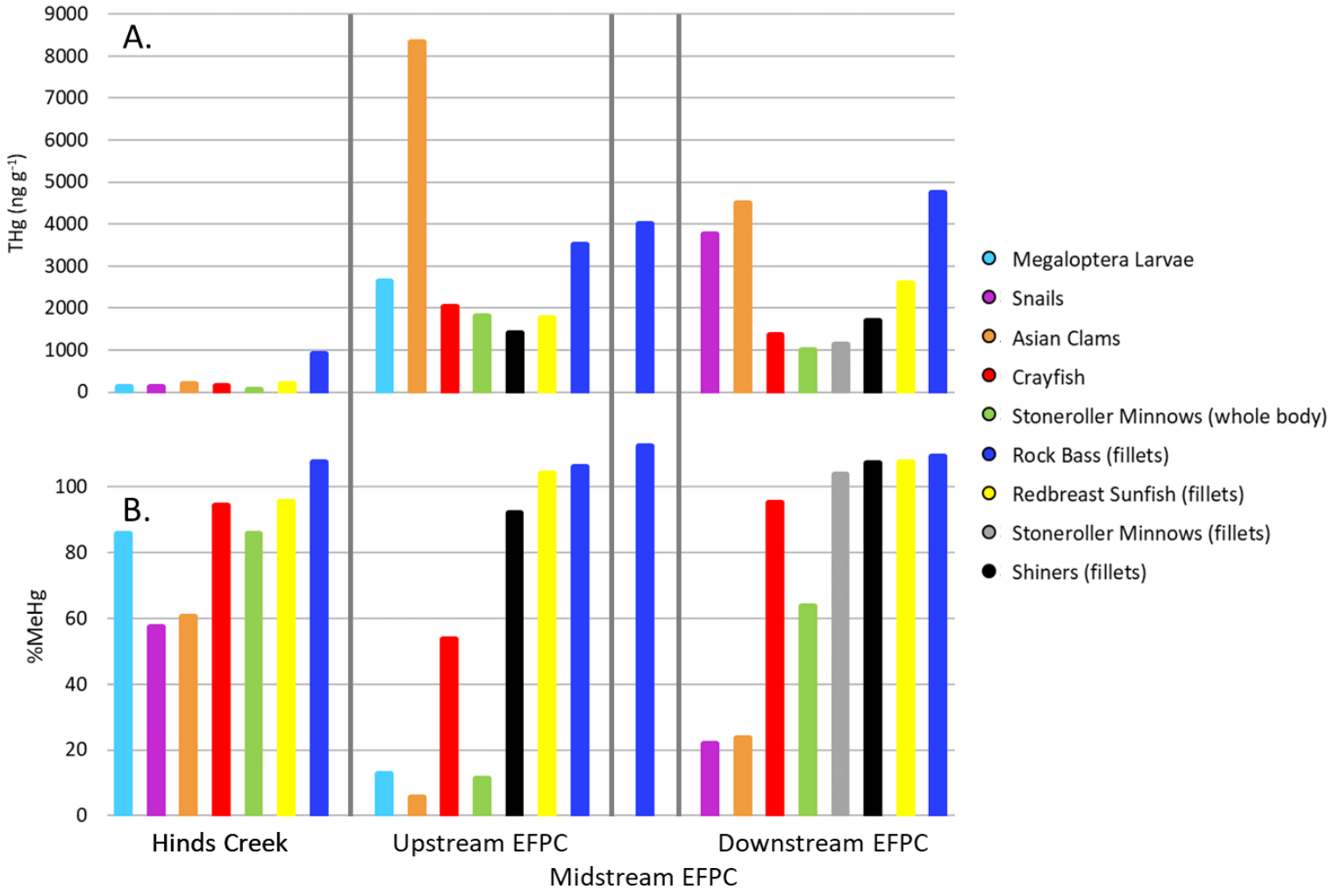

Figure S4.1. Average (A) THg concentrations and (B) %MeHg values of HC and EFPC biological samples.

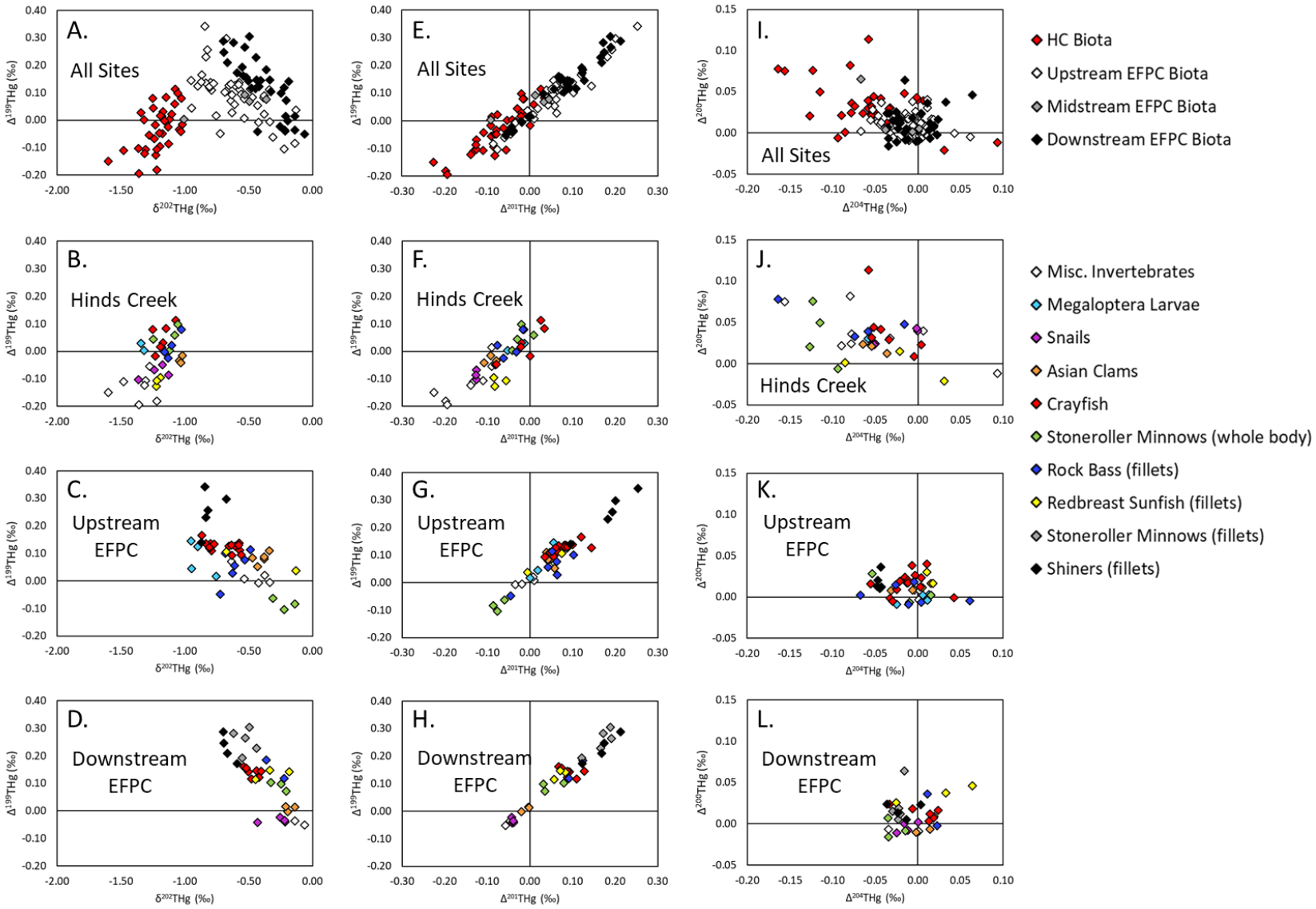
A.
All Sites
B.
Hinds Creek
C.
Upstream EFPC
D.
Downstream EFPC
E.
All Sites
F.
Hinds Creek
G.
Upstream EFPC
H.
Downstream EFPC
I.
All Sites
J.
Hinds Creek
K.
Upstream EFPC
L.
Downstream EFPC
Δ199THg (‰)
δ202THg (‰)
Δ201THg (‰)
Δ200THg (‰)
Δ204THg (‰)
HC Biota
Upstream EFPC Biota
Midstream EFPC Biota
Downstream EFPC Biota
Misc. Invertebrates
Megaloptera Larvae
Snails
Asian Clams
Crayfish
Stoneroller Minnows (whole body)
Rock Bass (fillets)
Redbreast Sunfish (fillets)
Stoneroller Minnows (fillets)
Shiners (fillets)

Figure S4.2. THg isotopic composition of HC and EFPC biological samples, measured via combustion, grouped by (A, E, and I) sampling site and (B, C, D, F, G, H, J, K, L) biological sample type.

Shown are Δ^{199}THg versus δ^{202}THg for (A) all sites, (B) HC, (C) upstream EFPC, and (D) downstream EFPC; Δ^{199}THg versus Δ^{201}THg for (E) all sites, (F) HC, (G) upstream EFPC, and (H) downstream EFPC; and Δ^{200}THg versus Δ^{204}THg for (I) all sites, (J) HC, (K) upstream EFPC, and (L) downstream EFPC.

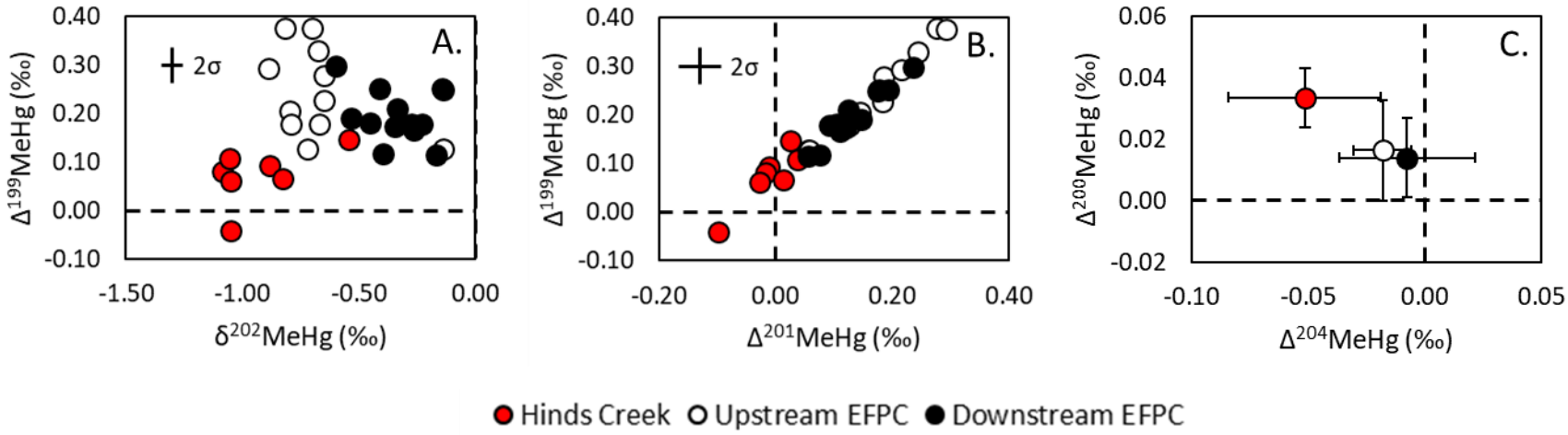

Figure S4.3. MeHg isotopic composition of HC and EFPC biological samples, measured via resin separation, grouped by sampling site. Shown are (A) Δ^{199}MeHg versus δ^{202}MeHg, (B) Δ^{199}MeHg versus Δ^{201}MeHg, and (C) Δ^{200}MeHg versus Δ^{204}MeHg.

Analytical uncertainty in MeHg delta values for biological samples is shown as the average uncertainty (2SD) across UM-Almadén analyses. For plots A and B, each symbol represents one biological sample, whereas for plot C, each symbol represents a site average, with error bars representing within-site variability across samples (1SD).

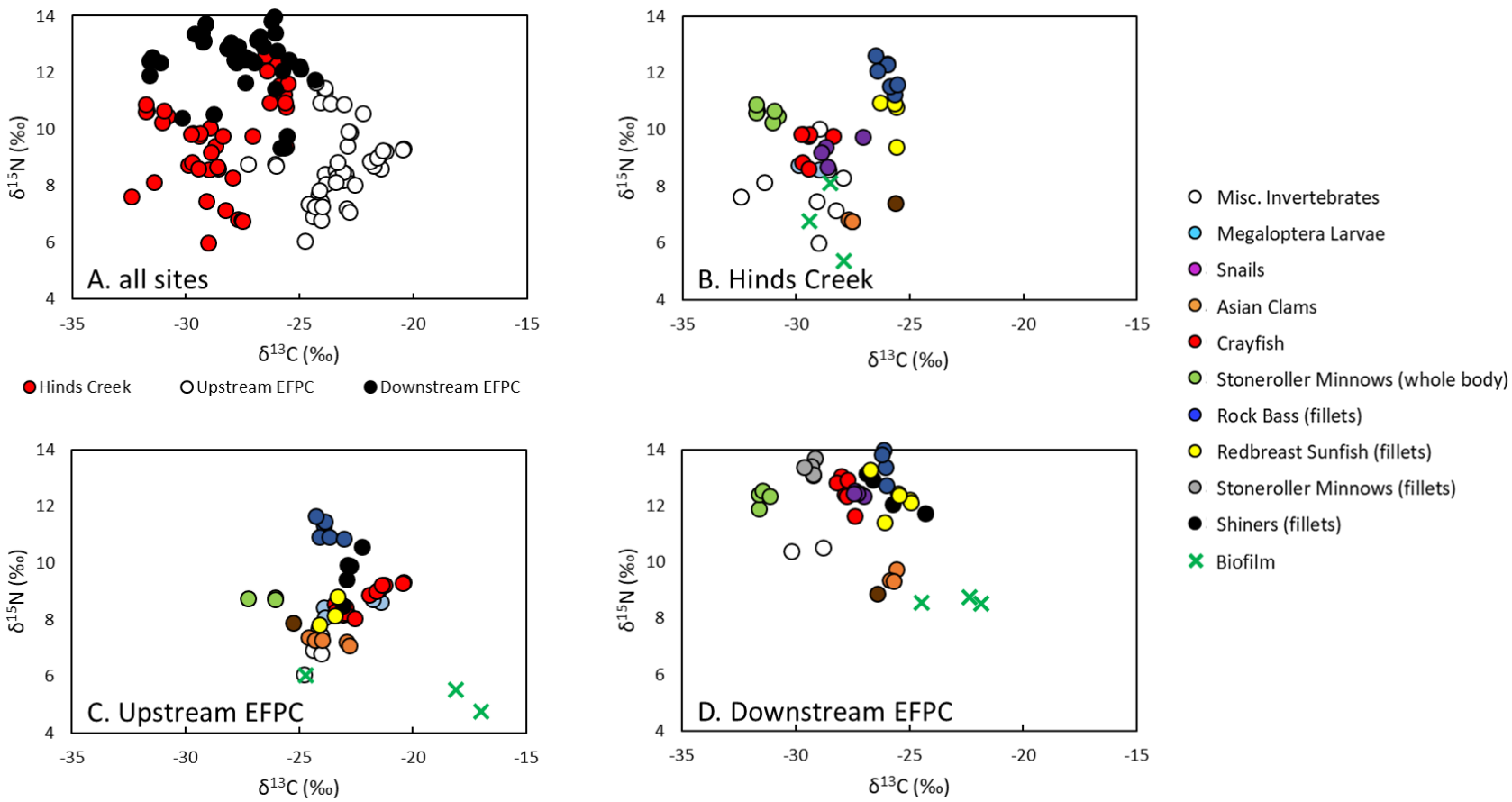

Figure S4.4. Carbon and nitrogen isotopic compositions of aquatic organisms and biofilm (A) grouped by site and grouped by biological sample types at (B) HC, (C) upstream EFPC, and (D) downstream EFPC.

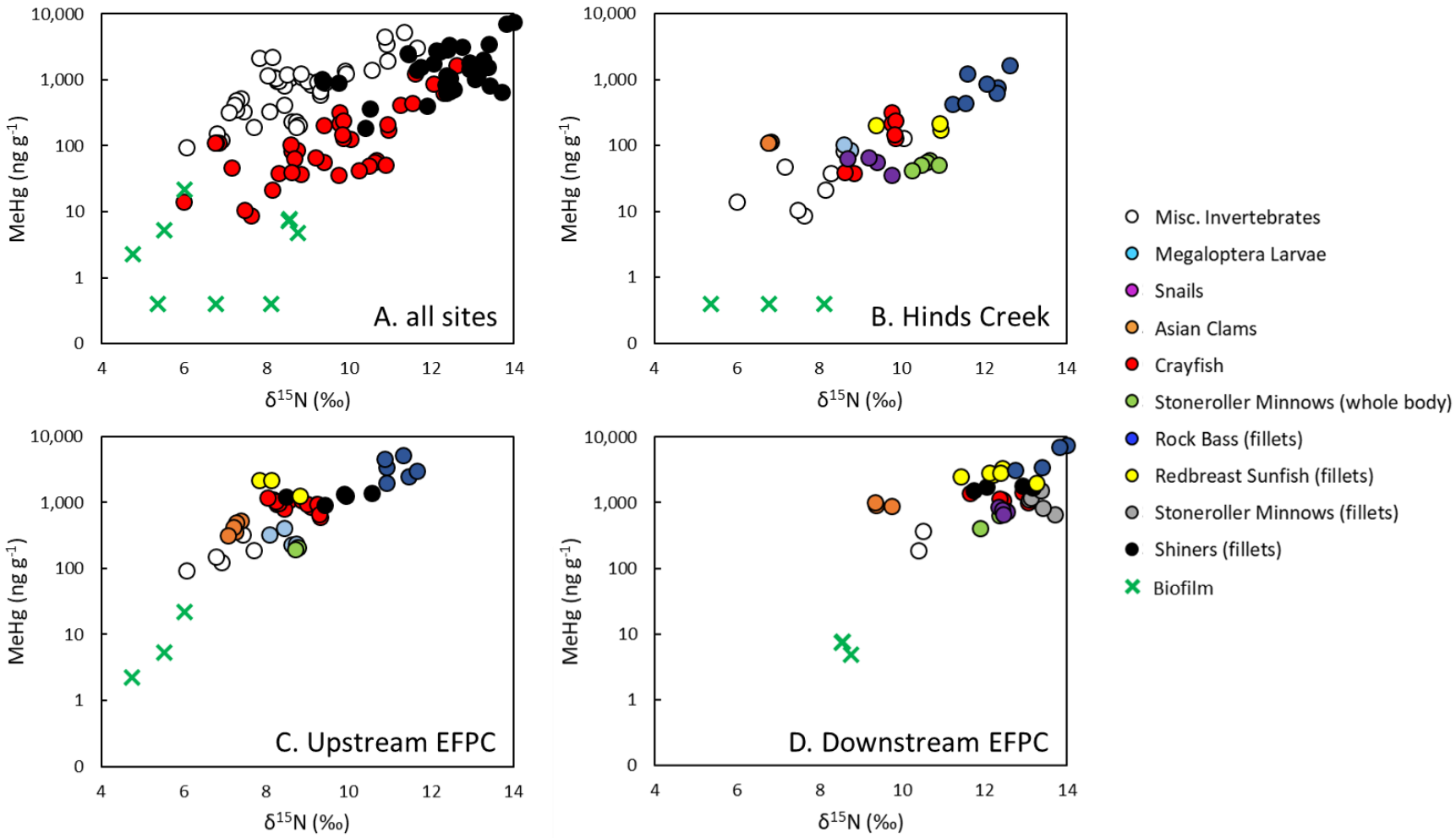

Figure S4.5. MeHg concentration (log scale) versus nitrogen isotopic composition of aquatic organisms and biofilm (A) grouped by site and grouped by biological sample types at (B) HC, (C) upstream EFPC, and (D) downstream EFPC.

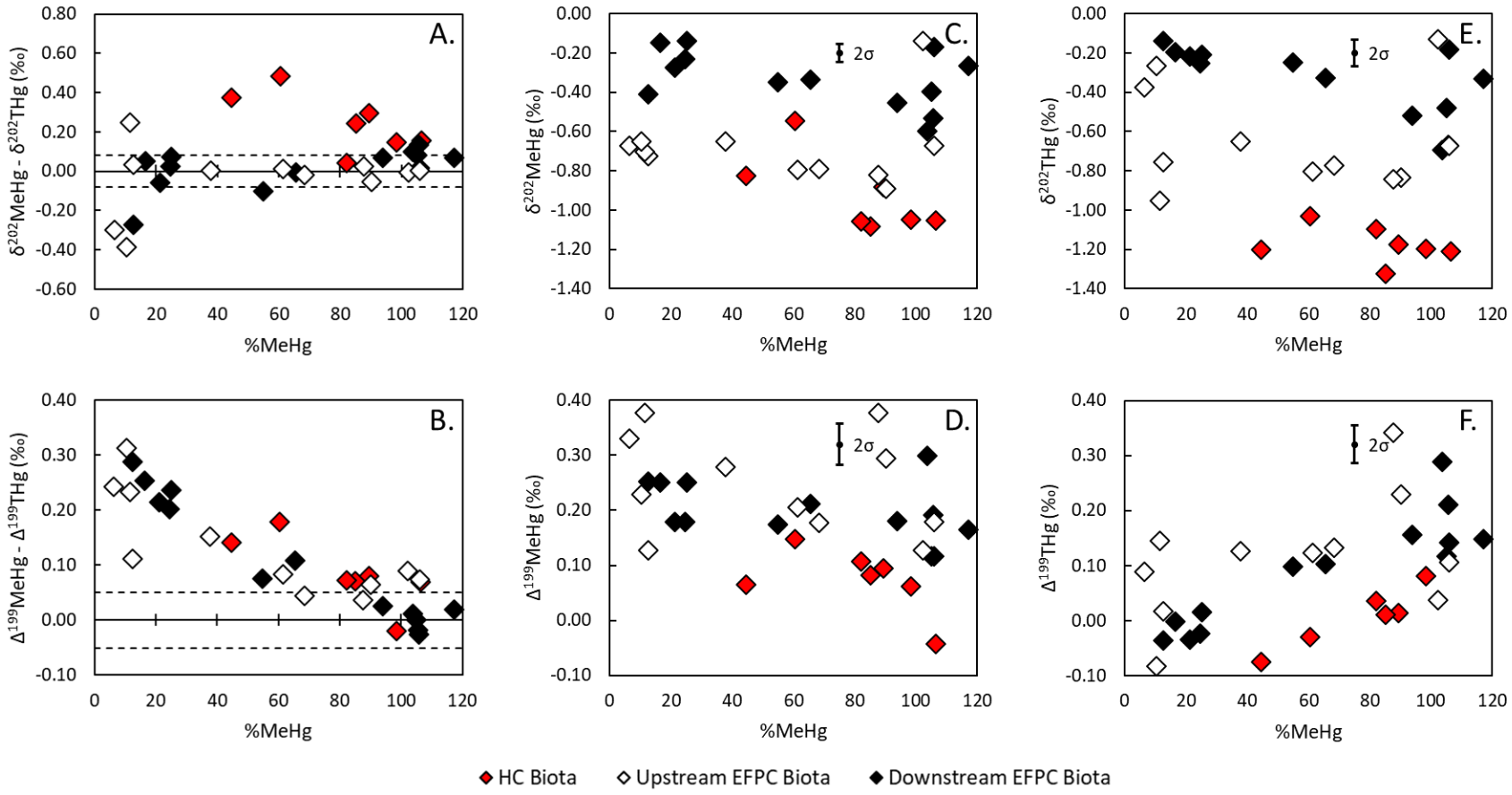

Figure S4.6. (A and B) Calculated offsets between MeHg and THg isotopic composition of biological samples from HC, upstream EFPC, and downstream EFPC for which MeHg was separated for direct isotopic analysis. Shown are (A) δ^{202}MeHg minus δ^{202}THg versus %MeHg and (B) Δ^{199}MeHg minus Δ^{199}THg versus %MeHg. Also shown are the (C and D) MeHg and (E and F) THg isotopic compositions of these biological samples versus %MeHg.

These plots demonstrate whether the variability in offsets between MeHg and THg isotopic composition among samples with similar %MeHg values are driven more by differences in MeHg or THg isotopic composition between samples. For example, the variability in calculated offsets between δ^{202}MeHg and δ^{202}THg for upstream EFPC biological samples with <20% MeHg is primarily driven by relatively large differences in δ^{202}THg values between samples, rather than by differences in δ^{202}MeHg values. Analytical uncertainty

in MeHg delta values for biological samples is shown as the average uncertainty (2SD) across UM-Almadén analyses. Analytical uncertainty in THg delta values for biological samples is shown as the average uncertainty (2SD) across combustion reference material analyses. Dashed lines above and below 0‰ on plots A and B represent propagated uncertainty (2SD) = $\sqrt{2SD_{MeHg}{}^2 + 2SD_{THg}{}^2}$

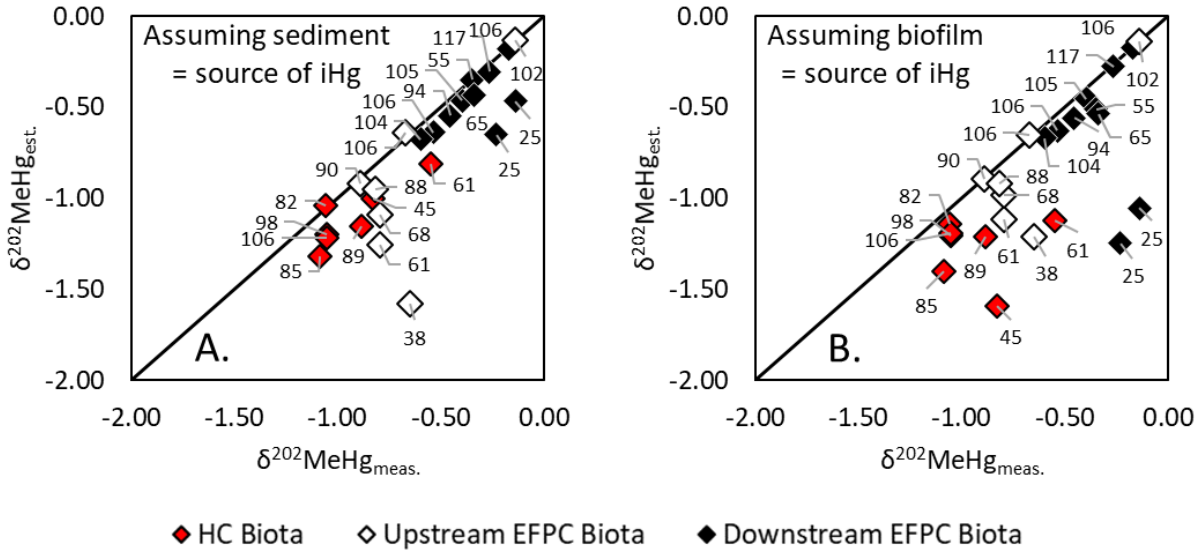

Figure S4.7. Estimated MeHg isotopic compositions of biological samples from HC and EFPC calculated via mass balance (Tsui et al. 2012) using measured THg isotopic compositions of the organisms and assumed iHg isotopic compositions based on the THg isotopic compositions of (A) streambed sediment and (B) biofilm from each of the sampling sites.

These values are plotted against directly measured MeHg isotopic compositions of biological samples measured via resin separation. Data point labels indicate %MeHg of each biological sample. Note that larger offsets between measured and estimated MeHg isotopic compositions were observed for samples with lower %MeHg. Also note that samples with lower %MeHg were more sensitive to whether streambed sediment or biofilm was chosen to represent the isotopic composition of iHg within the organism.

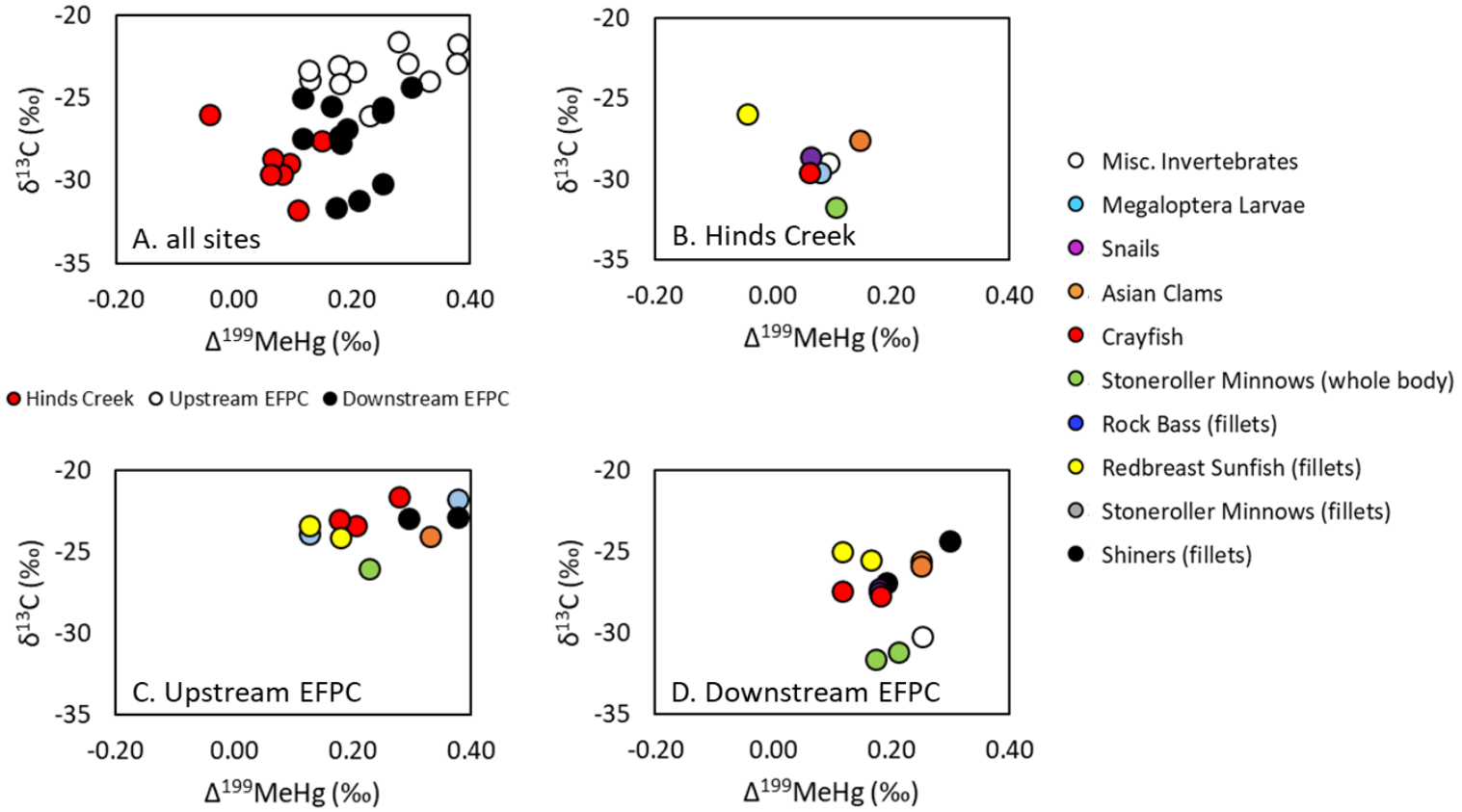

Figure S4.8. Carbon isotopic composition versus MeHg isotopic composition of aquatic organisms (A) grouped by site and grouped by biological sample types at (B) HC, (C) upstream EFPC, and (D) downstream EFPC.

Table S4.1a. Sample descriptions of Hinds Creek aquatic organisms.

Site ID	Sample ID	Organism Type	Sample Type	Sample Length	Sample Sex	Number of Individuals Composited	Sample Collection Date
HCK 20.6	15611	Rock Bass	fillet	–	–	1	May 2010
HCK 20.6	15612	Rock Bass	fillet	–	–	1	May 2010
HCK 20.6	15616	Rock Bass	fillet	–	–	1	May 2010
HCK 20.6	16961	Rock Bass	fillet	–	–	1	May 2011
HCK 20.6	16962	Rock Bass	fillet	–	–	1	May 2011
HCK 20.6	16965	Rock Bass	fillet	–	–	1	May 2011
HCK 20.6	16951	Redbreast Sunfish	fillet	–	–	1	May 2011
HCK 20.6	16952	Redbreast Sunfish	fillet	–	–	1	May 2011
HCK 20.6	16955	Redbreast Sunfish	fillet	–	–	1	May 2011
HCK 20.6	15604	Stoneroller Minnow	whole body	–	–	1	May 2010
HCK 20.6	15605	Stoneroller Minnow	whole body	–	–	1	May 2010
HCK 20.6	16957	Stoneroller Minnow	whole body	–	–	1	May 2011
HCK 20.6	16958	Stoneroller Minnow	whole body	–	–	1	May 2011
HCK 20.6	16959	Stoneroller Minnow	whole body	–	–	1	May 2011
HCK 20.6	1	Aquatic Earthworm	whole body	–	–	–	Aug 2014
HCK 20.6	2	Water Penny Beetle	whole body	–	–	–	Aug 2014
HCK 20.6	3	Dragonfly Larvae	whole body	–	–	–	Aug 2014
HCK 20.6	4	Riffle Beetle Larvae	whole body	–	–	–	Aug 2014
HCK 20.6	5	Typical Caddisfly Larvae	whole body	–	–	–	Aug 2014
HCK 20.6	6	Net-Spinning Caddisfly Larvae	whole body	–	–	–	Aug 2014
HCK 20.6	8	FH & SC Mayfly Larvae	whole body	–	–	–	Aug 2014
HCK 20.6	9	Burrowing Mayfly Larvae	whole body	–	–	–	Aug 2014
HCK 20.6	10	Snipe Fly Larvae	whole body	–	–	–	Aug 2014
HCK 20.6	11	Megaloptera Larvae	whole body	42-55 mm	–	–	Aug 2014
HCK 20.6	12	Megaloptera Larvae	whole body	31-45 mm	–	–	Aug 2014
HCK 20.6	13	Snail	soft tissue	29-33 mm	–	3	Aug 2014
HCK 20.6	14	Snail	soft tissue	24-29 mm	–	63	Aug 2014
HCK 20.6	15	Snail	soft tissue	20-24 mm	–	128	Aug 2014
HCK 20.6	16	Snail	soft tissue	15-20 mm	–	84	Aug 2014
HCK 20.6	17	Asian Clam	soft tissue	>1.5 cm	–	~50	Aug 2014
HCK 20.6	18	Asian Clam	soft tissue	>1.5 cm	–	~50	Aug 2014
HCK 20.6	19	Asian Clam	soft tissue	>1.5 cm	–	~50	Aug 2014

HCK 20.6	20	Crayfish	soft tissue	26 mm	male	1	Aug 2014
HCK 20.6	21	Crayfish	soft tissue	20-22 mm	male	4	Aug 2014
HCK 20.6	22	Crayfish	soft tissue	15-18 mm	male	44	Aug 2014
HCK 20.6	23	Crayfish	whole body	10-15 mm	male	45	Aug 2014
HCK 20.6	24	Crayfish	soft tissue	20-25 mm	female	15	Aug 2014
HCK 20.6	25	Crayfish	soft tissue	15-19 mm	female	33	Aug 2014
HCK 20.6	26	Crayfish	whole body	10-15 mm	female	52	Aug 2014

See Table S4.1c for notes.

Table S4.1b. Sample descriptions of upstream EFPC aquatic organisms.

Site ID	Sample ID	Organism Type	Sample Type	Sample Length	Sample Sex	Number of Individuals Composited	Sample Collection Date
EFK 24.2	15800	Rock Bass	fillet	–	–	1	June 2010
EFK 24.2	15998	Rock Bass	fillet	–	–	1	June 2010
EFK 24.2	15999	Rock Bass	fillet	–	–	1	June 2010
EFK 23.4	15801	Rock Bass	fillet	–	–	1	June 2010
EFK 23.4	15802	Rock Bass	fillet	–	–	1	June 2010
EFK 23.4	15803	Rock Bass	fillet	–	–	1	June 2010
EFK 23.4	15993	Redbreast Sunfish	fillet	–	–	1	June 2010
EFK 23.4	15995	Redbreast Sunfish	fillet	–	–	1	June 2010
EFK 23.4	103-R1	Shiner	fillet	–	–	1	June 2014
EFK 23.4	103-R2	Shiner	fillet	–	–	1	June 2014
EFK 23.4	103-R4	Shiner	fillet	–	–	1	June 2014
EFK 23.4	103-R5	Shiner	fillet	–	–	1	June 2014
EFK 23.4	103-R6	Shiner	fillet	–	–	1	June 2014
EFK 23.4	15988	Stoneroller Minnow	whole body	–	–	1	June 2010
EFK 23.4	15989	Stoneroller Minnow	whole body	–	–	1	June 2010
EFK 23.4	15990	Stoneroller Minnow	whole body	–	–	1	June 2010
EFK 23.4	71	Megaloptera Larvae	whole body	45-50 mm	–	3	Aug 2014
EFK 23.4	72	Megaloptera Larvae	whole body	60-70 mm	–	4	Aug 2014
EFK 23.4	73	Asian Clam	soft tissue	15-20 mm	–	16	Aug 2014
EFK 23.4	74	Asian Clam	soft tissue	10-15 mm	–	30	Aug 2014
EFK 23.4	75	Crayfish	soft tissue	32 mm	male	1	Aug 2014
EFK 23.4	76	Crayfish	soft tissue	25-30 mm	male	8	Aug 2014
EFK 23.4	77	Crayfish	soft tissue	22-25 mm	male	4	Aug 2014
EFK 23.4	78	Crayfish	soft tissue	16-18 mm	male	5	Aug 2014
EFK 23.4	79	Crayfish	soft tissue	30 mm	female	1	Aug 2014
EFK 23.4	80	Crayfish	soft tissue	26-28 mm	female	4	Aug 2014
EFK 23.4	81	Crayfish	soft tissue	21-24 mm	female	4	Aug 2014
EFK 23.4	82	Crayfish	soft tissue	15-19 mm	female	8	Aug 2014
EFK 22.3	51	Aquatic Earthworm	whole body	–	–	–	Aug 2014
EFK 22.3	52	Minnow Mayfly Larvae	whole body	–	–	–	Aug 2014
EFK 22.3	53	FH & SC Mayfly Larvae	whole body	–	–	–	Aug 2014
EFK 22.3	54	Net-Spinning Caddisfly Larvae	whole body	–	–	–	Aug 2014

EFK 22.3	55	Darners Dragonfly Larvae	whole body	–	–	–	Aug 2014
EFK 22.3	57	Megaloptera Larvae	whole body	10-40 mm	–	–	Aug 2014
EFK 22.3	58	Megaloptera Larvae	whole body	58-75 mm	–	–	Aug 2014
EFK 22.3	59	Asian Clam	soft tissue	20-22 mm	–	6	Aug 2014
EFK 22.3	60	Asian Clam	soft tissue	16-20 mm	–	28	Aug 2014
EFK 22.3	61	Asian Clam	soft tissue	10-14 mm	–	47	Aug 2014
EFK 22.3	62	Crayfish	soft tissue	25-30 mm	male	4	Aug 2014
EFK 22.3	63	Crayfish	soft tissue	20-25 mm	male	12	Aug 2014
EFK 22.3	64	Crayfish	soft tissue	15-20 mm	male	8	Aug 2014
EFK 22.3	65	Crayfish	soft tissue	38 mm	female	1	Aug 2014
EFK 22.3	67	Crayfish	soft tissue	25-27 mm	female	3	Aug 2014
EFK 22.3	68	Crayfish	soft tissue	20-24 mm	female	14	Aug 2014
EFK 22.3	69	Crayfish	soft tissue	15-20 mm	female	9	Aug 2014

See Table S4.1c for notes.

Table S4.1c. Sample descriptions of midstream and downstream EFPC aquatic organisms.

Site ID	Sample ID	Organism Type	Sample Type	Sample Length	Sample Sex	Number of Individuals Composited	Sample Collection Date
EFK 18.2	15714	Rock Bass	fillet	–	–	1	June 2010
EFK 18.2	15715	Rock Bass	fillet	–	–	1	June 2010
EFK 13.8	15704	Rock Bass	fillet	–	–	1	June 2010
EFK 13.8	15705	Rock Bass	fillet	–	–	1	June 2010
EFK 6.3	16967	Rock Bass	fillet	–	–	1	June 2011
EFK 6.3	16968	Rock Bass	fillet	–	–	1	June 2011
EFK 6.3	16972	Rock Bass	fillet	–	–	1	June 2011
EFK 6.3	15690	Redbreast Sunfish	fillet	–	–	1	June 2010
EFK 6.3	15691	Redbreast Sunfish	fillet	–	–	1	June 2010
EFK 6.3	15693	Redbreast Sunfish	fillet	–	–	1	June 2010
EFK 6.3	16976	Redbreast Sunfish	fillet	–	–	1	June 2011
EFK 6.3	102-R1	Shiner	fillet	12.8 cm	–	1	June 2014
EFK 6.3	102-R2	Shiner	fillet	10.3 cm	–	1	June 2014
EFK 6.3	102-R3	Shiner	fillet	9.3 cm	–	1	June 2014
EFK 6.3	102-R4	Shiner	fillet	7.2 cm	–	1	June 2014
EFK 6.3	100	Stoneroller Minnow	fillet	14.8 cm	–	1	June 2012
EFK 6.3	101-R1	Stoneroller Minnow	fillet	16.5 cm	–	1	July 2013
EFK 6.3	101-R2	Stoneroller Minnow	fillet	16.0 cm	–	1	July 2013
EFK 6.3	101-R3	Stoneroller Minnow	fillet	14.3 cm	–	1	July 2013
EFK 6.3	101-R4	Stoneroller Minnow	fillet	13.5 cm	–	1	July 2013
EFK 6.3	15680	Stoneroller Minnow	whole body	–	–	1	June 2010
EFK 6.3	15681	Stoneroller Minnow	whole body	–	–	1	June 2010
EFK 6.3	15682	Stoneroller Minnow	whole body	–	–	1	June 2010
EFK 6.3	30	FH & SC Mayfly Larvae	whole body	–	–	–	Aug 2014
EFK 6.3	31	Net-Spinning Caddisfly Larvae	whole body	–	–	–	Aug 2014
EFK 6.3	32	Snail	soft tissue	21-25 mm	–	12	Aug 2014
EFK 6.3	33	Snail	soft tissue	17-18 mm	–	51	Aug 2014
EFK 6.3	34	Snail	soft tissue	12-13 mm	–	76	Aug 2014
EFK 6.3	35	Snail	soft tissue	10-11 mm	–	78	Aug 2014
EFK 6.3	36	Asian Clam	soft tissue	21-23 mm	–	10	Aug 2014
EFK 6.3	37	Asian Clam	soft tissue	17-18 mm	–	16	Aug 2014
EFK 6.3	38	Asian Clam	soft tissue	12-13 mm	–	25	Aug 2014

EFK 6.3	40	Crayfish	soft tissue	30-33 mm	male	4	May & Aug 2014
EFK 6.3	41	Crayfish	soft tissue	25-30 mm	male	8	May & Aug 2014
EFK 6.3	42	Crayfish	soft tissue	23-24 mm	male	2	May & Aug 2014
EFK 6.3	43	Crayfish	soft tissue	15-19 mm	male	3	May & Aug 2014
EFK 6.3	45	Crayfish	soft tissue	32-33 mm	female	2	May & Aug 2014
EFK 6.3	46	Crayfish	soft tissue	28-29 mm	female	2	May & Aug 2014
EFK 6.3	48	Crayfish	soft tissue	15-20 mm	female	2	May & Aug 2014

Fish and aquatic invertebrates were collected from various sites along Hinds Creek (HC) and East Fork Poplar Creek (EFPC). Site ID refers to the sampling location identified by the number of kilometers upstream of the confluence either of the Clinch River and HC (HCK #), or of Poplar Creek and EFPC (EFK #). Note that FH & SC stands for flathead and spiny crawler mayfly larvae.

Table S4.2a. THg and MeHg concentrations, and C and N isotope ratios of Hinds Creek aquatic organisms.

Site ID	Sample ID	Organism Type	THg (ng g^{-1})	MeHg (ng g^{-1})	%MeHg	C (wt %)	N (wt %)	$\delta^{13}C_{VPDB}$ (‰)	$\delta^{15}N_{AIR}$ (‰)	n_1	n_2 (THg)	n_2 (MeHg)	n_3 (MeHg)	n_2 (C, N)
HCK 20.6	15611	Rock Bass	402	451	112	43.4	13.3	-25.68	11.24	1	1	1	–	1
HCK 20.6	15612	Rock Bass	445	476	107	42.7	13.4	-25.89	11.54	1	1	1	–	1
HCK 20.6	15616	Rock Bass	700 ± 7	751 ± 98	107	45.8	14.3	-26.00	12.32	2	2	2	–	2
HCK 20.6	16961	Rock Bass	811	929 ± 7	115	44.9	14.5	-26.43	12.06	1	1	2	2	1
HCK 20.6	16962	Rock Bass	1260	1329	105	42.9	13.8	-25.54	11.60	1	1	1	–	1
HCK 20.6	16965	Rock Bass	1842	1829	99	45.0	13.8	-26.53	12.61	1	1	1	–	2
HCK 20.6	16951	Redbreast Sunfish	182	188	103	42.5	11.8	-26.30	10.95	1	1	1	–	1
HCK 20.6	16952	Redbreast Sunfish	199	219	110	42.6	12.8	-25.61	9.38	1	1	1	–	1
HCK 20.6	16955	Redbreast Sunfish	204 ± 20	231	113	44.8	14.1	-25.64	10.86	2	2	1	–	2
HCK 20.6	15604	Stoneroller Minnow	80	65	80	44.1	5.9	-31.74	10.67	1	1	1	–	1
HCK 20.6	15605	Stoneroller Minnow	71 ± 3	59 ± 4	83	41.3	5.4	-31.78	10.75	2	2	2	–	2
HCK 20.6	16957	Stoneroller Minnow	60	55	92	46.5	6.8	-30.80	10.48	1	1	1	–	1
HCK 20.6	16958	Stoneroller Minnow	53	47	88	40.4	6.1	-31.05	10.25	1	1	1	–	1
HCK 20.6	16959	Stoneroller Minnow	52	–	–	44.9	6.3	-30.97	10.67	1	1	–	–	1
HCK 20.6	1	Aquatic Earthworm	113	42	37	33.2	8.0	-27.93	8.29	1	1	1	–	1
HCK 20.6	2	Water Penny Beetle	21	10	45	45.7	9.7	-32.42	7.62	1	1	1	–	1
HCK 20.6	3	Dragonfly Larvae	88	90	103	45.2	10.8	-28.58	8.60	1	1	1	–	1
HCK 20.6	4	Riffle Beetle Larvae	23	12	50	46.3	10.2	-29.11	7.47	1	1	1	–	1
HCK 20.6	5	Typical Caddisfly Larvae	25	16	62	49.3	9.6	-29.03	5.92	1	1	1	–	1
HCK 20.6	6	Net-Spinning Caddisfly Larvae	86	–	–	–	–	–	–	1	1	–	–	1
HCK 20.6	8	FH & SC Mayfly Larvae	50	23	47	47.7	10.7	-31.40	8.14	1	1	1	–	1
HCK 20.6	9	Burrowing Mayfly Larvae	71	52	73	41.3	10.5	-28.28	7.15	1	1	1	–	1

HCK 20.6	10	Snipe Fly Larvae	152	138 ± 16	89	41.5	10.3	-28.96	10.04	1	1	2	–	1
HCK 20.6	11	Megaloptera Larvae	105 ± 5	92	88	44.9	10.9	-29.91	8.75	1	2	1	–	1
HCK 20.6	12	Megaloptera Larvae	131	110 ± 8	84	44.9	11.3	-28.97	8.59	1	1	2	2	1
HCK 20.6	13	Snail	63	39	62	35.4	8.3	-27.06	9.75	1	1	1	–	1
HCK 20.6	14	Snail	178	61 ± 1	34	37.9	8.0	-28.71	9.40	1	1	2	2	1
HCK 20.6	15	Snail	106 ± 2	73	69	39.2	8.2	-28.91	9.19	1	2	1	–	1
HCK 20.6	16	Snail	107	70	65	37.2	8.1	-28.61	8.68	1	1	1	–	1
HCK 20.6	17	Asian Clam	205	122	59	45.2	10.1	-27.72	6.83	1	1	1	–	1
HCK 20.6	18	Asian Clam	195	119	61	42.9	9.8	-27.56	6.78	1	1	1	–	1
HCK 20.6	19	Asian Clam	195	119	61	43.7	10.0	-27.53	6.76	1	1	1	–	2
HCK 20.6	20	Crayfish	163	–	–	44.5	13.5	-28.40	9.76	1	1	1	–	1
HCK 20.6	21	Crayfish	233	238	102	42.8	12.6	-29.44	9.76	1	1	1	–	1
HCK 20.6	22	Crayfish	135	143	106	43.3	13.2	-29.68	9.85	1	1	1	–	1
HCK 20.6	23	Crayfish (whole body)	51	41	80	34.4	8.1	-29.74	8.83	1	1	1	–	1
HCK 20.6	24	Crayfish	262	262	100	43.7	13.3	-29.40	9.85	1	1	1	–	1
HCK 20.6	25	Crayfish	165	159	97	40.9	12.5	-29.77	9.83	1	1	1	–	1
HCK 20.6	26	Crayfish (whole body)	53	43	81	35.1	8.0	-29.46	8.62	1	1	1	–	2

See Table S4.2c for notes.

Table S4.2b. THg and MeHg concentrations, and C and N isotope ratios of upstream EFPC aquatic organisms.

Site ID	Sample ID	Organism Type	THg (ng g^{-1})	MeHg (ng g^{-1})	%MeHg	C (wt %)	N (wt %)	$\delta^{13}C_{VPDB}$ (‰)	$\delta^{15}N_{AIR}$ (‰)	n_1	n_2 (THg)	n_2 (MeHg)	n_3 (MeHg)	n_2 (C, N)
EFK 24.2	15800	Rock Bass	5490	5681	103	44.6	14.1	-23.91	11.33	1	1	1	–	1
EFK 24.2	15998	Rock Bass	3405	3714	109	46.4	14.6	-23.66	10.92	1	1	1	–	1
EFK 24.2	15999	Rock Bass	4412	4906	111	41.7	13.3	-23.04	10.87	1	1	1	–	1
EFK 23.4	15801	Rock Bass	2045	2123	104	40.2	12.9	-24.10	10.93	1	1	1	–	1
EFK 23.4	15802	Rock Bass	2435	2649	109	40.3	12.6	-23.89	11.45	1	1	1	–	1
EFK 23.4	15803	Rock Bass	3291 ± 142	3296 ± 8	100	49.5	13.9	-24.27	11.65	2	2	3	2	1
EFK 23.4	15993	Redbreast Sunfish	1308	1339	102	42.2	13.2	-23.33	8.82	1	1	1	–	1
EFK 23.4	15995	Redbreast Sunfish	2229 ± 118	2364 ± 28	106	44.4	13.1	-23.77	7.98	2	2	3	2	3
EFK 23.4	103-R1	Shiner	1289	1280	99	42.7	13.3	-23.09	8.49	1	1	1	–	1
EFK 23.4	103-R2	Shiner	1063	959 ± 15	90	44.6	13.8	-22.88	9.33	1	1	2	–	4
EFK 23.4	103-R4	Shiner	1557	1434	92	45.8	13.8	-22.78	9.90	1	1	1	–	1
EFK 23.4	103-R5	Shiner	1508	1323 ± 50	88	44.2	13.5	-22.86	9.93	1	1	2	–	1
EFK 23.4	103-R6	Shiner	1625	1478	91	45.2	13.6	-22.24	10.56	1	1	1	–	1
EFK 23.4	15988	Stoneroller Minnow	1647	169	10	–	–	–	–	1	1	1	–	–
EFK 23.4	15989	Stoneroller Minnow	1725	221	13	41.4	6.9	-27.27	8.76	1	1	1	–	1
EFK 23.4	15990	Stoneroller Minnow	2020 ± 75	215 ± 8	11	46.7	7.3	-26.07	8.75	2	2	2	–	2
EFK 23.4	71	Megaloptera Larvae	2689	250	9	45.2	11.2	-21.42	8.61	1	1	1	–	1
EFK 23.4	72	Megaloptera Larvae	2212	255 ± 10	12	48.9	11.0	-21.76	8.72	1	1	3	2	1
EFK 23.4	73	Asian Clam	9865	457	5	43.7	11.0	-22.92	7.21	1	1	1	–	1
EFK 23.4	74	Asian Clam	8064	348	4	42.7	10.6	-22.81	7.08	1	1	1	–	1
EFK 23.4	75	Crayfish	2164	1268	59	42.6	12.8	-22.57	8.03	1	1	1	–	1
EFK 23.4	76	Crayfish	2449 ± 103	921	38	43.5	13.2	-21.48	9.08	1	2	1	–	2

EFK 23.4	77	Crayfish	3713	1020	27	37.6	11.6	-21.24	9.22	1	1	1	–	1
EFK 23.4	78	Crayfish	1697	650	38	46.4	14.1	-20.43	9.31	1	1	1	–	1
EFK 23.4	79	Crayfish	1848	1168	63	43.2	13.5	-21.92	8.86	1	1	1	–	1
EFK 23.4	80	Crayfish	2740	1036 ± 93	38	41.8	12.8	-21.60	8.99	1	1	2	–	1
EFK 23.4	81	Crayfish	2516	1015	40	43.7	13.1	-21.35	9.24	1	1	1	–	1
EFK 23.4	82	Crayfish	2355	727	31	41.8	12.8	-20.46	9.29	1	1	1	–	1
EFK 22.3	51	Aquatic Earthworm	10902	209	2	28.0	6.2	-24.17	7.69	1	1	1	–	1
EFK 22.3	52	Minnow Mayfly Larvae	3422	134	4	46.8	10.7	-24.40	6.91	1	1	1	–	1
EFK 22.3	53	FH & SC Mayfly Larvae	2474 ± 38	103	4	43.3	10.2	-24.78	6.06	1	2	1	–	2
EFK 22.3	54	Net-Spinning Caddisfly Larvae	4209	164	4	44.0	10.7	-24.04	6.79	1	1	1	–	1
EFK 22.3	55	Darners Dragonfly Larvae	1270	358	28	43.6	11.3	-24.04	7.44	1	1	1	–	1
EFK 22.3	57	Megaloptera Larvae	3569	447 ± 11	13	49.1	11.1	-23.90	8.43	1	1	5	2	1
EFK 22.3	58	Megaloptera Larvae	2080	352 ± 10	17	47.3	11.4	-23.87	8.08	1	1	3	2	2
EFK 22.3	59	Asian Clam	10019	563	6	44.0	11.5	-24.59	7.38	1	1	1	–	1
EFK 22.3	60	Asian Clam	7539	532 ± 9	7	43.2	11.2	-24.32	7.27	1	1	3	–	1
EFK 22.3	61	Asian Clam	6195	391 ± 2	6	44.8	11.4	-24.00	7.26	1	1	4	2	1
EFK 22.3	62	Crayfish	1596	1175	74	48.1	14.9	-23.08	8.18	1	1	1	–	1
EFK 22.3	63	Crayfish	1580 ± 445	1091	69	44.7	14.0	-23.03	8.46	1	2	1	–	1
EFK 22.3	64	Crayfish	1569	1017	65	46.7	14.5	-22.93	8.26	1	1	1	–	1
EFK 22.3	65	Crayfish	1477	1131	77	46.3	14.5	-23.42	8.56	1	1	1	–	1
EFK 22.3	67	Crayfish	1505	861	57	45.5	14.3	-22.97	8.43	1	1	1	–	1
EFK 22.3	68	Crayfish	1698	1043 ± 13	61	45.9	14.1	-23.38	8.30	1	1	4	2	1
EFK 22.3	69	Crayfish	1640	1122 ± 12	68	46.5	14.6	-23.00	8.23	1	1	3	2	1

See Table S4.2c for notes.

Table S4.2c. THg and MeHg concentrations, and C and N isotope ratios of midstream and downstream EFPC aquatic organisms.

Site ID	Sample ID	Organism Type	THg (ng g^{-1})	MeHg (ng g^{-1})	%MeHg	C (wt %)	N (wt %)	$\delta^{13}C_{VPDB}$ (‰)	$\delta^{15}N_{AIR}$ (‰)	n_1	n_2 (THg)	n_2 (MeHg)	n_3 (MeHg)	n_2 (C, N)
EFK 18.2	15714	Rock Bass	3969	4101	103	49.7	12.5	-25.12	9.86	1	1	1	–	1
EFK 18.2	15715	Rock Bass	4161	5189	125	45.6	14.8	-23.63	10.46	1	1	1	–	1
EFK 13.8	15704	Rock Bass	3731	4204	113	44.9	14.4	-24.81	11.81	1	1	1	–	1
EFK 13.8	15705	Rock Bass	4118	4497	109	45.0	14.3	-25.10	11.95	1	1	1	–	1
EFK 6.3	16967	Rock Bass	3334	3788	114	41.8	12.8	-26.06	13.39	1	1	1	–	1
EFK 6.3	16968	Rock Bass	3109	3441	111	45.7	14.6	-26.00	12.75	1	1	1	–	1
EFK 6.3	16972	Rock Bass	7759 ± 203	8075 ± 240	104	45.1	14.5	-26.18	13.91	2	2	2	–	2
EFK 6.3	15690	Redbreast Sunfish	2000	2141	107	47.9	12.2	-26.74	13.27	1	1	1	–	1
EFK 6.3	15691	Redbreast Sunfish	2709	2712	100	45.4	12.7	-26.08	11.42	1	1	1	–	1
EFK 6.3	15693	Redbreast Sunfish	2782 ± 163	2947 ± 112	106	42.9	13.4	-24.97	12.18	2	2	2	–	2
EFK 6.3	16976	Redbreast Sunfish	2851 ± 44	3343 ± 359	117	45.1	14.2	-25.47	12.41	2	2	2	–	2
EFK 6.3	102-R1	Shiner	1742	1942	111	44.9	14.3	-26.60	12.92	1	1	1	–	1
EFK 6.3	102-R2	Shiner	1748	1845 ± 50	106	41.9	12.5	-26.88	13.16	1	1	3	2	1
EFK 6.3	102-R3	Shiner	1715	1868	109	43.7	13.2	-25.75	12.06	1	1	1	–	1
EFK 6.3	102-R4	Shiner	1604	1664 ± 24	104	43.3	13.0	-24.31	11.75	1	1	5	2	1
EFK 6.3	100	Stoneroller Minnow	1215	1247	103	49.3	12.7	-29.25	13.08	1	1	1	–	1
EFK 6.3	101-R1	Stoneroller Minnow	687	723	105	51.1	12.3	-29.14	13.71	1	1	1	–	1
EFK 6.3	101-R2	Stoneroller Minnow	905	914	101	48.2	12.0	-29.31	13.41	1	1	1	–	1
EFK 6.3	101-R3	Stoneroller Minnow	1278	1323	104	52.9	15.5	-29.23	13.13	1	1	1	–	1
EFK 6.3	101-R4	Stoneroller Minnow	1613	1716 ± 14	106	48.3	13.3	-29.63	13.37	1	1	2	2	2
EFK 6.3	15680	Stoneroller Minnow	786	431	55	43.3	6.0	-31.62	11.89	1	1	1	–	1
EFK 6.3	15681	Stoneroller Minnow	1106	785 ± 22	71	42.5	6.0	-31.61	12.41	1	1	2	–	2

EFK 6.3	15682	Stoneroller Minnow	1130 ± 2	740 ± 88	65	41.6	6.1	-31.31	12.45	2	2	2	–	2
EFK 6.3	30	FH & SC Mayfly Larvae	1633	204 ± 10	12	46.0	10.2	-30.19	10.40	1	1	4	2	1
EFK 6.3	31	Net-Spinning Caddisfly Larvae	5303 ± 320	392	7	34.6	8.2	-28.78	10.52	1	2	1	–	2
EFK 6.3	32	Snail	4291	782	18	34.4	8.1	-27.39	12.55	1	1	1	–	1
EFK 6.3	33	Snail	3967	927 ± 43	23	36.7	8.6	-27.01	12.35	1	1	2	2	2
EFK 6.3	34	Snail	3391	835 ± 1	25	33.0	7.9	-27.29	12.44	1	1	2	–	1
EFK 6.3	35	Snail	3390	719 ± 2	21	35.2	8.7	-27.46	12.46	1	1	2	–	1
EFK 6.3	36	Asian Clam	5828	959 ± 8	16	44.6	10.4	-25.58	9.75	1	1	2	–	1
EFK 6.3	37	Asian Clam	3946	989 ± 11	25	43.3	10.0	-25.84	9.36	1	1	2	–	1
EFK 6.3	38	Asian Clam	3723	1089	29	42.8	10.5	-25.68	9.34	1	1	1	–	1
EFK 6.3	40	Crayfish	1212	1177	97	33.2	10.3	-27.86	12.43	1	1	1	–	1
EFK 6.3	41	Crayfish	1271	1142 ± 28	90	47.7	14.7	-27.15	12.46	1	1	2	2	1
EFK 6.3	42	Crayfish	1207	1090	90	43.5	13.1	-28.01	13.05	1	1	1	–	1
EFK 6.3	43	Crayfish	2470	–	–	46.4	13.8	-28.19	12.85	1	1	–	–	1
EFK 6.3	45	Crayfish	1288	1234	96	44.5	13.6	-27.77	12.36	1	1	1	–	1
EFK 6.3	46	Crayfish	1448	1522	105	43.0	13.5	-27.41	11.66	1	1	1	–	1
EFK 6.3	48	Crayfish	1669	1568	94	45.9	14.1	-27.72	12.92	1	1	1	–	1

Fish and aquatic invertebrates were collected from various sites along Hinds Creek (HC) and East Fork Poplar Creek (EFPC). Site ID refers to the sampling location identified by the number of kilometers upstream of the confluence either of the Clinch River and HC (HCK #), or of Poplar Creek and EFPC (EFK #). Note that FH & SC stands for flathead and spiny crawler mayfly larvae. Here, n_1 denotes the number of sample replicates that were ground independently prior to analysis, n_2 (THg) denotes the number of combustion preparations, n_2 (MeHg) denotes the number of nitric acid digestion preparations, n_3 (MeHg) denotes the number of independent nitric acid digestion matrix spike tests performed on the material, and n_2 (C, N) denotes the number of sample preparations for C and N concentration (percentage by weight) and isotopic analysis. Percent MeHg (%MeHg) in the solid material was calculated by dividing the measured MeHg concentration (via nitric acid digestion) by the measured THg concentration (via combustion).

Table S4.3. C and N isotope ratios of reference materials and of Hinds Creek and EFPC biofilm.

Site ID	Sample Collection Date	Standard Name	Standard or Sample Type	n	C (wt %)	N (wt %)	$\delta^{13}C_{VPDB}$ (‰)	$\delta^{15}N_{AIR}$ (‰)
Reference Materials	–	IU Acetanilide	acetanilide	7	71.1 ± 1.0	10.4 ± 0.2	-29.49 ± 0.05	0.91 ± 0.20
	–	USGS41	L-glutamic acid	5	43.2 ± 0.2	9.9 ± 0.2	36.48 ± 0.16	47.45 ± 0.29
	–	USGS25	ammonium sulfate	6	–	–	–	-29.70 ± 0.24
	–	IAEA-N-2	ammonium sulfate	6	–	–	–	20.57 ± 0.12
	–	IAEA-600	caffeine	6	48.1 ± 1.4	28.8 ± 0.9	-27.77 ± 0.01	0.87 ± 0.09
	–	IAEA-CH-6	sucrose	6	40.6 ± 3.3	–	-10.67 ± 0.02	13.28 ± 3.31
	–	Oak	oak	4	46.9 ± 0.1	1.5 ± <0.1	-28.78 ± 0.08	1.01 ± 0.19
HCK 20.6	Oct 2011	–	biofilm	1	11.5	1.5	-29.41	6.78
HCK 20.6	April 2012	–	biofilm	1	8.4	1.3	-28.52	8.12
HCK 20.6	Aug 2012	–	biofilm	2	8.9	1.1	-27.89	5.37
EFK 22.3	Oct 2011	–	biofilm	1	14.3	2.1	-24.70	6.02
EFK 22.3	April 2012	–	biofilm	1	18.0	2.4	-18.10	5.52
EFK 22.3	Aug 2012	–	biofilm	1	21.2	2.4	-16.99	4.75
EFK 5.0	Oct 2011	–	biofilm	2	11.0	1.2	-22.35	8.76
EFK 5.0	April 2012	–	biofilm	1	14.5	2.0	-24.47	8.56

Biofilm was collected from Hinds Creek (HC) and East Fork Poplar Creek (EFPC). Site ID refers to the sampling location identified by the number of kilometers upstream of the confluence either of the Clinch River and HC (HCK #), or of Poplar Creek and EFPC (EFK #). Here, n denotes the number of sample preparations for C and N concentration (percentage by weight) and isotopic analysis.

Table S4.4. THg and MeHg concentrations and recovery for biological reference materials.

Standard Name	Standard Type	THg (ng g^{-1})	Combustion %Rec. of THg (± 1SD)	MeHg (ng g^{-1})	HNO_3 Digestion %Rec. of MeHg	%MeHg	n_1 (THg)	n_1 (MeHg)	n_2 (MeHg)
DORM-3	fish protein	372 ± 9 (382 ± 60)	97.5 ± 2.4	335 ± 13 (355 ± 56)	94.2 ± 2.3	90 (93)	7	15	4
TORT-2	lobster hepatopancreas	271 ± 5 (270 ± 60)	100.5 ± 1.7	162 ± 5 (152 ± 13)	106.7 ± 3.2	60 (56)	5	15	4
DOLT-2	dogfish liver	2119 ± 60 (1990 ± 100)	106.5 ± 3.0	793 ± 11 (693 ± 53)	114.4 ± 1.6	37 (35)	2	6	2
DOLT-5	dogfish liver	– (440 ± 180)	–	129 ± 3 (119 ± 58)	108.6 ± 2.9	– (27)	–	18	2

Certified THg and MeHg concentrations (± expanded uncertainty) of the biological reference materials are provided in parentheses below our measured THg and MeHg concentrations (±1SD). Recovery (%Rec) of THg after combustion and recovery of MeHg after nitric acid digestion were calculated relative to the certified THg and MeHg concentrations for each of the reference materials. Here, n_1 (THg) denotes the number of combustion preparations, n_1 (MeHg) denotes the number of nitric acid digestion preparations, and n_2 (MeHg) denotes the number of independent nitric acid digestion matrix spike tests performed on the material. Percent MeHg (%MeHg) in the solid material was calculated by dividing the measured MeHg concentration (via nitric acid digestion) by the measured THg concentration (via combustion), with the same calculation using certified MeHg and THg concentrations provided in parentheses (note that DOLT-5 was not analyzed for its THg concentration via combustion).

Table S4.5. THg isotopic composition of UM-Almadén, aqueous MeHgCl stock, and procedural standards.

Standard Type	n_1	n_2	Transfer or P+T %Rec. of THg (± 1SD)	δ^{202}THg (‰)	2σ (‰)	Δ^{204}THg (‰)	2σ (‰)	Δ^{201}THg (‰)	2σ (‰)	Δ^{200}THg (‰)	2σ (‰)	Δ^{199}THg (‰)	2σ (‰)
UM-Almadén (analyzed alongside combustion samples)	17	130	–	-0.56	0.01 *0.08*	0.01	0.01 *0.09*	0.04	0.00 *0.05*	0.01	0.01 *0.04*	0.02	0.00 *0.06*
UM-Almadén (analyzed alongside resin separation samples)	4	22	–	-0.55	0.02 *0.05*	0.01	0.03 *0.07*	0.03	0.00 *0.04*	0.01	0.01 *0.03*	0.02	0.01 *0.04*
Aqueous MeHgCl Stock (Brooks Rand)	3	6	–	-1.21	0.02 *0.04*	-0.01	0.02 *0.03*	0.05	0.01 *0.03*	0.02	0.02 *0.03*	0.10	0.02 *0.02*
Purge & Trap NIST SRM 3133	3	3	98.5 ± 0.7	0.01	0.03	-0.02	0.01	0.00	0.02	0.03	0.04	0.01	0.02
DORM-3 (Fish Protein)	7	24	99.0 ± 1.7	0.47	0.02 *0.08*	-0.09	0.02 *0.08*	1.48	0.01 *0.04*	0.07	0.01 *0.02*	1.80	0.01 *0.03*
DORM-3 (Fish Protein) Long-term average	32	–	–	0.48	0.02	-0.09	0.01	1.48	0.01	0.06	0.01	1.80	0.01
TORT-2 (Lobster Hepatopancreas)	5	16	96.7 ± 4.5	0.04	0.03 *0.05*	-0.09	0.01 *0.06*	0.61	0.01 *0.05*	0.06	0.01 *0.02*	0.75	0.01 *0.03*
TORT-2 (Lobster Hepatopancreas) Long-term average	89	–	–	0.06	0.02	-0.09	0.02	0.59	0.01	0.06	0.01	0.75	0.01
DOLT-2 (Dogfish Liver)	2	6	98.4 ± 2.7	-0.52	0.03 *0.05*	-0.02	0.02 *0.04*	0.62	0.04 *0.06*	0.02	0.05 *0.03*	0.72	0.05 *0.06*
DOLT-2 (Dogfish Liver) Long-term average	17	–	–	-0.51	0.01	-0.03	0.02	0.60	0.01	0.03	0.01	0.73	0.01

For UM-Almadén and the brominated aqueous MeHgCl stock, n_1 denotes the number of preparations (i.e., the number of session averages, with preparations at different concentrations counted separately). For the purge and trap procedural standard and combustion reference materials, n_1 denotes the number of independent preparations of the material. For all standards and reference materials, n_2 denotes the number of separate isotopic analyses on an individual preparation(s). Transfer or purge-and-trap (P+T) %Rec indicates the recovery of Hg during the transfer (for biological reference materials) or purge-and-trap pre-

concentration step. Isotope ratios show the average value (± 2SE) across independent preparations for each standard type. For UM-Almadén, the aqueous MeHgCl stock, and biological reference materials, the average uncertainty (2SD) across all analyses is also provided in italics. Long-term average isotopic compositions (± 2SE) are included for comparison (Blum and Johnson 2017).

Table S4.6a. THg isotopic composition of Hinds Creek aquatic organisms.

Site ID	Sample ID	Organism Type	Sample Type	Transfer %Rec. of THg	n	δ^{202}THg (‰)	2σ (‰)	Δ^{204}THg (‰)	2σ (‰)	Δ^{201}THg (‰)	2σ (‰)	Δ^{200}THg (‰)	2σ (‰)	Δ^{199}THg (‰)	2σ (‰)
HCK 20.6	15611	Rock Bass	fillet	103.2	2	-1.16	0.07	-0.02	0.07	-0.03	0.05	0.05	0.03	0.00	0.03
HCK 20.6	15612	Rock Bass	fillet	<85.0		Low transfer recovery.									
HCK 20.6	15616	Rock Bass	fillet	107.6 ± 5.0	4	-1.13	0.07	-0.06	0.07	-0.06	0.05	0.04	0.03	-0.03	0.03
HCK 20.6	16961	Rock Bass	fillet	<85.0		Low transfer recovery.									
HCK 20.6	16962	Rock Bass	fillet	95.3	2	-1.10	0.07	-0.16	0.07	-0.08	0.05	0.08	0.03	0.02	0.03
HCK 20.6	16965	Rock Bass	fillet	94.6	2	-1.03	0.07	-0.07	0.07	-0.02	0.05	0.03	0.03	0.08	0.03
HCK 20.6	16951	Redbreast Sunfish	fillet	93.6	1	-1.22	0.07	-0.09	0.07	-0.08	0.05	0.00	0.03	-0.13	0.03
HCK 20.6	16952	Redbreast Sunfish	fillet	96.8	1	-1.19	0.07	0.03	0.07	-0.08	0.05	0.02	0.03	-0.09	0.03
HCK 20.6	16955	Redbreast Sunfish	fillet	97.4 ± 0.7	2	-1.22	0.07	-0.02	0.07	-0.06	0.05	0.01	0.03	-0.11	0.03
HCK 20.6	15604	Stoneroller Minnow	WB	96.6	1	-1.06	0.07	-0.13	0.07	-0.02	0.05	0.02	0.03	0.10	0.03
HCK 20.6	15605	Stoneroller Minnow	WB	104.2 ± 2.0	2	-1.12	0.07	-0.11	0.07	-0.04	0.05	0.05	0.03	0.00	0.03
HCK 20.6	16957	Stoneroller Minnow	WB	87.7	1	-1.08	0.07	-0.09	0.07	0.01	0.05	0.01	0.03	0.06	0.03
HCK 20.6	16958	Stoneroller Minnow	WB	<85.0		Low transfer recovery.									
HCK 20.6	16959	Stoneroller Minnow	WB	90.4	1	-1.25	0.07	-0.12	0.07	-0.03	0.05	0.08	0.03	0.04	0.03
HCK 20.6	1	Aquatic Earthworm	WB	101.0	1	-1.22	0.07	-0.16	0.07	-0.20	0.05	0.08	0.03	-0.18	0.03
HCK 20.6	2	Water Penny Beetle	WB	97.3	1	-1.60	0.07	0.09	0.07	-0.23	0.05	-0.01	0.03	-0.15	0.03
HCK 20.6	3	Dragonfly Larvae	WB	98.5	1	-1.28	0.07	-0.03	0.07	-0.09	0.05	0.03	0.03	-0.06	0.03
HCK 20.6	4	Riffle Beetle Larvae	WB	98.8	1	-1.48	0.07	-0.08	0.07	-0.13	0.05	0.08	0.03	-0.11	0.03
HCK 20.6	5	Typical Caddisfly Larvae	WB	98.3	1	-1.31	0.07	-0.08	0.07	-0.11	0.05	0.04	0.03	-0.11	0.03
HCK 20.6	6	Net-Spinning Caddisfly Larvae	WB			Insufficient mercury for isotopic analysis.									
HCK 20.6	8	FH & SC Mayfly Larvae	WB	99.4	1	-1.31	0.07	-0.08	0.07	-0.14	0.05	0.02	0.03	-0.12	0.03
HCK 20.6	9	Burrowing Mayfly Larvae	WB	99.6	1	-1.36	0.07	0.01	0.07	-0.19	0.05	0.04	0.03	-0.19	0.03

HCK 20.6	10	Snipe Fly Larvae	WB	98.5	2	-1.18	0.07	-0.09	0.07	-0.09	0.05	0.02	0.03	0.01	0.03
HCK 20.6	11	Megaloptera Larvae	WB	98.0 ± 1.1	4	-1.34	0.07	-0.06	0.07	-0.01	0.05	0.03	0.03	0.03	0.03
HCK 20.6	12	Megaloptera Larvae	WB	100.6	2	-1.32	0.07	-0.05	0.07	-0.05	0.05	0.02	0.03	0.00	0.03
HCK 20.6	13	Snail	soft tissue	95.9	1	-1.36	0.07	0.00	0.07	-0.13	0.05	0.04	0.03	-0.10	0.03
HCK 20.6	14	Snail	soft tissue	114.2	2	-1.24	0.07	-0.05	0.07	-0.13	0.05	0.02	0.03	-0.07	0.03
HCK 20.6	15	Snail	soft tissue	100.2	2	-1.18	0.07	0.00	0.07	-0.08	0.05	0.04	0.03	-0.05	0.03
HCK 20.6	16	Snail	soft tissue	101.2	2	-1.13	0.07	-0.05	0.07	-0.13	0.05	0.02	0.03	-0.09	0.03
HCK 20.6	17	Asian Clam	soft tissue	102.0	2	-1.04	0.07	-0.06	0.07	-0.08	0.05	0.02	0.03	-0.03	0.03
HCK 20.6	18	Asian Clam	soft tissue	101.7	2	-1.03	0.07	-0.04	0.07	-0.11	0.05	0.01	0.03	-0.04	0.03
HCK 20.6	19	Asian Clam	soft tissue	99.4	2	-1.02	0.07	-0.05	0.07	-0.09	0.05	0.02	0.03	-0.02	0.03
HCK 20.6	20	Crayfish	soft tissue	96.1	1	-1.20	0.07	-0.06	0.07	-0.08	0.05	0.11	0.03	-0.05	0.03
HCK 20.6	21	Crayfish	soft tissue	95.2	1	-1.23	0.07	0.00	0.07	0.00	0.05	0.01	0.03	-0.02	0.03
HCK 20.6	22	Crayfish	soft tissue	98.7	2	-1.07	0.07	-0.05	0.07	0.03	0.05	0.04	0.03	0.11	0.03
HCK 20.6	23	Crayfish	WB	100.3	2	-1.17	0.07	-0.03	0.07	-0.02	0.05	0.03	0.03	0.03	0.03
HCK 20.6	24	Crayfish	soft tissue	96.0	2	-1.25	0.07	-0.05	0.07	-0.01	0.05	0.03	0.03	0.08	0.03
HCK 20.6	25	Crayfish	soft tissue	98.0	2	-1.15	0.07	0.00	0.07	0.03	0.05	0.02	0.03	0.08	0.03
HCK 20.6	26	Crayfish	WB	97.5	2	-1.19	0.07	-0.04	0.07	-0.02	0.05	0.04	0.03	0.02	0.03

See Table S4.6c for notes.

Table S4.6b. THg isotopic composition of upstream EFPC aquatic organisms.

Site ID	Sample ID	Organism Type	Sample Type	Transfer %Rec. of THg	n	δ^{202}THg (‰)	2σ (‰)	Δ^{204}THg (‰)	2σ (‰)	Δ^{201}THg (‰)	2σ (‰)	Δ^{200}THg (‰)	2σ (‰)	Δ^{199}THg (‰)	2σ (‰)
EFK 24.2	15800	Rock Bass	fillet	94.4	2	-0.72	0.07	-0.01	0.07	-0.05	0.05	-0.01	0.03	-0.05	0.03
EFK 24.2	15998	Rock Bass	fillet	102.7	2	-0.61	0.07	-0.03	0.07	0.04	0.05	0.01	0.03	0.06	0.03
EFK 24.2	15999	Rock Bass	fillet	106.6	2	-0.63	0.07	0.06	0.07	0.06	0.05	0.00	0.03	0.03	0.03
EFK 23.4	15801	Rock Bass	fillet	94.4	2	-0.68	0.07	0.00	0.07	0.10	0.05	-0.01	0.03	0.10	0.03
EFK 23.4	15802	Rock Bass	fillet	94.4	2	-0.49	0.07	-0.07	0.07	0.05	0.05	0.00	0.03	0.11	0.03
EFK 23.4	15803	Rock Bass	fillet	93.9 ± 0.6	4	-0.53	0.07	0.00	0.07	0.06	0.05	0.02	0.03	0.08	0.03
EFK 23.4	15993	Redbreast Sunfish	fillet	101.3	2	-0.13	0.07	0.01	0.07	-0.01	0.05	0.03	0.03	0.04	0.03
EFK 23.4	15995	Redbreast Sunfish	fillet	101.6 ± 9.6	4	-0.68	0.07	0.02	0.07	0.07	0.05	0.02	0.03	0.11	0.03
EFK 23.4	103-R1	Shiner	fillet	100.6	2	-0.87	0.07	-0.05	0.07	0.09	0.05	0.01	0.03	0.14	0.03
EFK 23.4	103-R2	Shiner	fillet	99.4	2	-0.84	0.07	-0.04	0.07	0.18	0.05	0.01	0.03	0.23	0.03
EFK 23.4	103-R4	Shiner	fillet	99.0	3	-0.82	0.07	-0.05	0.07	0.19	0.05	0.02	0.03	0.26	0.03
EFK 23.4	103-R5	Shiner	fillet	98.5	2	-0.84	0.07	-0.04	0.07	0.25	0.05	0.04	0.03	0.34	0.03
EFK 23.4	103-R6	Shiner	fillet	91.0	2	-0.67	0.07	-0.04	0.07	0.20	0.05	0.01	0.03	0.30	0.03
EFK 23.4	15988	Stoneroller Minnow	WB	102.6	2	-0.22	0.07	-0.01	0.07	-0.08	0.05	-0.01	0.03	-0.10	0.03
EFK 23.4	15989	Stoneroller Minnow	WB	107.5	2	-0.14	0.07	-0.05	0.07	-0.09	0.05	0.03	0.03	-0.08	0.03
EFK 23.4	15990	Stoneroller Minnow	WB	94.5	2	-0.31	0.07	0.02	0.07	-0.06	0.05	0.00	0.03	-0.06	0.03
EFK 23.4	71	Megaloptera Larvae	WB	98.7	3	-0.90	0.07	0.01	0.07	0.09	0.05	0.00	0.03	0.12	0.03
EFK 23.4	72	Megaloptera Larvae	WB	96.0	2	-0.95	0.07	-0.02	0.07	0.06	0.05	-0.01	0.03	0.15	0.03
EFK 23.4	73	Asian Clam	soft tissue	87.9	2	-0.47	0.07	-0.01	0.07	0.04	0.05	0.01	0.03	0.08	0.03
EFK 23.4	74	Asian Clam	soft tissue	99.4	2	-0.34	0.07	0.00	0.07	0.04	0.05	0.02	0.03	0.11	0.03
EFK 23.4	75	Crayfish	soft tissue	99.1	1	-0.63	0.07	-0.02	0.07	0.03	0.05	0.02	0.03	0.09	0.03
EFK 23.4	76	Crayfish	soft tissue	99.3 ± 2.5	4	-0.57	0.07	-0.03	0.07	0.07	0.05	-0.01	0.03	0.11	0.03

EFK 23.4	77	Crayfish	soft tissue	100.1	3	-0.56	0.07	-0.02	0.07	0.06	0.05	0.01	0.03	0.09	0.03
EFK 23.4	78	Crayfish	soft tissue	96.9	1	-0.57	0.07	-0.01	0.07	0.10	0.05	0.04	0.03	0.14	0.03
EFK 23.4	79	Crayfish	soft tissue	97.9	1	-0.61	0.07	0.04	0.07	0.14	0.05	0.00	0.03	0.13	0.03
EFK 23.4	80	Crayfish	soft tissue	97.6	2	-0.65	0.07	0.00	0.07	0.06	0.05	0.01	0.03	0.13	0.03
EFK 23.4	81	Crayfish	soft tissue	98.1	3	-0.64	0.07	0.00	0.07	0.08	0.05	0.03	0.03	0.13	0.03
EFK 23.4	82	Crayfish	soft tissue	96.4	2	-0.58	0.07	0.00	0.07	0.09	0.05	0.02	0.03	0.13	0.03
EFK 22.3	51	Aquatic Earthworm	WB	97.8	2	-0.42	0.07	0.00	0.07	-0.03	0.05	0.02	0.03	-0.01	0.03
EFK 22.3	52	Minnow Mayfly Larvae	WB	96.0	2	-0.33	0.07	0.00	0.07	-0.02	0.05	0.00	0.03	-0.01	0.03
EFK 22.3	53	FH & SC Mayfly Larvae	WB	95.2 ± 3.1	5	-0.54	0.07	0.00	0.07	0.01	0.05	0.01	0.03	0.01	0.03
EFK 22.3	54	Net-Spinning Caddisfly Larvae	WB	100.0	3	-0.38	0.07	0.01	0.07	0.01	0.05	0.00	0.03	0.02	0.03
EFK 22.3	55	Darners Dragonfly Larvae	WB	98.4	2	-0.64	0.07	0.00	0.07	0.06	0.05	0.01	0.03	0.07	0.03
EFK 22.3	57	Megaloptera Larvae	WB	99.4	3	-0.76	0.07	0.01	0.07	0.00	0.05	0.00	0.03	0.02	0.03
EFK 22.3	58	Megaloptera Larvae	WB	99.7	2	-0.95	0.07	0.01	0.07	0.02	0.05	0.00	0.03	0.04	0.03
EFK 22.3	59	Asian Clam	soft tissue	97.7	3	-0.43	0.07	0.02	0.07	0.06	0.05	0.02	0.03	0.05	0.03
EFK 22.3	60	Asian Clam	soft tissue	95.1 ± 1.7	6	-0.38	0.07	-0.03	0.07	0.04	0.05	0.01	0.03	0.08	0.03
EFK 22.3	61	Asian Clam	soft tissue	96.7	3	-0.38	0.07	0.01	0.07	0.05	0.05	0.01	0.03	0.09	0.03
EFK 22.3	62	Crayfish	soft tissue	97.1	2	-0.79	0.07	-0.01	0.07	0.05	0.05	0.02	0.03	0.11	0.03
EFK 22.3	63	Crayfish	soft tissue	97.3 ± 0.8	6	-0.80	0.07	-0.01	0.07	0.08	0.05	0.02	0.03	0.14	0.03
EFK 22.3	64	Crayfish	soft tissue	97.8	2	-0.83	0.07	-0.01	0.07	0.08	0.05	0.02	0.03	0.13	0.03
EFK 22.3	65	Crayfish	soft tissue	92.7	1	-0.81	0.07	-0.01	0.07	0.06	0.05	0.02	0.03	0.12	0.03
EFK 22.3	67	Crayfish	soft tissue	89.8	2	-0.87	0.07	0.01	0.07	0.12	0.05	0.04	0.03	0.17	0.03
EFK 22.3	68	Crayfish	soft tissue	98.0	2	-0.81	0.07	-0.06	0.07	0.08	0.05	0.02	0.03	0.12	0.03
EFK 22.3	69	Crayfish	soft tissue	93.8	2	-0.77	0.07	-0.03	0.07	0.07	0.05	0.00	0.03	0.13	0.03

See Table S4.6c for notes.

Table S4.6c. THg isotopic composition of midstream and downstream EFPC aquatic organisms.

Site ID	Sample ID	Organism Type	Sample Type	Transfer %Rec. of THg	n	δ^{202}THg (‰)	2σ (‰)	Δ^{204}THg (‰)	2σ (‰)	Δ^{201}THg (‰)	2σ (‰)	Δ^{200}THg (‰)	2σ (‰)	Δ^{199}THg (‰)	2σ (‰)
EFK 18.2	15714	Rock Bass	fillet	93.1	2	-1.01	0.07	-0.04	0.07	-0.09	0.05	0.00	0.03	0.00	0.03
EFK 18.2	15715	Rock Bass	fillet	104.4	1	-0.53	0.07	-0.07	0.07	0.01	0.05	0.07	0.03	0.09	0.03
EFK 13.8	15704	Rock Bass	fillet	104.7	2	-0.49	0.07	-0.01	0.07	0.03	0.05	0.00	0.03	0.07	0.03
EFK 13.8	15705	Rock Bass	fillet	102.8	1	-0.36	0.07	0.00	0.07	0.05	0.05	0.01	0.03	0.08	0.03
EFK 6.3	16967	Rock Bass	fillet	90.6	2	-0.36	0.07	0.01	0.07	0.12	0.05	0.04	0.03	0.18	0.03
EFK 6.3	16968	Rock Bass	fillet	<85.0		Low transfer recovery.									
EFK 6.3	16972	Rock Bass	fillet	93.6 ± 0.8	4	-0.22	0.07	0.02	0.07	0.09	0.05	0.00	0.03	0.12	0.03
EFK 6.3	15690	Redbreast Sunfish	fillet	102.6	2	-0.45	0.07	0.03	0.07	0.06	0.05	0.04	0.03	0.11	0.03
EFK 6.3	15691	Redbreast Sunfish	fillet	<85.0		Low transfer recovery.									
EFK 6.3	15693	Redbreast Sunfish	fillet	102.3 ± 0.0	4	-0.18	0.07	-0.03	0.07	0.08	0.05	0.03	0.03	0.14	0.03
EFK 6.3	16976	Redbreast Sunfish	fillet	95.6	2	-0.33	0.07	0.06	0.07	0.07	0.05	0.05	0.03	0.15	0.03
EFK 6.3	102-R1	Shiner	fillet	97.6	2	-0.59	0.07	-0.01	0.07	0.12	0.05	0.00	0.03	0.17	0.03
EFK 6.3	102-R2	Shiner	fillet	91.7	4	-0.67	0.07	0.00	0.07	0.17	0.05	0.02	0.03	0.21	0.03
EFK 6.3	102-R3	Shiner	fillet	89.3	2	-0.69	0.07	-0.02	0.07	0.17	0.05	0.01	0.03	0.25	0.03
EFK 6.3	102-R4	Shiner	fillet	98.8	2	-0.70	0.07	-0.04	0.07	0.21	0.05	0.02	0.03	0.29	0.03
EFK 6.3	100	Stoneroller Minnow	fillet	100.7	2	-0.55	0.07	-0.02	0.07	0.12	0.05	0.01	0.03	0.19	0.03
EFK 6.3	101-R1	Stoneroller Minnow	fillet	100.3	3	-0.49	0.07	-0.03	0.07	0.19	0.05	0.01	0.03	0.30	0.03
EFK 6.3	101-R2	Stoneroller Minnow	fillet	99.5	2	-0.44	0.07	-0.02	0.07	0.17	0.05	0.02	0.03	0.23	0.03
EFK 6.3	101-R3	Stoneroller Minnow	fillet	93.2	3	-0.53	0.07	-0.02	0.07	0.19	0.05	0.06	0.03	0.26	0.03
EFK 6.3	101-R4	Stoneroller Minnow	fillet	91.3	3	-0.62	0.07	-0.02	0.07	0.17	0.05	0.01	0.03	0.28	0.03
EFK 6.3	15680	Stoneroller Minnow	WB	100.9	2	-0.25	0.07	-0.04	0.07	0.03	0.05	0.01	0.03	0.10	0.03
EFK 6.3	15681	Stoneroller Minnow	WB	91.5	2	-0.21	0.07	-0.03	0.07	0.04	0.05	-0.02	0.03	0.07	0.03

EFK 6.3	15682	Stoneroller Minnow	WB	102.2 ± 3.6	4	-0.33	0.07	-0.01	0.07	0.08	0.05	-0.01	0.03	0.10	0.03
EFK 6.3	30	FH & SC Mayfly Larvae	WB	96.2	2	-0.14	0.07	0.00	0.07	-0.05	0.05	-0.01	0.03	-0.04	0.03
EFK 6.3	31	Net-Spinning Caddisfly Larvae	WB	102.9 ± 0.7	4	-0.06	0.07	-0.03	0.07	-0.06	0.05	-0.01	0.03	-0.05	0.03
EFK 6.3	32	Snail	soft tissue	100.0	3	-0.43	0.07	-0.01	0.07	-0.04	0.05	-0.01	0.03	-0.04	0.03
EFK 6.3	33	Snail	soft tissue	99.9	3	-0.21	0.07	-0.02	0.07	-0.04	0.05	-0.01	0.03	-0.04	0.03
EFK 6.3	34	Snail	soft tissue	101.1	3	-0.25	0.07	-0.02	0.07	-0.04	0.05	0.00	0.03	-0.02	0.03
EFK 6.3	35	Snail	soft tissue	100.0	3	-0.22	0.07	0.00	0.07	-0.04	0.05	0.00	0.03	-0.04	0.03
EFK 6.3	36	Asian Clam	soft tissue	101.1	3	-0.20	0.07	0.00	0.07	-0.02	0.05	-0.01	0.03	0.00	0.03
EFK 6.3	37	Asian Clam	soft tissue	99.5	3	-0.21	0.07	0.01	0.07	0.00	0.05	-0.01	0.03	0.01	0.03
EFK 6.3	38	Asian Clam	soft tissue	100.2	3	-0.14	0.07	0.02	0.07	0.00	0.05	0.01	0.03	0.01	0.03
EFK 6.3	40	Crayfish	soft tissue	101.4	3	-0.50	0.07	0.02	0.07	0.09	0.05	0.01	0.03	0.14	0.03
EFK 6.3	41	Crayfish	soft tissue	96.6	3	-0.42	0.07	-0.02	0.07	0.09	0.05	0.02	0.03	0.12	0.03
EFK 6.3	42	Crayfish	soft tissue	90.9	1	-0.54	0.07	0.01	0.07	0.07	0.05	0.01	0.03	0.16	0.03
EFK 6.3	43	Crayfish	soft tissue	97.1	3	-0.44	0.07	-0.01	0.07	0.09	0.05	0.02	0.03	0.15	0.03
EFK 6.3	45	Crayfish	soft tissue	99.4	2	-0.40	0.07	0.02	0.07	0.13	0.05	0.02	0.03	0.14	0.03
EFK 6.3	46	Crayfish	soft tissue	94.1	2	-0.48	0.07	0.01	0.07	0.11	0.05	0.00	0.03	0.12	0.03
EFK 6.3	48	Crayfish	soft tissue	99.6	1	-0.52	0.07	-0.03	0.07	0.07	0.05	0.02	0.03	0.16	0.03

Fish and aquatic invertebrates were collected from various sites along Hinds Creek (HC) and East Fork Poplar Creek (EFPC). Site ID refers to the sampling location identified by the number of kilometers upstream of the confluence either of the Clinch River and HC (HCK #), or of Poplar Creek and EFPC (EFK #). Note that FH & SC stands for flathead and spiny crawler mayfly larvae, and WB stands for whole body sample type. Here, n denotes the number of separate isotopic analyses on an individual preparation(s). The analytical uncertainty in the isotopic composition of THg in combustion samples is represented by the average uncertainty (2SD) across combustion reference material analyses (Table S4.5). THg isotope ratios were not reported for samples with <85% recovery (%Rec.) after the transfer procedure.

Table S4.7a. MeHg recovery and purity at various points throughout the MeHg separation procedure for reference materials and Hinds Creek aquatic organisms.

Site ID	Sample ID	Organism Type	%MeHg	n	Syringe Filtering %Rec. of MeHg (± 1SD)	1st Resin Step %Rec. of MeHg (± 1SD)	2nd Resin Step %Rec. of MeHg (± 1SD)	Cumulative Syringe Filtering + Resin %Rec. of MeHg (± 1SD)	%Purity after Syringe Filtering (± 1SD)	%Purity after 1st Resin Step (± 1SD)	%Purity after 2nd Resin Step (± 1SD)
Reference Materials	–	Aqueous MeHgCl Stock (Brooks Rand)		5	98.3 ± 1.1	98.6 ± 1.3	–	96.9 ± 1.8	102.9 ± 2.5	102.3 ± 0.7	–
	–	DORM-3 (fish protein)	90 (93)	4	95.9 ± 1.7	99.3 ± 1.1	–	95.3 ± 2.3	84.8 ± 2.7	100.7 ± 4.6	–
	–	TORT-2 (lobster hepatopancreas)	60 (56)	4	94.8 ± 2.5	99.0 ± 1.5	99.6 ± 0.1	93.5 ± 3.5	54.2 ± 0.7	87.4 ± 4.2	94.3 ± 3.2
	–	DOLT-2 (dogfish liver)	37 (35)	5	94.9 ± 3.3	99.0 ± 1.3	98.7 ± 0.5	93.2 ± 2.9	34.8 ± 0.9	93.3 ± 6.9	98.5 ± 2.9
	–	DOLT-5 (dogfish liver)	– (27)	5	96.4 ± 1.5	97.2 ± 4.5	100.7 ± 4.5	94.0 ± 2.2	33.8 ± 0.2	85.4 ± 9.0	96.5 ± 1.3
HCK 20.6	10	Snipe Fly Larvae	89	1	91.1	96.5	–	88.0	79.7	92.5	–
HCK 20.6	11	Megaloptera Larvae	88	1	97.7	99.4	98.9	96.1	80.0	98.7	102.2
HCK 20.6	12	Megaloptera Larvae	84	2	96.2 ± 2.5	99.3 ± 1.1	98.4 ± <0.1	94.0 ± 1.4	78.7 ± 2.0	96.8 ± 1.3	101.3 ± <0.1
HCK 20.6	14	Snail	34	2	not measured	not measured	98.5 ± 0.8	99.4 ± 7.0	not measured	91.8 ± 1.0	96.4 ± 0.7
HCK 20.6	16	Snail	65	1	not measured	not measured	98.7	93.5	not measured	87.9	93.9
HCK 20.6	17	Asian Clam	59	1	not measured	not measured	98.2	93.2	not measured	91.8	98.3
HCK 20.6	18	Asian Clam	61	1	not measured	not measured	97.8	92.6	not measured	92.4	99.8
HCK 20.6	19	Asian Clam	61	1	not measured	not measured	96.9	91.7	not measured	93.3	98.9
HCK 20.6	24	Crayfish	100	1	not measured	not measured	–	97.4	not measured	102.2	–
HCK 20.6	25	Crayfish	97	1	not measured	not measured	–	98.9	not measured	101.4	–

HCK 20.6	15604	Stoneroller Minnow	80	1	not measured	not measured	99.2	93.1	not measured	98.8	98.9
HCK 20.6	15605	Stoneroller Minnow	83	2	not measured	not measured	97.0 ± 1.0	92.8 ± 0.9	not measured	94.3 ± 0.4	96.8 ± 1.0
HCK 20.6	16951	Redbreast Sunfish	103	1	not measured	not measured	–	95.4	not measured	101.6	–
HCK 20.6	16952	Redbreast Sunfish	110	1	97.7	98.4	–	96.1	93.7	102.7	–

See Table S4.7b for notes.

Table S4.7b. MeHg recovery and purity at various points throughout the MeHg separation procedure for EFPC aquatic organisms.

Site ID	Sample ID	Organism Type	%MeHg	n	Syringe Filtering %Rec. of MeHg (± 1SD)	1st Resin Step %Rec. of MeHg (± 1SD)	2nd Resin Step %Rec. of MeHg (± 1SD)	Cumulative Syringe Filtering + Resin %Rec. of MeHg (± 1SD)	%Purity after Syringe Filtering (± 1SD)	%Purity after 1st Resin Step (± 1SD)	%Purity after 2nd Resin Step (± 1SD)
EFK 23.4	72	Megaloptera Larvae	12	1	94.9	97.5	97.3	89.9	10.3	55.9	95.6
EFK 23.4	80	Crayfish	38	1	97.7	98.1	98.6	94.5	45.1	94.7	102.7
EFK 23.4	103-R2	Shiner	90	1	96.0	99.6	–	95.5	84.6	100.8	–
EFK 23.4	103-R5	Shiner	88	1	96.6	101.4	–	97.9	86.5	100.7	–
EFK 23.4	15988	Stoneroller Minnow	10	1	100.1	96.9	98.6	95.6	10.2	57.3	97.1
EFK 23.4	15990	Stoneroller Minnow	11	1	98.5	96.7	100.4	95.6	10.6	53.4	95.5
EFK 23.4	15993	Redbreast Sunfish	102	1	94.0	99.7	95.7	89.7	86.5	98.4	99.5
EFK 23.4	15995	Redbreast Sunfish	106	1	94.3	97.8	98.5	90.8	88.9	101.2	100.8
EFK 22.3	57	Megaloptera Larvae	13	2	96.5 ± 0.1	97.2 ± 0.7	98.4 ± 1.1	92.2 ± 1.6	12.0 ± 0.3	65.4 ± 5.2	97.8 ± 0.3
EFK 22.3	61	Asian Clam	6	2	98.3 ± 2.4	90.1 ± 3.1	98.4 ± 2.3	87.1 ± 1.2	6.1 ± 0.2	52.9 ± 2.4	91.2 ± <0.1
EFK 22.3	68	Crayfish	61	2	96.7 ± 0.1	100.1 ± <0.1	97.8 ± 0.3	94.7 ± 0.4	62.8 ± 2.9	101.2 ± 0.9	104.3 ± 0.2
EFK 22.3	69	Crayfish	68	1	92.9	97.8	99.4	90.3	66.7	92.9	97.0
EFK 6.3	30	FH & SC Mayfly Larvae	12	2	96.2 ± <0.1	98.1 ± 1.0	97.1 ± 1.1	91.7 ± 0.1	12.7 ± 0.1	68.7 ± 1.1	96.3 ± 0.4
EFK 6.3	34	Snail	25	1	not measured	not measured	98.7	91.6	not measured	76.9	98.0
EFK 6.3	35	Snail	21	1	not measured	not measured	98.5	91.7	not measured	80.9	97.7
EFK 6.3	36	Asian Clam	16	1	not measured	not measured	100.1	90.4	not measured	74.8	98.5
EFK 6.3	37	Asian Clam	25	1	not measured	not measured	97.5	90.7	not measured	84.5	97.6

EFK 6.3	46	Crayfish	105	1	95.9	100.2	–	96.0	90.5	101.2	–
EFK 6.3	48	Crayfish	94	1	94.9	99.4	–	94.3	83.2	99.9	–
EFK 6.3	102-R2	Shiner	106	1	96.3	101.7	–	97.9	94.5	103.3	–
EFK 6.3	102-R4	Shiner	104	2	96.7 ± 0.5	99.5 ± 0.1	–	96.2 ± 0.4	94.8 ± 1.1	103.1 ± 2.1	–
EFK 6.3	15680	Stoneroller Minnow	55	1	94.8	100.9	100.3	95.9	54.0	95.3	105.4
EFK 6.3	15682	Stoneroller Minnow	65	1	95.7	100.4	98.9	95.0	63.9	96.9	103.3
EFK 6.3	15693	Redbreast Sunfish	106	1	100.7	98.0	–	98.6	98.3	103.0	–
EFK 6.3	16976	Redbreast Sunfish	117	1	98.6	101.1	–	99.8	95.0	101.1	–

Fish and aquatic invertebrates were collected from various sites along Hinds Creek (HC) and East Fork Poplar Creek (EFPC). Site ID refers to the sampling location identified by the number of kilometers upstream of the confluence either of the Clinch River and HC (HCK #), or of Poplar Creek and EFPC (EFK #). Note that FH & SC stands for flathead and spiny crawler mayfly larvae. Percent MeHg (%MeHg) in the solid material was calculated by dividing the measured MeHg concentration (via nitric acid digestion) by the measured THg concentration (via combustion), with the same calculation using certified MeHg and THg concentrations provided in parentheses for the biological reference materials (note that DOLT-5 was not analyzed for its THg concentration via combustion). These values match the %MeHg values provided in Table S4.2a-c and Table S4.4. Here, n denotes the number of independent nitric acid digestion samples that underwent resin separation. Recovery of MeHg after syringe filtering is relative to the measured MeHg concentration of the nitric acid digestion samples. Recovery of MeHg after the first resin separation step is relative to the measured MeHg concentration of the syringe-filtered samples. Recovery of MeHg after the second resin separation step is relative to the measured MeHg concentration of the first resin separation samples. Cumulative MeHg recovery after the final resin separation step is relative to the measured MeHg concentration of the nitric acid digestion samples. Percent purity was calculated by dividing the measured MeHg concentration by the measured THg concentration of each of the syringe filtered and resin separation samples. A dash for second resin step recovery and MeHg purity after the second resin step indicate that the sample underwent only one resin separation step. Note that for some biological samples, post-syringe filtering aliquots were not saved for MeHg and THg concentration analysis, and so syringe filtering recovery, first resin step recovery, and MeHg purity after syringe filtering could not be calculated ("not measured").

Table S4.8a. MeHg isotopic composition of reference materials and Hinds Creek aquatic organisms.

Site ID	Organism Type & Sample ID	Sample Type	n_1	n_2	P+T %Rec. (± 1SD)	δ^{202}MeHg (‰)	2σ (‰)	Δ^{204}MeHg (‰)	2σ (‰)	Δ^{201}MeHg (‰)	2σ (‰)	Δ^{200}MeHg (‰)	2σ (‰)	Δ^{199}MeHg (‰)	2σ (‰)
Reference Materials	MeHgCl Stock (Brooks Rand)	aqueous standard	3	3	100.9 ± 1.9	-1.24	0.05	-0.02	0.07	0.05	0.04	0.01	0.03	0.08	0.04
	DORM-3	fish protein	4	4	101.8 ± 1.7	0.64	0.05	-0.12	0.07	1.52	0.04	0.08	0.03	1.85	0.04
	TORT-2	lobster hepato-pancreas	4	4	101.1 ± 1.3	0.62	0.05	-0.11	0.07	0.85	0.04	0.07	0.03	1.04	0.04
	DOLT-2	dogfish liver	5	5	101.4 ± 3.8	0.21	0.05	-0.07	0.07	0.93	0.04	0.05	0.03	1.13	0.04
	DOLT-5	dogfish liver	4	4	101.9 ± 0.6	0.50	0.05	-0.03	0.07	0.85	0.04	0.08	0.03	1.01	0.04
HCK 20.6	Snipe Fly Larvae (10)	WB	1	1	97.3	-0.88	0.05	-0.04	0.07	-0.01	0.04	0.03	0.03	0.09	0.04
HCK 20.6	Megaloptera Larvae (11, 12, 12)	WB	1	1	102.7	-1.08	0.05	-0.08	0.07	-0.02	0.04	0.02	0.03	0.08	0.04
HCK 20.6	Snail (14, 14, 16)	soft tissue	1	1	100.4	-0.83	0.05	-0.03	0.07	0.01	0.04	0.03	0.03	0.07	0.04
HCK 20.6	Clam (17, 18, 19)	soft tissue	1	1	101.7	-0.55	0.05	-0.06	0.07	0.03	0.04	0.04	0.03	0.15	0.04
HCK 20.6	Crayfish (24, 25)	soft tissue	1	1	100.6	-1.05	0.05	-0.05	0.07	-0.03	0.04	0.02	0.03	0.06	0.04
HCK 20.6	Stoneroller Minnow (15604, 15605, 15605)	WB	1	1	100.4	-1.06	0.05	0.00	0.07	0.04	0.04	0.04	0.03	0.11	0.04
HCK 20.6	Redbreast Sunfish (16951, 16952)	fillet	1	1	100.5	-1.05	0.05	-0.10	0.07	-0.10	0.04	0.05	0.03	-0.04	0.04

See Table S4.8b for notes.

Table S4.8b. MeHg isotopic composition of EFPC aquatic organisms.

Site ID	Organism Type & Sample ID	Sample Type	n_1	n_2	P+T %Rec. (± 1SD)	δ^{202}MeHg (‰)	2σ (‰)	Δ^{204}MeHg (‰)	2σ (‰)	Δ^{201}MeHg (‰)	2σ (‰)	Δ^{200}MeHg (‰)	2σ (‰)	Δ^{199}MeHg (‰)	2σ (‰)
EFK 23.4	Megaloptera Larvae (72)	WB	1	1	102.5	-0.70	0.05	-0.02	0.07	0.28	0.04	-0.01	0.03	0.38	0.04
EFK 23.4	Crayfish (80)	WB	1	1	99.8	-0.65	0.05	-0.03	0.07	0.19	0.04	0.00	0.03	0.28	0.04
EFK 23.4	Shiner (103-R2)	fillet	1	1	99.8	-0.89	0.05	-0.03	0.07	0.22	0.04	0.05	0.03	0.29	0.04
EFK 23.4	Shiner (103-R5)	fillet	1	2	99.8	-0.82	0.05	-0.03	0.07	0.29	0.04	0.01	0.03	0.38	0.04
EFK 23.4	Stoneroller Minnow (15988, 15990)	WB	1	1	102.3	-0.65	0.05	0.00	0.07	0.18	0.04	0.01	0.03	0.23	0.04
EFK 23.4	Redbreast Sunfish (15993)	fillet	1	1	100.3	-0.14	0.05	-0.01	0.07	0.06	0.04	0.00	0.03	0.13	0.04
EFK 23.4	Redbreast Sunfish (15995)	fillet	1	1	99.8	-0.67	0.05	-0.04	0.07	0.11	0.04	0.01	0.03	0.18	0.04
EFK 22.3	Megaloptera Larvae (57)	WB	2	2	101.8 ± 2.3	-0.72	0.05	0.00	0.07	0.06	0.04	0.02	0.03	0.13	0.04
EFK 22.3	Asian Clam (61)	soft tissue	2	2	101.2 ± 0.7	-0.67	0.05	-0.01	0.07	0.24	0.04	0.04	0.03	0.33	0.04
EFK 22.3	Crayfish (68)	soft tissue	2	2	101.7 ± 0.4	-0.80	0.05	-0.02	0.07	0.14	0.04	0.03	0.03	0.21	0.04
EFK 22.3	Crayfish (69)	soft tissue	1	1	97.5	-0.79	0.05	-0.02	0.07	0.13	0.04	0.03	0.03	0.18	0.04
EFK 6.3	FH & SC Mayfly Larvae (30)	WB	2	2	100.4 ± 0.4	-0.41	0.05	-0.07	0.07	0.19	0.04	0.04	0.03	0.25	0.04
EFK 6.3	Snail (34)	soft tissue	1	1	99.8	-0.23	0.05	0.03	0.07	0.09	0.04	0.02	0.03	0.18	0.04
EFK 6.3	Snail (35)	soft tissue	1	1	101.2	-0.28	0.05	0.02	0.07	0.11	0.04	0.03	0.03	0.18	0.04

EFK 6.3	Asian Clam (36)	soft tissue	1	1	101.4	-0.15	0.05	0.04	0.07	0.18	0.04	0.00	0.03	0.25	0.04
EFK 6.3	Asian Clam (37)	soft tissue	1	1	99.7	-0.14	0.05	-0.03	0.07	0.17	0.04	0.02	0.03	0.25	0.04
EFK 6.3	Crayfish (46)	soft tissue	1	1	100.0	-0.40	0.05	0.00	0.07	0.08	0.04	0.02	0.03	0.12	0.04
EFK 6.3	Crayfish (48)	soft tissue	1	1	98.3	-0.45	0.05	-0.01	0.07	0.10	0.04	0.00	0.03	0.18	0.04
EFK 6.3	Shiner (102-R2)	fillet	1	2	99.7	-0.53	0.05	0.01	0.07	0.15	0.04	0.02	0.03	0.19	0.04
EFK 6.3	Shiner (102-R4)	fillet	2	4	101.4 ± 1.6	-0.60	0.05	-0.02	0.07	0.24	0.04	0.01	0.03	0.30	0.04
EFK 6.3	Stoneroller Minnow (15680)	WB	1	1	102.9	-0.35	0.05	-0.03	0.07	0.12	0.04	-0.01	0.03	0.17	0.04
EFK 6.3	Stoneroller Minnow (15682)	WB	1	1	103.1	-0.34	0.05	-0.01	0.07	0.13	0.04	0.01	0.03	0.21	0.04
EFK 6.3	Redbreast Sunfish (15693)	fillet	1	2	101.2	-0.17	0.05	-0.02	0.07	0.06	0.04	0.01	0.03	0.12	0.04
EFK 6.3	Redbreast Sunfish (16976)	fillet	1	2	100.3	-0.26	0.05	-0.01	0.07	0.11	0.04	0.01	0.03	0.17	0.04

Fish and aquatic invertebrates were collected from various sites along Hinds Creek (HC) and East Fork Poplar Creek (EFPC). Site ID refers to the sampling location identified by the number of kilometers upstream of the confluence either of the Clinch River and HC (HCK #), or of Poplar Creek and EFPC (EFK #). Note that FH & SC stands for flathead and spiny crawler mayfly larvae, and WB stands for whole body sample type. Here, n_1 denotes the number of resin separation samples and n_2 denotes the number of separate isotopic analyses on an individual preparation(s). Note that for some biological samples and reference materials, two or three resin separation samples were combined prior to isotopic analysis, as indicated by multiple sample IDs in parentheses below the organism type, or by a mismatch between n_1 in this table and n in Table S4.7a for the reference materials. Purge-and-trap (P+T) %Rec indicates the recovery of Hg during the purge-and-trap pre-concentration step. The analytical uncertainty in the isotopic composition of MeHg in resin separation samples is represented by the average uncertainty (2SD) across UM-Almadén analyses, which were analyzed alongside resin separation samples (Table S4.5).

Table S4.9. Offsets between measured δ^{202}MeHg values and estimated δ^{202}MeHg values using a mass balance approach for Hinds Creek and EFPC aquatic organisms.

Site ID	Sample ID	Organism Type	Sample Type	%MeHg	Measured δ^{202}MeHg (‰)	2σ (‰)	Calculated δ^{202}MeHg (‰) Assuming Sediment = Source of iHg	Calculated δ^{202}MeHg (‰) Assuming Biofilm = Source of iHg	Offset in δ^{202}MeHg (‰) Assuming Sediment = Source of iHg	Offset in δ^{202}MeHg (‰) Assuming Biofilm = Source of iHg
HCK 20.6	10	Snipe Fly Larvae	whole body	89	-0.88	0.05	-1.16	-1.21	-0.27	-0.33
HCK 20.6	11, 12, 12	Megaloptera Larvae	whole body	85	-1.08	0.05	-1.32	-1.40	-0.24	-0.32
HCK 20.6	14, 14, 16	Snail	soft tissue	45	-0.83	0.05	-1.00	-1.59	-0.17	-0.76
HCK 20.6	17, 18, 19	Asian Clam	soft tissue	61	-0.55	0.05	-0.81	-1.12	-0.27	-0.58
HCK 20.6	24, 25	Crayfish	soft tissue	98	-1.05	0.05	-1.19	-1.20	-0.14	-0.15
HCK 20.6	15604, 15605, 15605	Stoneroller Minnow	whole body	82	-1.06	0.05	-1.04	-1.14	0.02	-0.09
HCK 20.6	16951, 16952	Redbreast Sunfish	fillet	106	-1.05	0.05	-1.22	-1.19	-0.17	-0.14
EFK 23.4	72	Megaloptera Larvae	whole body	12	-0.70	0.05	–	–	–	–
EFK 23.4	80	Crayfish	soft tissue	38	-0.65	0.05	-1.58	-1.21	-0.93	-0.56
EFK 23.4	103-R2	Shiner	fillet	90	-0.89	0.05	-0.92	-0.89	-0.03	0.00
EFK 23.4	103-R5	Shiner	fillet	88	-0.82	0.05	-0.95	-0.92	-0.13	-0.10
EFK 23.4	15988, 15990	Stoneroller Minnow	whole body	10	-0.65	0.05	–	–	–	–
EFK 23.4	15993	Redbreast Sunfish	fillet	102	-0.14	0.05	-0.13	-0.14	0.01	0.00
EFK 23.4	15995	Redbreast Sunfish	fillet	106	-0.67	0.05	-0.64	-0.65	0.03	0.02
EFK 22.3	57	Megaloptera Larvae	whole body	13	-0.72	0.05	–	–	–	–
EFK 22.3	61	Asian Clam	soft tissue	6	-0.67	0.05	–	–	–	–
EFK 22.3	68	Crayfish	soft tissue	61	-0.80	0.05	-1.25	-1.11	-0.46	-0.32

EFK 22.3	69	Crayfish	soft tissue	68	-0.79	0.05	-1.09	-0.98	-0.30	-0.19
EFK 6.3	30	FH & SC Mayfly Larvae	whole body	12	-0.41	0.05	–	–	–	–
EFK 6.3	34	Snail	soft tissue	25	-0.23	0.05	-0.65	-1.25	-0.42	-1.02
EFK 6.3	35	Snail	soft tissue	21	-0.28	0.05	–	–	–	–
EFK 6.3	36	Asian Clam	soft tissue	16	-0.15	0.05	–	–	–	–
EFK 6.3	37	Asian Clam	soft tissue	25	-0.14	0.05	-0.47	-1.05	-0.33	-0.91
EFK 6.3	46	Crayfish	soft tissue	105	-0.40	0.05	-0.46	-0.45	-0.07	-0.06
EFK 6.3	48	Crayfish	soft tissue	94	-0.45	0.05	-0.55	-0.56	-0.09	-0.11
EFK 6.3	102-R2	Shiner	fillet	106	-0.53	0.05	-0.64	-0.63	-0.10	-0.09
EFK 6.3	102-R4	Shiner	fillet	104	-0.60	0.05	-0.68	-0.67	-0.08	-0.07
EFK 6.3	15680	Stoneroller Minnow	whole body	55	-0.35	0.05	-0.35	-0.51	0.00	-0.16
EFK 6.3	15682	Stoneroller Minnow	whole body	65	-0.34	0.05	-0.43	-0.54	-0.10	-0.20
EFK 6.3	15693	Redbreast Sunfish	fillet	106	-0.17	0.05	-0.18	-0.17	-0.01	0.00
EFK 6.3	16976	Redbreast Sunfish	fillet	117	-0.26	0.05	-0.30	-0.27	-0.04	-0.01

Fish and aquatic invertebrates were collected from various sites along Hinds Creek (HC) and East Fork Poplar Creek (EFPC). Site ID refers to the sampling location identified by the number of kilometers upstream of the confluence either of the Clinch River and HC (HCK #), or of Poplar Creek and EFPC (EFK #). Note that FH & SC stands for flathead and spiny crawler mayfly larvae. For biological samples containing ≥25% MeHg, MeHg isotopic compositions were estimated via mass balance (Tsui et al. 2012) according to Section 4.4.1.3, with the assumption that the isotopic composition of iHg within each of the organisms was equal to the THg isotopic composition of either streambed sediment or biofilm at each site. The δ^{202}THg values of HC, upstream EFPC, and downstream EFPC streambed sediment used in these calculations were -1.37‰, -0.09‰, and -0.13‰, respectively (Donovan et al. 2014, Crowther et al. 2021). The δ^{202}THg values of HC, upstream EFPC, and downstream EFPC biofilm used in these calculations were -0.89‰, -0.31‰, and 0.07‰, respectively (Demers et al. 2018). Offsets between directly measured and estimated δ^{202}MeHg values are provided ($\delta^{202}MeHg_{estimated} - \delta^{202}MeHg_{measured}$).

Table S4.10. Calculated iHg and photochemical demethylation-corrected MeHg isotopic compositions of Hinds Creek and EFPC aquatic organisms.

Site ID	Sample ID	Organism Type	$\delta^{20}iHg_{calc}$ (‰)	$\Delta^{204}iHg_{calc}$ (‰)	$\Delta^{201}iHg_{calc}$ (‰)	$\Delta^{200}iHg_{calc}$ (‰)	$\Delta^{199}iHg_{calc}$ (‰)	Photochemical Demethylation-Corrected $\delta^{202}MeHg$ (‰)	Photochemical Demethylation-Corrected $\Delta^{199}MeHg$ (‰) = Average $\Delta^{199}THg$ across Streambed Sediment and Biofilm
HCK 20.6	10	Snipe Fly Larvae	–	–	–	–	–	-1.04	-0.28
HCK 20.6	11, 12, 12	Megaloptera Larvae	–	–	–	–	–	-1.23	-0.28
HCK 20.6	14, 14, 16	Snail	-1.50	-0.06	-0.24	0.02	-0.19	-0.97	-0.28
HCK 20.6	17, 18, 19	Asian Clam	-1.77	-0.04	-0.28	-0.01	-0.30	-0.72	-0.28
HCK 20.6	24, 25	Crayfish	–	–	–	–	–	-1.19	-0.28
HCK 20.6	15604, 15605, 15605	Stoneroller Minnow	-1.29	-0.69	-0.37	0.03	-0.30	-1.22	-0.28
HCK 20.6	16951, 16952	Redbreast Sunfish	–	–	–	–	–	-1.15	-0.28
EFK 23.4	72	Megaloptera Larvae	-0.98	-0.03	0.03	-0.01	0.11	-0.87	-0.01
EFK 23.4	80	Crayfish	-0.65	0.02	-0.02	0.02	0.03	-0.77	-0.01
EFK 23.4	103-R2	Shiner	–	–	–	–	–	-1.02	-0.01
EFK 23.4	103-R5	Shiner	–	–	–	–	–	-0.98	-0.01
EFK 23.4	15988, 15990	Stoneroller Minnow	-0.22	0.00	-0.10	0.00	-0.12	-0.75	-0.01
EFK 23.4	15993	Redbreast Sunfish	–	–	–	–	–	-0.20	-0.01
EFK 23.4	15995	Redbreast Sunfish	–	–	–	–	–	-0.75	-0.01
EFK 22.3	57	Megaloptera Larvae	-0.76	0.02	-0.01	0.00	0.00	-0.78	-0.01
EFK 22.3	61	Asian Clam	-0.36	0.01	0.04	0.01	0.07	-0.82	-0.01

EFK 22.3	68	Crayfish	-0.82	-0.11	-0.03	0.00	-0.01	-0.89	-0.01
EFK 22.3	69	Crayfish	-0.73	-0.07	-0.06	-0.06	0.04	-0.87	-0.01
EFK 6.3	30	FH & SC Mayfly Larvae	-0.10	0.01	-0.08	-0.02	-0.08	-0.55	-0.09
EFK 6.3	34	Snail	-0.26	-0.03	-0.09	0.00	-0.09	-0.34	-0.09
EFK 6.3	35	Snail	-0.20	-0.01	-0.08	-0.01	-0.09	-0.39	-0.09
EFK 6.3	36	Asian Clam	-0.21	-0.01	-0.06	-0.01	-0.05	-0.29	-0.09
EFK 6.3	37	Asian Clam	-0.24	0.03	-0.06	-0.01	-0.06	-0.28	-0.09
EFK 6.3	46	Crayfish	–	–	–	–	–	-0.48	-0.09
EFK 6.3	48	Crayfish	–	–	–	–	–	-0.56	-0.09
EFK 6.3	102-R2	Shiner	–	–	–	–	–	-0.65	-0.09
EFK 6.3	102-R4	Shiner	–	–	–	–	–	-0.76	-0.09
EFK 6.3	15680	Stoneroller Minnow	-0.12	-0.04	-0.07	0.02	0.01	-0.46	-0.09
EFK 6.3	15682	Stoneroller Minnow	-0.31	-0.03	-0.01	-0.05	-0.10	-0.46	-0.09
EFK 6.3	15693	Redbreast Sunfish	–	–	–	–	–	-0.25	-0.09
EFK 6.3	16976	Redbreast Sunfish	–	–	–	–	–	-0.37	-0.09

Fish and aquatic invertebrates were collected from various sites along Hinds Creek (HC) and East Fork Poplar Creek (EFPC). Site ID refers to the sampling location identified by the number of kilometers upstream of the confluence either of the Clinch River and HC (HCK #), or of Poplar Creek and EFPC (EFK #). Note that FH & SC stands for flathead and spiny crawler mayfly larvae. For biological samples analyzed for both THg and MeHg isotopic composition and which contained <85% MeHg, iHg isotope ratios were calculated via mass balance according to Section 4.4.1.4. Uncertainty (2SD) in iHg isotope ratios was calculated by propagating the analytical uncertainty in THg (Table S4.6a-c) and MeHg (Table S4.8a-b) isotopic compositions (0.08‰ $\delta^{202}iHg_{calc}$; 0.10‰ $\Delta^{204}iHg_{calc}$; 0.06‰ $\Delta^{201}iHg_{calc}$; 0.04‰ $\Delta^{200}iHg_{calc}$; 0.05‰ $\Delta^{199}iHg_{calc}$). Note that the calculated Δ^{204}iHg value for the HC stoneroller minnow is anomalously low, likely due to inaccurate measurements of Δ^{204}THg and/or Δ^{204}MeHg values. For all biological samples analyzed for MeHg isotopic composition, MeHg isotope ratios were corrected to account for the isotope fractionation caused by photochemical demethylation according to Section 4.4.1.4 using a $\Delta^{199}Hg/\delta^{202}Hg$ slope of 2.43. Note that the corrected Δ^{199}MeHg values of HC aquatic organisms are equal to the average Δ^{199}THg value across HC streambed sediment (Donovan et al. 2014) and biofilm. Also note that the corrected Δ^{199}MeHg values of upstream and downstream EFPC aquatic organisms are equal to the average Δ^{199}THg values across EFPC streambed sediment (Donovan et al. 2014, Crowther et al. 2021), biofilm (Demers et al. 2018), and suspended particulates (Demers et al. 2018) collected from upstream (EFK 23.4 to EFK 22.3) and downstream (EFK 8.7 to EFK 5.0) sites.

References for Supporting Information

Blum, Joel D., and Marcus W. Johnson. 2017. "Recent developments in mercury stable isotope analysis." *Reviews in Mineralogy and Geochemistry* 82:733-757. doi: 10.2138/rmg.2017.82.17.

Crowther, Elizabeth R., Jason D. Demers, Joel D. Blum, Scott C. Brooks, and Marcus W. Johnson. 2021. "Use of sequential extraction and mercury stable isotope analysis to assess remobilization of sediment-bound legacy mercury." *Environmental Science: Processes & Impacts* 23:756-775. doi: 10.1039/d1em00019e.

Demers, Jason D., Joel D. Blum, Scott C. Brooks, Patrick M. Donovan, Ami L. Riscassi, Carrie L. Miller, Wang Zheng, and Baohua Gu. 2018. "Hg isotopes reveal in-stream processing and legacy inputs in East Fork Poplar Creek, Oak Ridge, Tennessee, USA." *Environmental Science: Processes & Impacts* 20 (4):686-707. doi: 10.1039/c7em00538e.

Donovan, Patrick M., Joel D. Blum, Jason D. Demers, Baohua Gu, Scott C. Brooks, and John Peryam. 2014. "Identification of multiple mercury sources to stream sediments near Oak Ridge, TN, USA." *Environmental Science & Technology* 48 (7):3666-3674. doi: 10.1021/es4046549.

Tsui, Martin Tsz Ki, Joel D. Blum, Sae Yun Kwon, Jacques C. Finlay, Steven J. Balogh, and Yabing H. Nollet. 2012. "Sources and transfers of methylmercury in adjacent river and forest food webs." *Environmental Science & Technology* 46:10957-10964. doi: 10.1021/es3019836.

Chapter 5 Conclusions

Due to its recalcitrant nature, it has long been believed that anthropogenic legacy mercury contamination in freshwater ecosystems is largely locked into the sediment and soil, limiting its impact on dissolved mercury concentrations in surface water and reducing its availability for methylation and subsequent accumulation in aquatic food webs. However, recent studies involving measurements of mercury stable isotope ratios in environmental samples have shown that sediment-bound legacy mercury can be remobilized within (Demers et al. 2018) and between (Sun et al. 2022) freshwater ecosystems, and may be available for methylation (Janssen et al. 2021). For waterbodies that both contain legacy mercury and continue to receive new inputs of mercury from anthropogenic sources, it can be difficult to quantify the relative importance of legacy sources and ongoing point and nonpoint sources as contributors of mercury to the surface water dissolved phase and to the aquatic food web. The research presented here provides a framework for using mercury isotopic measurements to assess the remobilization of sediment-bound legacy mercury to surface water and aquatic food webs. Additionally, this research outlines similarities and differences in biogeochemical cycling of mercury between point source impacted and natural background streams.

5.1 Remobilization of sediment-bound legacy mercury

5.1.1 Review of key findings of Chapter 2

In Chapter 2, I paired sequential extractions of sediment-bound mercury (Hg) with mercury isotopic analysis to assess how anthropogenic legacy mercury retained in East Fork

Poplar Creek (EFPC) streambed sediment may be remobilized to stream water. Previous studies had demonstrated that different pools of mercury within a single legacy source could have unique isotopic compositions (Stetson et al. 2009, Wiederhold et al. 2013, Yin et al. 2013, Wiederhold et al. 2015, Grigg et al. 2018, Brocza et al. 2019, Huang et al. 2021). I found that weakly-bound and strongly-bound pools of mercury within the sediment were isotopically similar to one another at each sampling site, and that the organically-bound mercury pool was isotopically distinct at upstream sites but converged with the isotopic composition of other sediment mercury pools along the flow path. The isotopic compositions of these sediment mercury pools were compared to previous mercury isotopic measurements of EFPC surface water, hyporheic pore water, suspended particulates, and biofilm (Demers et al. 2018). The results of this study suggested that strongly-bound legacy mercury in sediment may over time be released and then rapidly weakly re-adsorbed to the sediment, after which it may be re-released and contribute mercury to the dissolved phase, suspended particulates, and biofilm. These results provide evidence that despite being largely recalcitrant, legacy mercury within an industrially contaminated stream may be remobilized to the surface water and basal resources.

Another finding within Chapter 2 is that the isotopic composition of legacy mercury within EFPC streambed sediment appears to have been influenced by equilibrium isotope effects driven by isotope exchange between coexisting Hg(0) and Hg(II). As hypothesized by Bartov (2014) and observed experimentally by Zheng et al. (2019), equilibrium isotope effects can overwrite initial isotope fractionation by kinetic reactions. I found that these effects may have overwritten isotope fractionation patterns caused by mercury reduction and oxidation reactions in the environment surrounding the industrial point source and set the “baseline” mercury isotopic composition of EFPC streambed sediment. To my knowledge, this was the first study in which

isotope exchange between coexisting Hg(0) and Hg(II) was proposed to have been responsible for the mercury isotopic composition of environmental samples, though as suggested by Zheng et al. (2019), isotope exchange may occur ubiquitously during a variety of biogeochemical reactions. This could make it difficult to determine which types of kinetic reactions may have historically been dominant within an ecosystem containing both Hg(0) and Hg(II) contamination.

5.1.2 Future directions related to Chapter 2

The use of mercury isotopic measurements of environmental samples to identify dominant biogeochemical processes within an ecosystem relies on experimentally derived data linking isotope fractionation patterns to various types of environmentally relevant biogeochemical reactions. However, isotope fractionation has not been assessed for all environmentally relevant processes, including some that relate to the conclusions made in this study on sediment-bound legacy mercury. For example, the results of this study suggest that small amounts of strongly-bound mercury within sediment may be released and then rapidly re-adsorbed as weakly-bound mercury, and then later be released into the stream water. This conclusion relies on the assumption that dissolution of largely recalcitrant minerals such as mercury sulfide (HgS) followed by rapid re-adsorption to the sediment does not result in significant isotope fractionation, but this has not been tested. Future experimental studies should assess mercury isotope fractionation associated with dissolution of HgS through various mechanisms, including by dissolved organic matter, high levels of dissolved oxygen, and sulfur-oxidizing bacteria.

These results also suggest that mercury within biofilm and suspended particulates contributes to the organically-bound mercury fraction in the streambed sediment through physical mixing along the flow path. This conclusion relies on the assumption that the

organically-bound mercury pool within biofilm and suspended particulates is isotopically similar to bulk biofilm and suspended particulates. Future studies involving sequential extractions and mercury isotopic measurements to assess remobilization of mercury from sediment to other basal resources may want to consider performing these measurements on biofilm as well.

In this study, I also found that the isotopic composition of legacy mercury within EFPC streambed sediment may have been influenced by equilibrium isotope effects driven by isotope exchange between coexisting Hg(0) and Hg(II), which may have overwritten isotope fractionation patterns caused by earlier mercury reduction and oxidation reactions. Equilibrium isotope effects can alter isotopic fractionation patterns imparted by kinetic reactions, which can complicate investigations of mercury biogeochemical cycling within contaminated environments. This mechanism should be considered in future studies involving mercury isotopic measurements of sediment, especially if both Hg(0) and Hg(II) are known to have been present, such as within industrial sites or near mercury or gold mining sites.

5.2 Coupling of nitric acid digestion and anion-exchange resin separation to assess compound-specific methylmercury isotopic composition of organisms

5.2.1 Review of key findings of Chapter 3

In Chapter 3, I developed a method of extracting and isolating methylmercury (MeHg) from fish and aquatic invertebrates for compound-specific isotopic analysis. Direct measurements of the isotopic composition of MeHg within aquatic organisms and other environmental samples is useful for identifying sources of MeHg to the food web and for determining the relative importance of various biogeochemical reactions involved in the production and degradation of MeHg prior to its accumulation in the food web. Traditional

methods of estimating the isotopic composition of MeHg within aquatic food webs have involved mass balance (Tsui et al. 2012) or linear regression (Kwon et al. 2015) calculations, and relied only on measurements of total mercury (THg) and MeHg concentrations and THg isotopic composition. These estimation approaches work well when various types of organisms within a food web obtain inorganic mercury (iHg) and MeHg each from a single source. However, for some food webs, various types of organisms may obtain iHg and/or MeHg from a variety of sources, which complicates these estimation approaches. Thus, compound-specific MeHg isotopic analysis is especially beneficial for studies on complex food webs that obtain iHg and/or MeHg from multiple basal resources.

The MeHg separation method developed in this study involved a sequence of nitric acid digestion, batch anion-exchange resin separation, and pre-concentration by purge and trap. Nitric acid digestion is a relatively simple and widely accepted method of extracting mercury from biological materials without degrading the MeHg (Hammerschmidt and Fitzgerald 2005). However, this is the first time that this method has been incorporated into a procedure for isolating MeHg for isotopic analysis, replacing other MeHg extraction methods such as toluene extraction (Masbou et al. 2013), alkaline digestion (Zhang et al. 2021), and distillation (Rosera et al. 2020), which are either more toxic, difficult to optimize, or are unsuitable for certain types of samples. Additionally, nitric acid digestion allowed MeHg concentration and isotopic analyses to be performed on a single sample aliquot, which promotes a tight coupling between MeHg concentration, MeHg-to-THg ratios (%MeHg), and MeHg isotopic composition.

Through performing this method on aqueous standards, four biological reference materials, and five natural biological samples, and by independently measuring MeHg and THg concentrations after each step in the process, I found this method to reliably separate MeHg from

iHg for direct isotopic analysis. Cumulative recovery of MeHg after the resin separation procedure was >91% for all samples containing ≥12% MeHg, and ~87% for clam samples containing 6% MeHg. A majority of iHg impurities were removed by the resin, resulting in >91% MeHg purity for all samples after the resin separation procedure. Directly measured MeHg isotopic compositions of sample replicates had high reproducibility, and MeHg isotope ratios in biological reference materials matched those measured in other studies using different MeHg separation techniques. Overall, these results indicate that nitric acid digestion coupled with batch anion-exchange resin separation is a reliable method for isolating MeHg from iHg for compound-specific isotopic analysis, and that this method could improve studies aimed at identifying sources of MeHg to food webs and tracking biogeochemical cycling of MeHg within ecosystems.

5.2.2 Future directions related to Chapter 3

The nitric acid digestion and resin separation procedure developed for direct MeHg isotopic analysis could potentially be further optimized in the future to achieve higher MeHg purity for samples containing <10% MeHg. This may be done by utilizing a third resin separation step, using a larger amount of resin, or using resin columns rather than a batch method. Additionally, the procedure could potentially be optimized in the future to achieve higher MeHg recovery for samples containing <10% MeHg. The first step here would be to determine the reason for the lower MeHg recovery after the first resin separation step. This could be due to loss of MeHg to dissolved organic matter retained on the resin, or due to the formation of artifact MeHg during the MeHg concentration analysis of nitric acid digestion and syringe-filtered samples due to high levels of iHg in association with dissolved organic carbon in the sample prior to resin separation. This determination would likely require independent

verification of MeHg concentrations of biological samples using another mercury extraction technique, one that concentrates MeHg relative to iHg, in comparison to nitric acid digestion which releases MeHg and most of the iHg from the sample.

Further optimizing this MeHg separation procedure would be useful not only for measuring the MeHg isotopic composition of organisms containing <10% MeHg, but more importantly, for assessing the isotopic composition of MeHg within streambed sediment, biofilm, and other basal resources containing very low %MeHg, in some cases <0.1% (Olsen et al. 2016). Direct MeHg isotopic analysis of aquatic organisms at different trophic levels allows for an assessment of the range of MeHg isotopic compositions within the food web, which can reveal whether different types of organisms are obtaining MeHg from a common source or from multiple different sources. However, in order to link MeHg in aquatic organisms to the basal resource from which it originated, the isotopic composition of MeHg within various basal resources must either be measured directly or must be estimated based on assumptions of the relative amounts of microbial and photochemical demethylation occurring within different basal resources. Direct measurements of the MeHg isotopic composition of various types of organisms and basal resources within an ecosystem would allow for direct comparisons and a more confident determination of the primary sources of MeHg to a food web.

5.3 Comparison of sources and in-stream processes influencing bioaccumulation of methylmercury within natural background and point source impacted streams

5.3.1 Review of key findings of Chapter 4

In Chapter 4, I measured THg and MeHg concentrations and THg isotopic compositions of a large set of fish and aquatic invertebrate samples collected from multiple locations along

East Fork Poplar Creek (EFPC), the point source contaminated stream that was the focus of Chapter 2, as well as from Hinds Creek (HC), which is a regional background stream. For both HC and EFPC, relationships between THg isotopic composition and %MeHg values of aquatic organisms were nonlinear, suggesting that different types of organisms within each of the food webs had obtained iHg and/or MeHg from multiple isotopically distinct sources and preventing the MeHg isotopic compositions of lower trophic level organisms from being estimated. To facilitate investigation into the sources of MeHg to these food webs, I used the MeHg separation method developed in Chapter 3 for compound-specific MeHg isotopic analysis of a subset of biological samples from these two streams. These THg and MeHg isotopic compositions of aquatic organisms, along with THg isotopic measurements of streambed sediment, biofilm, and other environmental samples, were used together to identify sources of iHg and MeHg to the food webs of both streams, and to assess similarities and differences in mercury biogeochemical cycling between the point source impacted and regional background sites.

Aquatic organisms collected from HC, upstream EFPC, and downstream EFPC each had unique ranges in MeHg isotopic composition, suggesting that that MeHg within each of the food webs was derived from different sources and/or underwent different types or degrees of biogeochemical processing prior to its accumulation in the food web. The iHg and MeHg within the HC food web was found to have ultimately been derived from a combination of precipitation and dry atmospheric deposition. Aquatic organisms from HC appeared to have obtained iHg primarily from streambed sediment, and appeared to have obtained MeHg largely from biofilm and/or suspended particulates and a smaller portion from streambed sediment. In contrast, iHg and MeHg within the EFPC food web is largely derived from a combination of legacy mercury and ongoing releases of mercury from the upstream industrial point source. Some types of

organisms from EFPC appeared to have obtained iHg primarily from streambed sediment, which largely contains legacy mercury. Other types of organisms appeared to have obtained iHg primarily from suspended particulates, which at upstream sites contain a high proportion of newly released mercury, and at downstream sites contain a high proportion of legacy mercury, due to physical mixing with fine-grained streambed sediment along the flow path (Demers et al. 2018, Crowther et al. 2021). Similar to HC, aquatic organisms from EFPC appeared to have obtained MeHg largely from biofilm and/or suspended particulates, though some types of organisms, including top predator fish, appeared to have obtained a significant portion of their MeHg from streambed sediment. Together, these results suggest that both legacy mercury in streambed sediment, as well as newly released mercury from the upstream point source in suspended particulates and biofilm, contribute iHg and MeHg to the EFPC food web.

In addition to identifying sources of iHg and MeHg to the aquatic food webs of HC and EFPC, the THg and MeHg isotopic compositions of aquatic organisms were also used to investigate MeHg biogeochemical processing within each of the streams. Photochemical demethylation was found to be ubiquitous across each of the sampling sites, and based on odd-MIF signatures is presumed to occur within biofilm and suspended particulates more so than in streambed sediment. Additionally, I found that microbial demethylation is an important process within HC, which aligns with previous mercury isotopic studies on other waterbodies containing natural background levels of mercury (Kwon et al. 2014, Kwon et al. 2015, Li et al. 2016, Xu et al. 2016, Janssen et al. 2019). In contrast, I also found that isotope fractionation induced by microbial methylation is clearly dominant over that induced by microbial demethylation within EFPC. This observation aligns with previous studies on rates of microbial methylation and demethylation within EFPC biofilm (Olsen et al. 2016) as well as previous mercury isotopic

studies on other waterbodies containing very high levels of mercury (Donovan et al. 2016, Feng et al. 2019).

5.3.2 Future directions related to Chapter 4

Compound-specific MeHg isotopic analysis of aquatic organisms was very useful for determining the range in MeHg isotopic composition within the food webs of HC and EFPC, especially since the relationships between THg isotope ratios and %MeHg of aquatic organisms were nonlinear. Linking these measured MeHg isotopic compositions to specific basal resources, however, relied on assumptions about the relative amounts of photochemical demethylation occurring within different materials. In this study, I assumed that MeHg within biofilm and suspended particulates undergoes a higher degree of photochemical demethylation than MeHg within streambed sediment; thus, biofilm and suspended particulates would have higher Δ^{199}MeHg values than streambed sediment. This allowed us to suggest different basal resources as potential sources of MeHg to different types of organisms based on the relative magnitude of the Δ^{199}MeHg values of the organisms. However, for future studies, direct measurements of MeHg isotopic composition of streambed sediment, biofilm, and suspended particulates within HC and EFPC would allow for a more direct link between sources and receptors of MeHg, without relying as heavily on these assumptions.

In this study and through review of the literature, I found evidence of a trend that microbial demethylation is typically an important reaction within both natural background sites and point source impacted sites with sediment THg concentrations of less than ~1000 ng g^{-1}, but that isotope fractionation induced by microbial methylation is more likely to be dominant over that induced by microbial demethylation in highly contaminated waterbodies with sediment THg concentrations of greater than ~1000 ng g^{-1}. However, isotope fractionation induced by microbial

methylation also appeared to be dominant in a small number of waterbodies with relatively low sediment THg concentrations (Janssen et al. 2019), demonstrating that this trend does not always hold true. These observations warrant further study into the biogeochemical factors controlling rates of microbial methylation and demethylation, and whether those factors fundamentally differ across a range of minimally-to-highly mercury contaminated aquatic ecosystems.

References

Bartov, Gideon. 2014. "Mercury Stable Isotope Geochemistry as a Tool for Tracing Sources and Chemical Transformations in the Environment."Ph.D. Thesis, Department of Geology, University of Illinois at Urbana-Champaign.

Brocza, Flora M., Harald Biester, Jan-Helge Richard, Stephan M. Kraemer, and Jan G. Wiederhold. 2019. "Mercury isotope fractionation in the subsurface of a Hg(II) chloride-contaminated industrial legacy site." *Environmental Science & Technology* 53:7296-7305. doi: 10.1021/acs.est.9b00619.

Crowther, Elizabeth R., Jason D. Demers, Joel D. Blum, Scott C. Brooks, and Marcus W. Johnson. 2021. "Use of sequential extraction and mercury stable isotope analysis to assess remobilization of sediment-bound legacy mercury." *Environmental Science: Processes & Impacts* 23:756-775. doi: 10.1039/d1em00019e.

Demers, Jason D., Joel D. Blum, Scott C. Brooks, Patrick M. Donovan, Ami L. Riscassi, Carrie L. Miller, Wang Zheng, and Baohua Gu. 2018. "Hg isotopes reveal in-stream processing and legacy inputs in East Fork Poplar Creek, Oak Ridge, Tennessee, USA." *Environmental Science: Processes & Impacts* 20 (4):686-707. doi: 10.1039/c7em00538e.

Donovan, Patrick M., Joel D. Blum, Michael Bliss Singer, Mark Marvin-DiPasquale, and Martin T. K. Tsui. 2016. "Isotopic composition of inorganic mercury and methylmercury downstream of a historical gold mining region." *Environmental Science & Technology* 50:1691-1702. doi: 10.1021/acs.est.5b04413.

Feng, Caiyan, Zoyne Pedrero, Lázaro Lima, Susana Olivares, Daniel de la Rosa, Sylvain Berail, Emmanuel Tessier, Florence Pannier, and David Amouroux. 2019. "Assessment of Hg contamination by a Chlor-Alkali Plant in riverine and coastal sites combining Hg speciation and isotopic signature (Sagua la Grande River, Cuba)." *Journal of Hazardous Materials* 371:558-565. doi: 10.1016/j.jhazmat.2019.02.092.

Grigg, Andrew R. C., Ruben Kretzschmar, Robin S. Gilli, and Jan G. Wiederhold. 2018. "Mercury isotope signatures of digests and sequential extracts from industrially contaminated soils and sediments." *Science of The Total Environment* 636:1344-1354. doi: 10.1016/j.scitotenv.2018.04.261.

Hammerschmidt, Chad R., and William F. Fitzgerald. 2005. "Methylmercury in mosquitoes related to atmospheric mercury deposition and contamination." *Environmental Science & Technology* 39:3034-3039. doi: 10.1021/es0485107.

Huang, Shuyuan, Yuhan Zhao, Supeng Lv, Weiguo Wang, Weili Wang, Yuanbiao Zhang, Yunlong Huo, Xiuwu Sun, and Yaojin Chen. 2021. "Distribution of mercury isotope

signatures in Yundang Lagoon, Xiamen, China, after long-term interventions." *Chemosphere* 272:129716. doi: 10.1016/j.chemosphere.2021.129716.

Janssen, Sarah E., Karen Riva-Murray, John F. Dewild, Jacob M. Ogorek, Michael T. Tate, Peter C. Van Metre, David P. Krabbenhoft, and James F. Coles. 2019. "Chemical and physical controls on mercury source signatures in stream fish from the northeastern United States." *Environmental Science and Technology* 53:10110-10119. doi: 10.1021/acs.est.9b03394.

Janssen, Sarah E., Michael T. Tate, David P. Krabbenhoft, John F. DeWild, Jacob M. Ogorek, Christopher L. Babiarz, Anthony D. Sowers, and Peter L. Tuttle. 2021. "The influence of legacy contamination on the transport and bioaccumulation of mercury within the Mobile River Basin." *Journal of Hazardous Materials* 404 Part A:124097. doi: 10.1016/j.jhazmat.2020.124097.

Kwon, Sae Yun, Joel D. Blum, Celia Y. Chen, Dustin E. Meattey, and Robert P. Mason. 2014. "Mercury isotope study of sources and exposure pathways of methylmercury in estuarine food webs in the northeastern U.S." *Environmental Science & Technology* 48:10089-10097. doi: 10.1021/es5020554.

Kwon, Sae Yun, Joel D. Blum, Knute J. Nadelhoffer, J. Timothy Dvonch, and Martin Tsz-Ki Tsui. 2015. "Isotopic study of mercury sources and transfer between a freshwater lake and adjacent forest food web." *Science of The Total Environment* 532:220-229. doi: 10.1016/J.SCITOTENV.2015.06.012.

Li, Miling, Amina T. Schartup, Amelia P. Valberg, Jessica D. Ewald, David P. Krabbenhoft, Runsheng Yin, Prentiss H. Balcom, and Elsie M. Sunderland. 2016. "Environmental origins of methylmercury accumulated in subarctic estuarine fish indicated by mercury stable isotopes." *Environmental Science & Technology* 50 (21):11559-11568. doi: 10.1021/acs.est.6b03206.

Masbou, Jeremy, David Point, and Jeroen E. Sonke. 2013. "Application of a selective extraction method for methylmercury compound specific stable isotope analysis (MeHg-CSIA) in biological materials." *Journal of Analytical Atomic Spectrometry* 28:1620-1628. doi: 10.1039/c3ja50185j.

Olsen, Todd A., Craig C. Brandt, and Scott C. Brooks. 2016. "Periphyton biofilms influence net methylmercury production in an industrially contaminated system." *Environmental Science & Technology* 50:10843-10850. doi: 10.1021/acs.est.6b01538.

Rosera, Tylor J., Sarah E. Janssen, Michael T. Tate, Ryan F. Lepak, Jacob M. Ogorek, John F. DeWild, Christopher L. Babiarz, David P. Krabbenhoft, and James P. Hurley. 2020. "Isolation of methylmercury using distillation and anion-exchange chromatography for isotopic analyses in natural matrices." *Analytical and Bioanalytical Chemistry* 412:681-690. doi: 10.1007/s00216-019-02277-0.

Stetson, Sarah J., John E. Gray, Richard B. Wanty, and Donald L. Macalady. 2009. "Isotopic variability of mercury in ore, mine-waste calcine, and leachates of mine-waste calcine from areas mined for mercury." *Environmental Science & Technology* 43:7331-7336. doi: 10.1021/es9006993.

Sun, Ruoyu, Holger Hintelmann, Johan A. Wiklund, Marlene S. Evans, Derek Muir, and Jane L. Kirk. 2022. "Mercury isotope variations in lake sediment cores in response to direct mercury emissions from non-ferrous metal smelters and legacy mercury remobilization." *Environmental Science & Technology* 56:8266-8277. doi: 10.1021/acs.est.2c02692.

Tsui, Martin Tsz Ki, Joel D. Blum, Sae Yun Kwon, Jacques C. Finlay, Steven J. Balogh, and Yabing H. Nollet. 2012. "Sources and transfers of methylmercury in adjacent river and forest food webs." *Environmental Science & Technology* 46:10957-10964. doi: 10.1021/es3019836.

Wiederhold, Jan G., Ulf Skyllberg, Andreas Drott, Martin Jiskra, Sofi Jonsson, Erik Björn, Bernard Bourdon, and Ruben Kretzschmar. 2015. "Mercury isotope signatures in contaminated sediments as a tracer for local industrial pollution sources." *Environmental Science & Technology* 49:177-185. doi: 10.1021/es5044358.

Wiederhold, Jan G., Robin S. Smith, Hagar Siebner, Adam D. Jew, Gordon E. Brown Jr., Bernard Bourdon, and Ruben Kretzschmar. 2013. "Mercury isotope signatures as tracers for Hg cycling at the New Idria Hg Mine." *Environmental Science & Technology* 47:6137-6145. doi: 10.1021/es305245z.

Xu, Xiaoyu, Qianggong Zhang, and Wen-Xiong Wang. 2016. "Linking mercury, carbon, and nitrogen stable isotopes in Tibetan biota: Implications for using mercury stable isotopes as source tracers." *Scientific Reports* 6:25394. doi: 10.1038/srep25394.

Yin, Runsheng, Xinbin Feng, Jianxu Wang, Zhengduo Bao, Ben Yu, and Jiubin Chen. 2013. "Mercury isotope variations between bioavailable mercury fractions and total mercury in mercury contaminated soil in Wanshan Mercury Mine, SW China." *Chemical Geology* 336:80-86. doi: 10.1016/j.chemgeo.2012.04.017.

Zhang, Wei, Guangyi Sun, Runsheng Yin, Xinbin Feng, Zuxiu Yao, Xuewu Fu, and Lihai Shang. 2021. "Separation of methylmercury from biological samples for stable isotopic analysis." *Journal of Analytical Atomic Spectrometry* 36:2415-2422. doi: 10.1039/d1ja00236h.

Zheng, Wang, Jason D. Demers, Xia Lu, Bridget A. Bergquist, Ariel D. Anbar, Joel D. Blum, and Baohua Gu. 2019. "Mercury stable isotope fractionation during abiotic dark oxidation in the presence of thiols and natural organic matter." *Environmental Science & Technology* 53:1853-1862. doi: 10.1021/acs.est.8b05047.